
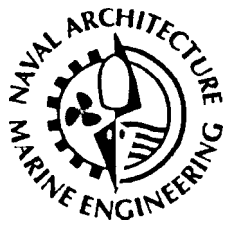



**Universities of Glasgow and Strathclyde**

**Department of Naval Architecture and Marine Engineering**

# Weight-Optimised Steel Catenary Risers and Their Applications in Harsh Deepwater Environment

**by**

**Jie Xia**

**A thesis presented in fulfilment of the requirements for the degree of Doctor of Philosophy**

**December 2008**

*To my dearest parents Jindi Chen and Changsheng Xia,*

*to my dearest husband Zhihai Xu,*

*this thesis is dedicated to them.*

# Acknowledgements

First and foremost, I would like to thank my doctoral study supervisor, Professor Purnendu K. Das. If it were not by his trust, support, and guidance, I would not have been able to start my doctoral study and have carried it on all the way till this stage. I am indeed very grateful.

Special thanks to Dr. Daniel Karunakaran of Subsea 7 who provided me not only the vessel data but also insight in the design of steel catenary risers with his profound experience, Mr. Nigel Winder of DNV Software who generously supplied me not only the academic use of DNV DeepC & Riflex, but also training course in Oslo, Dr. Helge Skåtun and Dr. Styrk Finne of DNV Software who were of tremendous help in my use of DNV DeepC & Riflex, and Professor Chengi Kuo of the Department who has always been willing to share his immense knowledge and practical experience and inspired me to do things better than it had been.

The administrative staffs of the Department are a delight to know and work with, Thelma Will, Fiona Cameron, always ready to help, and always with a warm smile.

Deep appreciation to Mr. Qiuxin Gao and his family for their great help and warm care for me, Dr. Li Xu and her family for her constructive advice on fatigue analysis and their generous help and concern whenever I was in need, and Dr. Xuan Phuc Pham for his greatest inspiration to my determination, perseverance, and English communication skill.

Heartfelt thanks also go to my office mates, Dr. Yunlong Zheng, Yang Zhang, Liang Shen, Nana Yang, Yanzhuo Xue, Hao Cui, Baogang San, Youhong Xiao, Xingyuan Zhao, Yanmin Xu, Clemens R. Strasser, Kwang Sic Chung, Camille Azzi, Marija Filipovski, Herbert Chuah, Imtaz Ali Khan, for their great supports and nicest friendship that has brought the color to my doctoral study life.

Last but not least, endless thanks to my dearest parents and husband, for their continuous long-distance love, unlimited support, understanding and encouragement during this period of time, helping me get through all the difficulties and accomplish this thesis.

I sincerely thank you all. If it were not you all, I would not have been able to come this far and have this opportunity to express my gratefulness and appreciation.

Jie Xia
18 December 2008

# Abstract

In recent years, offshore reservoirs have been developed in deeper and deeper water environments. Steel catenary risers (SCRs) are being considered used in conjunction with a semi-submersible in deepwater and harsh environments such as Northern North Sea, which presents significant design challenges. To increase the understanding of SCR behaviour and improve the design of such systems in deepwater harsh environments, the design modelling framework of deepwater SCR with weight-optimised coating was developed and investigated.

The research began by reviewing extensive publications relevant to the understanding of SCRs, limitations in their usage in deepwater and harsh environments had been addressed and establishing a methodology that could effectively unlock the physics and efficiently solve the problem.

At a first step, a parametric study on the strength design and analysis for a deepwater SCR with conventional coating, connected to a semi-submersible was carried out to deal with the factors that mainly influence the loading conditions of the riser. However, after every possible regulation of the major design parameters, the

dynamic performance of the deepwater SCR with conventional coating was improved but far from meeting the design code requirements.

From the outcome configuration with conventional coating, the deepwater SCR was further optimised by weight coating with various distribution plan, thickness and densities. Extreme dynamic analysis showed that the obtained deepwater SCR with weight-optimised coating could satisfy the strength requirements according to the design codes.

Following dynamic analysis, fatigue damage verification was executed from nonlinear random time domain analysis results by using specified bilinear S-N curve and rainflow cycle counting. Fatigue analysis results showed that the deepwater SCR with weight-optimised coating can meet the service life requirement. This suggested that weight-optimised coating as a mitigation method for deepwater SCR was effective and adequate for improving its both dynamic and fatigue performance.

Investigation was also conducted on the safety of the deepwater SCR with weight-optimised coating. Limit state functions with various models were assessed and compared. A bilinear S-N model based limit state function with wide band correction was found appropriate for fatigue reliability analysis, showing a matching result with fatigue life prediction.

A full design procedure for the deepwater SCR with weight-optimised coating, meeting design requirements including strength, fatigue life, and reliability was concluded, which can be applicable for SCRs with various deep water depths. While it is acknowledged that current model may be limited by its semi-empirical basis and issues associated with modelling simulation, it is noted that considerable possibilities for future research and development remains to be explored.

# Contents

# List of Tables

# List of Figures

# Nomenclature

## Roman

| | |
|---|---|
| $a$ | crack size |
| $a_0$ | initial crack size |
| $a_1$ | mass proportional damping coefficient |
| $a_2$ | stiffness proportional damping coefficient |
| $a_{cr}$ | critical crack size |
| $a_J$ | JONSWAP formulation parameter |
| $A$ | cross-sectional area |
| $A_B$ | Bretschneider spectrum parameter |
| $A_{PM}$ | Pierson-Moskovitz spectrum parameter |
| $B$ | stress modelling error |
| $B_B$ | Bretschneider spectrum parameter |
| $B_{PM}$ | Pierson-Moskovitz spectrum parameter |
| $C$ | Paris coefficient |

| | |
|---|---|
| $C_a$ | allowable stress factor |
| $C_{am}$ | added mass coefficient |
| $C_d$ | drag coefficient |
| $C_f$ | design case factor |
| $C_m$ | inertia coefficient |
| $C_R$ | global Rayleigh damping |
| $d$ | cylinder diameter |
| $D$ | fatigue damage |
| $D_i$ | fatigue damage per load cycle |
| $e$ | local axial misalignment |
| $f_j$ | fraction of the time spent in $j$ th sea state (to account for long-term sea effect) |
| $f_z$ | zero mean crossing frequency |
| $f(S)$ | probability density function of the stress ranges |
| $f_{\mathbf{X}}(\mathbf{x})$ | joint probability density function |
| $F$ | force |
| $g$ | acceleration of gravity |
| $g(\mathbf{X})$ | limit state function |
| $H_{max}$ | maximum wave height |
| $H_r$ | regular wave height |
| $H_s$ | significant wave height |
| $I_i$ | indication function |
| $k$ | number of stress blocks |
| $K$ | fatigue strength coefficient |
| $K_1$ | fatigue strength coefficient for the first slope of a bilinear S-N curve |
| $K_2$ | fatigue strength coefficient for the second slope of a bilinear S-N curve |
| $L$ | thickness exponent on fatigue strength |
| $L_A$ | riser arc length |

$L_{AT}$ riser arc length from top end to TDP under static loadings

$L_B$ riser arc length from the end point of section sagH to TDP under static loadings

$L_{BT}$ riser arc length before TDP, including sections upN, straightH, straightL and sagH

$L_{sagH}$ riser arc length for section sagH with heavy coating

$L_{straightH}$ riser arc length for section straightH with heavy coating

$L_{straightL}$ riser arc length for section straightL with light coating

$L_{TDAL}$ riser arc length for section TDAL with light coating

$L_{upN}$ riser arc length for section upN with normal coating

$m$ fatigue exponent coefficient

$m_1$ fatigue exponent coefficient for the first slope of a bilinear S-N curve

$m_2$ fatigue exponent coefficient for the second slope of a bilinear S-N curve

$m_P$ Paris exponent

$M$ tangential mass matrix

$M_k(a)$ magnificent factor

$M_y$ bending moment

$n_i$ number of constant amplitude range $S_i$ stress cycles in block $i$

$N$ number of fatigue cycles

$N_f$ number of samples falling into failure region

$N_i$ number of cycles to failure at constant stress range $S_i$

$N_{SW}$ number of cycles for which change in slope appears

$N_T$ total sampling number

$N(S_i)$ number of cycles to failure at stress range $S_i$

$N(T_s)$ total number of stress cycles in time $T_s$

$p_f$ probability of failure

$Q$ tangential stiffness matrix

| | |
|---|---|
| $R_i$ | correlation matrix |
| Re | Reynolds number |
| $S$ | stress range |
| $S_i$ | stress range per load cycle |
| $S_{SW}$ | stress range for which change of slope curve |
| $t$ | thickness through which a crack will most likely grow |
| $t_{fat}$ | fatigue thickness |
| $t_{ref}$ | reference thickness equal 25 mm for welded connections other than tubular joints |
| $T$ | time for fatigue failure |
| $T_e$ | effective tension |
| $T_i$ | wave period |
| $T_p$ | peak wave period |
| $T_r$ | corresponding regular wave period |
| $T_s$ | riser service life |
| $T_z$ | zero up-crossing wave period |
| $T_\omega$ | wave period |
| $\boldsymbol{u}^*$ | design point |
| $U_r$ | relative velocity of water to structure |
| $\dot{U}_r$ | acceleration of water relative to the structure |
| $\dot{U}_s$ | acceleration of structure |
| $\dot{U}_w$ | acceleration of water |
| $\nu_{0_j}$ | zero mean crossing frequency of stress process in $j$ th sea state |
| $wd$ | water depth |
| $X$ | random variables |
| $Y(a)$ | crack geometry |
| $Y_{plate}(a)$ | geometry function corresponding to a semi-elliptical surface crack |

# Greek

| | |
|---|---|
| $\alpha$ | generalised Philip's constant |
| $\alpha_i$ | direction cosines of the vector $\beta$ |
| $\beta$ | reliability index |
| $\beta_N$ | parameter in the integration methods defining the functional change in velocity |
| $\beta_w$ | spectral width parameter |
| $\gamma$ | peakedness parameter |
| $\gamma_{FM}$ | modelling error in $Y$ |
| $\gamma_N$ | parameter in the integration methods defining the functional change in displacement |
| $\gamma(a,x)$ | incomplete Gamma function |
| $\Gamma(a,x)$ | complementary incomplete Gamma function |
| $\delta_j$ | wide band correction factor in $j$ th sea state |
| $\Delta$ | Palmgren-Miner's damage index |
| $\Delta_F$ | fatigue resistant limit |
| $\Delta K$ | range of stress intensity factor |
| $\Delta K_{th}$ | threshold value |
| $\Delta t$ | time step |
| $\zeta_i$ | modal damping ratio |
| $\eta$ | allowable fatigue damage ratio |
| $\theta_N$ | parameter in the integration methods defining the functional change in acceleration |
| $\lambda_j$ | $j$ th moment of the stress spectrum |
| $\mu$ | mean value |
| $\nu$ | kinematic viscosity |
| $\rho$ | water density |

| | |
|---|---|
| $\rho(m_i, K_i)$ | correlation coefficient of $m_i$ and $K_i$ $(i = 1,2)$ |
| $\sigma$ | standard deviation |
| $\sigma_A$ | basic allowable combined stress |
| $\sigma_j$ | standard deviation of stress process in $j$ th sea state |
| $\sigma_s$ | RMS value of stress range $S$ |
| $\sigma_{VM}$ | maximum von Mises stress in the pipe |
| $\sigma_w$ | spectral width parameter |
| $\sigma_{wa}$ | left width parameter |
| $\sigma_{wb}$ | right width parameter |
| $\sigma_y$ | specified minimum yield strength |
| $\varphi$ | standard normal density function |
| $\Phi$ | standard normal CDF |
| $\omega$ | angular wave frequency |
| $\omega_i$ | eigenfrequency |
| $\omega_p$ | angular spectral peak frequency |
| $\Omega$ | stress parameter |

## Acronyms

| | |
|---|---|
| ALS | Accidental Limit State |
| API | American Petroleum Institute |
| ASTM | American Society for Testing and Materials |
| CALREL | CAL-RELiability |
| CDF | Cumulative Distribution Function |
| CoG | Centre of Gravity |
| COV | Coefficient of Variation |
| CPU | Central Processing Unit |
| CR | Conventional SCR |
| CRA | Corrosion Resistant Alloy |

| | |
|---|---|
| CT | Coating Thickness |
| DFF | Design Fatigue Factor |
| DS | Directional Simulation |
| ECA | Engineering Criticality Assessment |
| EPFM | elastic-plastic fracture mechanics |
| FD | Frequency Domain |
| FE | Finite Element |
| FLS | Fatigue Limit State |
| FM | Fracture Mechanics |
| FORM | First Order Reliability Method |
| FPS | Floating Production System |
| FPSO | Floating Production, Storage and Offloading vessel |
| GoM | Gulf of Mexico |
| GUI | Graphical User Interface |
| H | Heavy Coating |
| ID | Internal Diameter |
| IM | Importance Sampling |
| JIP | Joint Industry Project |
| L | Light Coating |
| LCC | Level Crossing Counting |
| LEFM | Linear Elastic Fracture Mechanics |
| LRFD | Load and Resistance Factor Design |
| LSD | Limit State Design |
| MCS | Monte Carlo Simulation |
| MODU | Mobile Offshore Drilling Unit |
| MPP | Most Probable Failure Point |
| N | Normal Coating |
| NDE | Non-Destructive Examination |
| NDT | Non-Destructive Test |
| NNS | Northern North Sea |
| OD | Outside Diameter |
| OPS | Orthogonal Plane Sampling |

| | |
|---|---|
| OS | Offshore Standard |
| PC | Peak Counting |
| PDF | Probability Density Function |
| PE | Polyethylene |
| PP | Polypropylene |
| PU | Polyurethane |
| RAO | Response Amplitude Operator |
| RC | Range Counting |
| RFC | Rainflow Counting |
| RMS | Root Mean Square |
| SCF | Stress Concentration Factor |
| SCR | Steel Catenary Riser |
| SMYS | Specified Minimum Yield Strength |
| SORM | Second Order Reliability Method |
| TD | Time Domain |
| TDP | Touch Down Point |
| TDZ | Touch Down Zone |
| TLP | Tension Leg Platform |
| TSJ | Taper Stress Joint |
| TTR | Top Tensioned Riser |
| ULS | Ultimate Limit State |
| VIV | Vortex Induced Vibration |
| WoA | West of Africa |
| WR | Weight-Optimised SCR |
| WSD | Working Stress Design; Wave Scatter Diagram |
| WT | Wall Thickness |

*Chapter 1*

# Introduction

## 1.1 Background

There is no immediately available, affordable substitute for oil and gas. Hydrocarbon energy is the driver of modern economies and the whole edifice of modern society is built upon it. Hydrocarbon energy is vital in order to create and sustain economic and social development. 80% of the world is starting to use oil and gas. In a word, our global economy and modern society could not exist without oil and gas.

75% of the earth's surface is covered by oceans so it is no surprise that as onshore oil and gas reserves are depleted that exploration and production has extended into offshore basins that fringe the world's continents. Today around 60% of the world's petroleum production comes from offshore operations in waters of more than half the coastal nations on earth. As near-shore oil production in shallow water has been declining, demand for energy is driving oil and gas exploration and production into increasingly challenging environments, from deepwater (500 to 1500 m) toward ultra deepwater (1500 to 3000 m). Today oil and gas is produced off the Louisiana coast in the Gulf of Mexico in over 8,000 ft (2438.4 m) of water.

Development of deepwater fields requires overcoming numerous design challenges, while new technologies are often used in conjunction with proven technologies to meet the demands of harsher operating conditions and larger production capabilities, which makes the possible use of lower-cost, efficient steel catenary risers (SCRs).

The SCR concept has become an attractive choice and recently been used in almost every new deepwater field development around the world. Shell pioneered the implementation of the SCR concept in 1994 on its Auger tension leg platform (TLP) in 872 m (2860 ft) water depth. Since then, SCRs have been vital to deepwater field developments. They have been widely used around the world in water depths ranging from less than 457 m (1500 ft, Price TLP in EW 1003) to 2438 m (8000 ft, Independence Hub semi-submersible in MC 920) for both production and export. Their use has given a new dimension to oil exploration and transportation in water depths where other riser concepts could not tolerate the environmental loads or would have become very costly.

However, SCR designs are very sensitive to floating support platform or vessel motion characteristics to which they are typically attached. For example, the application of SCRs for semi-submersibles and floating production, storage and offloading vessels (FPSOs) in deepwater harsh environments presents design challenges, due to the large wave-induced motions on the platform, and large vessel offsets caused by wind, current, and slow-drift wave motions. Large heave motions cause buckling at the touch down point (TDP). In addition to pipe stresses, the main design issues for the SCR concept is fatigue related which arise from vessel motions and soil-riser interaction.

These problems can be addressed with a weight-optimised SCR concept which was first developed by Subsea 7 with Statoil participation (Karunakaran, 2006).

A feasible riser configuration can be achieved by varying the weight along the riser length with different density coatings. For deepwater SCRs, the key design issues are local buckling and severe fatigue damage at touch down zone (TDZ). Heavy stresses

at TDZ are due to the "compression waves" induced by vessel motions, and also the up and down motion of long riser sections at TDZ. Further, in harsh environments the wave and vessel motion-induced dynamics of the straight section of the SCR also influence the stresses at TDZ.

Hence, a feasible configuration can be obtained only by controlling the dynamic stresses at TDZ. The features of the riser design are:

- Lightest possible cross-section at TDZ. This helps reduce the propagation of compression waves from vessel heave motion. Also, it reduces the dynamic stresses at TDZ caused by the up and down movement of long riser sections at TDZ.

- Heavy riser cross-section on the straight part of the SCR. This reduces the dynamics of the straight section, lessening the dynamic stresses at TDZ. However, for deepwater applications this also increases both the hang-off loads and the dynamic axial stress closer to the hang-off.

## 1.2 Aims of the Thesis

The aims of the thesis are as follows:

- To perform a critical review on the existing approaches adopted for the design and analysis.
- To identify problems related to the performance of SCRs for use in deepwater and hostile environment.
- To propose an applicable fatigue mitigation method based on weight optimisation of protective coatings for SCRs.
- To devise an effective reliability-based fatigue assessment methodology to assist in the design and analysis of SCR in deepwater.

# 1.3 Research Approach and Strategy

## *1.3.1 Research Approach*

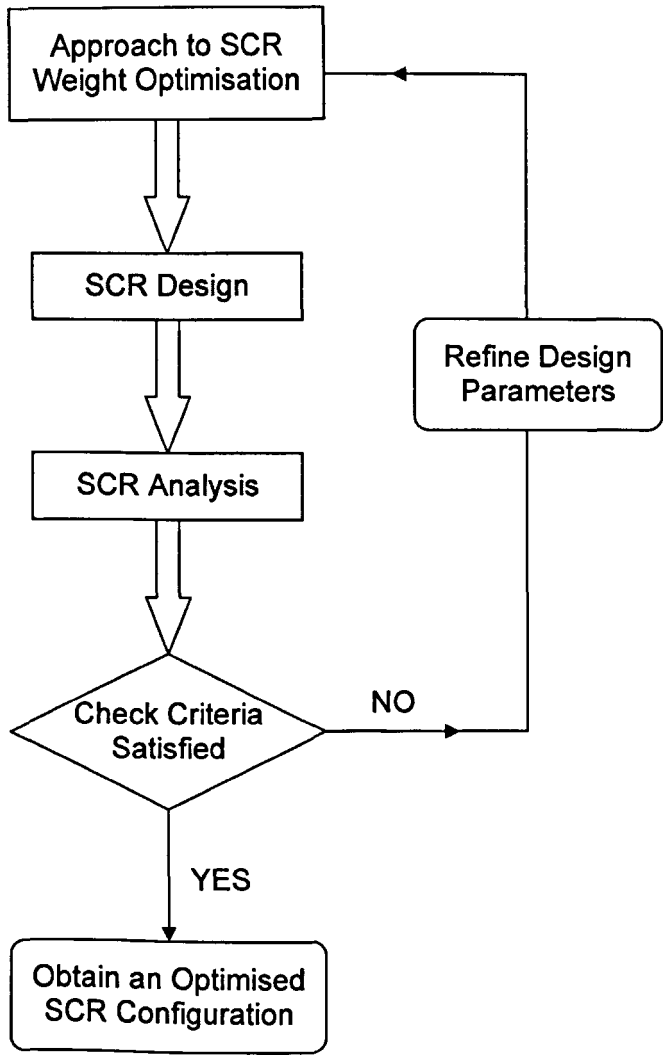


➢ Design Process

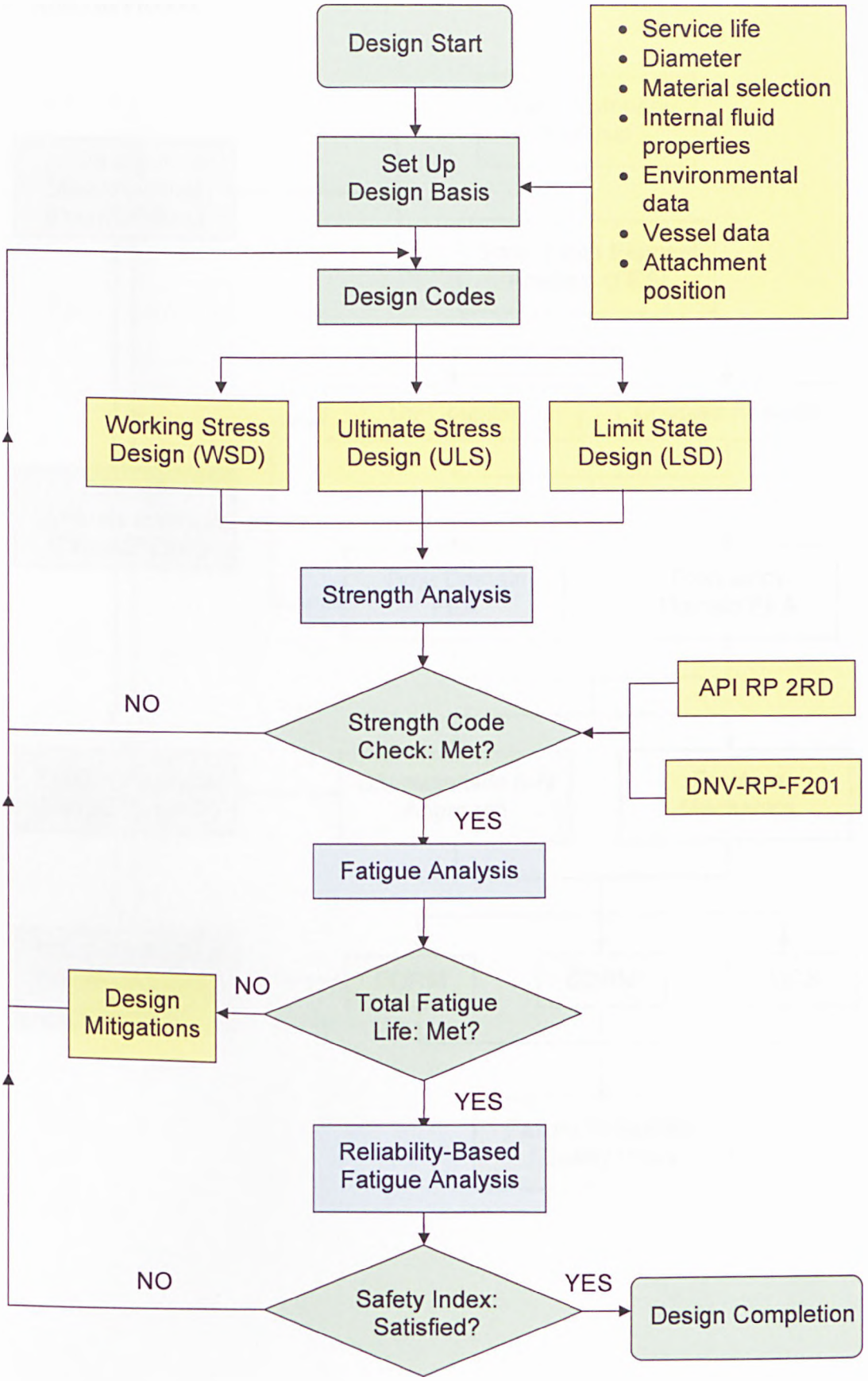
Design Start
Set Up Design Basis
Service life
Diameter
Material selection
Internal fluid properties
Environmental data
Vessel data
Attachment position
Design Codes
Working Stress Design (WSD)
Ultimate Stress Design (ULS)
Limit State Design (LSD)
Strength Analysis
Strength Code Check: Met?
NO
API RP 2RD
DNV-RP-F201
YES
Fatigue Analysis
Total Fatigue Life: Met?
NO
Design Mitigations
YES
Reliability-Based Fatigue Analysis
Safety Index: Satisfied?
NO
YES
Design Completion

- Analysis Process

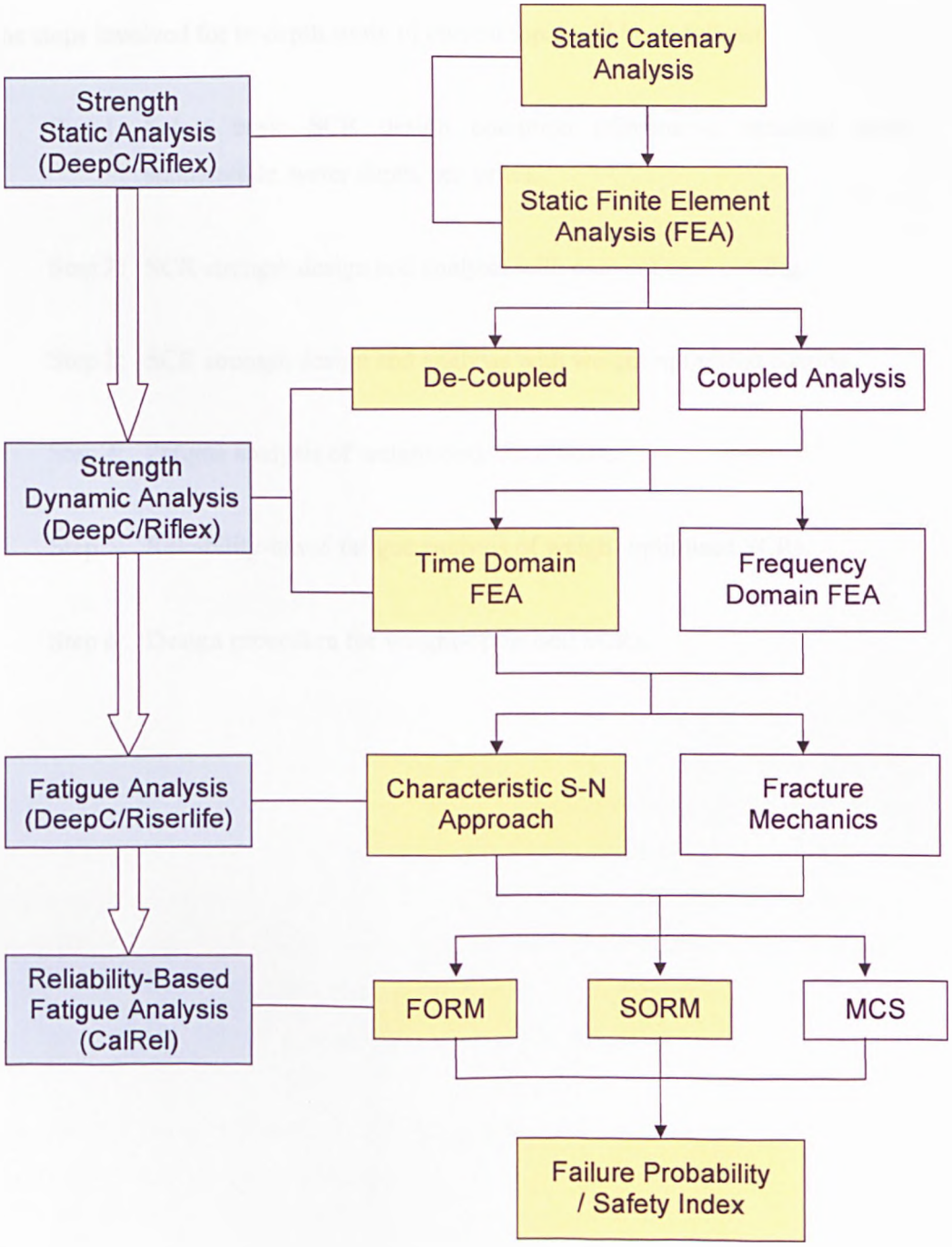

### *1.3.2 Research Strategy*

The steps involved for in-depth study of current topic will be as follows:

Step 1: Select basic SCR design condition (dimension, attached semi-submersible, water depth, sea state).

Step 2: SCR strength design and analysis with conventional coating.

Step 3: SCR strength design and analysis with weight-optimised coating.

Step 4: Fatigue analysis of weight-optimised SCRs.

Step 5: Reliability-based fatigue analysis of weight-optimised SCRs.

Step 6: Design procedure for weight-optimised SCRs.

Chapter 2

# Critical Review

## 2.1 What Is a Riser?

A riser system is essentially conductor pipes connected between floaters on the surface and the subsea facilities at the seabed for drilling, production, water injection, gas lift, or export purposes. As water depth increases the cost of the riser system becomes a higher proportion of the total field development cost. Riser systems play bigger and bigger role as part of the offshore and becomes the most important part of deepwater infrastructure. Riser systems provide one of the most challenging areas of design of deepwater systems. Once broken, it will result in great damage. So it's important to determine the reasonable environmental design criteria.

Riser can be categorised into the following main types (Deepwater Engineering & Technology Research Centre, 2008):

- Marine drilling risers (MODU risers)
- Top tensioned risers (TTRs or dry tree risers)
  - Drilling

  - Production
- Compliant risers
  - Steel catenary risers (SCRs)
  - Flexible risers
- Hybrid risers

where MODU stands for mobile offshore drilling unit.

The most widely used and field proven deepwater riser concepts include SCRs, hybrid risers with a single line or bundled multi-lines, flexible risers with different configurations, and TTRs as shown in Figure 2.1.1.

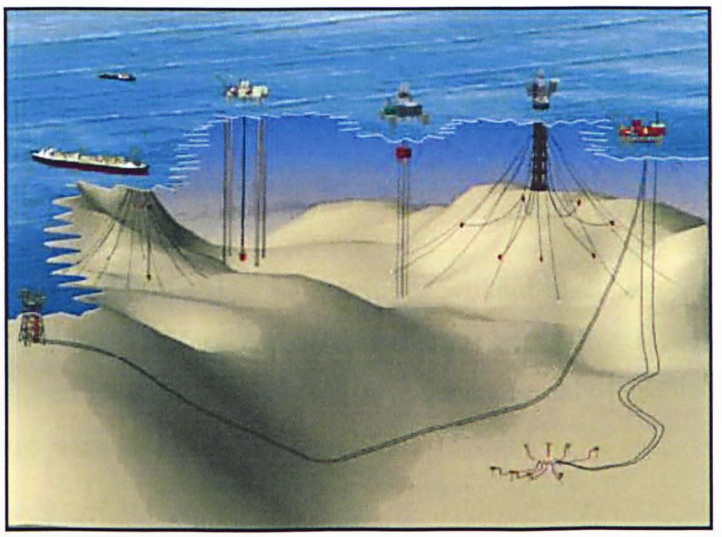

**Figure 2.1.1** Illustration of Deepwater Riser Concepts (Song and Stanton, 2007a).

Among the riser concepts, SCRs have been enjoying a widespread acceptability for deep and ultra-deepwater oil and gas production in recent years. Compared with other deepwater riser concepts, SCR is much more attractive because of its relative low cost, conceptual simplicity, significant structural capacity, ease of fabrication and offshore installation and suitable for wide range of diameters and water depths (Figure 2.1.2). By the end of 2006, more than 100 deepwater and ultra-deepwater

SCRs have been widely adopted for all types of deepwater floaters (SPAR, TLP, semi-submersible, and FPSO) worldwide mainly in the deepwater fields of Gulf of Mexico (GoM), West of Africa (WoA), and offshore Brazil (Song and Stanton, 2007b).

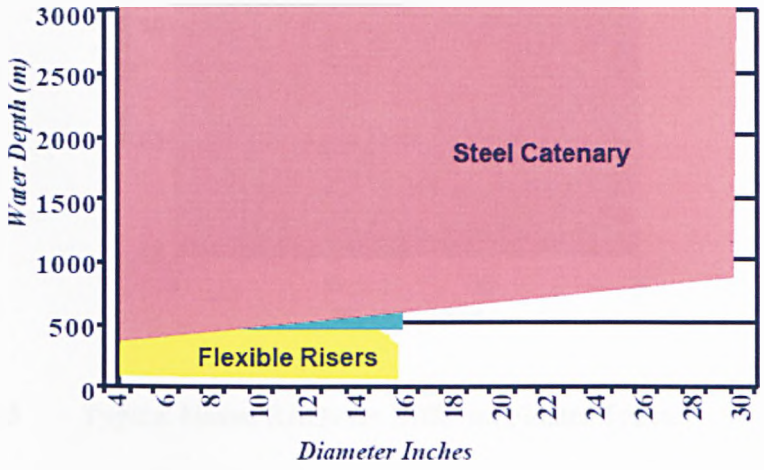


**Figure 2.1.2** Compliant Riser Applications.

SCR consists primarily of a steel pipe, with or without insulation and casing, free hanging from the vessel to form a simple catenary (Lim, 2006). Because of the large deflection required by this configuration, it is generally only feasible for very long lengths, in large water depths.

Major design concerns of the SCR pipes connected to a floating structure are the dynamic motion and the fatigue damage. The SCRs are very sensitive to the platform or vessel motion characteristics to which they would be attached as well to the environmental loads. The feasibility of the SCRs is strongly linked to the dynamic performance of the host facility. Figure 2.1.3 shows comparisons of typical heave Response Amplitude Operators (RAOs) for different floater types. All of the Spar, TLP and semi-submersible have proven to work well for SCRs at deep water, and the Spar and the semi-submersible with SCRs are qualified for ultra deepwater as well through recent DeepStar Projects.

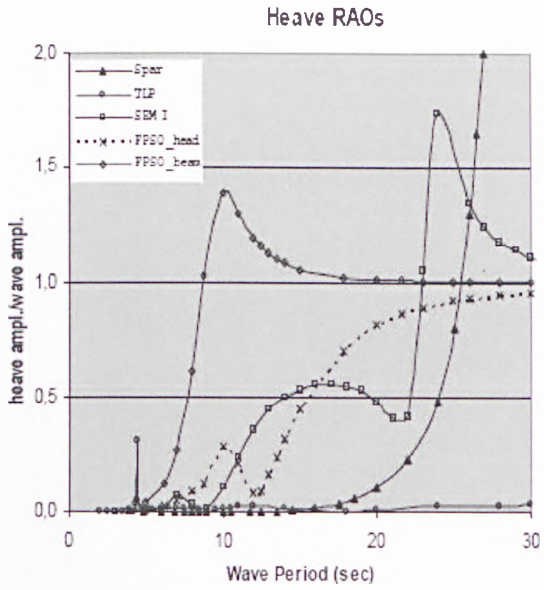


**Figure 2.1.3** Typical Heave RAOs for Different Floater Types.

Semi-submersible units offer a number of benefits, including large payload capacity, limited sensitivity to water depth, quayside integration and the ability to relocate after field abandonment. However, SCRs used in conjunction with a semi-submersible in deepwater environments present significant design challenges. Figure 2.1.4 shows the typical RAOs of a semi-submersible.

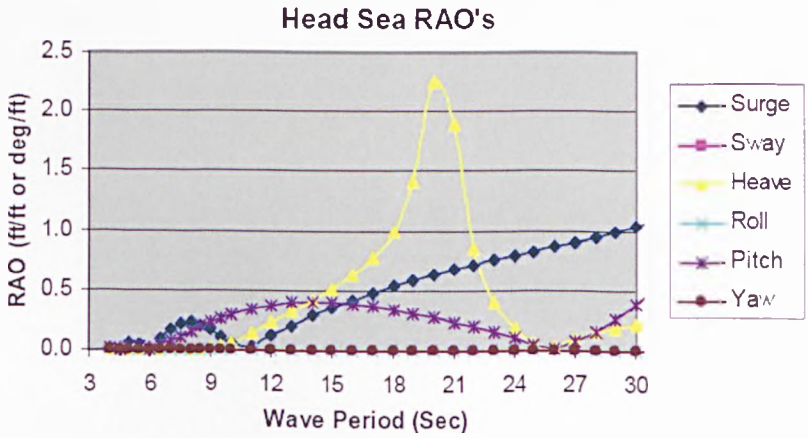


**Figure 2.1.4** Typical Semi-Submersible RAOs (FloaTEC, 2008).

Large heave motions introduced at the upper end of a catenary riser can lead to compression, large bending moments and potential buckling at the TDP area and result in difficulty meeting strength and fatigue design criteria at the TDP and at the riser hang off location. The challenge is even more significant when SCRs are considered for harsh environments such as Northern North Sea (NNS), where extreme and long-term environmental conditions are amongst the most severe in the world, causing the risers to be highly dynamic and fatigue sensitive. Special efforts are needed to develop an optimised, feasible SCR configuration to be used in conjunction with a semi-submersible for such harsh environment. Figure 2.1.5 shows a typical general arrangement of a SCR connected to a semi-submersible.

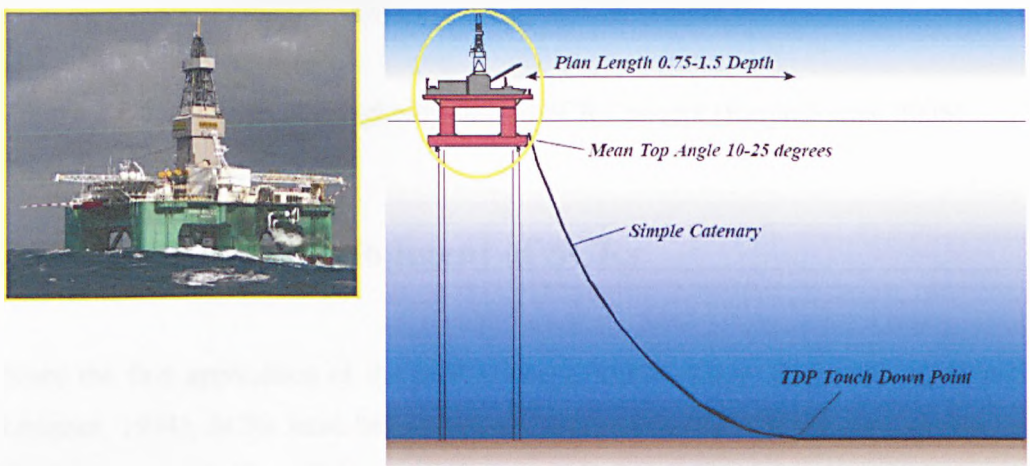


**Figure 2.1.5** Typical Semi-Submersible – SCR General Arrangement (Brugmans, 2005; Hatton, 1999).

Previous industry work suggested that an SCR strength and fatigue response can be improved using weight-optimised coating which means using heavy and light coatings strategically placed along the riser. Limited application attempts have been made at SCRs on a semi-submersible (Karunakaran, Meling, Kristoffersen, and Lund, 2005) and a turret moored FPSO (Foyt, Griffin, Campbell, Wang, and Kan, 2007) respectively in deepwater environments so far. A typical weight-optimised SCR concept is shown in Figure 2.1.6.

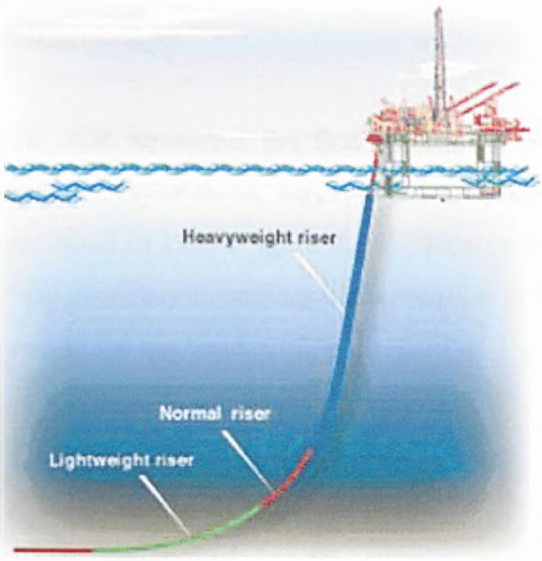


**Figure 2.1.6** Typical Weight-Optimised SCR Concept (Karunakaran, 2006).

## 2.2 Historical Development of SCRs

Since the first application of the SCR concept (Phifer, Kopp, Swanson, Allen, and Langner, 1994), SCRs have been currently used worldwide for the new deepwater field development. The brief review of some of the key SCR projects is as follows:

The Shell's Auger TLP in the Gulf of Mexico is the first floating production facility to implement steel catenary risers for oil and gas export in 1994. In this arrangement, the SCRs were installed in a water depth of 872 m (2860 ft) using a flex joint connected to the TLP pontoon.

Since Auger TLP to date, SCRs have been installed on several Gulf of Mexico TLPs, and Spar-type structures such as Marlin TLP, Allegheny SeaStar TLP, and Hoover/Diana-DDCV in water depth of 897 m (2950 ft), 1000 m (3290 ft), and 1460 m (4800 ft), respectively (Mekha, 2001). In these applications the steel catenary riser

configuration offers solutions to difficult deep water conditions, simplifying riser design and offering cost advantages.

The Petrobras P-XVIII SCR represents the first application of SCRs to installed semi-submersible based FPS systems in water depth of 910 m (2985 ft) in the Marlim Field, offshore Brazil in 1997 (Figure 2.2.1). Because the dynamic motions were more severe, it was necessary to employ higher tension in the SCR, in order to reduce bending moments in the sag bend.

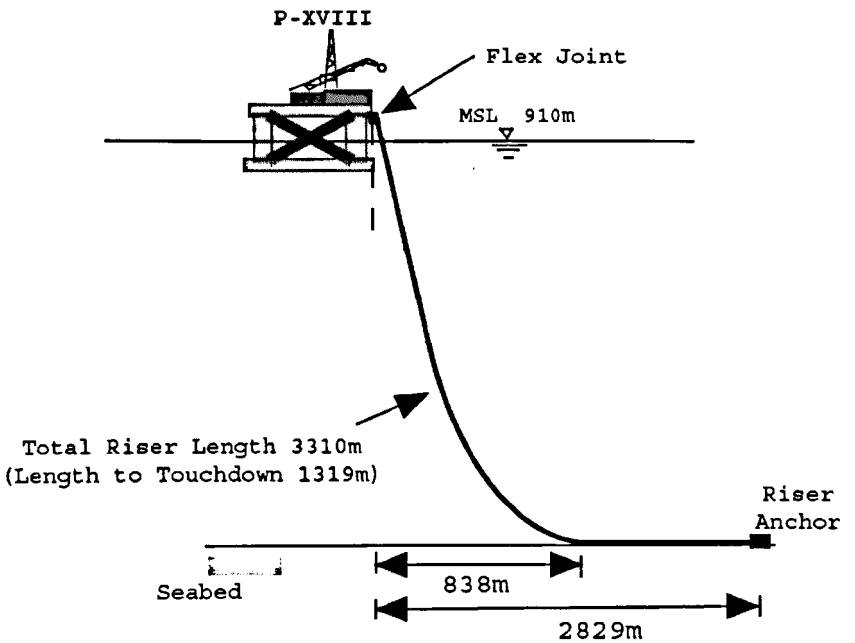


**Figure 2.2.1** Petrobras P-XVIII SCR Design Configuration (Sertã, Mourelle, Grealish, Harbert, and Souza, 1996).

The Bonga SCRs were the first to be installed on an FPSO vessel on Front Runner offshore WoA in 2004 (Bai and Bai, 2005, p.439).

To date, the deepest SCR that has been engineered and installed is for the Independence Hub Facility (IHF) at a water depth of 2438 m (8,000 ft) in the Atwater Valley region of the Gulf of Mexico (Figure 2.2.2) (Song, Mekha, and

Sebastian, 2006; Song and Stanton, 2007a). Initially, the gas production riser system consists of two 10-inch SCRs and four 8-inch SCRs attached to a deep draft semi-submersible as the host platform.

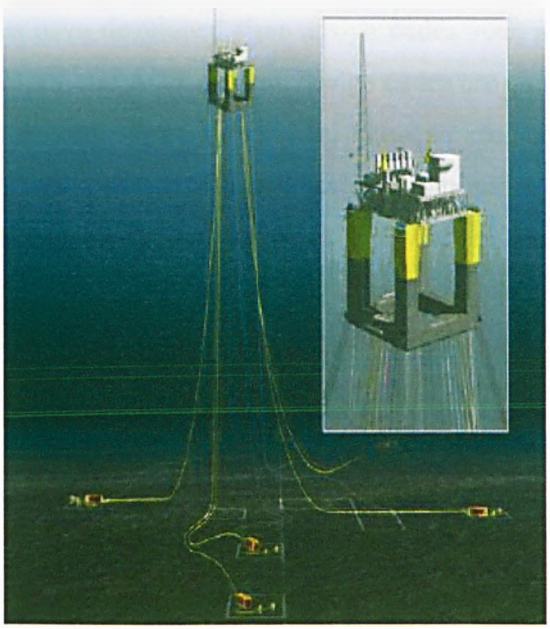

**Figure 2.2.2** Illustration of Enterpriser IHF SCR Project.

The oil industry has improved the basic semi-submersible hull form progressively to meet demands for increasing payload capacity, while retaining acceptable dynamic motions and improving station-keeping capability. Today, the leading edge driver for semi-submersible design has become the application of steel catenary risers as a preferred flowpath solution for high-rate production in ultra-deep water.

Current use of SCR concept is limited to deep water applications, but the potential for cost reduction and design flexibility of the concept is expected to result in more widespread use of the catenary arrangement. Furthermore, in difficult conditions, such as high temperature, high pressure applications, steel catenaries possibly offer the only viable design solution currently available.

## 2.3 SCR Code-Based Design

"Codes of practice attempt to force designers to exploit all means available so as to maximise safety, durability and economy." (Jeary, 1998, p.16) Authorities and classification societies have developed riser design codes such as ISO, API, NPD, HSE, NS, BS, CSA, DNV and ABS. Several design codes are currently available for designing a deepwater riser. These are divided between specially developed riser codes, extensions of pipeline codes to address riser design, or codes of practice which have been specially developed for pipes designed for export service. These codes constitute the typical general compliance and guidance documents used by industry. More detailed design, fabrication, installation and operation practices are authored and followed by operating companies. The most widely applied design codes for deepwater SCRs are API RP 2RD (1999), API RP 1111 (1999) and DNV-RP-F201 (2001). Other codes that have been partially used for deepwater SCR design include: ASME B31.8 (2000), DOT 49 CFR PT 192 (2007), ISO 15589-2 (2004), BS 7608 (1999), and DNV-RP-F204 (2005).

The design of SCRs must satisfy many static, dynamic and fatigue requirements according to the selected design based code. Design codes are distinguishable according to two fundamental design approaches (see Table 2.3.1):

- Working stress design (WSD)
- Limit state design (LSD)

**Table 2.3.1** Riser Design Approaches: WSD vs. LSD.

| Design Approach | WSD | LSD |
|---|---|---|
| Brief Description | The traditional approach to steel design, which relates allowable loading to the yield stress of the material. | An ultimate strength approach that relates allowable loading to the ultimate strength of the material, under a reliability-based design framework. |
| Applicability | API RP 2RD (Appendix A.1, A.2) | API RP 1111 |
| | DNV-OS-F201 (Appendix A.3) | |
| Merits | Very well established and relatively easier to use. | Relying on statistics and probabilities of failure, leading to a more consistent design and safety levels against failure which in turn leads to cost savings and more efficient structures. |
| Drawbacks | More conservative; structural safety is taken care of by using a single safety factor which leads to a varying safety level strongly dependent on the load conditions. | Availability of sufficient statistical data is essential to produce reliable factors. |

In general, pipeline or riser design for the oil and gas industry begins with material selection and pipe diameter sizing to meet fundamental flow assurance requirements. Pipe wall thickness selection for most offshore pipelines and risers is determined by considering stresses resulting from the internal and external pressure under operating, installation and test loading conditions. Both WSD and LSD approach are commonly used to design for these loads. Since WSD and LSD approach follow different philosophies, it is preferable to follow one approach for riser design rather than mix approaches in order to produce a consistent design and safety level. However, for certain failure modes of the riser, such as local buckling, the resistance to failure is independent of the material properties; as such, it does not strictly fall under WSD criteria and is more of a LSD criteria. Therefore, WSD and LSD codes are

sometimes specified together to define different design requirements for the same riser design. Caution should be exercised when several codes are followed at the same time to ensure consistency of the design and stress/strain checks.

The LSD approach has been included in the 2001 edition of the DNV-OS-F201 code and will be included in the API RP 2RD code which is currently being revised. It is reasonable to expect that existing risers designed per the WSD method would satisfied the LSD method since the former is expected to be more conservative than the latter. However, to date, no risers have been designed using the LSD method (Mansour, 2007).

So far, successful SCR code-based design experience has been gained through projects illustrated by such as Sertã, Mourelle, Grealish, Harbert, and Souza (1996), Hatton (1999), Mekha (2001), Patel, Kumar, Master and Karunakaran (2001), Torres, Mourelle, and Silva (2001), Wichers and Devlin (2001), Gore and Mekha (2002), Kavanagh, Lou, and Hays (2003), Pollack, Davies, and Riggs (2003), Kavanagh et al. (2004), Jesudasen, McShane, McDonald, Vandenbossche, and Souza (2004), Gonzalez, Mourelle, Mauricio, Lima, and Moreira (2005), Nolop et al. (2007), Quintin, Legras, Huang, and Wu (2007), Song and Stanton (2007), Galvin and Hill (2007).

## 2.4 SCR Strength Analysis Methods

When designing structural components, two load contributions are of special importance:

- Extreme loads
- Fatigue loads (reviewed in section 2.5)

Extreme loads can be thought of as loads that will cause the structure to fail due to the stress exceeding the material yield strength. Thus, the SCR design goal by

strength analysis is to avoid, by a proper low probability, that the material is exposed to such excessive loads.

### 2.4.1 Static Analysis

The initial state of any analysis of suspended pipe is the computation of its profile under a set of static forces. The static problem must be solved before undertaking subsequent dynamic analyses. As nonlinearity and large displacements are involved, the analysis is iterative. Starting from an initial configuration satisfying the boundary condition, one option is to employ a time domain analysis (described in the next section) and allow the riser to settle to its static position after the transients have been damped out. A review on the existing methods and the analysis techniques can be found in the works of Jain (1994) and Patel and Seyed (1995). Recent distinctive research efforts made to develop analytical methods to evaluate the response of catenary risers subjected to static loading were found by Wichers and Devlin (2001), Averbuch, Cunff, Costa, and Biolley (2003), and Tanaka and Martins (2006).

### 2.4.2 Time Domain vs. Frequency Domain Dynamic Analysis

For deepwater risers, dynamic analysis is a key issue that requires deep and comprehensive investigation of the associated system, proper formulation of the theoretical model and finally, the use of an efficient solution method. The dynamic analysis is a time simulation of the motions of the model over a specified period of time, starting from the position derived by the static analysis.

Usually, dynamic analysis can be performed in the time domain (TD) or frequency domain (FD). The preferred method is a function of the accuracy required versus the computational efficiency. Riser analysis involves inherent nonlinearities due to soil-pipe interaction, drag, damping, etc. In FD analysis, the nonlinearities must be linearised, either by dropping higher order terms in the equation of motion, or using approximations. In TD analysis, the nonlinearities are included. Consequently, TD

analysis is inherently more accurate than FD analysis; however, FD analysis is considerably faster. Detailed reviews on previous works were presented by Jain (1994) and Patel and Seyed (1995). Today, TD and FD are both available in several commercial software packages for riser analysis, such as ABAQUS, ANSYS, ANFLEX, DeepLines, Flexcom, OrcaFlex, and Riflex (see section 2.6), which are all based on the finite element (FE) approximation..

The response of SCRs in dynamic loading conditions is complex. The behaviour of SCRs is nonlinear in nature. Significant geometric nonlinearity can be exhibited near the attachment to the vessel and TDP on the seabed. Due to the nonlinearity of response, FD methods used for analysis of rigid risers are unlikely to provide reliable results and nonlinear TD methods are required. A TD simulation is better suited than FD analysis to capture possible nonlinear effects associated with wave forces and structural motions. But efforts to increase both the accuracy and efficiency of the analysis procedures with FD have never been stopped by, for instance, Garrett, Chappell, and Gordon (2002), Garrett (2005), and Low and Langley (2006a, 2006b).

### *2.4.3 Coupled vs. Uncoupled*

Mooring lines and risers have relatively small effect on the floating host vessel's wave frequency motions. However, they have significant impact on the vessel's low frequency response, which in turn affects mainly the riser fatigue.

In a coupled analysis, the vessel, mooring lines, and risers are accounted for in the same model. The mooring lines and risers are modelled using the finite element method (FEM) and their stiffness, mass, and damping are accounted for. Most recent attempts for coupled global analysis application have been made by Heurlier et al. (2001), Wichers and Devlin (2001), Garrett, Chappell, and Gordon (2002), Tahar and Kim (2003), Ye, Shanks, and Fang (2003), Hansen, Wang, Sodahl, and Ward (2004), Kim (2004), Garrett (2005), Arnesen et al. (2006), Low and Langley (2006a), and Lee and Clauss (2007). However, coupled analysis is computationally demanding,

especially for small finite element mesh size and large number of mooring lines and risers. Consequently, coupled analysis is typically performed only when necessary (Mansour, 2007).

The methodology of an uncoupled analysis assumes that the representative offset (static and low frequency) and platform wave frequencies (wave frequency) are computed in separate models by different programs. Once the vessel motions are obtained, either from coupled or uncoupled analysis, they are imported as input into the riser analysis software for the uncoupled riser analysis. Most current riser analyses are still based on uncoupled analysis which is more conservative but with less computation cost.

## 2.5 SCR Fatigue Analysis Approaches

Fatigue loads can be thought of as the loss of strength that a material experiences when subjected to a cyclic stress history. The process often starts at the surface of a material where small imperfections such as weld defects cause stress concentrations. Failure by fatigue is a progressive irreversible cracking process, which unless detected and remedied, can lead to a catastrophic rupture. "Between 50-90 per cent of all structural failures occur through a fatigue mechanism", reported by Fuchs and Stephens (1980). The percentage may vary with the types of structure and service environment, but incorporating fatigue into design of engineering structures is of great importance.

Almost all structures are experiencing some kind of varying load. However, fatigue failures are more likely to happen in ship and offshore structures because they are exposed to sea waves (and winds) that impose a great number of fluctuating loads on the ship during its service lifetime. These repeated loads can cause fatigue damage or failure at a stress level usually well below the design allowable of material. This implies that not only the extreme load values are important; the small-amplitude time

history of the load affects component reliability due to fatigue damage. Hence, incorporating fatigue into SCR design is of great importance.

Correctly calculating riser fatigue is a complex problem. The two major approaches for fatigue analysis and design of weld joints are

- the characteristic stress-cycle (S-N) curve approach and
- the fracture mechanics (FM) approach

which will be illustrated more detailedly in section 5.2. The S-N curve approach is based on experimental measurement of fatigue life in terms of cycles to failure for different structural details and loading levels. On the other hand, the FM approach is based on the existence of an initial crack and subsequent growth under cyclic loading.

So far, S-N curve approach is the most common approach for the assessment of SCR fatigue (Campbell, 1999; Mekha, Mirza, and Lang, 2000; Torres, Mourelle, and Silva, 2001; Borgen, 2002; Mekha, 2002; Senra, Jacob, Torres, and Mourelle, 2002; Buitrago, Weir, and Kan, 2003; Kopp, Perkins, Prentice, and Stevens, 2003; Langner, 2003; Macdonald, and Maddox, 2003; Mekha and Heijermans, 2003; Ye, Shanks, and Fang, 2003; Dantas et al., 2004; Mansour, 2004; Dantas et al., 2005; Karunakaran, Meling, Kristoffersen, and Lund, 2005; Sheehan, Grealish, Smith, and Harte, 2005; Karunakaran and Meling, 2006; Xu, Jesudasen, Fang, and Else, 2006; Yao and Sun, 2006; Brooks, Masson, and Reeves, 2007; Netto, Lourenço, and Botto, 2007 and 2008; Vandenbossche et al., 2007; Izquierdo et al., 2008).

Fracture mechanics is used only for the engineering criticality assessment (ECA) study to define acceptable flaw size at the riser girth welds (Landes, Lee, Bose, and Ito, 2001; Campbell, Jones, and Korloo, 2003; IIJIMA, 2005; Luk and Wang, 2007; Netto, Lourenço, and Botto, 2007 and 2008).

## 2.6 Reviewing the Available SCR Analysis Software

There are several both general purpose and riser-specific software packages that are currently available for the analysis and design of risers; the most widely used are (Table 2.6.1):

**Table 2.6.1** Riser Analysis Software.

| Software (Vendor) | Approach | | | Use | Availability for Academic Use in NAME of UGS | Popularity |
|---|---|---|---|---|---|---|
| | Nonlinear FEM | TD | FD | | | |
| ABAQUS (SIMULIA) | √ | √ | √ | Limited | √ | ★★★ |
| ANSYS (ANSYS) | √ | √ | √ | Limited | √ | ★ |
| ANFLEX | √ | √ | √ | Limited | | ★★★ |
| DeepLines (PRINCIPIA) | √ | √ | √ | Limited | | ★ |
| Flexcom (MCS) | √ | √ | | Wide | | ★★★★★★ |
| Freecom (MCS) | √ | | √ | Limited | | ★ |
| OrcaFlex (Orcina) | √ | √ | √ | Wide | √ | ★★★★ |
| Riflex (MARINTEK) | √ | √ | √ | Limited | √ | ★★★★ |

Note that FEM, FD, TD and NAME of UGS denote finite element method, frequency domain, time domain, and the Department of Naval Architecture and Marine Engineering of Universities of Glasgow and Strathclyde, respectively.

All software programs listed are finite element analysis (FEA) tools using hybrid formulation (stiffness matrix with force penalty terms to avoid the numerical instability induced by the disparity between the axial and bending stiffness of the

SCR). For solving the equation of motion, either implicit, explicit, or both methods are used. Each method has its advantages and disadvantages (accuracy versus computation efficiency). At the same level of accuracy and comparable modelling details, results produced by the different packages are very close (as should be expected since the FEA method is very well established).

ABAQUS (www.simulia.com) is a comprehensive, general-purpose FE program, and is renowned for its superiority in using time domain analysis and non-linear response capabilities. It also has optional add-on and interface products for offshore engineering. The use of ABAQUS for riser analysis is generally required when significant nonlinear effects need to be considered. These nonlinear effects are generally transient in nature and, therefore, require a time-domain solution approach to estimate the peak loads experienced by the riser. For riser analysis, ABAQUS can be used particular in the following:

- Riser static and dynamic analysis including Abaqus/Aqua (Korth, Chou, and McCullough, 2002; Song, Mekha, and Sebastian, 2006; Khan and Ahmad, 2007a, 2007b);
- Nonlinear material behaviour (metal plasticity and hyperelasticity);
- Pipe-soil interaction (Langner, 2003; Bridge and Laver, 2004; Hesar, 2004; Cheng, Song, Mekha, Torstrick, and Liu, 2007);
- Buckling including lateral buckling of seabed pipe line (Bjørset, Remseth, Leira, and Larsen, 2003; Torselletti, Vitali, and Bruschi, 2005);
- Crack propagation analysis (Pasqualino, Valeriano, and Alves, 2002; Chandwani, Timbrell, and Wiehahn, 2005; IIJIMA, 2005);
- Highly nonlinear geometry with contact including pipe reeling (Netto, Lourenço, and Botto, 2007);
- Nonlinear dynamics with Abaqus/Explicit (Sen and Hesar, 2007).

ANSYS (www.ansys.com) is also a general-purpose FE computer program for engineering analysis and used for the design and analysis of offshore structures. But

ANSYS is not used so often as ABAQUS for riser analysis (Campos and Martins, 2001; Bridge and Laver, 2004; Sánchez and Salas, 2005).

ANFLEX, Flexcom (www.mcs.com), DeepLines (www.principia.fr), OrcaFlex (www.orcina.com), and Riflex (www.sintef.no) are 3D nonlinear dynamic riser specific FEM programs.

For ANFLEX (1999) is a Petrobras's in-house computer codes developed and implemented as part of projects from CENPES with "COPPE/UFRJ" – The Engineering Post-Graduating Coordination of the Federal University of Rio de Janeiro", it's only limitedly used inside Petrobras and Federal University of Rio de Janeiro (Torres, Mourelle, and Silva, 2001; Morais and Jacob, 2002; Senra, Jacob, Torres, and Mourelle, 2002; Torres et al., 2002; Vieira, Jacob, Fernandes, and Franciss, 2002; Siqueira, Sousa, and Mourelle, 2003; Torres et al., 2003; Dantas et al., 2004; Franciss and Riberiro, 2004; Dantas et al., 2005; Gonzalez, Mourelle, Mauricio, Lima, Moreira, 2005; Andrade, Siqueira, Mourelle, and Caldwell, 2007).

The Institut Français du Pétrole (IFP, French Institute of Oil) software package DeepLines has been marketed in the offshore structure behaviour since 1998. Although it is particularly suited to projects involving great water depths and has the advantage of being able to model all the types of connections used in offshore oil and gas development systems, it doesn't seem to be popular for riser analysis (Averbuch, Cunff, Costa, and Biolley, 2003).

Unlike ANFLEX and DeepLines, Flexcom and OrcaFlex enjoy a wide usage for analysing riser systems which can be found in piles of literature:

- Flexcom: Sertã, Mourelle, Grealish, Harbert, and Souza (1996); Connaire, Kavanagh, Ahilan, and Goodwin (1999); Mekha, Mirza, and Lang (2000); Willis (2000); Sele, Dretvik, Nygård, and Støme (2001); Willis (2001); Willis and West (2001); Willis (2002); Sele, Dretvik, Nygård, and Støme (2001); Brinkmann, and Whooley (2002); Thompson, Grealish, Young, and Wang

(2002); Hogg, Harte, and Grealish (2003); Langner (2003); Bai, Tang, O'Sullivan, Uppu, and Ramakrishnan (2004); Mansour (2004); Chai, and Varyani (2005); Sheehan, Grealish, Smith, and Harte (2005); Arnesen, Dalane, Aramanadka, Herfjord, Snell, and Stansberg, (2006); Song, Mekha, and Sebastian (2006); Xu, Jesudasen, Fang, and Else (2006); Grealish, Kavanagh, Connaire, and Batty (2007); Vandenbossche et al. (2007); Amicis, Mahoney, Grealish, and Connaire (2008).

- OrcaFlex: Borgen (2002); Petruska, Zimmermann, Krafft, Thurmond, and Duggal (2002); Borgen, Fosterud, and Larsen (2003); Ong and Pellegrino (2003); Pesce et al. (2003a); Simos, Fujarra, and Alves (2003); Cunliffe, Baxter, McCarthy, and Trim (2004); Silveira and Martins (2004); Low and Langley (2006); Sen (2006); Quintin, Legras, Huang, and Wu (2007); Sen and Hesar (2007); Zimmermann, Petruska, and Duggal (2007).

Riflex is developed and maintained by MARINTEK, and marketing and sale is handled by DNV Software (www.dnv.com/software). It doesn't have graphical user interface (GUI) which limited its usage. But after being integrated with DeepC (DNV Software, www.dnv.com/software) as its pre-processing and post-processing tool, it has become more popular for riser analysis (Willis, 2000; Patel, Kumar, Master, and Karunakaran, 2001; Bjørset, Remseth, Leira, and Larsen, 2003; Bhat, Dutta, Wu, and Sarkar, 2004; Giertsen, Verley, and Schrøder, 2004; Mungall et al., 2004; Karunakaran, Meling, Kristoffersen, and Lund, 2005; Arnesen et al., 2006; Karunakaran and Meling, 2006; Larsen and Passano, 2006; Passano and Larsen, 2006 and 2007; Aggarwal et al., 2007; Rustad, Larsen, and Sørensen, 2007; Chatjigeorgiou, 2008).

Because Freecom is only a FD program for riser analysis, it's not used so frequently as other TD programs. Few applications can be found by Hogg, Harte, and Grealish (2003) and Sheehan, Grealish, Smith, and Harte (2005).

## 2.7 SCR Reliability-Based Fatigue Analysis Methods

Structural reliability methods have been the subject of considerable interest in recent years with the adoption of risk-based approaches to the safety management of engineering structures in various industrial sectors, including offshore installations.

Probabilistic structural integrity assessment methods provide an alternative approach to deterministic methods which, in some circumstances, can also lead to unduly conservative predictions of structural integrity. This is particularly apparent in the application of deterministic S-N fatigue and fracture mechanics assessment procedures to the assessment of welded joints in offshore installations as these require the use of data which are often subject to considerable uncertainty, necessitating the use of conservative estimates of parameter values to ensure safety.

The recognition of this by the offshore and other industries has led to considerable effort being expended over the years on the development of procedures for probabilistic structural integrity assessment (Wirsching and Chen, 1988; Kung and Wirsching, 1992; Siddiqui and Ahmad, 2001; Shabakhty, Gelder, and Boonstra, 2002; Zhao, Stacey, and Prakash, 2002; Bjørset, Leira, and Remseth, 2004; Ku et al., 2004; Moan, Ayala-Uraga, and Wang, 2004; Madhavan and Veena, 2006; Ayala-Uraga and Moan, 2007). But still only a few have been done for riser analysis (Sen, 2006; Akpan, Koko, Rushton, Tavassoli, and Else, 2007; Khan and Ahmad, 2007a and 2007b; Nazir, Khan, and Amyotte, 2008).

## 2.8 Reviewing the Available General-Purpose Reliability Analysis Software

Over the past two decades, various software packages featuring stochastic methods have been developed and applied to numerous problems of academic and engineering interest. Table 2.8.1 lists the software packages.

**Table 2.8.1** General-Purpose Reliability Software Packages (Pellissetti and Schuëller, 2006).

| Software Package | Algorithms | | | |
|---|---|---|---|---|
| | FORM/SORM | MCS | Adv. MCS | Response Surface |
| ANSYS PDS & Design Xplorer (Reh, Beley, Mukherjee, and Khor, 2006) | | √ | | √ |
| CAIREL (Liu, Lin, and Kiureghian, 1989) | √ | √ | √ | |
| COSSAN (Schuëller, and Pradlwarter, 2005) | | √ | √ | |
| NESSUS (Riha, Thacker, Millwater, Wu, and Enright, 2000) | √ | √ | √ | √ |
| OpenSees (Mazzoni, McKenna, Scott, and Fenves, 2006) | √ | √ | √ | |
| PERMAS-RA/STRUREL (Gollwitzer, Kirchgässner, Fischer, and Rackwitz, 2006) | √ | √ | √ | √ |
| PHIMECA (Lemaire, and Pendola, 2006) | √ | √ | √ | |
| Proban (Tvedt, 2006) | √ | √ | √ | √ |
| ProFES (Wu, Shin, Sues, and Cesare, 2006) | √ | √ | √ | √ |
| UNIPASS (Lin, and Khalessi, 2006) | √ | √ | √ | √ |

CALREL (CAL-RELiability) was initially developed by Liu, Lin, and Kiureghian (1989) as a general-purpose structural reliability FORTRAN code designed to compute probability integrals. Over the years, the code has evolved into a powerful tool for structural reliability analysis with a large collection of alternative analysis methods and computational algorithms (Kiureghian, Haukaas, and Fujimura, 2006). It incorporates four general techniques for computing the probability of failure: (1)

FORM, (2) SORM, (3) Monte Carlo simulation, and (4) directional simulation with exact or approximate surfaces.

## 2.9 Critical Views on the Current Status of SCR Design Application and Analysis Methods

The concept of the SCR is now well established in the industry. The technology has advanced through numerous studies and joint industry projects (JIPs). However, the resulting deepwater developments are constantly pushing SCR technology to its limit. For relatively harsher and deeper water environments and larger motion host platforms, such as semi-submersibles and FPSOs, the conventional SCRs might not meet the design codes requirements.

The number one challenge of deepwater SCR design is still fatigue. Comprehensive summarisation on traditional SCR fatigue design mitigations can be found in reviews by Yao and Sun (2006) and Song and Stanton (2007). One new concept of SCR fatigue mitigation which was not included is weight-optimised coating, first suggested and accepted as lightweight coating on TDZ (Karunakaran, Dutta, Clausen, and Lund, 2002; Aggarwal et al., 2005; Arnesen et al., 2006) and later developed as weight-optimised coating on SCRs connected to a semi-submersible by a cooperation project of Subsea 7 and Statoil (Karunakaran, Meling, Kristoffersen, and Lund, 2005; Karunakaran, 2006; Karunakaran and Meling, 2006) which was also tried on SCRs connected to an FPSO (Foyt, Griffin, Campbell, Wang, and Kan, 2007).

The concept of weight-optimised coating is newly built and hence its application is yet limited. Whether it is an effective way to reduce SCR fatigue? How to apply the concept for practical use efficiently? Whether it can be put into wider use or not? Answers are needed.

## 2.10 Areas Requiring Research Attention

A number of problems related to deepwater SCR which deserve attention can be outlined as follows:

- Deepwater SCR design challenges: strength and fatigue response at TDZ and its mitigation methods

As water depth increases, riser systems play bigger and bigger role as part of the offshore infrastructure. Although SCRs have been enjoying a widespread acceptability for deepwater oil and gas production in recent years, to make sure the feasibility of SCRs outside the limits of what has been done to-date is always challenging. SCR feasibility is controlled by strength and fatigue response in the TDZ. The pragmatic ways to enhance strength and fatigue performance of SCRs seem more important than ever. More research into the feasibility of the new concept of weight-optimised coating as a strength and fatigue response mitigation method for SCRs is needed.

- To propose a generalised guidance for the applications of weight-optimised SCRs

Previous industry work and studies on weight-optimised SCRs applied for a deepwater semi-submersible (Karunakaran and Meling, 2006) and an FPSO (Foyt, Griffin, Campbell, Wang, and Kan, 2007) showed that SCR strength and fatigue response could be improved by using weight-optimised coating. But there have not been given any clear answers about how to place strategically the coatings with various densities along the riser, how much effect it can have on the global strength and fatigue response, and how this mitigation method can work under different deep water depths. Therefore, a generalised guidance for applying the weight-optimised coating approach for deepwater SCRs is needed to assist riser engineer to improve SCR performance in harsh deepwater environment.

- SCR reliability-based fatigue analysis method for optimising weight of protective coating

Fatigue life prediction in SCRs is a complicated process involving many factors and has been discussed at length by Campbell (1999). The irregular nature of the sea, evaluation of stress concentration factors in welded joints and possible dynamic effects, etc. contribute to the complexity of the fatigue life assessment. Due to the inherent random nature of various input parameters affecting the response of the risers, reliability analysis assumes greater importance in the design of SCRs. Computation of fatigue reliability is also useful for planning in-service in-spection of SCRs and for checking the design and certification. However, existing approaches for SCR design and analysis are typically based on deterministic methods. In order to account for uncertainties associated with the deterministic fatigue predictions, a suitable probabilistic reliability framework for the weight-optimised SCR is required for investigation.

Chapter 3

# Deepwater SCR Strength Design and Analysis with Conventional Coating

## 3.1 Introduction

In this chapter, an attempt would be made to examine whether a conventional SCR with normal coating would be feasible for the semi-submersible application in a deepwater and harsh environment, such as Northern North Sea (NNS).

To devise an acceptable design of SCRs for production and export of oil and gas, it is essential to ensure that the risers can have adequate strength for use in severe conditions and also meet the required fatigue life target which is an iterative process.

Riser configurations are typically developed in two phases: Firstly, extreme load analysis is done for giving a basic configuration which has satisfactory maximum stress levels. Secondly, a fatigue analysis would follow which may require minor modifications to the basic configuration and determines the quality of details needed to meet design life requirements.

Uncoupled, dynamic and fatigue analyses were conducted with DNV DeepC & Riflex program. The software is applicable for both the preliminary static analysis to determine general configuration as well as for the full dynamic response analysis.

The uncoupled analysis consists of two phases. The ship motion is first computed based on a simplified response of the mooring lines. In the second step, the motion given by the RAO is imposed as top end excitations to study the dynamics of the risers and mooring lines.

At this stage of design, sensitivity analyses to optimise SCR configuration, including departure angle, diameter, wall thickness, and length, should be performed.

## 3.2 Strength Design Criteria

The riser design criteria are defined in the regulations and in practice must comply with the API (API RP 2RD, 1999) and DNV (DNV-OS-F201, 2001) regulations. This in turn implies that the following requirements should be met:

a) The developed configurations should satisfy the criteria of ultimate limit state (ULS), accidental limit state (ALS) and fatigue limit state (FLS);

b) The extreme stresses should be checked by the working stress method;

c) The design lifetime shall be obtained using a safety factor of 10 on the calculated fatigue lives. The minimum fatigue life required for the risers is 20 years.

These requirements would now be briefly considered.

### 3.2.1 Limit State Control

According to DNV and Norwegian rules and regulations, see e.g. DNV-OS-F201 (2001), Norsok Standard N-001 (2004) and N-003 (2007), an offshore structure is to be controlled against overload failures at two levels: ULS control and ALS control.

The extreme response is checked by the extreme load conditions. Riser strength was assessed in terms of maximum stresses which need to be kept below the allowable limits as per the codes. For example, the maximum von Mises stress, $\sigma_{VM}$, along the riser must satisfy the requirements of the following relationship (API RP 2RD, 1999):

$$\sigma_{VM} \leq C_f \sigma_A \tag{3.2.1}$$

where

$\sigma_A$ $C_a\sigma_y$ = basic allowable combined stress

$C_a$ $\frac{2}{3}$ = allowable stress factor

$\sigma_y$ specified minimum yield strength (SMYS)

$C_f$ design case factor as given in Table 3.2.1

$\sigma_{VM}$ maximum von Mises stress in the pipe

**Table 3.2.1** Design Case Factors and Allowable Stress (API-RP-2RD, 1999; DNV-OS-F201, 2001).

| Limit State Category | $C_f$ | Allowable Stress |
|---|---|---|
| ULS | 1.2 | $0.8\sigma_y$ |
| ALS | 1.5 | $1.0\sigma_y$ |

### 3.2.2 *Extreme Load Response and Limit State Control Design*

Critical loading occurs when the waves and current lie in the same plane as the catenary. The most common positions for the floating support structure include:

- Zero mean offset position: The floating structure is in its initial position without displacement in any direction.
- Near offset position: The platform is displaced in the plane of the SCR moving away from the SCR TDA causing the departure angle to increase with a shorter section of the SCR lying on the seabed.
- Far offset position: The platform is displaced in the plane of the SCR moving towards the SCR TDA causing the departure angle to decrease with a longer section of the SCR lying on the seabed.
- Cross offset position: The platform is displaced out of the plane of the SCR with the platform in the in-plane zero mean offset position.

The schematic of a typical SCR is shown in Figure 3.2.1.

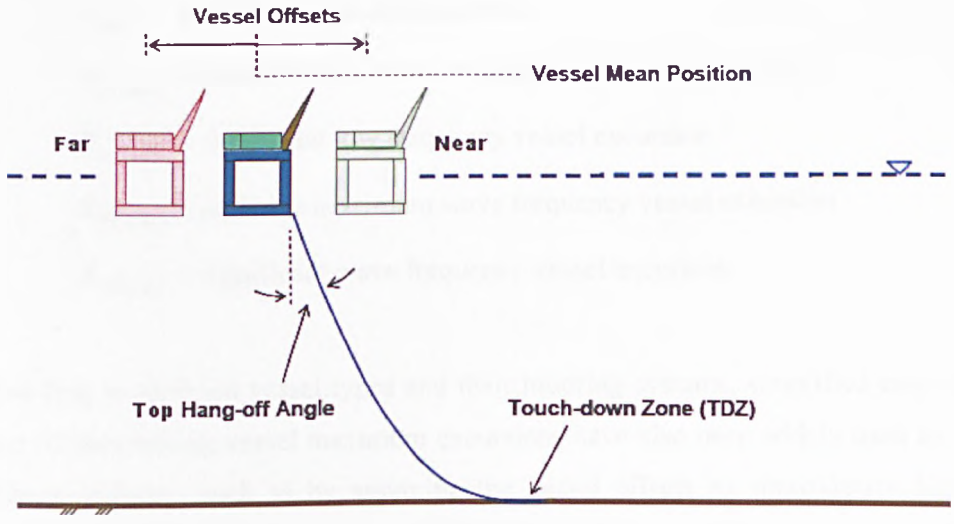


**Figure 3.2.1** Typical SCR Profile and Nomenclature.

Vessel extreme excursions can be calculated by a balance of mean wave drift, current and wind induced static forces. The low frequency response of the moored vessel can be derived from the time domain integration of governing second order response equations. The wave frequency response can be derived using appropriate RAOs combined with wave elevation. The maximum excursion can be taken as the mean offset plus the combined wave frequency and low frequency vessel motions (Hogg, Harte, and Grealish 2003):

$$X_{\max} = X_{mean} + X_{LF(\max)} + X_{WF(sig)} \qquad (3.2.2)$$

$$\text{if } X_{LF(\max)} > X_{WF(\max)}$$

$$X_{\max} = X_{mean} + X_{WF(\max)} + X_{LF(sig)} \qquad (3.2.3)$$

$$\text{if } X_{WF(\max)} > X_{LF(\max)}$$

where

$X_{mean}$ = mean vessel excursion

$X_{\max}$ = maximum vessel excursion

$X_{LF(\max)}$ = probable maximum low frequency vessel excursion

$X_{LF(sig)}$ = significant low frequency vessel excursion

$X_{WF(\max)}$ = probable maximum wave frequency vessel excursion

$X_{WF(sig)}$ = significant wave frequency vessel excursion

According to different vessel types and their mooring systems, simplified empirical ways of determining vessel maximum excursions have also been widely used by the offshore industry, such as by assuming the vessel offsets as approximate double amplitude (Zimmermann, Petruska, and Duggal, 2002) or proportions of water depth (Karunakaran and Meling, 2006).

The strength requirements under specific loads (API RP 2RD, 1999) and their corresponding vessel offsets applied in the current study referred to Karunakaran and Meling (2006) are given respectively as follows:

- ULS condition – Intact mooring — 10% water depth
  $\sigma_{VM} \leq 0.8\sigma_y$
- ALS condition – One mooring line failure — 12% water depth
  $\sigma_{VM} \leq 1.0\sigma_y$

The riser configuration is developed by satisfying the ULS and ALS design conditions. The basic configurations are obtained by performing nonlinear dynamic response analysis using a time domain analysis package DNV DeepC & Riflex. Dynamic strength is analysed for the SCR in near and far positions. The semi-submersible motions caused by wave are applied at the vessel centre of gravity. The associated current profile is conservatively assumed to be in the motion direction for each load case.

## 3.3 SCR Nonlinear Analysis Procedure

SCR nonlinear analysis includes the follows:

a) **Nonlinear static analysis** under static load components: should take into account dead weight, current and static offset of the platform applied to the top of the riser. During a number of static load steps it shall end up with the line ends in specific static position of support points.

b) **Nonlinear time-domain dynamic analysis**: This analysis starts with the static equilibrium positions and performs a time domain simulation of the system exposed to all types of loads.

Highlights of these two steps will now be summarised.

### *3.3.1 Nonlinear Static Analysis*

An initial static analysis is performed to determine the neutral riser configuration for a specified set of conditions. The static analysis is based on a complete nonlinear formulation. The computations include:

- Establishment of initial configurations based on catenary approximation which starts with the stress free configuration of the line.

- Iteration for equilibrium position by incremental reduction of unbalanced forces (Newton-Raphson iteration procedure) by application of nonlinear FEA. During a number of static load steps it ends up with the line ends in specified static position of support points.

### *3.3.2 Nonlinear Time-Domain Dynamic Analysis*

Following from static configuration obtained by static analysis, all the nonlinear dynamic response analyses were conducted in the full TD approach by DNV DeepC & RIFLEX. Vessel motion was applied at the Centre of Gravity (CoG) of the semi-submersible platform via RAOs.

Typical numerical integration methods include the finite-difference, Houbolt, Wilson-θ and Newmark-β methods. A large majority of solutions used in offshore applications utilise the Newmark-β method to integrate the governing equations in time. The popularity of this method arises from its unconditional stability, zero period elongation, low amplitude decay, good accuracy and ease of implementation (Bathe, 1982). Newmark-β family with constant average acceleration method is used here for step by step numerical integration of the dynamic equilibrium equations. $\gamma_N$, $\beta_N$ and $\theta_N$ are parameters in the integration methods defining the functional change in displacement, velocity and acceleration vectors over time step $\Delta t$. Values of $\gamma_N$, $\beta_N$ and $\theta_N$ are as follows:

$\gamma_N$ = 1/2 (no artificial damping)

$\beta_N$ = 1/4

$\theta_N$ = 1

The strength analysis is performed based on a 3-hour 100 year extreme wave condition. Extreme strength response is considered to be acceptable if, along the entire riser at zero mean offset position, the maximum von Mises stress does not exceed 80% of the yield stress. It is also desirable to maintain positive effective tension in SCR at all load cases.

## 3.4 SCR Design Conditions

In this project, an SCR for oil export connected to a semi-submersible in deepwater area of NNS is taken as the study case. The basic design parameters for the SCR study case is primarily based on the working condition in the previous studies by Karunakaran et al. (2005, 2006).

Environment Conditions

For design purposes, the most popular assumption is to estimate the 100-year response by exposing the structure to the simultaneous action of 100-year wind, 100-year wave and 10-year current. The riser is designed for the 100-year wave condition in combination with 10-year current profile. The water depth at this location is selected to be 1000 m. The wave data are for a typical NNS location. The extreme sea state is modelled by irregular waves. The 100-year sea state is:

- Significant wave height $H_s$ 15.5 m
- Corresponding wave peak period $T_p$ 16 s

The corresponding 10-year current are:

- At surface 0.93 m/s
- -50 m 0.68 m/s
- -300 m 0.47 m/s
- -1000 m 0.00 m/s

The combination of these sea states is severe and represents much of the typical harsh environment worldwide. The most critical loading conditions generally occur when wave action is in the plane of the catenary.

Hydrodynamic Coefficients

Wave and current action produce hydrodynamic loads on the riser. The current velocity usually varies with depth and can also vary in direction. A number of wave theories are available to model the water particle velocity and acceleration in waves such as Airy wave theory (Airy, 1841).

Morrison's equation (O'Brien and Morison, 1952) provides a means of converting information on water particle velocity and acceleration into hydrodynamic loads on the structure. When the structure is moving Morison's equation can be written as (Barltrop and Adams, 1991):

$$F = \frac{1}{2} C_d \rho d U_r |U_r| + C_m \rho A \dot{U}_w - C_{am} \rho A \dot{U}_s \tag{3.4.1}$$

or

$$F = \frac{1}{2} C_d \rho d U_r |U_r| + \rho A \dot{U}_w + C_{am} \rho A \dot{U}_r \tag{3.4.2}$$

where

$F$ force per unit length

$C_d$ drag coefficient

$C_m$ inertia coefficient ($C_m = 1 + C_a$)

$C_{am}$ added mass coefficient

$\rho$ water density

$d$ cylinder diameter

$A$ cross-sectional area

$U_r$ relative velocity of water to structure

$\dot{U}_w$ acceleration of water

$\dot{U}_s$ acceleration of structure

$\dot{U}_r$ acceleration of water relative to the structure

The equation is implemented (in a modified form) along with wave theories in computer programs which allow the automatic calculation of the resolved relative velocities and riser and water particle accelerations.

Values of $C_d$ and $C_m$ depend on the shape and surface roughness of the riser. Typical values of $C_d$ and $C_m$ for SCRs are as follows:

- Drag coefficient $C_d$ 1.0
- Inertia coefficient $C_m$ 2.0

Riser Material Selection

Current material technology for SCR application includes carbon steel pipe, clad pipe, steel forgings, titanium for stress joints, and flex joints. In systems where corrosion resistance is not required, carbon steel linepipe is the less expensive and most common used material for SCR even though their properties could vary. Normally, API X52 through X70, with yield strength from 52 ksi (359 MPa) to 70 ksi (483 MPa) (API Spec 5L, 2000), line pipe has been widely used for SCR pipe.

As fatigue will be the most challenging design criteria, internal corrosion allowance with possibility of fatigue initiation from bottom of local corrosion attacks mainly due to $CO_2$ and potential $H_2S$ in the production dream will drastically reduce the fatigue resistance. Hence solid corrosion resistant alloy (CRA) will be utilised to obtain satisfactory fatigue life. For some SCRs on recent deepwater projects clad pipe and duplex / super duplex material have been specified, and this has required the development of new welding and non-destructive tests (NDT) procedures, which can sometimes prove difficult to control under offshore conditions. The super duplex material is NACE and NORSOK approved. "Super" duplex grades have enhanced pitting and crevice corrosion resistance compared with the ordinary austenitic or duplex types. Super duplex stainless steels have excellent corrosion resistance, increased resistance to chloride attack, good resistance to stress corrosion cracking, tensile and yield strength higher than conventional austenitic or ferritic grades of stainless steel, good weldability and good formability. Stainless steel super-duplex grade F55 can be used for pipes for the oil and gas industries and offshore technology.

- Production SCR ASTM A182 Grade F55
- SMYS 550 MPa

Note that although super-duplex stainless steel can provide high strength and good corrosion resistance, it is expensive. Therefore, it will be neither a first nor an economical choice for deepwater SCR unless necessary.

Riser Coating

For preliminary design, the whole riser was wrapped with normal coating.

- Normal coating (N) density = 800 kg/m$^3$ (normally 750 ~ 950 kg/m$^3$)
- Coating thickness 75 mm (0.075m)

Internal Fluid

- Oil density = 800 kg/m$^3$

Upper End Termination (Hang off System)

To terminate an SCR at a floater, a hang-off system is required. In general, three types of hang off systems have been used. They are flex joint, taper stress joint (TSJ), and pull tube as shown in Figure 3.4.1 below. Of these, the flex joint option is the most common and has been assumed throughout all of the analysis cases in this study.

**Figure 3.4.1** Typical SCR Hang off Systems.

The selection of a hang-off system depends upon its functional requirements in terms of required angular deflection, SCR size and expected top tension. Different hang-off systems provide different tie-back design flexibility. The pros and cons and limitations of various hang-off systems are presented in Table 3.4.1.

Bending of steel catenaries near the water surface, as a result of wave action, can be both relieved and compounded by vessel motion. Differences between vessel and riser response can lead to high bending moments at the vessel attachment point.

These may be accommodated by use of taper stress joints or flex-joints, typically found at the base of vertical rigid risers. To avoid excessive loading on the platform, flex joints form the preferable solution and can better accommodate variations in riser performance characteristics.

Therefore, the top end of the riser was assumed to be equipped with a flex joint attached to the riser termination point. In the global analysis, the top end was simplified as pinned; in other words it was free to rotate (Karunakaran, Meling, Kristoffersen, and Lund, 2005; Passano and Larsen, 2006).

**Table 3.4.1** Various Hang-off Systems.

| Hang-off System | Pros | Cons | Limitations |
|---|---|---|---|
| Flex Joint | Decoupling the riser from the platform pitch and roll motions → reducing the stresses in the upper region of the riser and supporting porch structure; better accommodating variations in riser performance characteristics; a reliable technical solution particularly for fatigue design | A relatively sophisticated component | Appropriate inspection procedures needed under high temperature and pressure fluctuation environment |
| TSJ | A one-piece metallic component without any moving parts → less complicated than a flex joint | As the riser size increases or the platform pitch and roll motions become more severe, the tapered stress joint design becomes more challenging | Suitable in cases where the relative rotation between the platform and the riser is not excessive |
| Pull Tube | Avoiding the use of any subsea mechanical connections on the riser → simple and economical | Little room for flexibility; potential for wear between the riser and the end of the pull tube → good inspection procedures required | With larger diameter risers, there is increasing risk of the riser getting stuck in the pull tube due to the high bending stiffness |

Vessel Motion

Floating vessels experience first-order short period motions in response to wave action. This first-order short-period motion is important for SCR dynamic analysis and can be defined using Response Amplitude Operators (RAOs). The RAO values define the amplitude and phase of the vessel motion relative to the wave for a particular wave frequency. RAO data usually takes the form of sets of twelve values for each wave frequency of interest. These twelve values are the amplitude and phase for heave, surge, sway, yaw, roll, and pitch. DNV Riflex calculates vessel motion using wave and RAO data and applies the relevant motion to the riser by means of special boundary conditions. Short-period motion of fixed is negligible compared to riser motion and deflection. Other motions occur slowly and can be modelled by applying an offset to the vessel.

The RAOs of a semi-submersible in harsh environment from a former project of Subsea 7 was used in the study.

Soil-Riser Interaction

When the riser is subjected to oscillatory motion, there is a complex interaction between riser movement and the seabed at TDP. This forces the riser into the soil and thereby increases the soil resistance. The common practice is to model the soil riser interaction by linear soil stiffness and friction.

The representative parameters used in the global analysis are as follows:

- Transverse friction stiffness 0.5
- Transverse soil stiffness 10 kPa
- Normal soil stiffness 600 kPa

## 3.5 Structural Modelling and Parametric Design

The key parameters for a typical SCR structural modelling are given as follows:

- Dynamic simulation time duration 3600 s (1 hour)
- Nonlinear time domain simulation time step 0.1 s
- Time step of wave motion time series 1 s
- Mass damping coefficient $a_1$ 0.0
- Stiffness damping coefficient $a_2$ 0.015

All the study cases are carried out with a same random model.

### *3.5.1 Sensitivity to Analysis Parameters*

The TD approach is computationally intensive. Three major factors will influence the simulation's convergence, accuracy, speed and efficiency dependent on different study models. Other analysis parameters can be chosen as the default values set up by the program. Accordingly, a sensitivity study is performed for the following parameters:

- Time interval
- Structural damping
- Mesh length

For each study case, all the parameter values are fixed except the value of the specific parameter which is under investigation, as shown in Table 3.5.1.

**Table 3.5.1** Analysis Parameters for Sensitivity Study.

| Parameter \ Study Case | | a | b | c | d |
|---|---|---|---|---|---|
| Dynamic Simulation Duration (h) | | 1, 3 | 1 | | |
| Structural Damping | Mass Damping Coefficient $a_1$ | 0.0 | | | |
| | Stiffness Damping Coefficient $a_1$ | 0.15 | 0.0, 0.01, 0.015, 0.03, 0.5, 1.0 | 0.15 | |
| Mesh Length (m) | | 4 | | 3, 4, 5, 6, 8 | 4 |
| Dynamic Simulation Time Step (s) | | 0.1 | | | 0.02, 0.05, 0.1, 0.2, 0.5 |

**a) Sensitivity to Dynamic Simulation Duration**

Normally a 3 h simulation will give a proper convergence for a riser dynamic analysis. However, longer simulation time means not only higher central processing unit (CPU) consumption and also bigger hard disk occupation, especially for a large amount of parametric study cases. An SCR study case with two different simulation durations is compared (Table 3.5.2) on the computer with following properties:

- CPU — Intel Core 2 Duo, Processor T5500, 1.66 GHz
- Memory — 1 GB
- Operating System — Microsoft Windows XP

SCR Base Case

- Internal diameter (ID) — 0.254 m (10 in)
- Wall thickness (WT) — 0.03 m
- Top hang-off angle — 10 deg
- Riser length — 3000 m
- Mesh length — 4 m
- Vessel offset — 0 m, mean position

- *Dynamic simulation duration* *1, 3 h*

Sensitivity of maximum dynamic von Mises stress envelopes to dynamic simulation durations 1 and 3 h are shown in Figure 3.5.1, among which the maximum values are compared in Table 3.5.2.

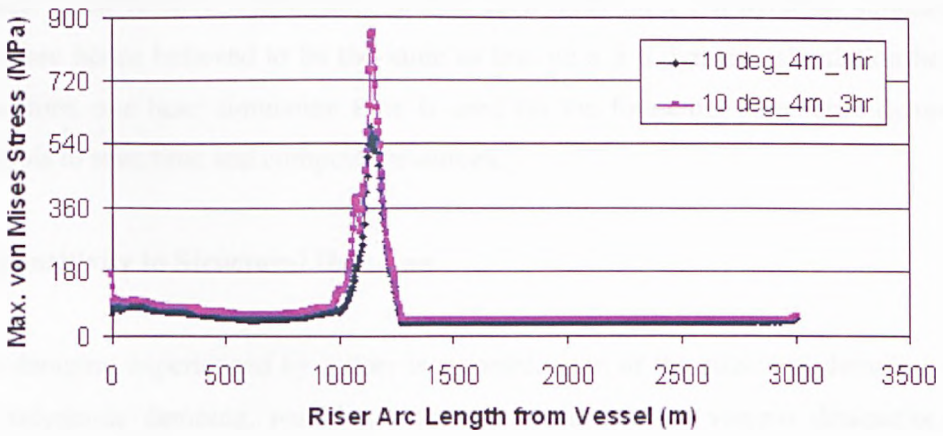


**Figure 3.5.1** Sensitivity of Maximum Dynamic von Mises Stress Envelope to Simulation Time Durations 1 and 3 h.

**Table 3.5.2** Sensitivity to Different Dynamic Simulation Durations.

| Dynamic Analysis Parameter | Dynamic Simulation Time (h) | |
|---|---|---|
| | 3 | 1 |
| Maximum Dynamic von Mises Stress (MPa) | 853.40 | 588.70 (–34.5%) |
| Maximum Dynamic von Mises Stress Point Position along Riser Arc Length from Vessel (m) | 1144.206 | 1136.206 (–2.7%) |
| CPU Calculation Time (min) | 202 | 44 (–78.2%) |
| Dynamic Result File Size (GB) | 4.27 | 1.42 (–66.7%) |

The maximum dynamic von Mises stress of 1 h simulation time was much lower than the 3 h simulation case (34.5% less). But the overall stress range trends were

similar for both cases except the short length of 40 m with peak stress levels (see Figure 3.5.1). The position of the maximum dynamic von Mises stress point of 1 h simulation case was closer to the vessel by 8 m (2.7% of the whole riser length) than that of the 3 h simulation case.

For parametric dynamic studies, the cases are compared by their peak dynamic stress values. Their relative relationships among each other on a 1 h dynamic simulation basis are hence believed to be the same as that on a 3 h dynamic simulation basis. Therefore, one hour simulation time is used for the following parametric dynamic analysis to save time and computer resources.

**b) Sensitivity to Structural Damping**

The damping experienced by a riser is a combination of the structural damping and hydrodynamic damping, resulting from both radiation and viscous dissipation of energy (Faltinsen, 1990; Mekha, Johnson, and Roesset, 1996). The structural damping is due to the strain and elasticity properties of steel.

The global Rayleigh damping model is established as a linear combination of the global tangential mass- and stiffness matrices (DNV Software, 2005):

$$C_R = a_1 M + a_2 Q \tag{3.5.1}$$

where

| | |
|---|---|
| $M, Q$ | tangential mass and stiffness matrix respectively and evaluated at the static equilibrium |
| $a_1, a_2$ | mass and stiffness proportional damping coefficient respectively |

The structural matrix of the global Rayleigh damping is given by equation 3.5.1 and is orthogonal with respect to the eigenvectors.

$$\zeta_i = \frac{1}{2}\left[\frac{a_1}{\omega_i} + a_2\omega_i\right] \tag{3.5.2}$$

where $\omega_i$ is the eigenfrequency. When the global Rayleigh damping model is used for compliant structures undergoing large rigid body displacements, the mass proportional damping is usually omitted to avoid non-physical structural damping due to rigid body motions (i.e. $a_1 = 0$) (Bech and Skallerud, 1992). Therefore, the damping matrix for an SCR based on proportional Rayleigh damping is assumed proportional to the global stiffness matrix

$$C_R = a_2 Q \tag{3.5.3}$$

The stiffness proportional damping, $a_2 Q$, will lead to a modal damping ratio,

$$\zeta_i = \frac{1}{2}a_2\omega_i = \frac{1}{2}a_2 \cdot \frac{2\pi}{T_i} = \frac{a_2\pi}{T_i} \tag{3.5.4}$$

where $T_i$ is wave period in second. In the wave zone, maximum loading occurs when vessel motions are small, which for semi-submersible platforms occurs with wave periods of approximately 10 seconds. Therefore, $T_i$ is normally set as 10 s. Accordingly, the structural damping will be 15.7% at the eigenperiod of $T$ = 10 s for $a_2$ = 0.5, which is unrealistic high. In practical application, $a_2$ is selected to give realistic energy dissipation at the peak period of loading. Therefore, the magnitude of the stiffness damping is dependent on the value of $a_2$ and also the wave frequency or period.

The effect of structural damping was investigated by using different $a_2$ values, see Table 3.5.3 and Figure 3.5.2 and 3.5.3.

SCR Base Case

- ID 0.254 m (10 in)
- WT 0.03 m
- Top hang-off angle 10 deg
- Riser length 3000 m
- Mesh length 4 m
- Vessel offset 0 m, mean position
- Dynamic simulation time 1 hour
- *Stiffness damping coefficient* $a_2$ *0.0, 0.001, 0.015, 0.03, 0.5, and 1.0*

**Table 3.5.3** Sensitivity of Maximum von Mises Stress to Different $a_2$ Values.

| $a_2$ | Structural Damping (%) | Dynamic (MPa) |
|---|---|---|
| 0.0 | 0 | 596.3 |
| 0.001 | 0.3 | 591.7 |
| 0.015 | 0.5 | 588.7 |
| 0.03 | 0.9 | 581.0 |
| 0.5 | 15.7 | 382.1 |
| 1.0 | 31.4 | 299.7 |

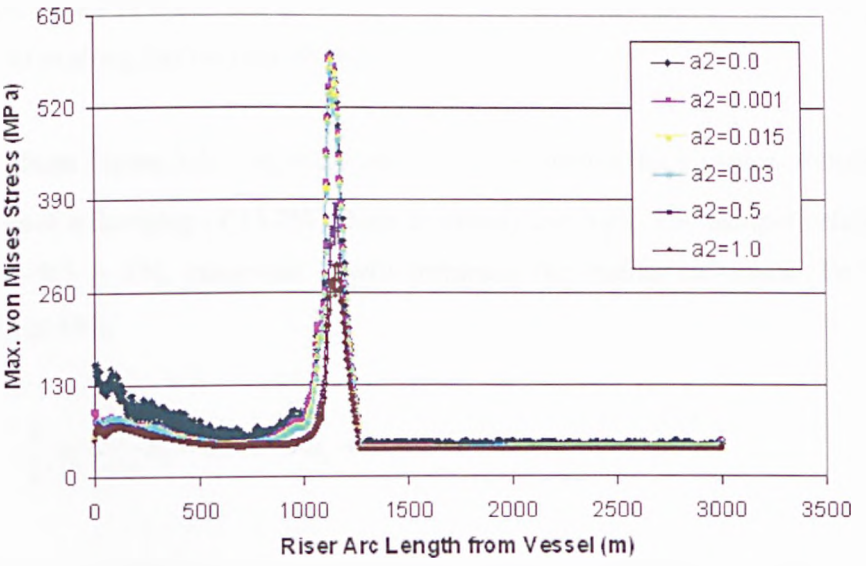


**Figure 3.5.2** Sensitivity of Maximum Dynamic von Mises Stress Envelope to Stiffness Damping Coefficients $a_2$ 0.0, 0.001, 0.015, 0.03, 0.5, and 1.0.

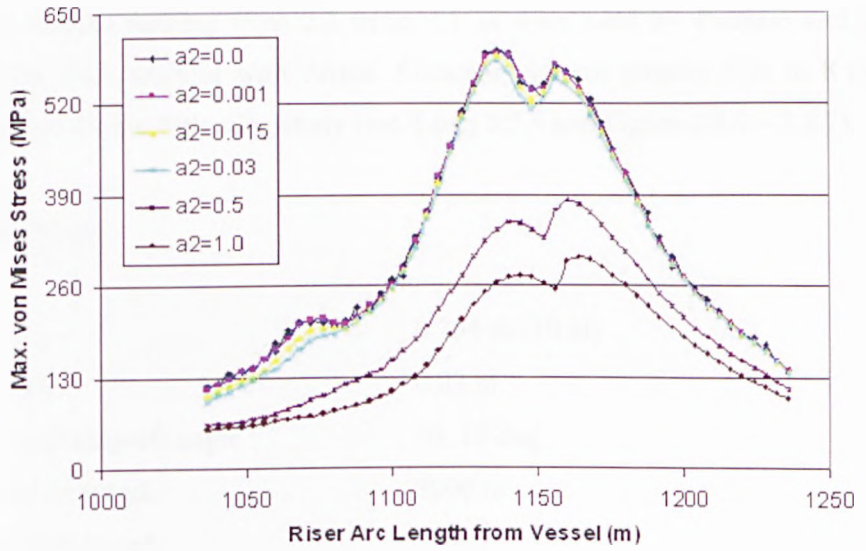


**Figure 3.5.3** Sensitivity of Peak Value of Maximum Dynamic von Mises Stress Envelope to Stiffness Damping Coefficients $a_2$ 0.0, 0.001, 0.015, 0.03, 0.5, and 1.0.

The peak values of maximum dynamic von Mises stress envelopes within a length of about 200 m along the riser are shown in Figure 3.5.3.

As seen from Figure 3.5.3, $a_2$ = 0.5 and 1.0 are unrealistic high values. Actually $a_2$ = 0.03 gave a damping of 15.7% which is already too high. The damping should be less than 0.5 ~ 1%; otherwise it will influence the results too much. For 0.5% damping at 10 s,

$$\frac{\pi}{T}a_2 = \frac{\pi}{10}a_2 = 0.5\% \Rightarrow a_2 = 0.016$$

Therefore, $a_2$ = 0.015 was chosen for the following riser dynamic analyses.

**c) Sensitivity to Mesh Length**

The riser is modelled with beam elements. Shorter mesh length may consume larger CPU calculating cost while longer mesh length may cause unstable results. Constant element lengths ranging from 2.2 m to 4.1 m were used by Passano and Larsen (2006) for riser analysis with Riflex. Constant element lengths 3 m to 8 m were investigated for the following study (see Table 3.5.4 and Figure 3.5.4 ~ 3.5.7).

SCR Base Case

- ID 0.254 m (10 in)
- WT 0.03 m
- Top hang-off angle 10, 15 deg
- Riser length 3000 m
- *Mesh length* *3, 4, 5, 6, and 8 m*
- Vessel offset 0 m, mean position

Table 3.5.4 shows mesh densities of 3 m to 5 m provide relatively stable results for both static and dynamic analysis with relatively shorter CPU calculation time. The

peak values of maximum dynamic von Mises stress envelope within a length of about 35 m along the riser are shown in Figure 3.5.6 ~ 3.5.7.

Either shorter mesh length or longer mesh length with smaller simulation time step will cause a large amount of time series results from time domain analysis of a 10800 s simulation length which needs a longer transferring data time included in the CPU calculation time and also a huge storage space in computer. This problem will be more highlighted during fatigue analysis. Therefore, an appropriate mesh length with a relatively stable simulation result but shorter CPU calculation time and smaller storage space needs to be decided in the beginning by a parametric study. A mesh length of 4 m was chosen for the following study.

**Table 3.5.4** Sensitivity of SCR Model to Various Mesh Lengths.

| Top Angle (deg) | Mesh Length (m) | Static Maximum von Mises Stress (MPa) | Maximum Dynamic von Mises Stress (MPa) | CPU Calculation Time (min) | Dynamic Result File Size (GB) |
|---|---|---|---|---|---|
| 10 | 3 | 154.60 | 586.90 | 55 | 1.89 |
| | 4 | 154.60 | 588.70 | 44 | 1.42 |
| | 5 | 154.70 | 587.90 | 35 | 1.14 |
| | 6 | 154.70 | 593.00 | 30 | 0.975 |
| | 8 | 154.80 | 596.80 | 18 | 0.740 |
| 15 | 3 | 100.30 | 655.50 | 60 | 1.89 |
| | 4 | 100.30 | 658.50 | 48 | 1.42 |
| | 5 | 100.30 | 659.80 | 38 | 1.14 |
| | 6 | 100.30 | 678.70 | 27 | 0.975 |
| | 8 | 100.40 | 663.70 | 21 | 0.740 |

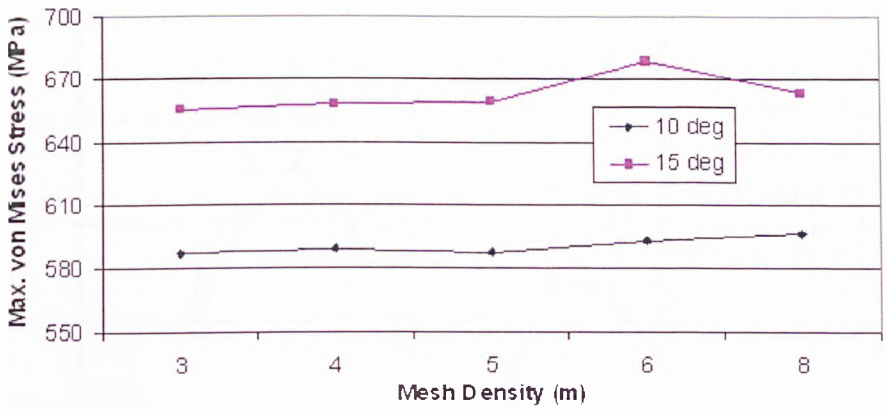


**Figure 3.5.4** Sensitivity of Maximum Dynamic von Mises Stress to Mesh Lengths 3, 4, 5, 6, and 8 m.

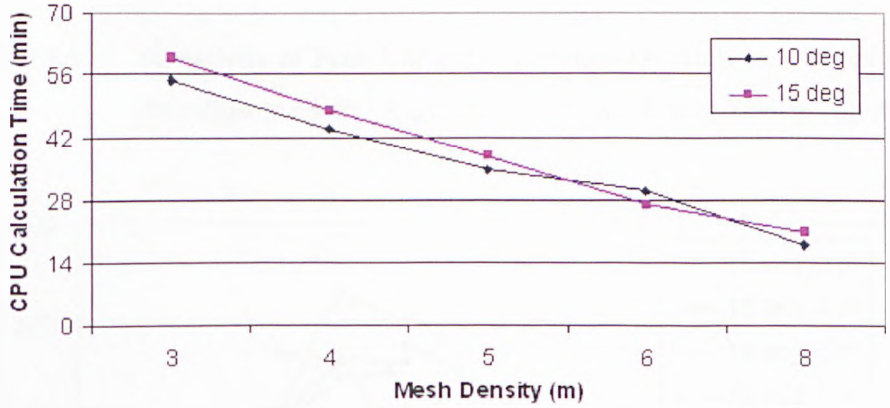


**Figure 3.5.5** Sensitivity of CPU Calculation Time to Mesh Lengths 3, 4, 5, 6, and 8 m.

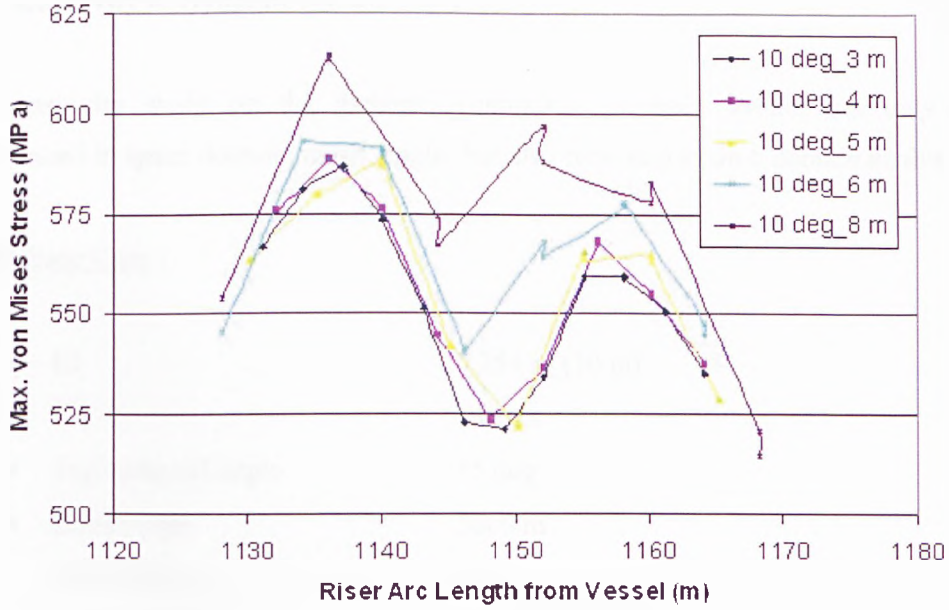


**Figure 3.5.6** Sensitivity of Peak Value of Maximum Dynamic von Mises Stress Envelope to Mesh Lengths 3, 4, 5, 6, and 8 m of 10 deg Top Angle.

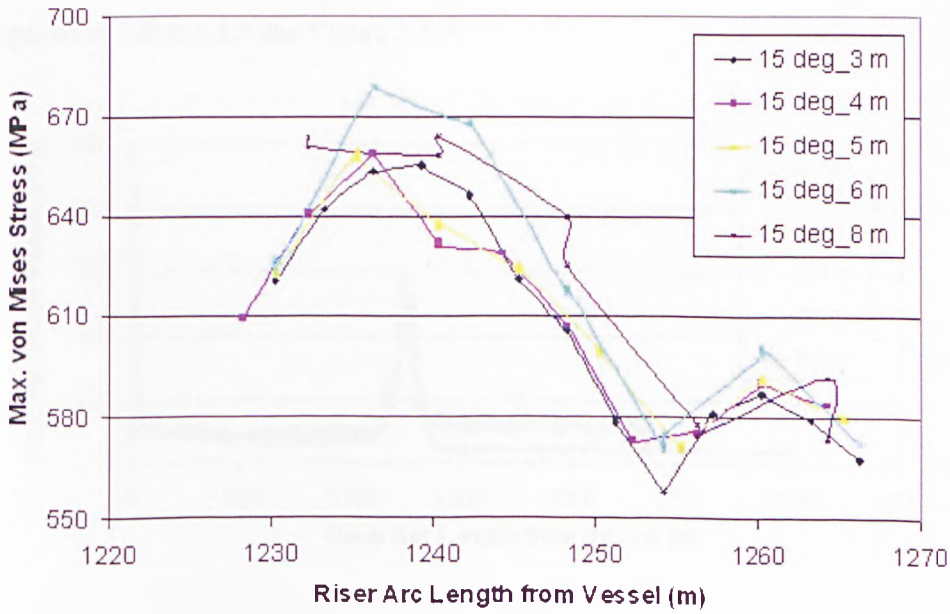


**Figure 3.5.7** Sensitivity of Peak Value of Maximum Dynamic von Mises Stress Envelope to Mesh Lengths 3, 4, 5, 6, and 8 m of 15 deg Top Angle.

**d) Sensitivity to Dynamic Simulation Time Step**

A sensitivity study on the dynamic simulation accuracy should not only be performed in space domain, mesh length, but also time step in time domain analysis.

SCR Base Case

- ID 0.254 m (10 in)
- WT 0.03 m
- Top hang-off angle 15 deg
- Riser length 3000 m
- Mesh length 4 m
- Vessel offset 0 m, mean position
- *Dynamic simulation time step* *0.02, 0.05, 0.1, 0.2, and 0.5 s*

Sensitivity of maximum dynamic von Mises stress envelopes to various simulation time steps are shown in Figure 3.5.8, among which the maximum values are compared in Table 3.5.5 and Figure 3.5.9.

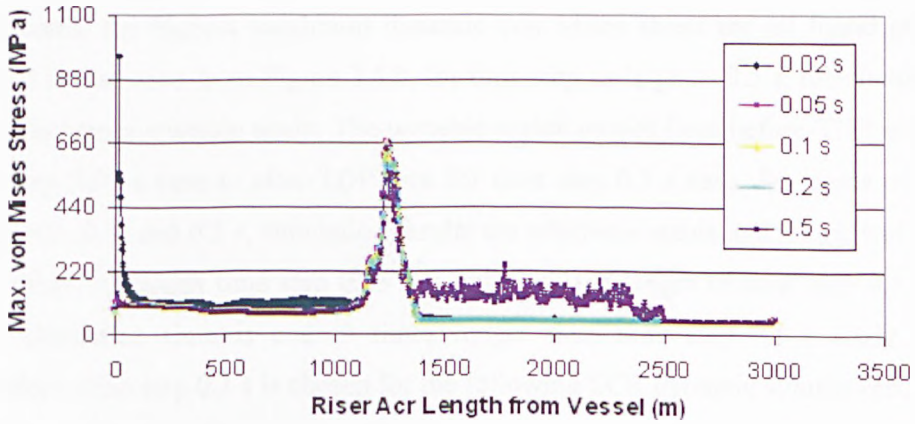


**Figure 3.5.8** Sensitivity of Maximum Dynamic von Mises Stress Envelope to Time Steps 0.02, 0.05, 0.1, 0.2, and 0.5 s.

**Table 3.5.5** Sensitivity to Various Time Steps for SCR Dynamic Simulations.

| Time Step (s) | Maximum Dynamic von Mises Stress (MPa) | CPU Simulation Time (h) |
|---|---|---|
| 0.02 | 667.50 (5273.00*) | 5.00* |
| 0.05 | 664.60 | 3.42 |
| 0.1 | 658.80 | 0.82 |
| 0.2 | 648.80 | 0.67 |
| 0.5 | 644.50 | 0.30 |

It will be noted that for time step as small as 0.02 s, the amount of data generated from the dynamic simulation time series were too large and exceeded the size of Riflex dynamic work memory. So the riser length was reduced from 3000 m to 2000 m to reduce the simulation data. Even though the processing data was remarkably reduced compared with other cases, its CPU simulation time was still much longer than the others. Although the maximum dynamic von Mises stress envelope has a good agreement with cases of time steps 0.05, 0.1, and 0.2 s around and after TDP, the simulation results are unstable before TDP even with unusually high stress values at the top end of the riser. Therefore, 667.50 MPa is the highest maximum dynamic von Mises stress around TDP while 5273.00 MPa is the highest at the top end. For other cases, the highest maximum dynamic von Mises stress are all found around TDP. It is also seen from Figure 3.5.8, for time step as large as 0.5 s, the simulation results becomes unstable again. The unstable region moves from before-TDP area for time step 0.02 s case to after-TDP area for time step 0.5 s case. For cases of time steps 0.05, 0.1, and 0.2 s, simulation results are relatively stable and match well with each other. Although time step 0.05 s is only half the length of time step 0.1 s, its CPU simulation time is over 3 times longer than time step 0.1 s study case. Therefore, time step 0.1 s is chosen for the following SCR dynamic simulations.

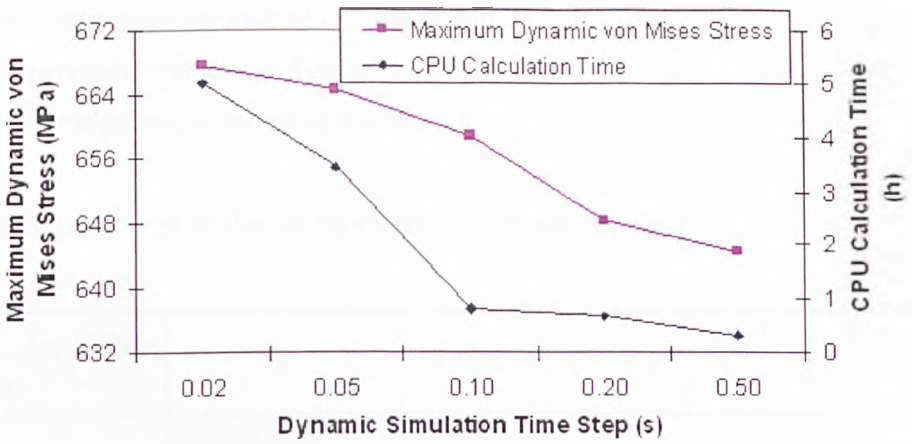


**Figure 3.5.9** Sensitivity of Maximum Dynamic von Mises Stress and CPU Simulation Time to Time Steps 0.02, 0.05, 0.1, 0.2, and 0.5 s.

### *3.5.2 Sensitivity to SCR Design Parameters*

Evaluation of effect of various parameters on the SCR strength response can provide valuable guide for the preliminary design of SCRs. The main parameters studied here are as follows:

a) Wave spectrum formulation
b) Riser top hang-off angle
c) Riser internal diameter (ID)
d) Riser wall thickness (WT)
e) Hydrodynamic drag coefficient $C_d$
f) Choice of normal soil stiffness: properties of the soil where the SCR touches the seabed
g) Wave conditions: Mild vs. Harsh
h) Riser length
i) Water depth

All the study cases are carried out with a same random model. For each study case, all the parameter values are fixed except the value of the specific parameter which is under investigation, as shown in Table 3.5.6.

**Table 3.5.6** SCR Design Parameters for Sensitivity Study.

| Parameter \ Study Case | a | b | c | d | e | f | g | h | i |
|---|---|---|---|---|---|---|---|---|---|
| Wave Spectrum Formulation | 5 Parameter JONSWAP, 3 Parameter JONSWAP, Bretschneider Spectrum | 3 parameter JONSWAP | | | | | | | |
| Top Hang-off Angle (deg) | 15 | 10 - 18 | 15 | | | | | | |
| Internal Diameter (ID) (in) | 10 | | 8 ~ 20 | 10 | | | | | |
| Riser Wall Thickness (WT) (m) | 0.03 | | | 0.026 ~ 0.036 | 0.03 | | | | |
| Hydrodynamic Drag Coefficient | 1.0 | | | | 0.7 ~ 1.2 | 1.0 | | | |
| Hydrodynamic Inertia Coefficient | 2.0 | | | | | | | | |
| Normal Soil Stiffness (kPa) | 600 | | | | | 100 ~ 5000 | 600 | | |
| Transverse Soil Stiffness (kPa) | 10 | | | | | | | | |
| Wave Conditions | NNS | | | | | | Brazil, WoA, GoM, NNS, India | NNS | |
| Riser Length (m) | 3000 | | | | | | | 1500 ~ 3000 | N/A |
| Water Depth (m) | 1000 | | | | | | | | 500 ~ 3000 |

**a) Sensitivity to Wave Spectrum Formulation**

There are two basic wave spectra that are commonly used by the offshore engineering:

- The Pierson-Moskovitz (PM / ISSC spectrum) (Pierson and Moskowitz, 1964);
- The JONSWAP spectrum, which was developed specially for the North Sea in joint industry study (Hasselmann et al., 1973).

During many years the Pierson-Moskovitz spectrum was said to be valid for the entire world, except for the North Sea, where JONSWAP was used. More recently, however, variations of the JONSWAP spectrum have been found to suit some other parts of the world better than the Pierson-Moskovitz curve.

Other wave spectra available in DNV DeepC (DNV Software, 2008) are

- Bretschneider spectrum (a modified PM formulation, also known as a 2 parameter PM spectrum);
- Torsethaugen spectrum.

The equations that control these spectra are described in Appendix B. User defined parameters for various wave spectrum formulations are shown in Table 3.5.7.

**Table 3.5.7** Wave Spectrum Formulations.

| Wave Spectrum | User Defined Parameters | | | | |
|---|---|---|---|---|---|
| | $\gamma$ | $H_s$ | $T_p$ | $\sigma_{wa}$ | $\sigma_{wb}$ |
| Pierson-Moskovitz Spectrum | | √ | | | |
| 3 Parameter JONSWAP | √ | √ | √ | | |
| 5 Parameter JONSWAP | √ | √ | √ | √ Default = 0.07 | √ Default = 0.09 |
| Bretschneider Spectrum | | √ | √ | | |

where

| | |
|---|---|
| $\gamma$ | peakedness parameter |
| $H_s$ | significant wave height |
| $T_p$ | wave peak period |
| $\sigma_{wa}$ | left width parameter |
| $\sigma_{wb}$ | right width parameter |

For a PM spectrum, $T_p$ and zero up-crossing wave period $T_z$ are related by

$$T_z = T_p / 1.408 \tag{3.5.5}$$

The JONSWAP formulation is the PM multiplied by a peakedness factor $\gamma^{a_J}$ (see Appendix B), where $a_J$ is JONSWAP formulation parameter.

If $\gamma = 1.0$, the JONSWAP reduces to the PM. Sometimes the value of $\gamma$ is modified based on site-specific data, but DNV DeepC allows no other values for $\gamma$. Wave energy is more concentrated in the JONSWAP spectrum around the peak spectral energy wave period. The relationship between the peak spectral period and the zero up-crossing period is

$$T_z = T_p / 1.28 \tag{3.5.6}$$

Figure 3.5.10 shows the NNS wave presented by different two parameter spectrum formulations in DNV DeepC. A sensitivity analysis of various wave spectrum formulations for a same wave condition is conducted.

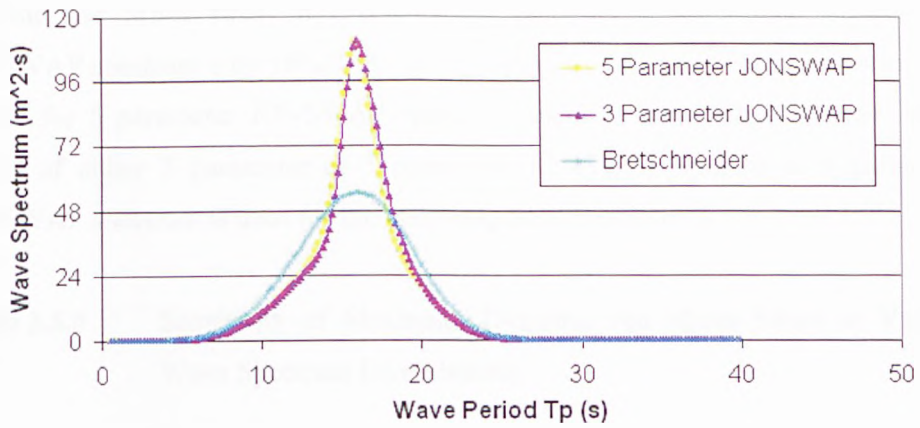


**Figure 3.5.10** Comparison of Various Wave Spectrum Formulations for NNS Wave $H_s$ = 15.5 m, $T_p$ = 16 s.

SCR Base Case

- ID 0.254 m (10 in)
- WT 0.03 m
- Top hang-off angle 15 deg
- Riser length 3000 m
- Mesh length 4 m
- Vessel offset 0 m, mean position
- Significant wave height $H_s$ 15.5 m
- Wave peak period $T_p$ 16 s
- *Wave spectrum formulation* *5 Parameter JONSWAP, 3 Parameter JONSWAP, and Bretschneider Spectrum*

Sensitivity of maximum dynamic von Mises stress envelopes to various wave spectrum formulations are shown in Figure 3.5.12, among which the maximum values are compared in Table 3.5.8 and Figure 3.5.11. It can be seen that the overall envelope curves are similar while the values of Bretschneider spectrum's are much lower than the other two JONSWAP spectrums' around TDA. The maximum

dynamic von Mises stress of Bretschneider spectrum is lower than 3 parameter JONSWAP spectrum's by 18%. If the default values of spectral width parameters are chosen for 5 parameter JONSWAP spectrum, there is not much difference in the results of either 3 parameter or 5 parameter JONSWAP spectrums. 3 parameter JONSWAP spectrum is used for the following SCR simulations.

**Table 3.5.8** Sensitivity of Maximum Dynamic von Mises Stress to Various Wave Spectrum Formulations.

| Wave Spectrum | Dynamic (MPa) |
|---|---|
| 5 Parameter JONSWAP (5J) | 658.10 |
| 3 Parameter JONSWAP (3J) | 657.20 |
| Bretschneider (B) | 539.80 |

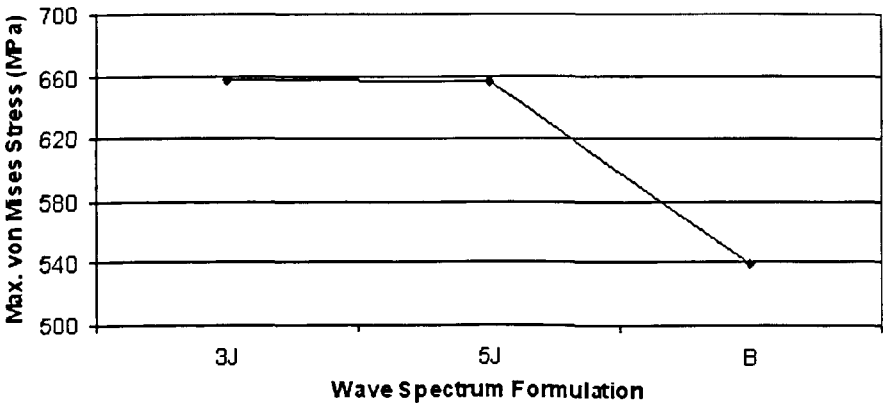


**Figure 3.5.11** Sensitivity of Maximum Dynamic von Mises Stress to Various Wave Spectrum Formulations.

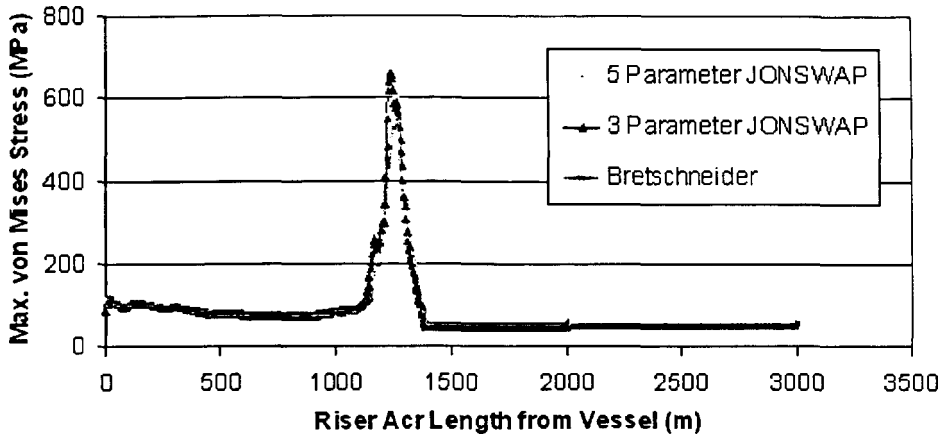


**Figure 3.5.12** Sensitivity of Maximum Dynamic von Mises Stress Envelope to 5 Parameter JONSWAP, 3 Parameter JONSWAP, and Bretschneider Spectrum.

**b) Sensitivity to Top Hang-off Angle**

The top hang-off angle (or top / departure angle) of the riser from the vessel is the most important parameter for the global configuration design of an SCR (Song and Stanton, 2007a). The top hang-off angle is defined by the length of the riser, and orientation of the hang-off porch on the vessel. Table 3.5.9 summarizes the typical SCR top hang-off angles for different types of floaters.

**Table 3.5.9** Typical SCR Hang-off Angles.

| Floater Type | Spar | Semi-Submersible | TLP | FPSO |
|---|---|---|---|---|
| Hang-off Angle (°) | 8 - 14 | 10 - 18 | 10 - 14 | 12 - 16 |

A sensitivity analysis of the effect of top hang-off angle is performed.

SCR Base Case

- ID 0.254 m (10 in)
- WT 0.03 m
- *Top hang-off angle* *10 - 18 deg*
- Riser length 3000 m
- Mesh length 4 m
- Vessel offset 0 m, mean position

The SCR base case is studied with different top hang-off angles. Maximum static and dynamic von Mises stresses are compared in Table 3.5.10 and Figure 3.5.13 ~ 3.5.16. With the increase of riser top hang-off angle by each one degree, the maximum static von Mises stress was decreased averagely by 8.14% while the maximum dynamic von Mises stress was increased averagely by 2.54% (see Table 3.5.10). But for both static and dynamic cases, the von Mises stresses at the top of the riser at the connection to the vessel.

**Table 3.5.10** Sensitivity of Maximum von Mises Stress to Top Hang-off Angles 10 – 18 deg.

| Top Angle (deg) | Static (MPa) | Dynamic (MPa) |
|---|---|---|
| 10 | 154.60 | 588.70 |
| 11 | 142.00 (–8.15%) | 597.70 (+1.53%) |
| 12 | 129.50 (–8.80%) | 604.20 (+1.09%) |
| 13 | 118.50 (–8.49%) | 617.90 (+2.27%) |
| 14 | 109.50 (–7.59%) | 634.40 (+2.67%) |
| 15 | 100.30 (–8.40%) | 658.80 (+3.85%) |
| 16 | 92.70 (–7.58%) | 678.40 (+2.98%) |
| 17 | 85.13 (–8.17%) | 702.20 (+3.51%) |
| 18 | 78.36 (–7.95%) | 719.10 (+2.41%) |

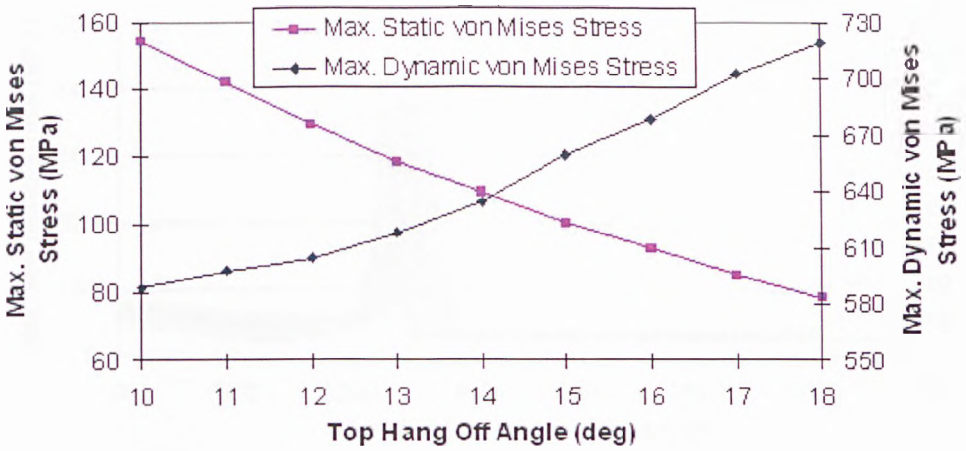


**Figure 3.5.13** Sensitivity of Maximum Static and Dynamic von Mises Stress to Top Hang-off Angles 10 – 18 deg.

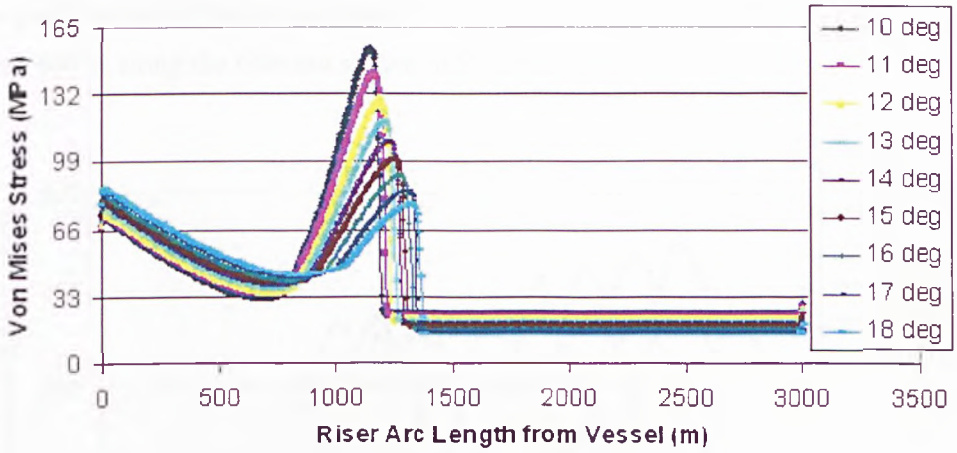


**Figure 3.5.14** Sensitivity of Static von Mises Stress to Top Hang-off Angles 10 – 18 deg.

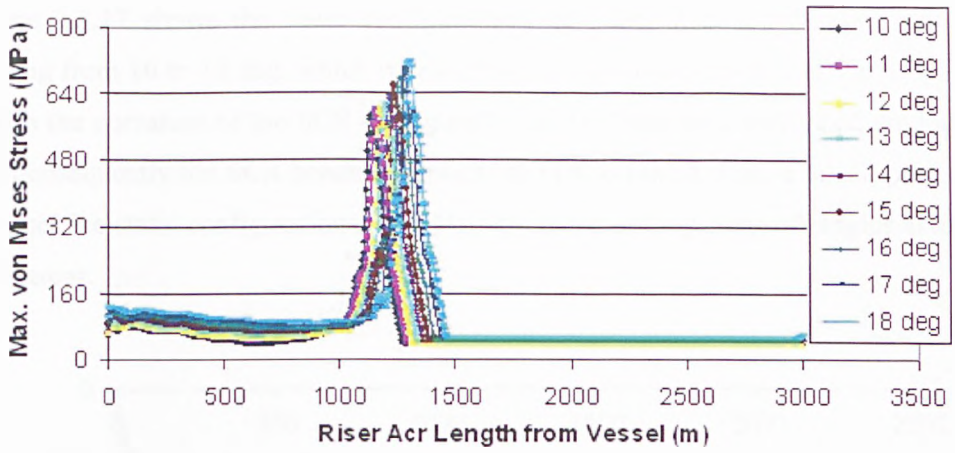


**Figure 3.5.15** Sensitivity of Maximum Dynamic von Mises Stress Envelope to Top Hang-off Angles 10 – 18 deg.

The peak values of maximum dynamic von Mises stress envelopes within a length of about 400 m along the riser arc shown in Figure 3.5.16.

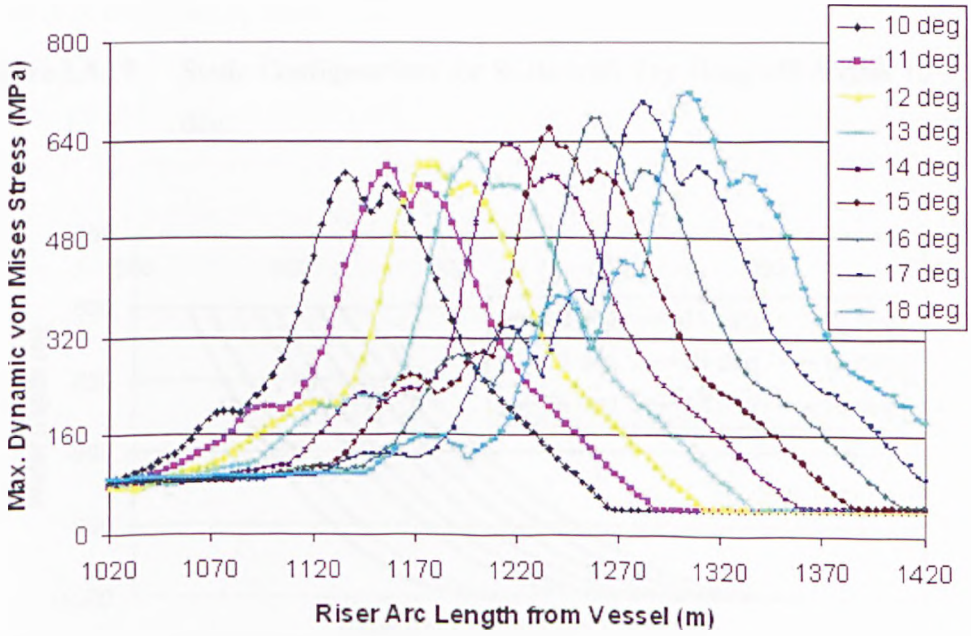


**Figure 3.5.16** Sensitivity of Peak Value of Maximum Dynamic von Mises Stress Envelope to Top Hang-off Angles 10 – 18 deg.

Figure 3.5.17 shows the static configurations of SCRs with top hang-off angles varying from 10 to 18 deg, which reveals that with the increase of riser top hang-off angles the curvature of the SCR configuration at TDP has been steepened gradually and consequently the SCR bending moment at TDP is raised. Figure 3.5.18 partially enlarges the static configurations of SCRs with increased top hang-off angles around TDP areas.

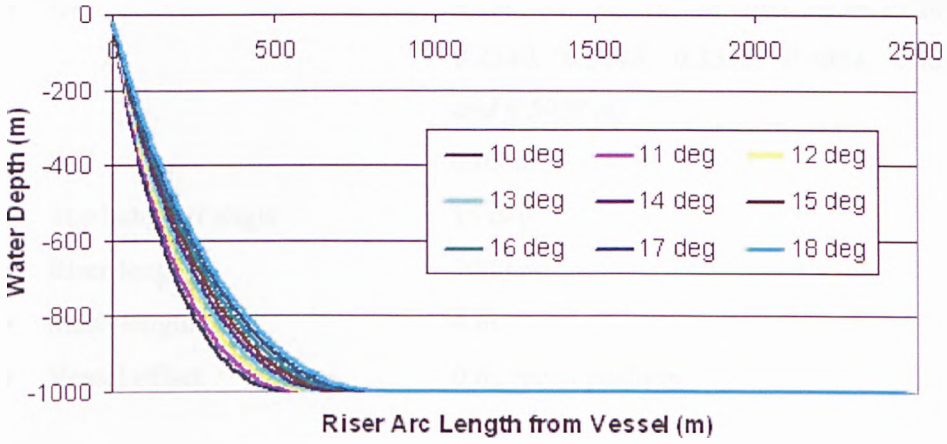


**Figure 3.5.17** Static Configurations for SCRs with Top Hang-off Angles 10 – 18 deg.

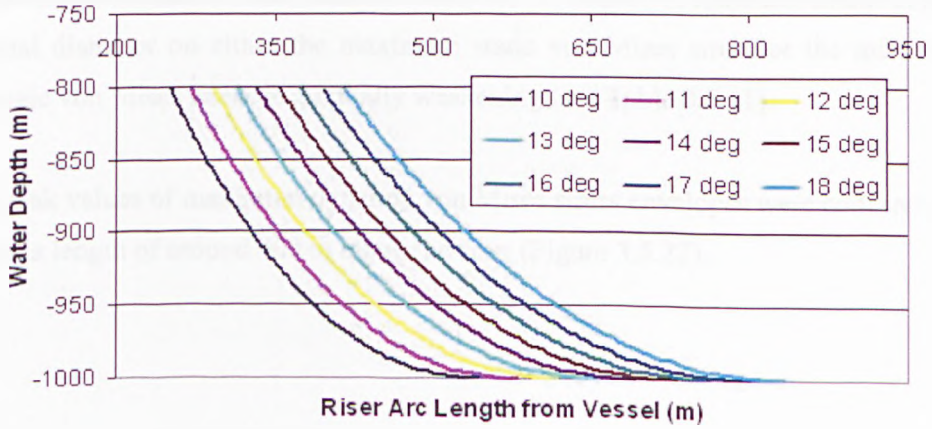


**Figure 3.5.18** Static Configurations around TDP for SCRs with Top Hang-off Angles 10 – 18 deg.

**c) Sensitivity to Internal Diameter (ID)**

Diameter is one of the critical factors for determining the dynamic performance of risers. An SCR base case with various internal diameters is examined.

SCR Base Case

| | |
|---|---|
| • *ID* | *8, 10, 12, 14, 16, 18, and 20 in (0.2032, 0.2540, 0.3048, 0.3556, 0.4064, 0.4572, and 0.5080 m)* |
| • WT | 0.03 m |
| • Top hang-off angle | 15 deg |
| • Riser length | 3000 m |
| • Mesh length | 4 m |
| • Vessel offset | 0 m, mean position |

Maximum static and dynamic von Mises stresses are compared in Table 3.5.11 and Figure 3.5.19 ~ 3.5.22. With the increase of riser internal diameter by every 2 inches (0.0508 m), the maximum static von Mises stress was increased averagely by 11.23% while the maximum dynamic von Mises stress was decreased averagely by 5.31%. But with the increase of riser internal diameter, the impact of same increment of riser internal diameter on either the maximum static von Mises stress or the maximum dynamic von Mises stress is gradually weakening (see Table 3.5.11).

The peak values of maximum dynamic von Mises stress envelopes were concentrated within a length of around 400 m along the riser (Figure 3.5.22).

**Table 3.5.11** Sensitivity of Maximum von Mises Stress to IDs 8 – 20 in.

| ID | | Static (MPa) | Dynamic (MPa) |
|---|---|---|---|
| (in) | (m) | | |
| 8 | 0.2032 | 87.83 | 733.80 |
| 10 | 0.2540 | 100.30 (+14.20%) | 658.80 (–10.22%) |
| 12 | 0.3048 | 113.30 (+12.96%) | 608.50 (–7.64%) |
| 14 | 0.3556 | 126.10 (+11.30%) | 583.40 (–4.12%) |
| 16 | 0.4064 | 139.70 (+10.79%) | 571.70 (–2.01%) |
| 18 | 0.4572 | 152.50 (+9.16%) | 549.60 (–3.87%) |
| 20 | 0.5080 | 166.20 (+8.98%) | 527.70 (–3.98%) |

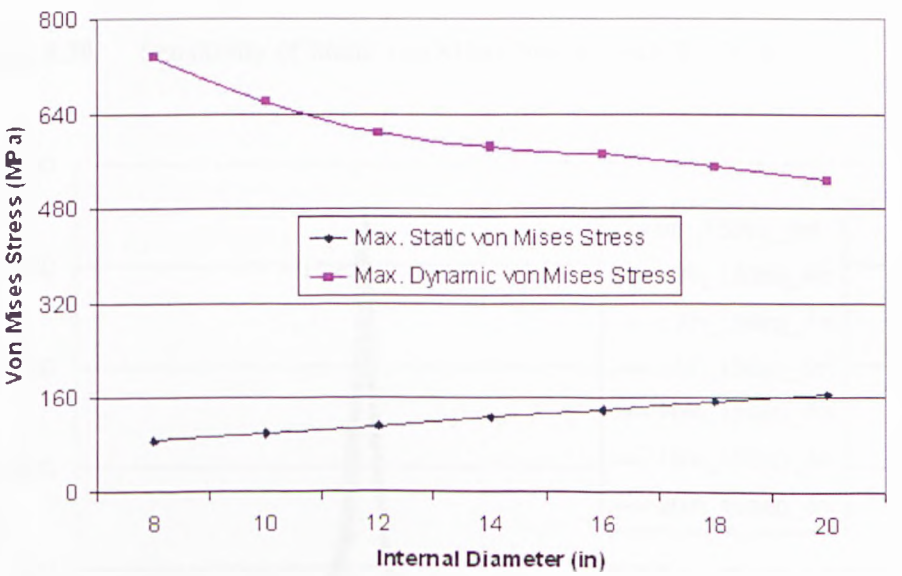


**Figure 3.5.19** Sensitivity of Maximum Static and Dynamic von Mises Stress to IDs 8 – 20 in.

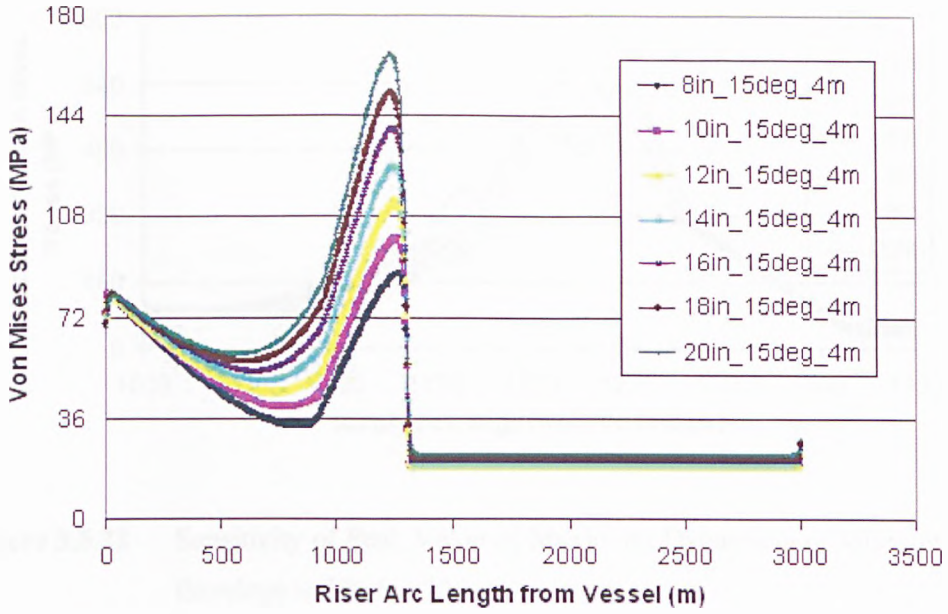


**Figure 3.5.20** Sensitivity of Static von Mises Stress to IDs 8 – 20 in.

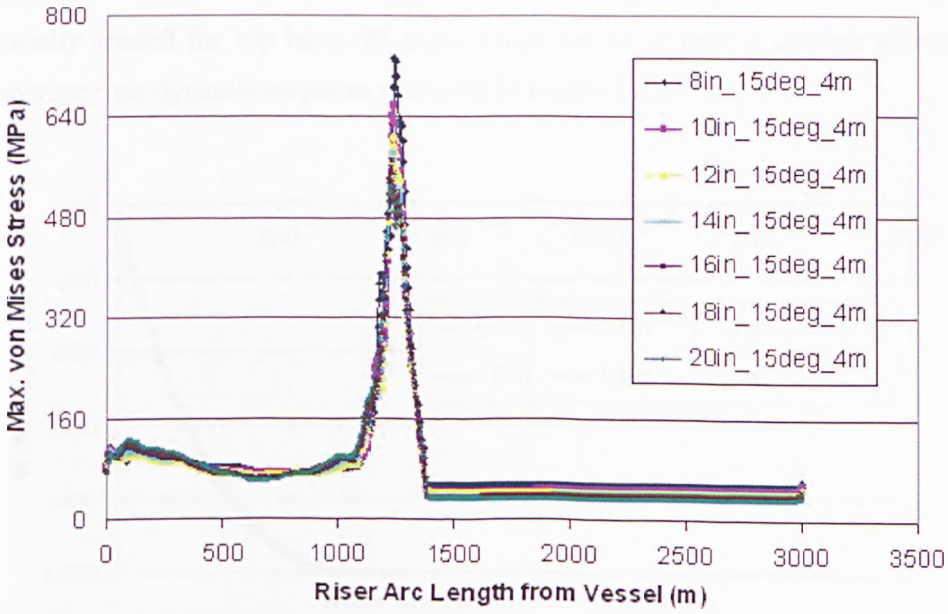


**Figure 3.5.21** Sensitivity of Maximum Dynamic von Mises Stress Envelope to IDs 8 – 20 in.

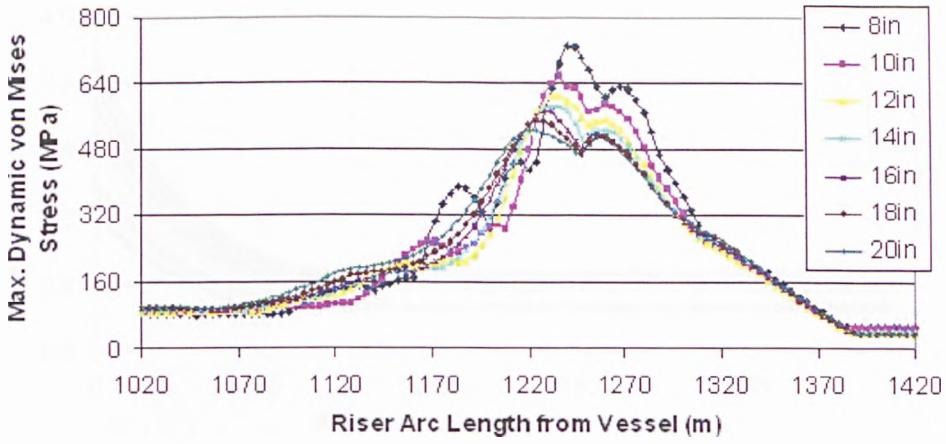


**Figure 3.5.22** Sensitivity of Peak Value of Maximum Dynamic von Mises Stress Envelope to IDs 8 – 20 in.

Figure 3.5.23 shows the static configurations of SCRs with internal diameters varying from 8 to 20 in were almost the same while Figure 3.5.24 reveals that with increased riser diameter but same wall thickness the axial force of SCRs was raised especially around the top hang-off areas which seems to have a positive effect on improving riser dynamic response as shown in Figure 3.5.21.

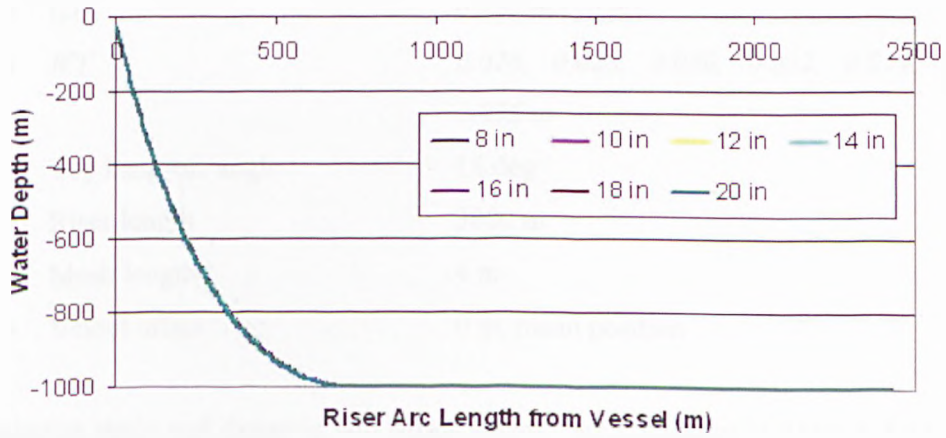


**Figure 3.5.23** Static Configurations for SCRs with IDs 8 – 20 in.

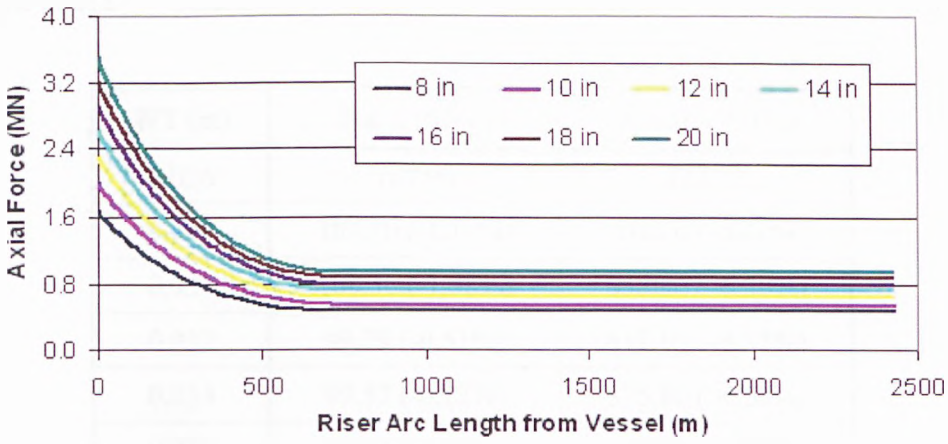


**Figure 3.5.24** Sensitivity of SCR Axial Force to IDs 8 – 20 in.

**d) Sensitivity to Riser Wall Thickness (WT)**

Wall thickness sizing is another decisive factor together with diameter for the riser dynamic performance. A 10 in ID SCR with varied wall thickness is analysed.

SCR Base Case

- ID 0.254 m (10 in)
- *WT* *0.026, 0.028, 0.030, 0.032, 0.034, and 0.036 m*
- Top hang-off angle 15 deg
- Riser length 3000 m
- Mesh length 4 m
- Vessel offset 0 m, mean position

Maximum static and dynamic von Mises stresses are compared in Table 3.5.12 and Figure 3.5.25 ~ 3.5.28. With the increase of riser wall thickness by each 0.02 m, the maximum static von Mises stress was decreased averagely by 0.66% while the maximum dynamic von Mises stress was also decreased averagely by 6.06%.

**Table 3.5.12** Sensitivity of Maximum von Mises Stress to WTs 0.026 – 0.036 m.

| WT (m) | Static (MPa) | Dynamic (MPa) |
|---|---|---|
| 0.026 | 102.90 | 743.20 |
| 0.028 | 101.70 (-1.17%) | 703.10 (–5.40%) |
| 0.030 | 100.30 (-1.38%) | 658.80 (–6.30%) |
| 0.032 | 99.79 (-0.51%) | 617.10 (–6.33%) |
| 0.034 | 99.57 (-0.22%) | 576.80 (–6.53%) |
| 0.036 | 99.57 (-0.00%) | 543.70 (–5.74%) |

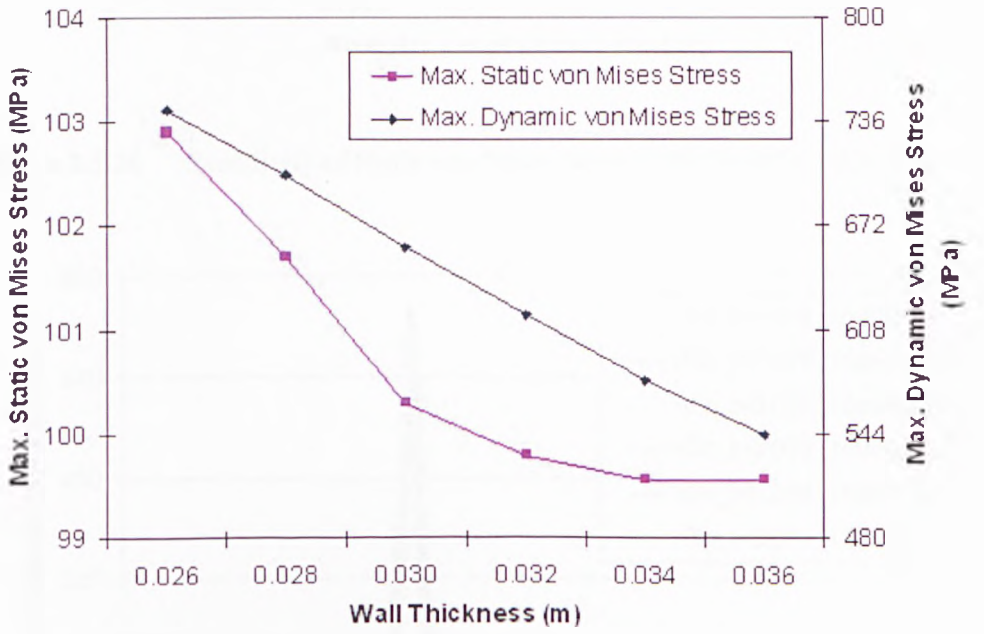


**Figure 3.5.25** Sensitivity of Maximum Static and Dynamic von Mises Stress to WTs 0.026 – 0.036 m.

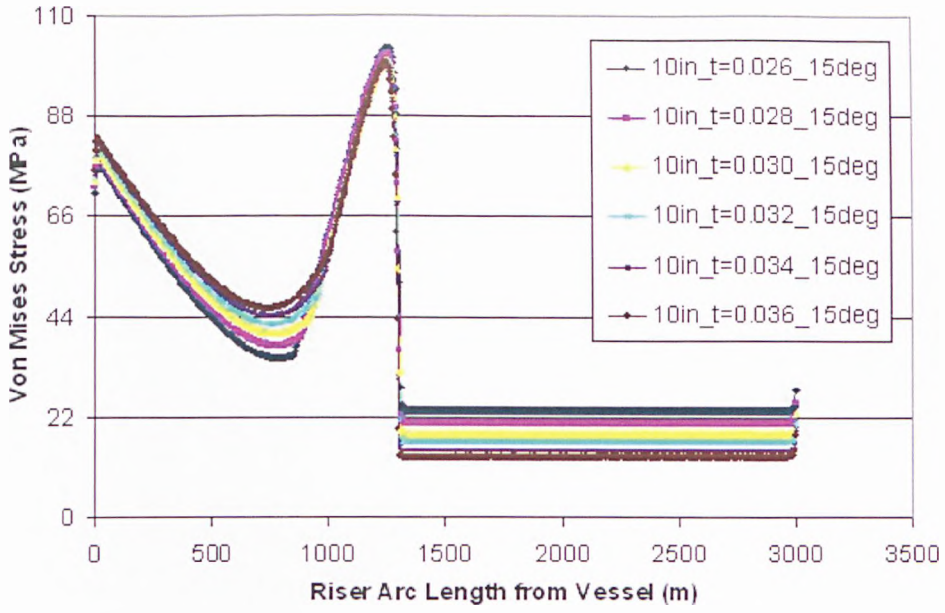


**Figure 3.5.26** Sensitivity of Static von Mises Stress to WTs 0.026 – 0.036 m.

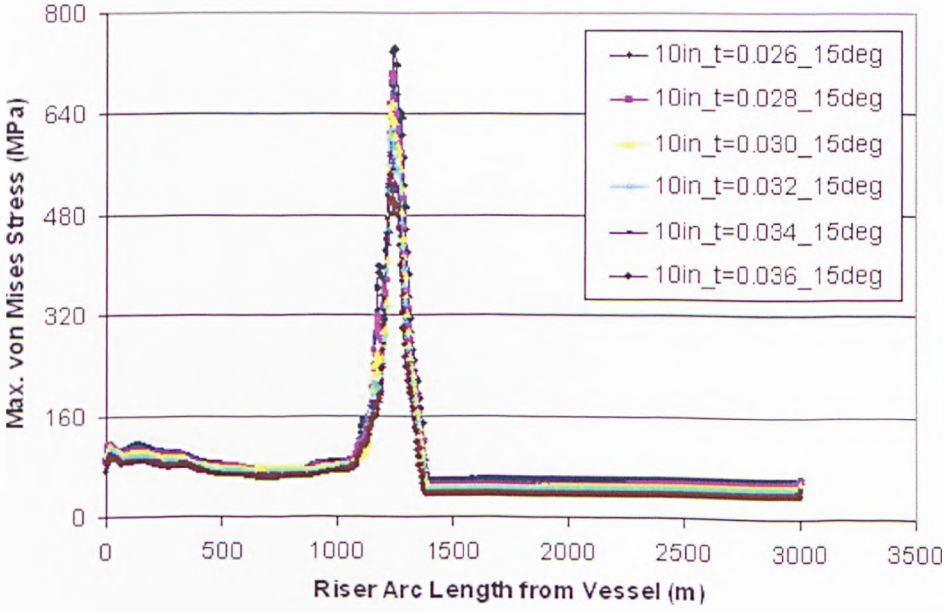


**Figure 3.5.27** Sensitivity of Maximum Dynamic von Mises Stress Envelope to WTs 0.026 – 0.036 m.

The peak values of maximum dynamic von Mises stress envelopes were concentrated within a length of about 400 m along the riser, as shown in Figure 3.5.28.

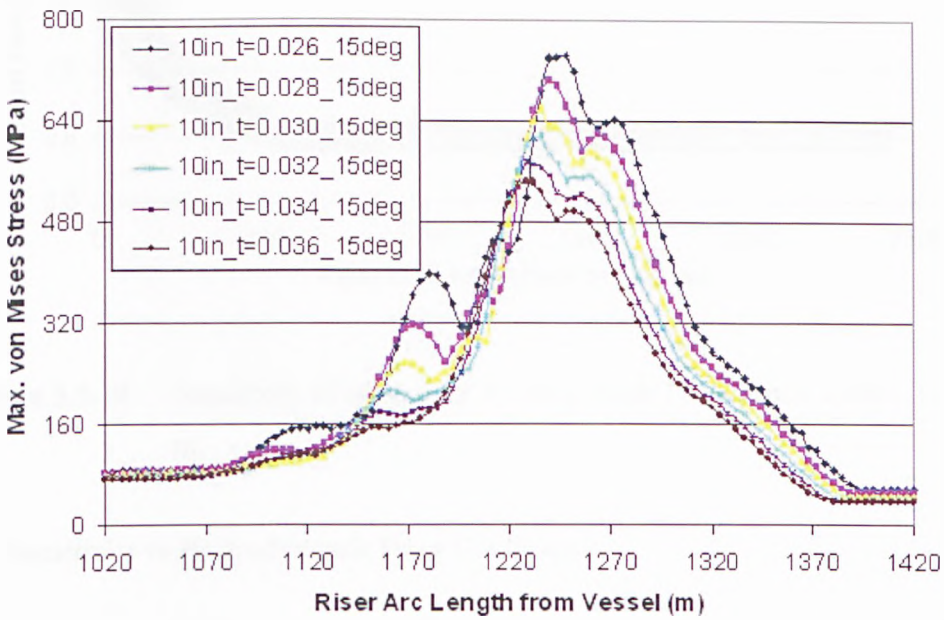


**Figure 3.5.28** Sensitivity of Peak Value of Maximum Dynamic von Mises Stress Envelope to Wall Thicknesses 0.026 – 0.036 m.

Similar as sensitivity to riser diameter, the static configurations of SCRs with wall thicknesses varying from 0.026 to 0.036 m were almost the same while Figure 3.5.29 reveals that with increased riser wall thickness but same internal diameter the axial force of SCRs was raised especially around the top hang-off areas which seems to have a positive effect on improving riser dynamic response as shown in Figure 3.5.27.

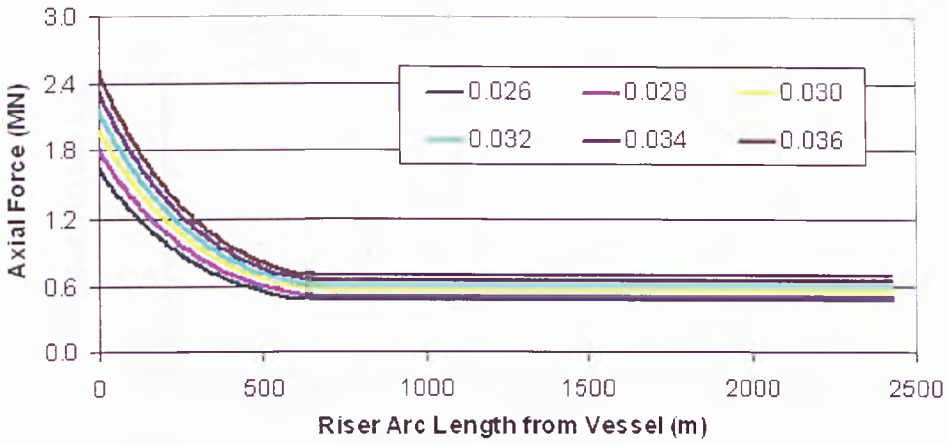


**Figure 3.5.29** Sensitivity of SCR Axial Force to Wall Thicknesses 0.026 – 0.036 m.

**e) Sensitivity to Hydrodynamic Drag Coefficient**

Drag estimation is important to riser design, particularly for deepwater locations with strong currents. The horizontal hydrodynamic load will affect many aspects of design. One effect that could possibly impact the hydrodynamic drag coefficient (defined as the drag force per unit length of the cylinder) is variation in flow regime (i.e. Reynolds number). The relationship between drag coefficient $C_d$ and Reynolds number Re for a smooth cylinder in steady uniform flow is illustrated in Figure 3.5.30 and Table 3.5.13.

The Reynolds number is defined as

$$\mathrm{Re} = \frac{Vd}{\nu} \tag{3.5.7}$$

where $V$ is water particle velocity, $d$ is cylinder diameter and $\nu$ is the kinematic viscosity.

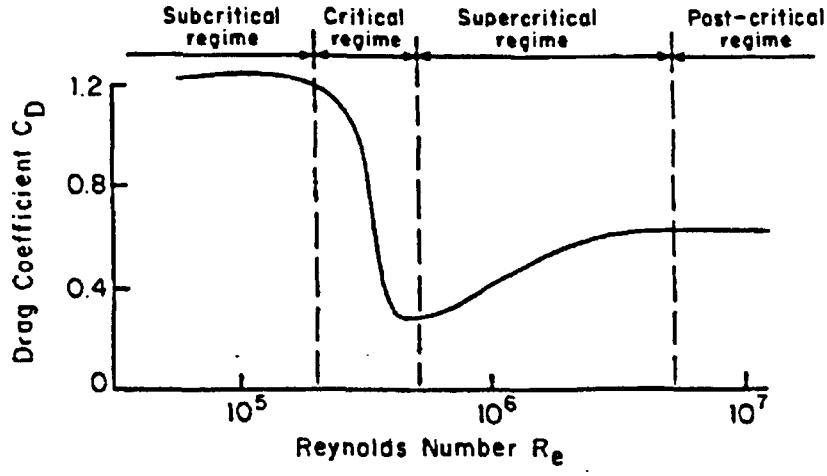


**Figure 3.5.30** Variation of Drag Coefficient $C_d$ with Reynolds Number Re for a Smooth Cylinder in Steady Uniform Flow.

**Table 3.5.13** Range of Hydrodynamic Coefficients for Flow Normal to Riser Axis.

| | Flow Condition | Re | $C_d$ | $C_m$ |
|---|---|---|---|---|
| Smooth Pipe | Supercritical | $Re > 10^6$ | 0.7 | 2.0 |
| | Critical | $10^5 < Re < 10^6$ | 0.6 – 1.2 | |
| | Subcritical | $Re < 10^5$ | 1.2 | |

A sensitivity analysis is conducted to assess the riser response to the variation in hydrodynamic drag coefficient.

SCR Base Case

- ID 0.254 m (10 in)
- WT 0.03 m
- Top hang-off angle 15 deg
- Riser length 3000 m
- Mesh length 4 m

- Vessel offset — 0 m, mean position
- *Drag coefficient* $C_d$ — *0.7, 0.8, 0.9, 1.0, 1.1 and 1.2*
- Inertia coefficient $C_m$ — 2.0

Since hydrodynamic drag coefficient mainly affects the riser dynamic loadings, the SCR static von Mises stresses remained almost the same as shown in Figure 3.5.31. Maximum dynamic von Mises stresses are compared in Table 3.5.14 and Figure 3.5.32 ~ 3.5.34. With the increase of hydrodynamic drag coefficient by each 0.1, the maximum dynamic von Mises stress was increased averagely by 48.96 MPa (8.27%) which means that the increase of hydrodynamic drag force will worsen the riser dynamic performance.

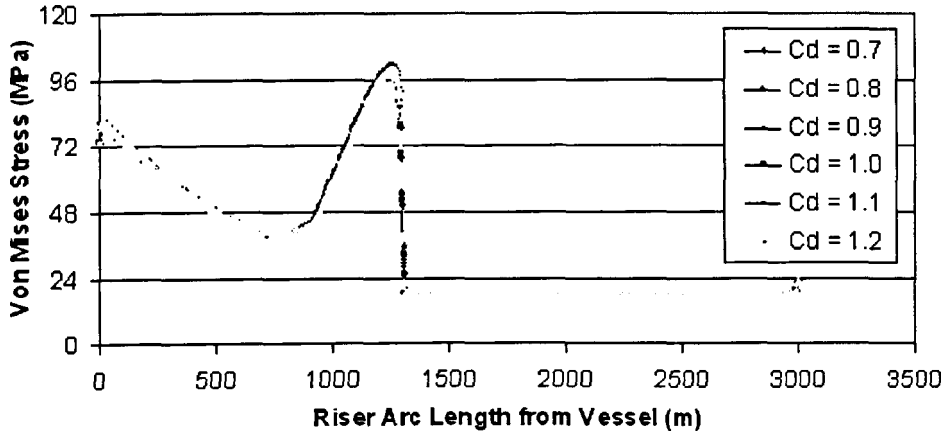


**Figure 3.5.31** Sensitivity of Static von Mises Stress to Drag Coefficients 0.7 – 1.2.

**Table 3.5.14** Sensitivity of Maximum von Mises Stress to Drag Coefficients 0.7 – 1.2.

| $C_d$ | Dynamic (MPa) |
|---|---|
| 0.7 | 503.00 |
| 0.8 | 555.80 (+10.50%) |
| 0.9 | 600.80 (+8.10%) |
| 1.0 | 658.80 (+9.65%) |
| 1.1 | 704.50 (+6.94%) |
| 1.2 | 747.80 (+6.15%) |

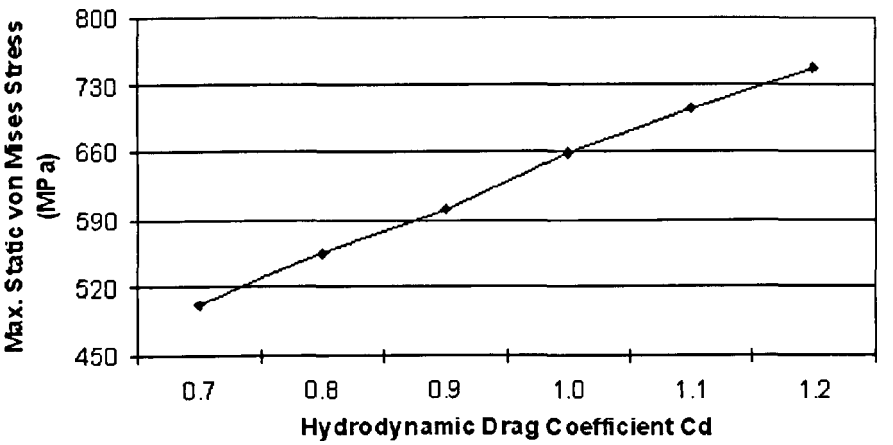


**Figure 3.5.32** Sensitivity of Maximum Dynamic von Mises Stress to Drag Coefficients 0.7 – 1.2.

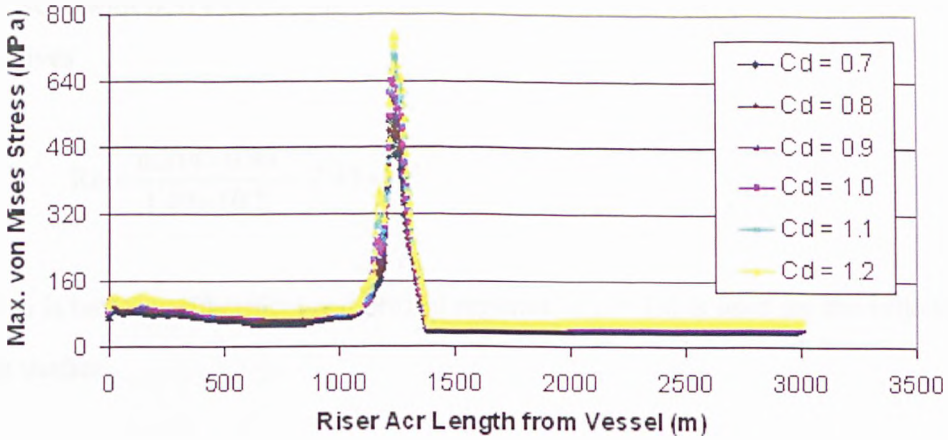


**Figure 3.5.33** Sensitivity of Maximum Dynamic von Mises Stress Envelope to Drag Coefficients 0.7 – 1.2.

The peak values of maximum dynamic von Mises stress envelopes were concentrated within a length of about 400 m along the riser, as shown in Figure 3.5.34.

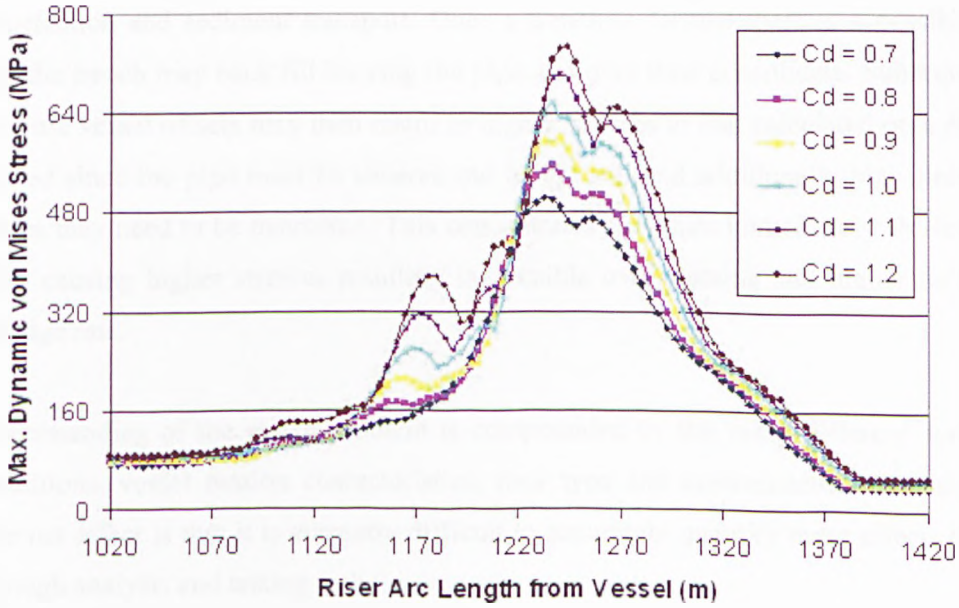


**Figure 3.5.34** Sensitivity of Peak Value of Maximum Dynamic von Mises Stress Envelope to Drag Coefficients 0.7 – 1.2.

The SCR with 0.314 m outside diameter (OD) and maximum current strength 0.93 m/s gives

$$\mathrm{Re} = \frac{0.314 \times 0.93}{1.19 \times 10^{-6}} = 2.45 \times 10^{5}$$

which is between subcritical and critical regimes. $C_d$ = 1.0 is used for the following case studies.

**f) Sensitivity to Normal Soil Stiffness**

The response of the riser at the seabed TDP and the interaction with the seabed is complex. Until recently most analysis was conducted assuming the seabed is rigid or that it exhibits a linear stiffness. However, these assumptions are not necessarily conservative. There is evidence that risers can trench to significant depth, 2-3 diameters, in certain conditions. The formation of the trench is not well understood but is thought to be a combination between soil deformation and remoulding, soil liquefaction and sediment transport. Once a trench is formed there is a possibility that the trench may back fill burying the pipe and over time consolidate. Subsequent extreme vessel offsets may then result in higher stresses to that calculated on a rigid seabed since the pipe must be sheared out of the soil and additionally high suction forces may need to be overcome. This concentrates curvature immediately above the TDP causing higher stresses resulting in possible overstressing and higher fatigue damage rate.

Understanding of the above problem is compounded by the many different seabed conditions, vessel motion characteristics, riser type and environmental conditions. The net effect is that it is currently difficult to accurately quantify these effects both through analysis and testing techniques.

A linear stiffness is employed in the current study, and the impact of soil stiffness on the riser response is assessed for a range of soil conditions. The analysis conducted

for the rigid seabed case is repeated for normal soil stiffness of between 100 kPa and 5000 kPa.

SCR Base Case

- ID — 0.254 m (10 in)
- WT — 0.03 m
- Top hang-off angle — 15 deg
- Riser length — 3000 m
- Mesh length — 4 m*
- Vessel offset — 0 m, mean position
- Drag coefficient $C_d$ — 1.0
- Inertia coefficient $C_m$ — 2.0
- Transverse soil stiffness — 10 kPa
- *Normal soil stiffness* — *100, 300, 400, 500, 600, 700, 1000, 2000, 3000, and 5000 kPa*

As for mesh length, when the normal soil stiffness was larger than 1000 kPa, the dynamic results with mesh length of 4 m became unstable and usually large. A sensitivity study was performed for the cases with high normal soil stiffness to obtain a mesh length with stable results. The results of the mesh length sensitivity analysis are shown in Figure 3.5.35 ~ 3.5.39 from which 2 m, 3 m, and 2.5 m were chosen as mesh length for cases with normal soil stiffness 2000, 3000, and 5000 kPa respectively.

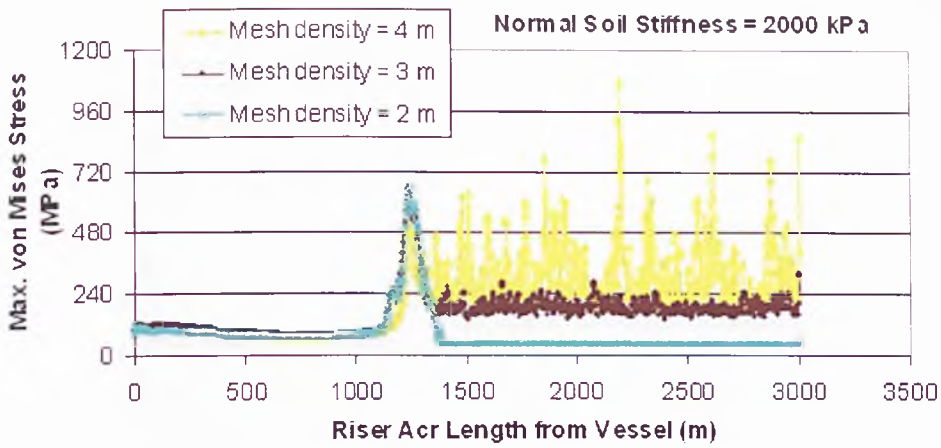


**Figure 3.5.35** Sensitivity of Maximum Dynamic von Mises Stress Envelope of Normal Soil Stiffness 2000 kPa to Mesh Lengths 4, 3, and 2 m.

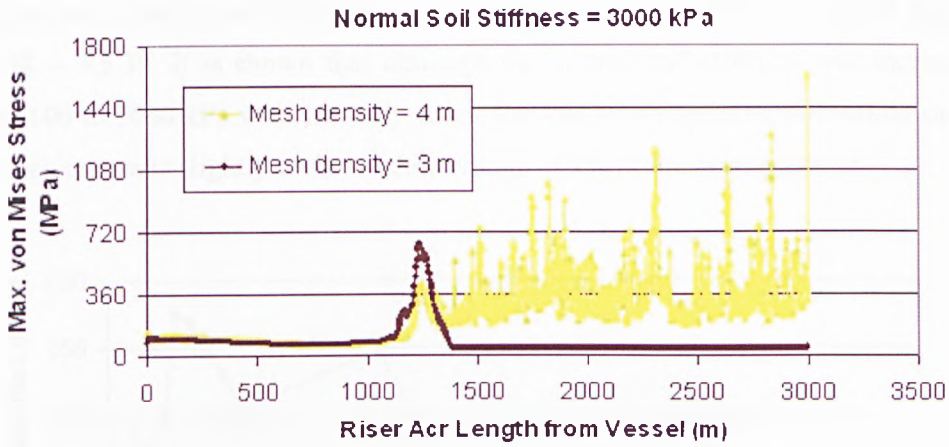


**Figure 3.5.36** Sensitivity of Maximum Dynamic von Mises Stress Envelope of Normal Soil Stiffness 3000 kPa to Mesh Lengths 4 and 3 m.

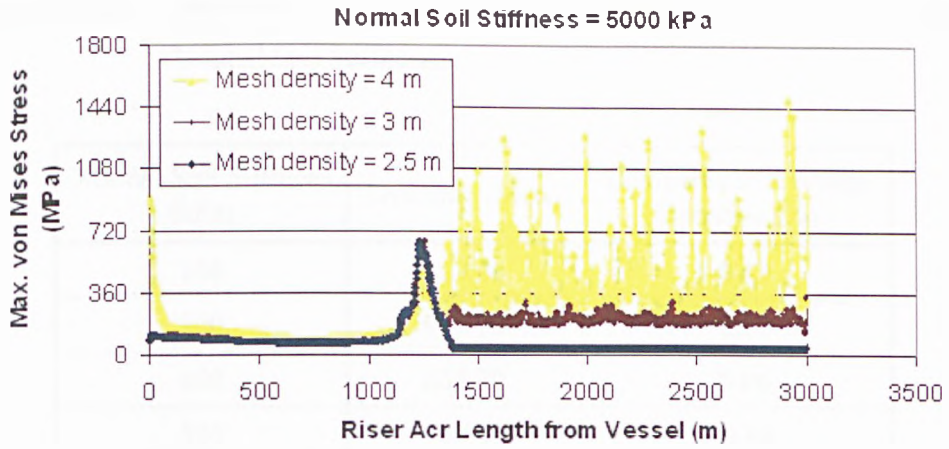


**Figure 3.5.37** Sensitivity of Maximum Dynamic von Mises Stress Envelope of Normal Soil Stiffness 5000 kPa to Mesh Lengths 4, 3, and 2.5 m.

Maximum dynamic von Mises stresses are compared in Table 3.5.15 and Figure 3.5.38 ~ 3.5.39. It is shown that although the normal soil stiffness was increased from 100 to 5000 kPa with 10 study cases, the maximum dynamic von Mises stress for each case was slightly varied within a range of 1% of the average value.

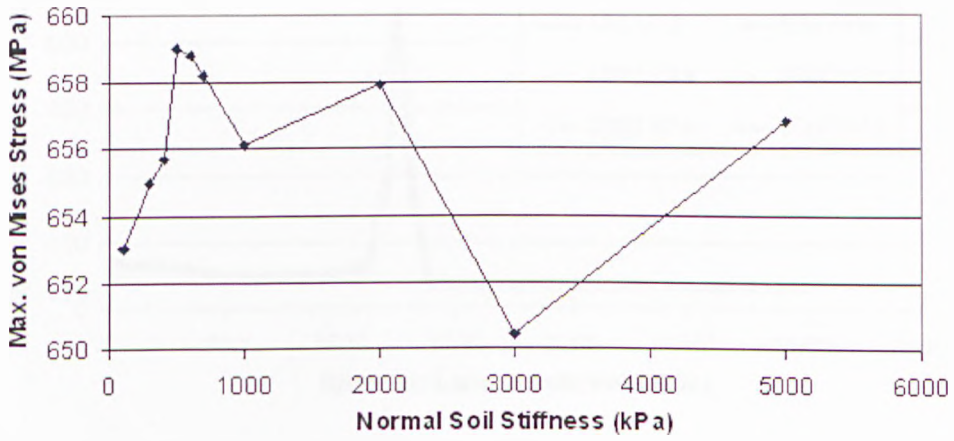


**Figure 3.5.38** Sensitivity of Maximum Dynamic von Mises Stress to Various Normal Soil Stiffness.

**Table 3.5.15** Sensitivity of Maximum Dynamic von Mises Stress to Various Normal Soil Stiffness.

| Normal Soil Stiffness (kPa) | Dynamic (MPa) | Compared to Average Dynamic (%) |
|---|---|---|
| 100 | 653.00 | –0.47 |
| 300 | 655.00 | –0.17 |
| 400 | 655.70 | –0.06 |
| 500 | 659.00 | +0.44 |
| 600 | 658.80 | +0.41 |
| 700 | 658.20 | +0.32 |
| 1000 | 656.10 | +0.00 |
| 2000 | 657.90 | +0.28 |
| 3000 | 650.40 | –0.87 |
| 5000 | 656.80 | +0.11 |
| Average = 656.09 | | |

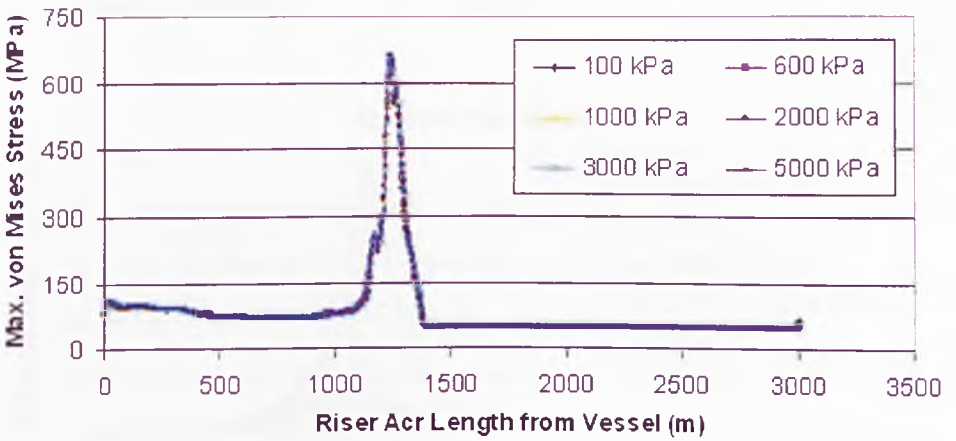


**Figure 3.5.39** Sensitivity of Maximum Dynamic von Mises Stress Envelopes to Various Normal Soil Stiffness.

**g) Sensitivity to Wave Conditions**

The typical wave conditions of some offshore regions around the world are listed in Table 3.5.16 and Figure 3.5.40. A sensitivity analysis of riser response to the various wave conditions is investigated.

SCR Base Case

- ID 0.254 m (10 in)
- WT 0.03 m
- Top hang-off angle 15 deg
- Riser length 3000 m
- Mesh length 4 m
- Vessel offset 0 m, mean position
- Drag coefficient $C_d$ 1.0
- Inertia coefficient $C_m$ 2.0
- Transverse soil stiffness 10 kPa
- Normal soil stiffness 600 kPa

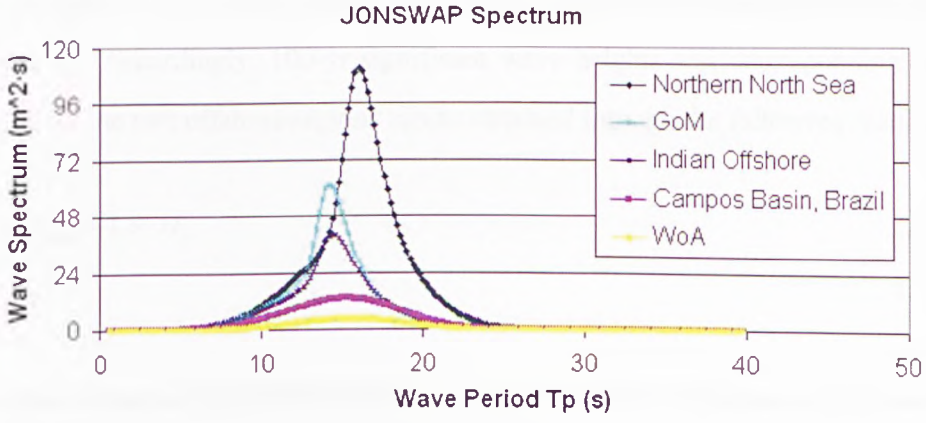


**Figure 3.5.40** 3 Parameter JONSWAP Spectra for Wave Conditions of Various Offshore Regions.

**Table 3.5.16** Wave Conditions of Various Offshore Regions.

| Case | Significant Wave Height $H_s$ (m) | Corresponding wave peak period $T_p$ (s) | Peakedness Factor $\gamma$ | Offshore Region |
|---|---|---|---|---|
| 1 | 4.6 | 15.6 | 1.0 | *West of Africa (Hogg, Harte, and Grealish, 2003) |
| 2 | 7.8 | 15.3 | 1.0 | Campos Basin, Brazil (Keppel FELS Limit, 2007) |
| 3 | 10.9 | 14.4 | 2.08 | *Indian Offshore (Patel, Kumar, Master, and Karunakaran, 2001) |
| 4 | 12.2 | 14.2 | 2.93 | Gulf of Mexico (Petruska, Zimmermann, Krafft, Thurmond, and Duggal, 2002) |
| 5 | 15.5 | 16 | 2.93 | Northern North Sea (Karunakaran, Meling, Kristoffersen, and Lund, 2005) |

where peakedness factor $\gamma$ is as defined in equation B.1.1.

Note that the 100-yr design wave heights and corresponding wave periods for West of Africa and Indian Offshore provided in the papers respectively were the regular wave heights $H_r$ (i.e. maximum wave height $H_{max}$) and corresponding regular wave periods $T_r$. Accordingly, 100-yr significant wave heights and corresponding wave periods for the two offshore regions can be obtained through the following relations:

$$H_r = H_{max} = 1.9 \cdot H_s \tag{3.5.8}$$

$$T_r = T_p \tag{3.5.9}$$

Maximum dynamic von Mises stresses for various offshore regions are compared in Table 3.5.17 and Figure 3.5.41. It is seen that the wave conditions of Campos Basin, WoA and Indian Offshore are relatively mild while the wave conditions of NNS is far much harsher than the other regions. With a same SCR design model, the maximum dynamic von Mises stress in NNS exceeded that in GoM, Indian Offshore,

Campos Basin, and WoA by 0.67, 2.26, 4.24, and 6.62 times respectively. The harsh environment can really affect the riser response greatly which makes feasible SCR design in mild environments unfeasible.

**Table 3.5.17** Sensitivity of Maximum Dynamic von Mises Stress to Various Offshore Regions.

| Offshore Region | Dynamic (MPa) | Utilisation Ratio (Maximum Stress / Yield Stress) |
|---|---|---|
| West of Africa (WoA) | 86.51 | 0.16 << 0.8 |
| Campos Basin, Brazil | 125.80 | 0.23 << 0.8 |
| Indian Offshore | 201.80 | 0.48 < 0.8 |
| Gulf of Mexico (GoM) | 395.10 | 0.72 < 0.8 |
| Northern North Sea (NNS) | 658.80 | 1.20 >> 0.8 |

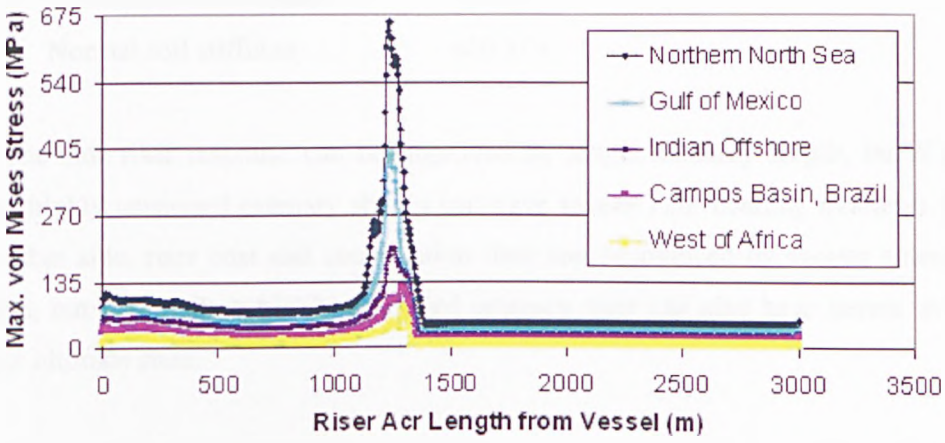


**Figure 3.5.41** Sensitivity of Maximum Dynamic von Mises Stress Envelope to Various Offshore Regions.

**h) Sensitivity to Riser Length**

A sensitivity analysis of riser response to the riser length is performed.

SCR Base Case

- ID 0.254 m (10 in)
- WT 0.03 m
- Top hang-off angle 15 deg
- *Riser length* *1500, 1750, 2000, 2250, 2500, 2750, and 3000 m*
- Mesh length 4 m
- Vessel offset 0 m, mean position
- Drag coefficient $C_d$ 1.0
- Inertia coefficient $C_m$ 2.0
- Transverse soil stiffness 10 kPa
- Normal soil stiffness 600 kPa

On one side riser response can be improved by longer catenary length, but if too long, highly tensioned catenary shapes can have severe TDP bending moments. On the other side, riser cost and computation time can be reduced by shorter catenary length, but if too short, highly tensioned catenary riser can also have severe stress under ultimate state.

Maximum static and dynamic von Mises stresses are compared in Table 3.5.18 and Figure 3.5.42 ~ 3.5.44. The riser length was varied from 1500 to 3000 m but the von Mises stress distribution along the riser for both static and dynamic loadings remained almost the same which means the 1500 m length of the riser of a 3000 m long SCR on the seabed near the bottom end has nearly no effect on the overall riser response for a mean vessel position. However, the maximum dynamic von Mises stresses for riser length as short as 1500 m and as long as 3000 m were both higher than the risers with length between them. 1 h ULS check for both near and far vessel

positions were executed for riser lengths 1500, 2000, and 3000 m and results are compared in Table 3.5.19 and Figure 3.5.45 and 3.5.46. It is shown that the stress levels along the risers were similar for all three cases and three vessel positions except the dynamic von Mises stress of 1500 m long riser at far vessel position was much higher than the other two risers. Therefore, the 2000 m and 3000 m long risers can be considered to have similar response under current loading conditions, and to lower computation cost the riser length can be reduced to 2000 m long.

**Table 3.5.18** Sensitivity of Maximum von Mises Stress to Riser Lengths 1500, 1750, 2000, 2250, 2500, 2750, and 3000 m.

| Riser Length (m) | Static (MPa) | Dynamic (MPa) |
|---|---|---|
| 1500 | 100.20 | 658.90 |
| 1750 | 100.20 | 654.20 |
| 2000 | 100.20 | 657.20 |
| 2250 | 100.30 | 656.50 |
| 2500 | 100.30 | 656.40 |
| 2750 | 100.30 | 655.80 |
| 3000 | 100.30 | 658.80 |

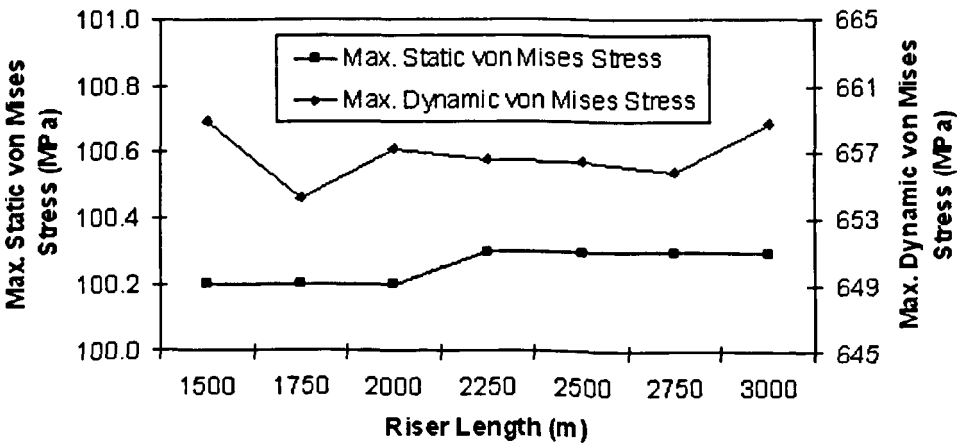


**Figure 3.5.42** Sensitivity of Maximum Static and Dynamic von Mises Stress to Riser Lengths 1500, 1750, 2000, 2250, 2500, 2750, and 3000 m.

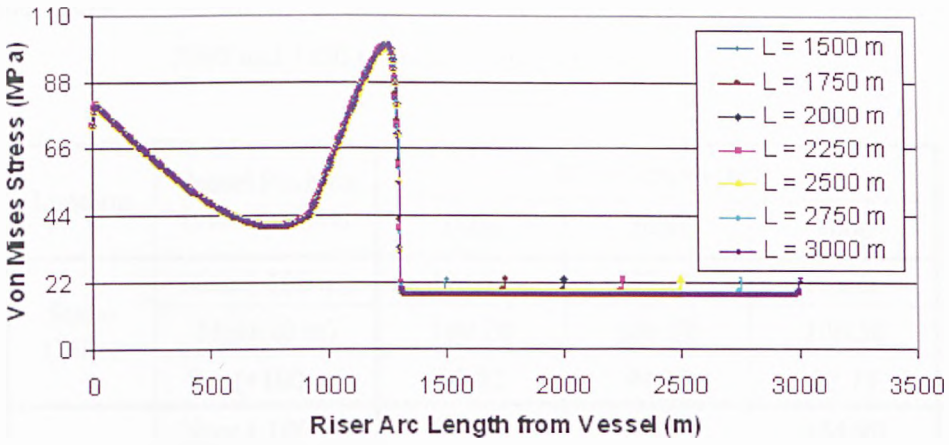


**Figure 3.5.43** Sensitivity of Static von Mises Stress to Riser Lengths 1500, 1750, 2000, 2250, 2500, 2750, and 3000 m.

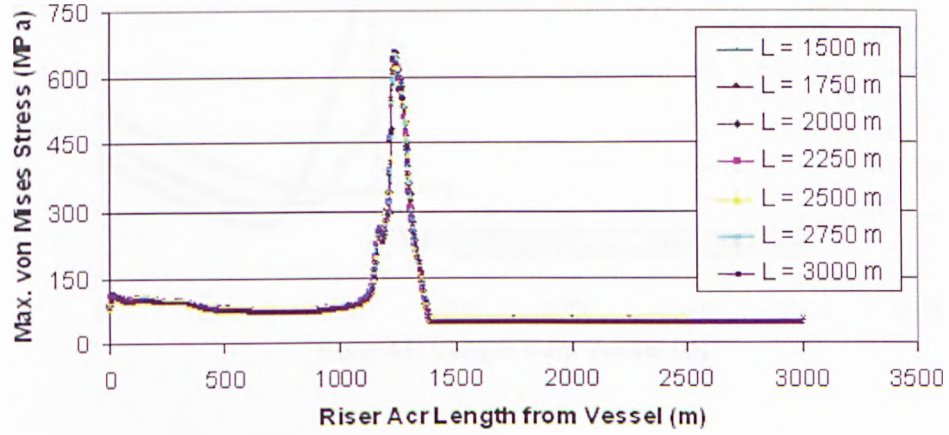


**Figure 3.5.44** Sensitivity of Maximum Dynamic von Mises Stress Envelope to Riser Lengths 1500, 1750, 2000, 2250, 2500, 2750, and 3000 m.

**Table 3.5.19** Sensitivity of Maximum von Mises Stress to Riser Lengths 1500, 2000 and 3000 m under 1 h ULS Check.

| Loading | Vessel Position (vessel offset) | Riser Length (m) | | |
|---|---|---|---|---|
| | | 1500 | 2000 | 3000 |
| Static (MPa) | Near (-100 m) | 173.50 | 173.60 | 173.60 |
| | Mean (0 m) | 100.20 | 100.20 | 100.30 |
| | Far (+100 m) | 97.82 | 97.79 | 97.75 |
| Dynamic (MPa) | Near (-100 m) | 563.80 | 565.50 | 564.90 |
| | Mean (0 m) | 658.90 | 657.20 | 658.80 |
| | Far (+100 m) | 969.40 | 768.00 | 754.50 |

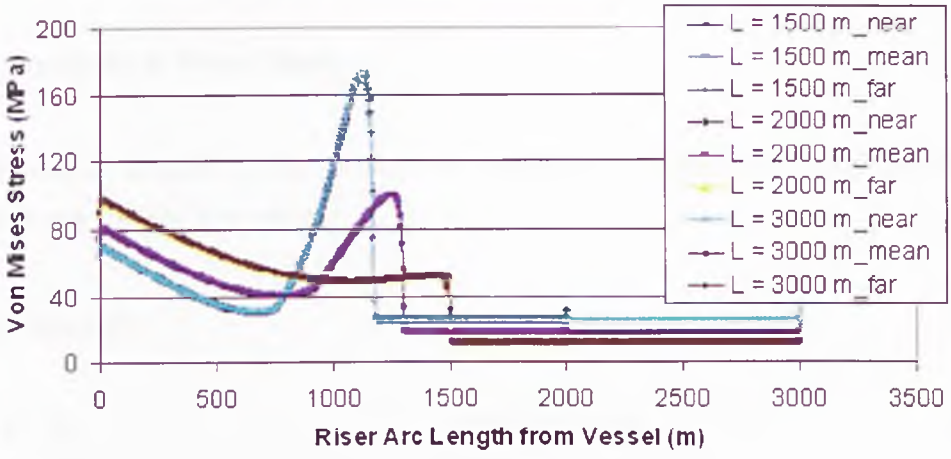


**Figure 3.5.45** Sensitivity of Static von Mises Stress to Riser Lengths 1500, 2000 and 3000 m under 1 h ULS Check.

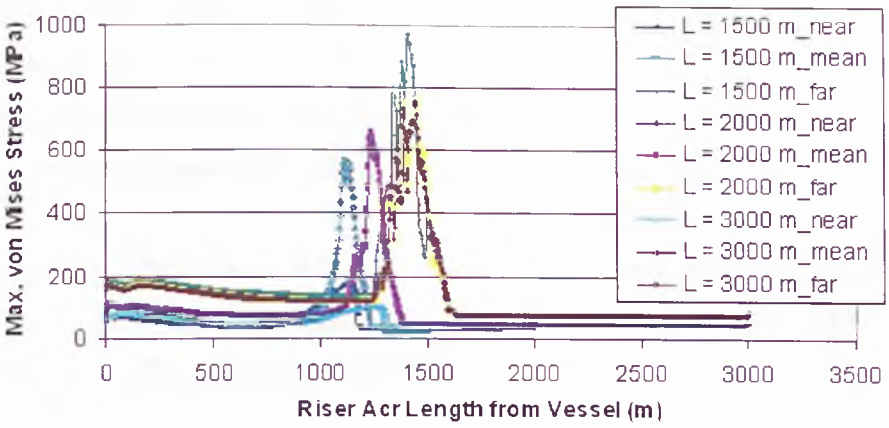


**Figure 3.5.46** Sensitivity of Maximum Dynamic von Mises Stress Envelope to Riser Lengths 1500, 2000 and 3000 m under 1 h ULS Check.

**i) Sensitivity to Water Depth**

A sensitivity analysis of riser response to various water depths for a range between 500 m and 3000 m is conducted.

SCR Base Case

- ID 0.254 m (10 in)
- WT 0.03 m
- Top hang-off angle 15 deg
- Mesh length 4 m
- Vessel offset 0 m, mean position
- Drag coefficient $C_d$ 1.0
- Inertia coefficient $C_m$ 2.0
- Transverse soil stiffness 10 kPa
- Normal soil stiffness 600 kPa
- Offshore region NNS
- *Water depth* *500, 800, 1000, 1500, 2000, 2500, and 3000 m*

Overall static von Mises stress and maximum dynamic von Mises stress envelope for various water depths are shown in Figure 3.5.47 and 3.5.49. The maximum static and dynamic von Mises stresses at top hang-off area and TDA respectively for various water depths are compared in Table 3.5.20 and Figure 3.5.48 and 3.5.50.

**Table 3.5.20** Sensitivity of Maximum von Mises Stress of Top Hang-off Area and TDA Respectively to Water Depths 500, 800, 1000, 1500, 2000, 2500, and 3000 m.

| Water Depth (m) | Static (MPa) | | Dynamic (MPa) | |
|---|---|---|---|---|
| | Top Hang-off Area | TDA | Top Hang-off Area | TDA |
| 500 | 50.80 | 169.00 | 85.48 | 597.40 |
| 800 | 67.33 | 117.70 | 94.59 (+10.66%) | 638.30 (+6.85%) |
| 1000 | 80.59 | 100.20 | 113.30 (+19.78%) | 657.20 (+2.96%) |
| 1500 | 115.40 | 81.47 | 133.00 (+17.39%) | 727.10 (+10.64%) |
| 2000 | 151.40 | 75.74 | 170.80 (+28.42%) | 738.40 (+1.55%) |
| 2500 | 188.00 | 75.32 | 217.90 (+27.58%) | 691.60 (–6.34%) |
| 3000 | 224.30 | 78.50 | 260.90 (+19.73%) | 769.20 (+11.28%) |

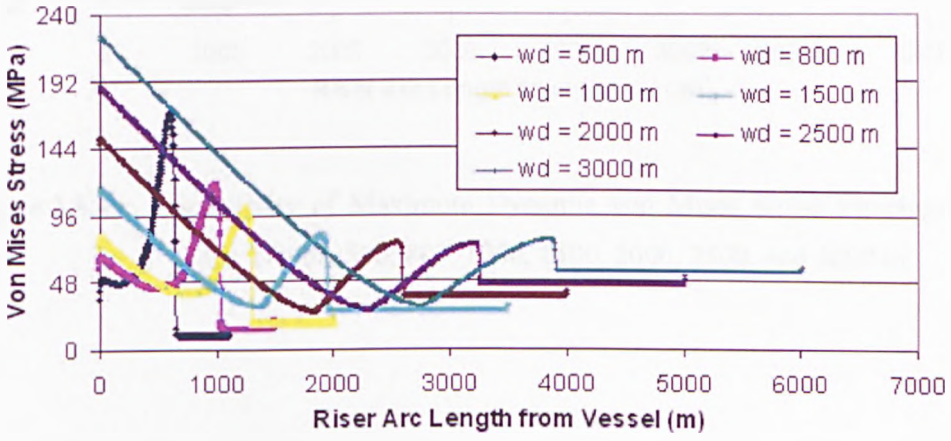


**Figure 3.5.47** Sensitivity of Static von Mises Stress to Water Depths 500, 800, 1000, 1500, 2000, 2500, and 3000 m.

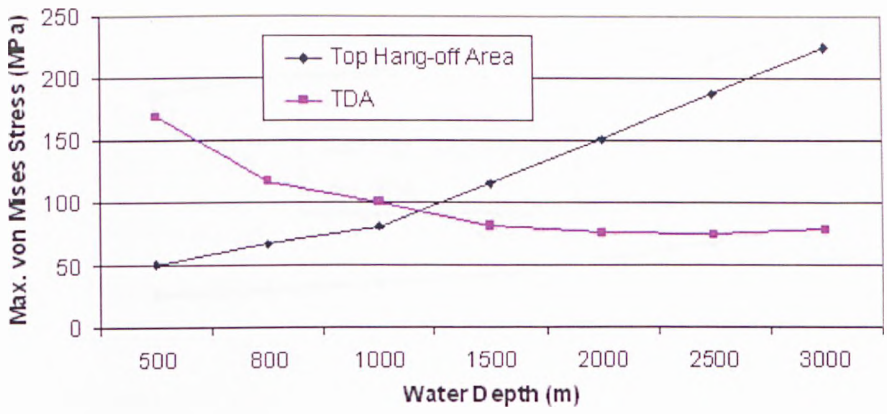


**Figure 3.5.48** Sensitivity of Maximum Static von Mises Stress of Top Hang-off Area and TDA Respectively to Water Depths 500, 800, 1000, 1500, 2000, 2500, and 3000 m.

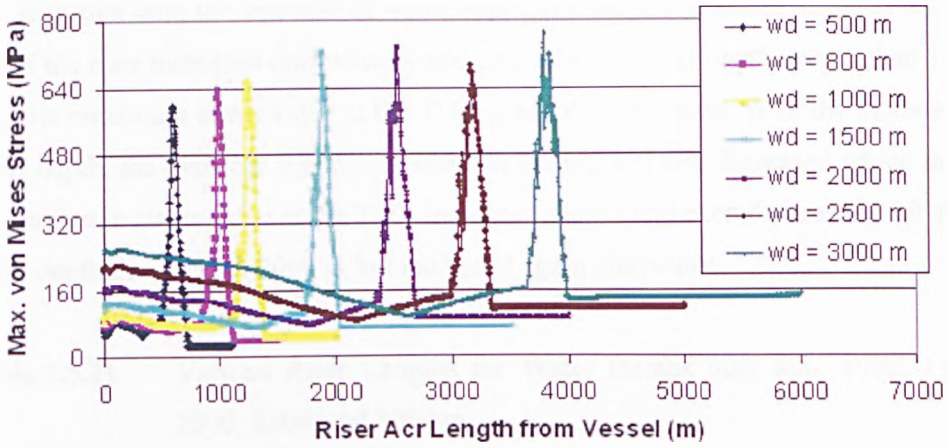


**Figure 3.5.49** Sensitivity of Maximum Dynamic von Mises Stress Envelope to Water Depths 500, 800, 1000, 1500, 2000, 2500, and 3000 m.

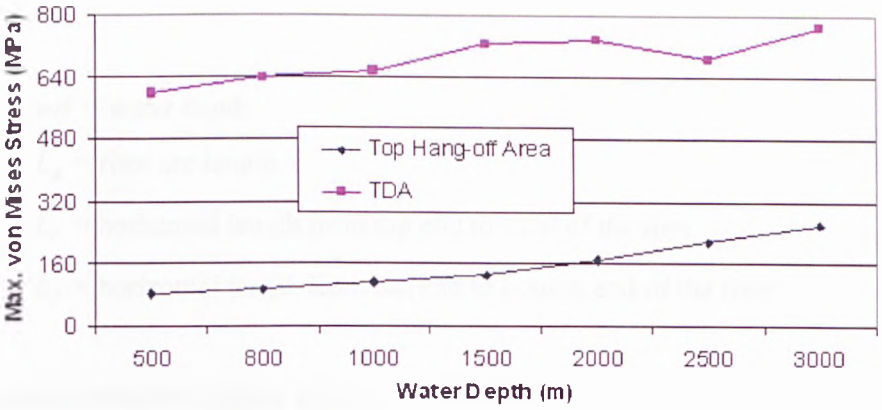


**Figure 3.5.50** Sensitivity of Maximum Dynamic von Mises Stress of Top Hang-off Area and TDA Respectively to Water Depths 500, 800, 1000, 1500, 2000, 2500, and 3000 m.

It is seen that with the increase of water depth, the static von Mises stress at the top end of the riser increased dramatically and peaked after water depth deeper than 1000 m while maximum stress value at the TDA gradually decreased. With the increase of water depth, the dynamic von Mises stress at the top end also increased which made the maximum stress value at the TDA increased slowly and even decreased a bit after water depth deeper than 2000 m but increased again afterwards.

**Table 3.5.21** Various Riser Lengths for Water Depths 500, 800, 1000, 1500, 2000, 2500, and 3000 m.

| $wd$ (m) | $L_A$ (m) | $L_T$ (m) | $L_T/L_A$ | $L_E$ (m) | $L_E/L_A$ |
|---|---|---|---|---|---|
| 500 | 1100 | 403.98 | 0.37 | 820 | 0.75 |
| 800 | 1500 | 627.97 | 0.42 | 1044 | 0.70 |
| 1000 | 2000 | 794.94 | 0.40 | 1427 | 0.71 |
| 1500 | 3500 | 1130.78 | 0.32 | 2131 | 0.61 |
| 2000 | 4000 | 1493.74 | 0.37 | 2834 | 0.71 |
| 2500 | 5000 | 1853.60 | 0.37 | 3538 | 0.71 |
| 3000 | 6000 | 2207.43 | 0.37 | 4238 | 0.71 |

where

$wd$ = water depth

$L_A$ = riser arc length

$L_T$ = horizontal length from top end to TDP of the riser

$L_E$ = horizontal length from top end to bottom end of the riser

Illustration is shown in Figure 3.5.51.

It can be derived from Table 3.5.21 that a proper proportions of $L_T$ to $L_A$ and $L_E$ to $L_A$ are approximately 0.37 and 0.70 respectively, which can be applied as a starting point for SCR structural preliminary design.

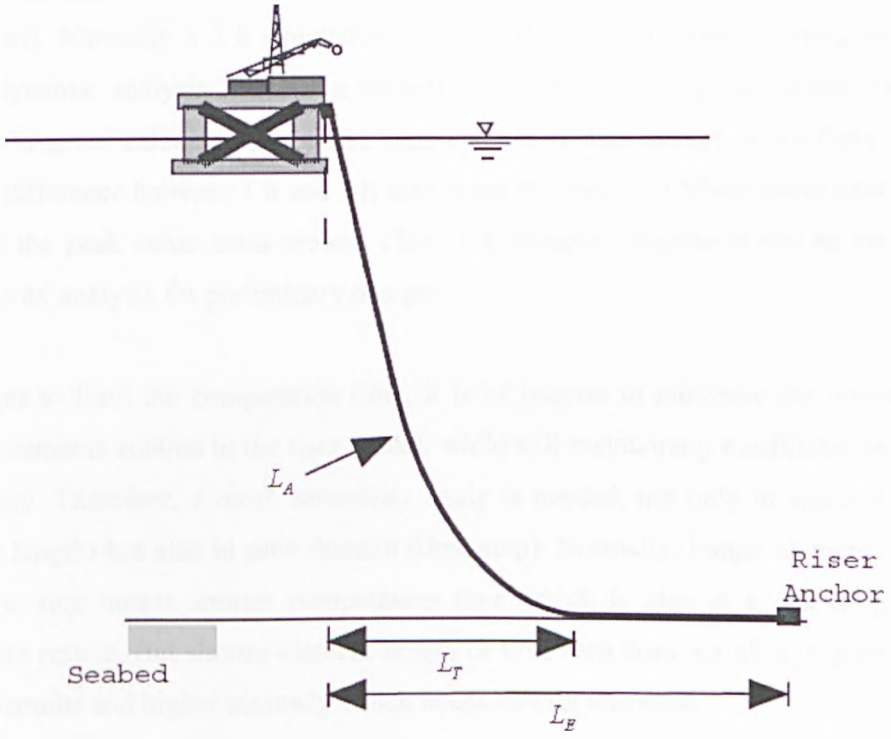


**Figure 3.5.51** Riser Length Definition.

## 3.6 Discussion and Conclusion

Many problems are encountered through inadequate assessment of modelling parameters. Therefore, a comprehensive sensitivity analysis of extreme loading conditions was carried out to optimise catenary length and geometry for an attempt on a feasible design of an SCR connected to a semi-submersible in NNS.

Firstly, before any structural modelling, much care and patience must be exercised in order to obtain reliable results. Sensitivity analyses based on a same random model need to be conducted to ensure that modelling features such as mesh length, time step size, and dynamic simulation duration are suitable. Values of mass and stiffness damping, if used, must also be carefully selected.

Underestimation of the time required to produce meaningful results will cause problems. Normally a 3 h simulation is required to give a proper convergence for riser dynamic analysis. But for a several thousand meter long deepwater riser, it means hours of calculation time and huge amount of data storage. Since there is not much difference between 1 h and 3 h maximum dynamic von Mises stress envelopes except the peak value areas around TDA, 1 h dynamic simulation can be used for sensitivity analysis for preliminary design.

In order to limit the computation time, it is of interest to minimise the number of finite elements applied in the riser model, while still maintaining a sufficient level of accuracy. Therefore, a mesh sensitivity study is needed, not only in space domain (mesh length) but also in time domain (time step). Normally, longer element length or time step means shorter computation time which is also at a risk of getting unstable results. But shorter element length or time step does not always guarantees stable results and higher accuracy which needs careful attention.

The global Rayleigh damping model was used during SCR dynamic simulation and the mass proportional damping is usually omitted while the stiffness damping is dependent on the value of $a_2$ (see equation 3.5.1) and also the wave frequency or

period. For a reasonable damping of 0.5%, $a_2$ = 0.015 is an appropriate stiffness damping coefficient for riser dynamic analysis.

After the modelling features being carefully selected, sensitivity study on SCR design parameters can then be carried out under extreme environmental loadings.

As for riser dynamic analysis, wave load is the major concerned loading condition. Several wave spectrum formulations are commonly used for offshore engineering and available in DNV DeepC while JONSWAP spectrum is more suitable for North Sea offshore region.

The SCR is generally highly stressed near TDP at seabed. Extreme loading results in an increase in the stress level, which may become unacceptable in extreme conditions. Steps can be taken to improve response by optimising riser top hang-off angle, internal diameter (ID), wall thickness (WT), and hydrodynamic drag coefficient $C_d$. The effect of the variation of these parameters on the riser response is compared in the following Table 3.6.1.

**Table 3.6.1** Effect of the Variation of Top Hang-off Angle, ID, WT, and $C_d$ on the Riser Response.

| Design Parameter | Increase by Each Unit | Static Response (%) | Dynamic Response (%) |
|---|---|---|---|
| Top Hang-off Angle | + 1 deg | – 8.14 | + 2.54 |
| ID (0.03 m WT) | + 1 in (0.0254 m) | + 5.62 | – 2.66 |
| WT (10 in ID) | + 0.01 m | – 0.33 | – 3.03 |
| $C_d$ | + 0.1 | – 0.20 | + 8.27 |

It is seen from the table that decrease the top hang-off angle by each 1 deg or increase the ID and WT by each 1 in (0.0254 m) and 0.01 m respectively can reduce the maximum dynamic stress level by similar amount. As for hydrodynamic drag coefficient, although the flow regime was getting less critical with increase of drag

coefficient, the stress level of the riser was becoming more critical and even with 0.1 variation of the coefficient, the average change in stress level could be as high as 8.27%. Therefore, for every specific offshore region, the typical flow regime around the area should be appropriately defined for the calculation of Re value and careful determination of drag coefficient.

Riser length is another important parameter for SCR design. Longer length may lower the riser dynamic stress level but will increase the computation cost and also riser cost in terms of both materials and installation time while shorter length is an opposite case. Sensitivity analysis is needed to obtain an optimised riser length with a balance between dynamic response and computation and riser cost. The proportions of horizontal length from top end to TDP to riser arc length ($L_T/L_A$) and horizontal length from top end to bottom end to riser arc length ($L_E/L_A$) are suggested to be 0.76 and 0.70 respectively as a starting point for SCR preliminary design.

Unlike the parameters above, soil stiffness has little influence on the maximum dynamic von Mises stress, but element length may need to be reduced to get stable results when soil stiffness becomes larger.

In this chapter, a same SCR design model has been compared in different offshore regions with various wave loading conditions and different water depth. The SCR is generally highly stressed near the TDP at the seabed. Extreme loading results in an increase in the stress level, which may become unacceptable in extreme conditions in offshore regions with harsh environment. The harsh environment had a significant impact and caused an applicable riser in mild environments into severe dynamic response condition which needed mitigation methods for improvement to achieve acceptable response.

The dynamic response of an SCR is highly influenced by vessel motion, particularly heave motions at the vessel connection point. When water depth gets deeper, actually the vessel motion on the water surface will have less effect on the TDA response on the seabed. Therefore, deeper water depth has a bigger effect on the top hang-off area

of the riser rather than the TDA which made the maximum stress level on TDA increase more slowly than the top hang-off area. Hence with the increase of water depth, attention should be raised for the design of riser top termination.

The significance effect of all the parameters studied on the riser response and computation cost is shown in Table 3.6.2.

**Table 3.6.2** Significance Effect of Parameters on the Riser Response and Computation Cost.

| Parameter | | Effect on Riser Response | Effect on Computation Cost |
|---|---|---|---|
| Analysis | Dynamic Simulation Duration | Significant | Significant |
| | Structural Damping | Minor Significance | Insignificant |
| | Mesh Length | Significant | Significant |
| | Dynamic Simulation Time Step | Minor Significance | Significant |
| Design | Wave Spectrum Formulation | Significant | Insignificant |
| | Top Hang-off Angle | Significant | Insignificant |
| | Internal Diameter | Significant | Insignificant |
| | Riser Wall Thickness | Significant | Insignificant |
| | Hydrodynamic Drag Coefficient $C_d$ | Significant | Insignificant |
| | Normal Soil Stiffness | Minor Significance | Insignificant |
| | Wave Conditions | Significant | Insignificant |
| | Riser Length | Minor Significance | Insignificant |
| | Water Depth | Significant | Insignificant |

Chapter 4

# Deepwater SCR Strength Design and Analysis with Weight-Optimised Coating

## 4.1 Introduction

The maximum dynamic von Mises stress envelope for a mean vessel offset extreme wave load case is shown in Figure 4.1.1, and this is typical of SCR response. Von Mises stresses peak sharply at the seabed TDP due to the high bending in this region which is a critical design point for SCRs. When SCRs move to harsh environment and deepwater mitigations need to be applied to improve the riser response at TDP for service feasibility.

Previous studies for SCR applications on other floating hosts indicated that a heavy section in the sag-bend region and light section along the touch down region improves response. Improvements can be achieved by increasing coating thickness or changing the type of coating used in the affected area. To improve the response of the SCR on a semi-submersible in both strength and fatigue performance, an optimisation study on SCR configuration with weight-optimised coating is carried

out. The general arrangement used as the base case for this study is shown in Figure 2.1.6.

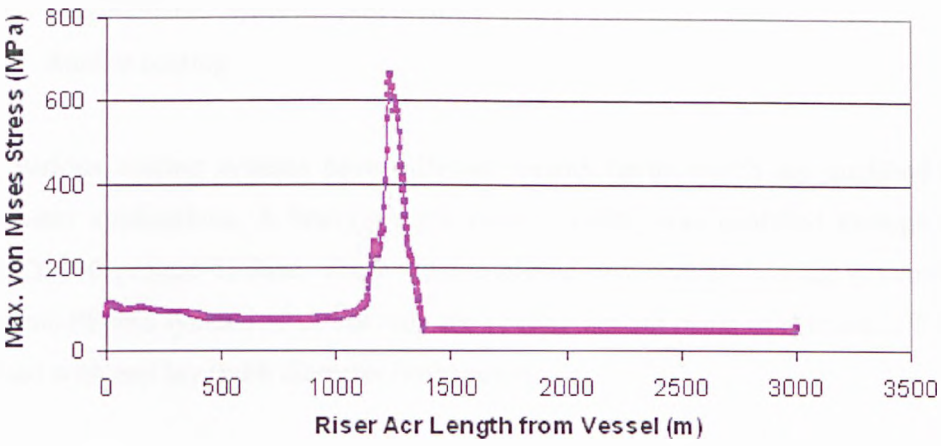


**Figure 4.1.1** Typical Maximum Dynamic von Mises Response Envelope of an SCR.

## 4.2 Design Details of SCR Coatings

Polymeric external coatings are generally used on flow lines and risers for:

- Corrosion protection
- Mechanical protection
- Thermal protection

However, coatings can also be applied for weight optimisation by varying its density and thickness.

In some cases a single material provides all of these functions, whilst in other concepts, multilayer systems are used, where different layers provide the various functions.

The most common coating systems used in the oil and gas industry are:

- Multilayer polypropylene (PP) or polyethylene (PE)
- Polyurethane / syntactic polyurethane (PU)
- Rubber coating

The various coating systems have different density limits which are qualified for deepwater applications. A heavy weight rubber coating was qualified through the DEMO2000 project Ti-Rise. There exist qualified low density coating systems of syntactic PP and syntactic PU, but only the coating system made of syntactic PP can be used with reel lay (with diameter limitations).

Thermal insulation is not always a requirement hence other means of weight optimisation exist. Additional weight can be achieved by increasing the steel wall thickness, and buoyancy can be achieved by attaching buoyancy modules. In the present study, weight optimisation was accomplished by using external coating due to its simplicity during installation.

Some details about the selected coating systems are given in the Appendix C.

## 4.3 Proposing an Approach to Optimising SCR Coatings

An initial weight-optimised SCR configuration is adopted based on the use of heavy ≥800 kg/m$^3$ and light 670 kg/m$^3$ density coatings along the length to vary the weight of the riser at key locations. To obtain an acceptable configuration, a total of 12 configurations which vary the light and heavy section lengths and thicknesses are evaluated for strength and fatigue response, among which a configuration is found to satisfy both fatigue and strength criteria. A comparison between the weight-optimised configuration and the conventional SCR is given in Figure 4.3.5 and 4.3.6.

SCR Base Case

Based on the former parametric study for design of SCRs in Chapter 3, the following parameters were chosen:

- ID 0.254 m (10 in)
- WT 0.03 m
- Top hang off angle 15 deg
- Riser Length 3000 m
- Mesh length 4 m
- Vessel offset 0 m, mean position

Then riser configurations were developed with varying weight of cross-sections along the length. The densities for various are as follows:

- Normal Coating (N) 800 kg/m$^3$ (normally 750 ~ 950 kg/m3)
- Light Coating (L) 670 kg/m$^3$ (normally 650 ~ 700 kg/m3)
- Heavy Coating (H) 2800 kg/m$^3$
- Coating Thickness (CT) 0.075 m (75 mm)

To obtain an acceptable configuration, dozens of configurations with various lengths and arrangements of light and heavy sections, based on the results by Karunakaran, Meiling, Kristoffersen, and Lund (2005) were evaluated for strength response. Among these, twelve configurations (A ~ L) were compared for their improving effect on SCR strength response in Table 4.3.1 and Figure 4.3.2 ~ 4.3.4. A typical weight-optimised SCR configuration is shown in Figure 4.3.1.

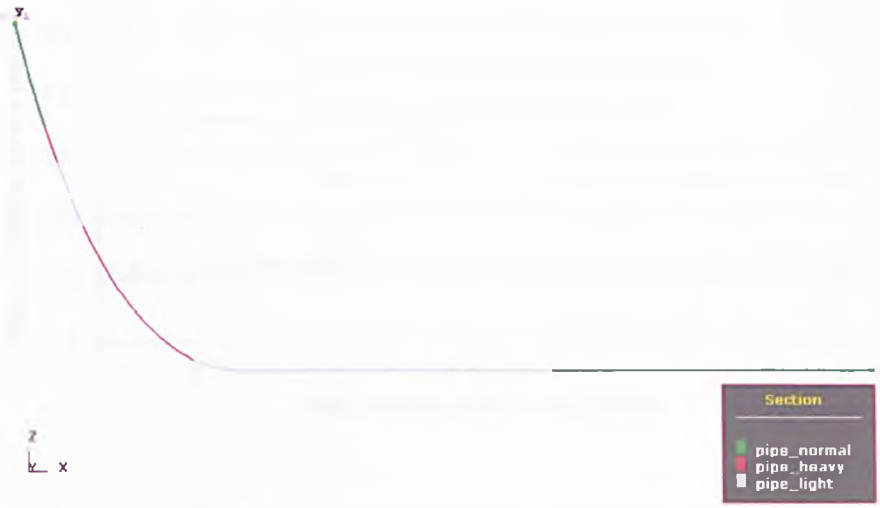


**Figure 4.3.1** Typical Weight-Optimised SCR Configuration.

**Table 4.3.1** Maximum von Mises stresses of various configurations with Riser Arc Length 3000 m.

| Case | Up N (m) | Straight H (m) | Straight L (m) | Sag H (m) | TDA L (m) | Bottom N (m) | Maximum Dynamic von Mises Stress (MPa) |
|---|---|---|---|---|---|---|---|
| A | 300 | 100 | 200 | 500 | 800 | 1100 | 288.30 |
| B | 300 | 100 | 200 | 400 | 900 | 1100 | 360.00 |
| C | 300 | 100 | 200 | 600 | 700 | 1100 | 352.70 |
| D | 300 | 100 | 200 | 550 | 750 | 1100 | 256.30 |
| E | 300 | 100 | 200 | 550 | 850 | 1000 | 256.30 |
| F | 300 | 100 | 200 | 550 | 950 | 900 | 256.20 |
| G | 300 | 100 | 200 | 550 | 1050 | 800 | 256.20 |
| H | 300 | 100 | 200 | 550 | 1150 | 700 | 256.20 |
| I | 300 | 100 | 200 | 550 | 1250 | 600 | 256.20 |
| J | 200 | 200 | 200 | 550 | 950 | 900 | 258.70 |
| K | 300 | 200 | 100 | 550 | 950 | 900 | 262.10 |
| L | 300 | 100 | 100 | 650 | 950 | 900 | 258.40 |

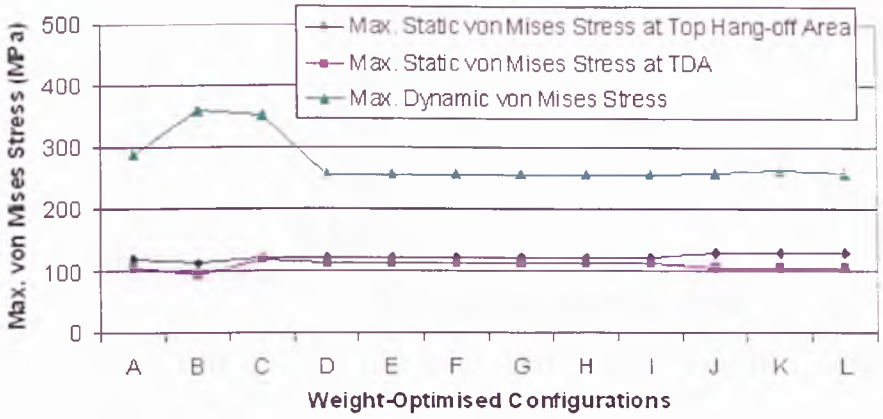


**Figure 4.3.2** Maximum Static and Dynamic von Mises Stresses for Weight-Optimised Configurations A ~ L with Riser Arc Length 3000 m.

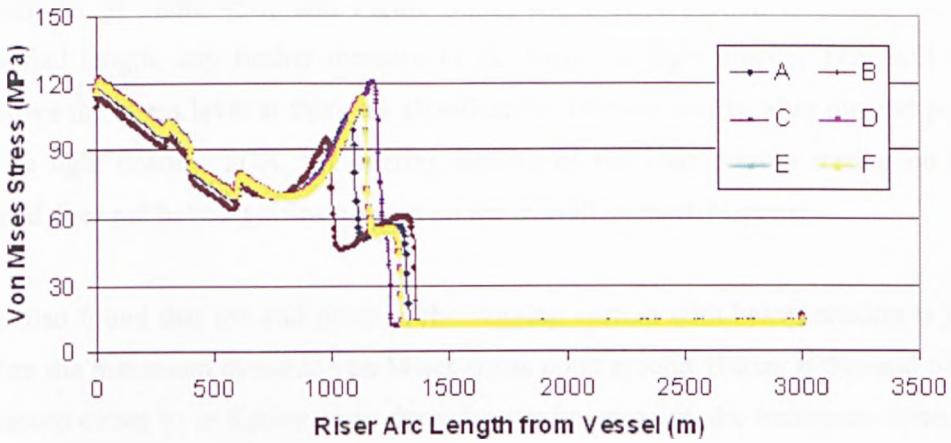


**Figure 4.3.3** Static von Mises Stresses for Weight-Optimised Configurations A ~ F with Riser Arc Length 3000 m.

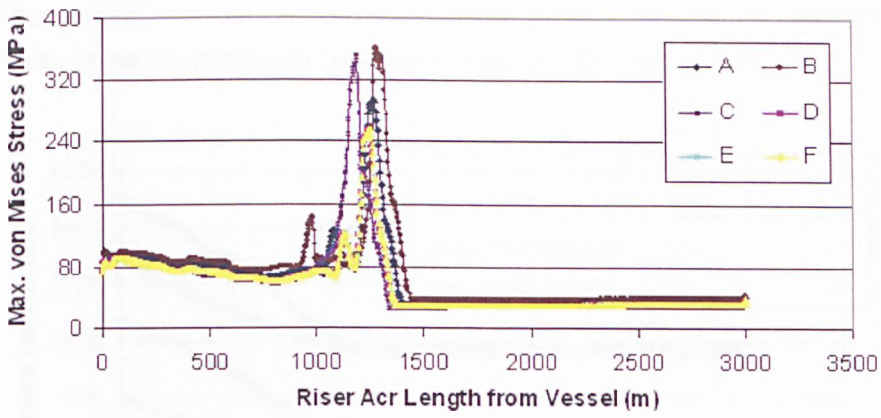


**Figure 4.3.4** Maximum Dynamic von Mises Stress Envelopes for Weight-Optimised Configurations A ~ F with Riser Arc Length 3000 m.

As shown in Table 4.3.1 and Figure 4.3.2, when TDA section is longer than a specified length, any further increase in the length of light coating TDP will not improve the stress level at this area significantly. In other words, after the end point of the light coating TDA, the coating density of the riser portion resting on the seabed does not have significant effect on the overall strength response.

It is also found that the end point of the sagging section with heavy coating is just before the maximum dynamic von Mises stress point around 100 m. If this end point is moved closer to or further away from the maximum point, the maximum dynamic von Mises stress will increase.

The severity of environmental conditions and vessel motions results in highly dynamic risers. Tension fluctuations are large and in extreme load cases low tension or even compression can occur near the TDP. Figure 4.3.5 shows the distribution of effective (axial) force along the length of the riser depicting a very small amount of compression on the seabed for weight-optimised configuration F while the compression level is much higher for the conventional riser. However, the top tension of the weight-optimised riser is much higher than the conventional riser which needs attention for riser top termination design. Figure 4.3.6 shows the comparison of maximum and minimum bending moment along the riser between

weight-optimised riser and conventional riser. It is seen that weight-optimised coating can lower the maximum bending moment at TDA remarkably.

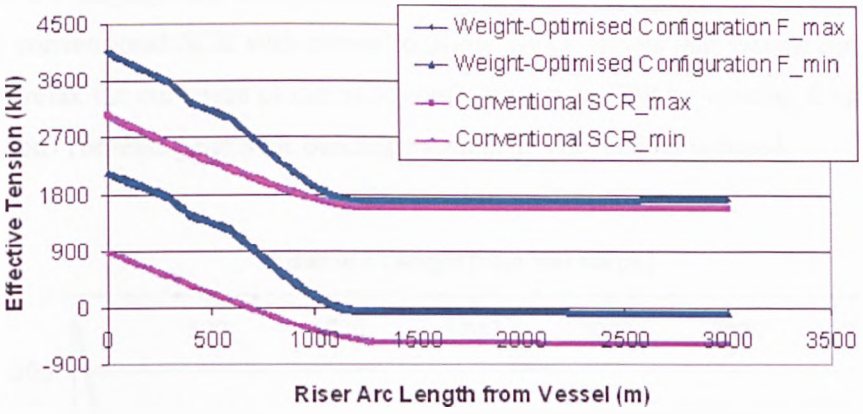


**Figure 4.3.5** Maximum and Minimum Effective Tension Envelopes $T_e$ for Weight-Optimised Configuration F and Conventional SCR with Riser Arc Length 3000 m.

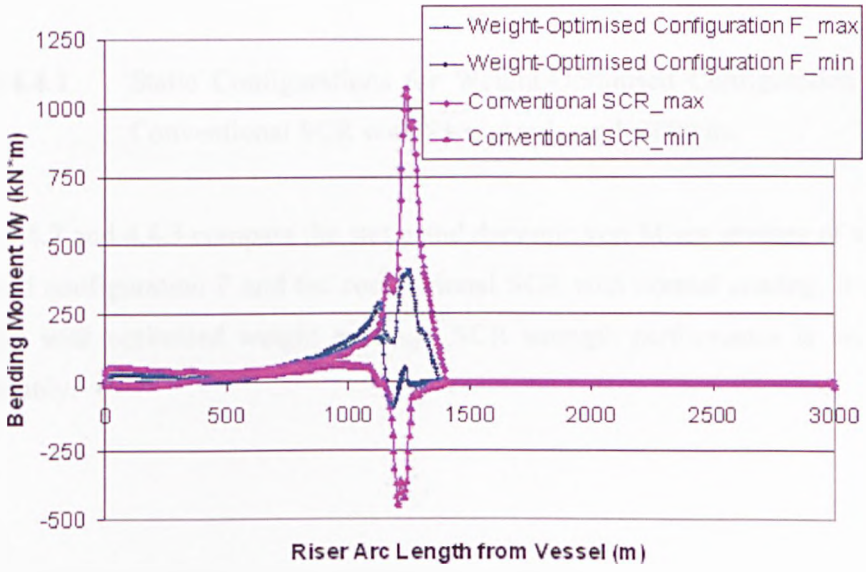


**Figure 4.3.6** Maximum and Minimum Bending Moment $M_y$ Envelopes for Weight-Optimised Configuration F and Conventional SCR with Riser Arc Length 3000 m.

## 4.4 Modified Configuration of SCR

Figure 4.4.1 displays the static configurations of weight-optimised configuration F and the conventional SCR with normal coating, which shows that weight-optimised coatings relax the curvature of the SCR configuration at TDP by moving it up to the sag section. Therefore, the SCR bending moment at TDP can be reduced.

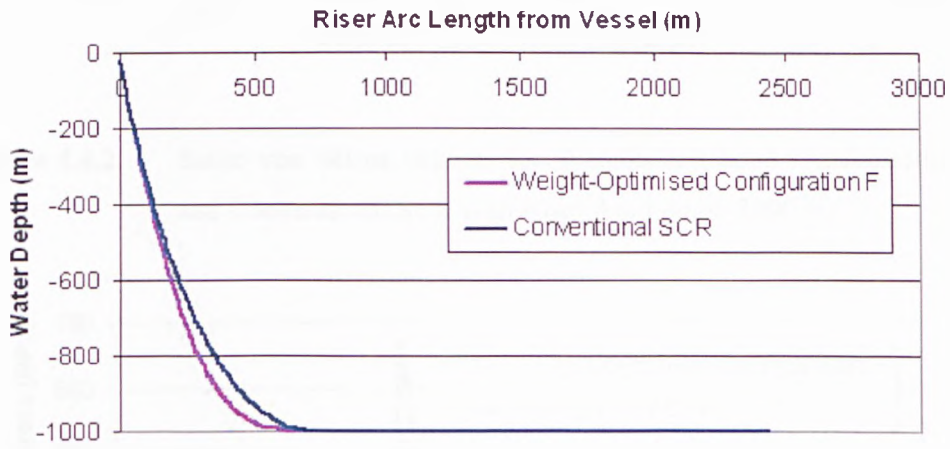


**Figure 4.4.1** Static Configurations for Weight-Optimised Configuration F and Conventional SCR with Riser Arc Length 3000 m.

Figure 4.4.2 and 4.4.3 compare the static and dynamic von Mises stresses of weight-optimised configuration F and the conventional SCR with normal coating. It can be seen that with optimised weight coatings, SCR strength performance is improved considerably.

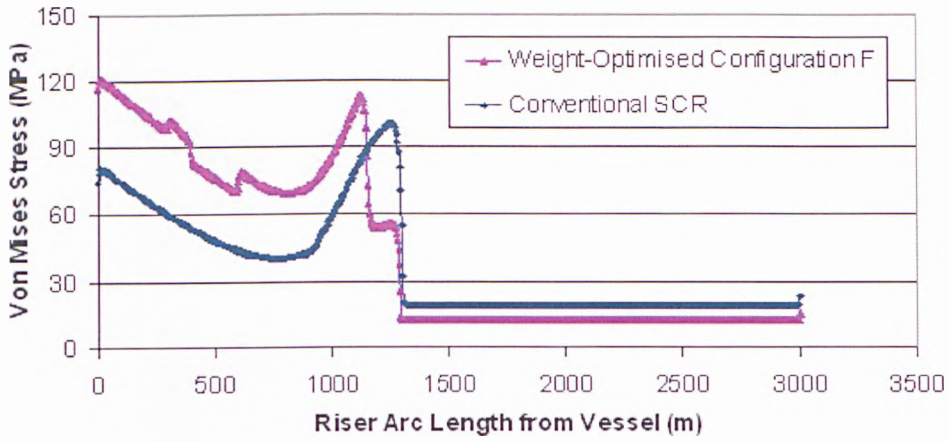


**Figure 4.4.2** Static von Mises stresses for Weight-Optimised Configuration F and Conventional SCR with Riser Arc Length 3000 m.

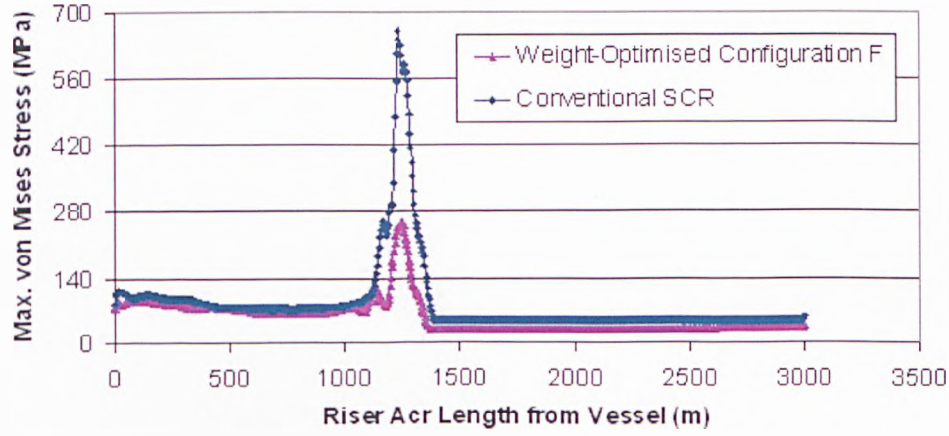


**Figure 4.4.3** Maximum Dynamic von Mises Stress Envelopes for Weight-Optimised Configuration F and Conventional SCR with Riser Arc Length 3000 m.

Being compared of the dynamic response performance, configuration F is chosen to be the base case for ULS and ALS check.

ULS & ALS Check

For ULS assessment, the dynamic simulation time normally needs to be three hours for convergence. Unfortunately, the maximum dynamic von Mises stress for near position (-100 m offset) was 618.40 MPa and its utilization was 1.12 which is far greater than the criteria 0.8.

From comparison in Table 4.3.1, it seems that there could be no better arrangement and distribution of weight coatings than configuration F to improve the overall dynamic response condition. However, up to now the thickness and density of coatings haven't been changed. What kind of role can they play?

SCR Base Case: Configuration F

Configuration F with various coating thicknesses and densities are studied for strength assessment (see Table 4.4.1 and Figure 4.4.4 ~ 4.4.5).

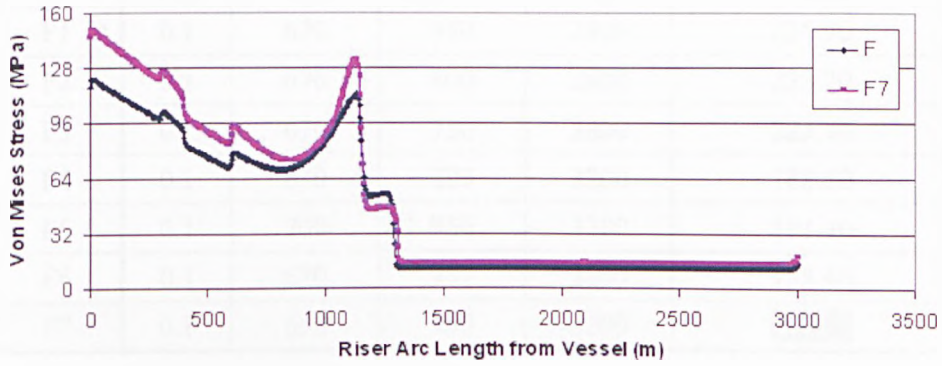


**Figure 4.4.4** Static von Mises Stresses for Configurations F and F7 with Riser Arc Length 3000 m.

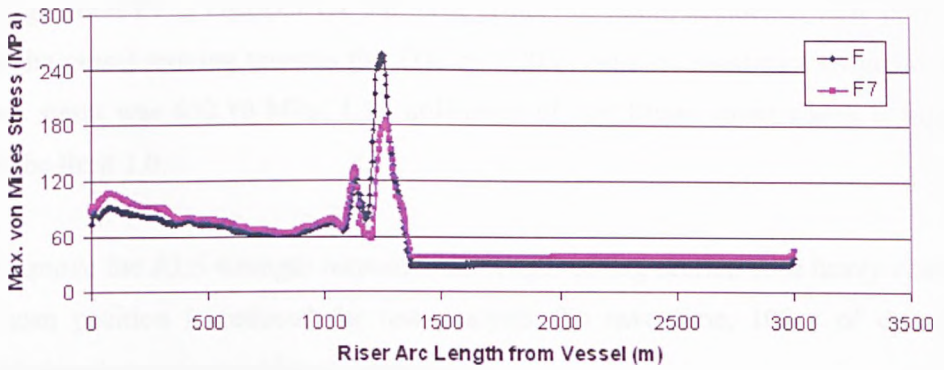


**Figure 4.4.5** Maximum Dynamic von Mises Stress Envelopes for Configurations F and F7 with Riser Arc Length 3000 m.

**Table 4.4.1** Maximum von Mises Stresses of Configuration F of Riser Arc Length 3000 m with Various Coating Thicknesses and Densities.

| Case | CT (m) | Coating Density ($kg/m^3$) | | | Maximum von Mises Stress (MPa) |
|---|---|---|---|---|---|
| | | L | N | H | |
| F | 0.075 | 670 | 800 | 2800 | 256.20 |
| F1 | 0.1 | 670 | 950 | 2800 | 225.90 |
| F2 | 0.1 | 670 | 800 | 2800 | 223.70 |
| F3 | 0.1 | 670 | 750 | 2800 | 225.90 |
| F4 | 0.1 | 670 | 800 | 3200 | 188.80 |
| F5 | 0.1 | 700 | 950 | 3200 | 191.40 |
| F6 | 0.1 | 670 | 950 | 3200 | 188.40 |
| F7 | 0.1 | 650 | 950 | 3200 | 185.90 |

As compared, configuration F with increased coating thickness and increased normal and heavy densities reduces the maximum dynamic von Mises stress by nearly 30% off. But it's still not for sure that whether it can pass ALS check or not. For near position, the vessel moves to the TDP by 100 m. This means that the end point of the sagging section with heavy coating is closer to the TDP (maximum von Mises stress point) by 100 m. This greatly increases the stress level of near position.

Configuration F7 is checked for the most critical position, accidental near position with the vessel moving towards the TDP by 120 m, and the maximum dynamic von Mises stress was 652.10 MPa, 1.19 utilization of von Mises stress which is bigger than the limit 1.0.

To improve the ALS strength response, the length of Sag section with heavy coating at mean position is reduced for test analysis. To save time, 100 s of dynamic simulation time is executed (see Table 4.4.2).

**Table 4.4.2** 100 s ALS Check for Various Configurations with Riser Arc Lengths 3000 m and 2000 m.

| Case | Sag Section Length (m) | TDA Section Length (m) | Accidental Near Position (MPa) | |
|---|---|---|---|---|
| | | | $L_A$ = 3000 m | $L_A$ = 2000 m |
| F7 | 550 | 950* | 344.0 | 343.7 |
| M | 500 | 1000 | 333.6 | / |
| N | 450 | 1050 | 112.0 | / |
| O | 480 | 1020 | 123.5 | / |
| P | 490 | 1010* | 205.6 | 205.5 |

Note that for arc length 2000 m riser, there is no BottomN part as shown in Table 4.3.1 and the TDAL lengths for configurations F7 and P are 850 m and 910 m respectively.

From Table 4.4.2 it is seen that reduced sagging section length with heavy coating can lower the maximum dynamic von Mises stress remarkably. Configuration N had the lowest stress level for accidental near position which means it may have much higher stress levels for other positions near mean position and may cause low fatigue life. So configuration P was chosen for further assessment. In addition, Configuration F and P had been checked also for riser arc length 2000 m and the results in Table

4.4.2 show that the overall stress level for riser length cases were similar and it was even a little better for shorter length 2000 m case.

Configuration P is performed for a full ALS check with a three-hour dynamic simulation time for both lengths. The results are shown in Table 4.4.3 and Figure 4.4.6 ~ 4.4.9. Both risers satisfied the requirements for ULS and ALS conditions.

**Table 4.4.3** ULS & ALS Check for Configuration P with Riser Arc Lengths 3000 m and 2000 m.

| Case | | | P | |
|---|---|---|---|---|
| | | | $L_A$ = 3000 m | $L_A$ = 2000 m |
| ULS | Near Position | Maximum von Mises stress (MPa) | 225.6 | 207.6 |
| | | Von Mises stress utilization | 0.41 < 0.8 | 0.38 < 0.8 |
| | Far Position | Maximum von Mises stress (MPa) | 414.2 | 398.2 |
| | | Von Mises stress utilization | 0.75 < 0.8 | 0.72 < 0.8 |
| ALS | Near Position | Maximum von Mises stress (MPa) | 500.6 | 497.4 |
| | | Von Mises stress utilization | 0.91 < 1.0 | 0.90 < 1.0 |
| | Far Position | Maximum von Mises stress (MPa) | 411.0 | 437.0 |
| | | Von Mises stress utilization | 0.75 < 1.0 | 0.79 < 1.0 |

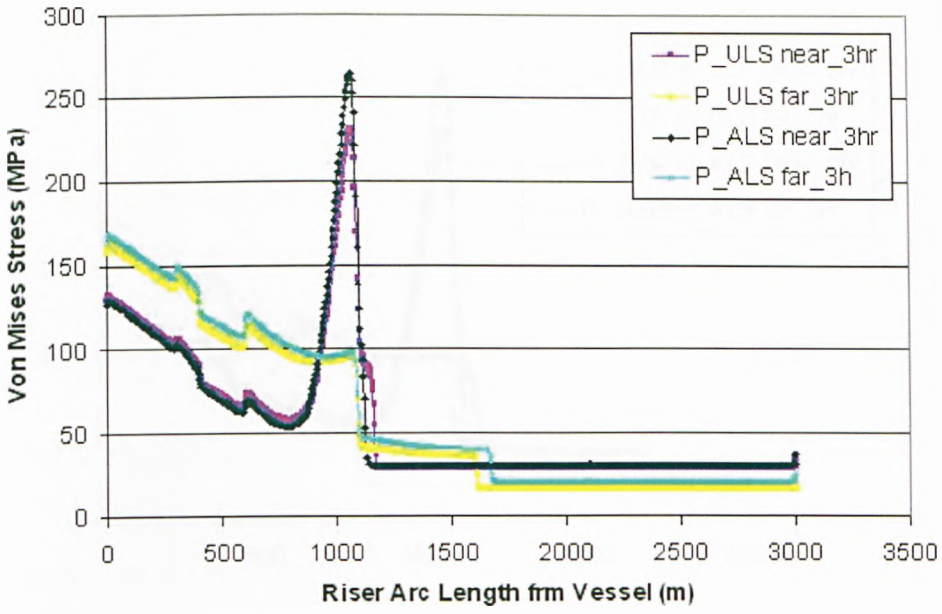


**Figure 4.4.6** Static von Mises Stresses for Configuration P with Riser Arc Length 3000 m.

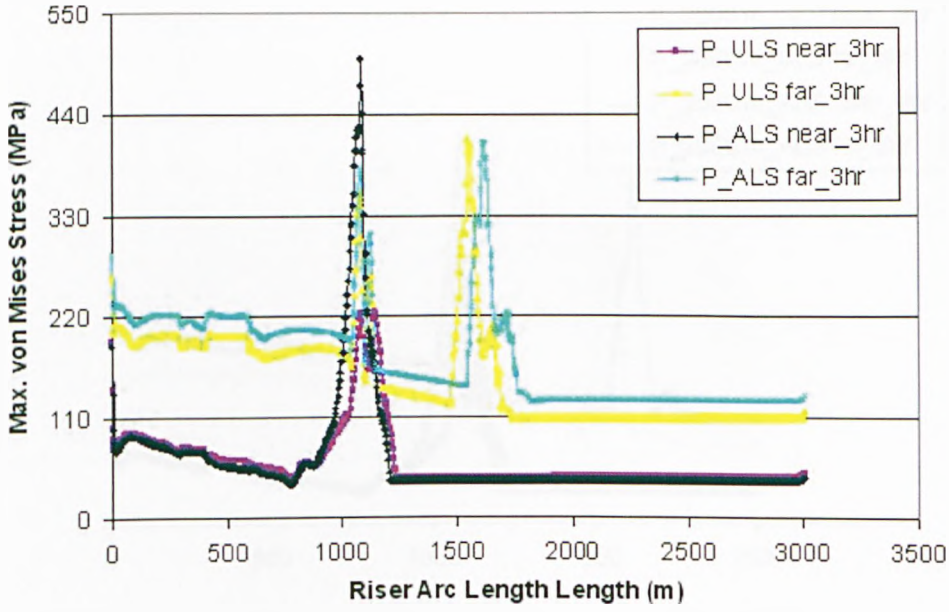


**Figure 4.4.7** Maximum Dynamic von Mises Stress Envelopes for Configuration P with Riser Arc Length 3000 m.

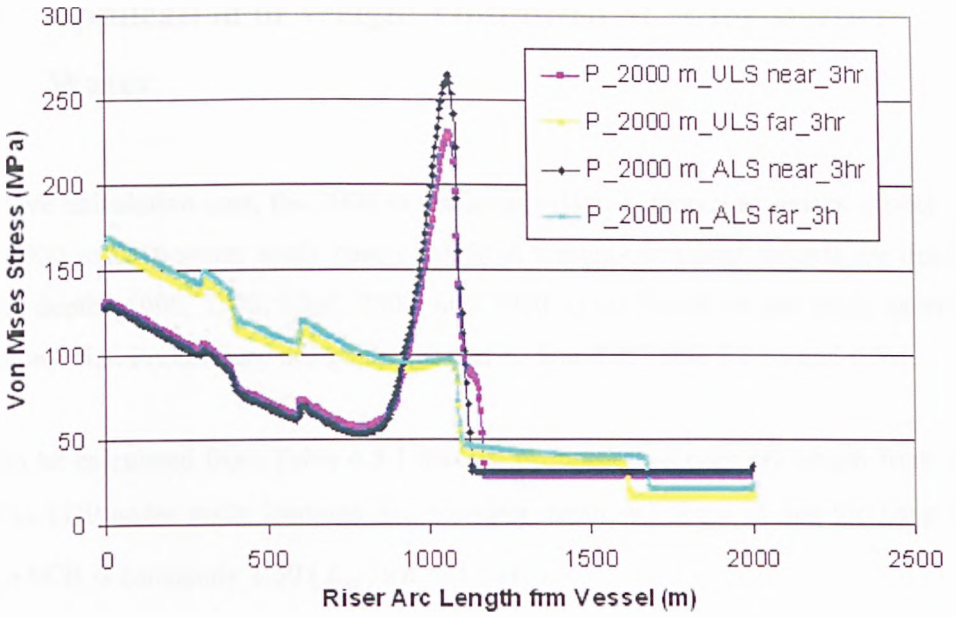


**Figure 4.4.8** Static von Mises Stresses for Configuration P with Riser Arc Length 2000 m.

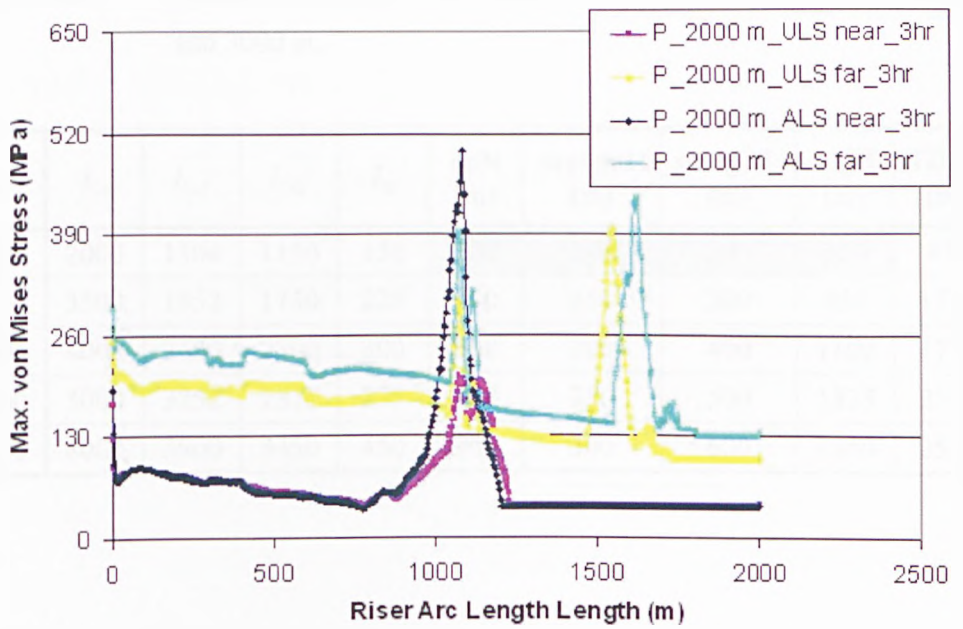


**Figure 4.4.9** Maximum Dynamic von Mises Stress Envelopes for Configuration P with Riser Arc Length 2000 m.

## 4.5 Application of Weight-Optimised SCR for Deeper Water

To save calculation cost, the 2000 m arc length riser is chosen as design model for the 1000 m deep water study base case. SCR weight-optimised models for deeper water depths 1000, 1500, 2000, 2500, and 3000 m are based on the study cases in Section 3.5.2. Preliminary design details can be found in Table 3.5.19 and 4.5.1.

It can be calculated from Table 4.5.1 that the proportion of riser arc length from top end to TDP under static loadings $L_{AT}$ to water depth $wd$ for a 15 deg top hang-off 10 in SCR is constantly 1.30 ($L_{AT}/wd = 1.30$).

As a preliminary weight-optimised design for deeper water depths, configuration F7 with riser arc length 2000 m for 1000 m water depth is set as a starting base case.

**Table 4.5.1** Weight-Optimised SCRs for Water Depths 1000, 1500, 2000, 2500, and 3000 m.

| $wd$ | $L_A$ | $L_{AT}$ | $L_{BT}$ | $L_B$ | upN (m) | straightH (m) | straightL (m) | sagH (m) | TDAL (m) |
|---|---|---|---|---|---|---|---|---|---|
| 1000 | 2000 | 1304 | 1150 | 150 | 300 | 100 | 200 | 550 | 850 |
| 1500 | 3500 | 1952 | 1730 | 225 | 450 | 150 | 300 | 830 | 1770 |
| 2000 | 4000 | 2600 | 2300 | 300 | 600 | 200 | 400 | 1100 | 1700 |
| 2500 | 5000 | 3252 | 2875 | 375 | 750 | 250 | 500 | 1375 | 2125 |
| 3000 | 6000 | 3900 | 3450 | 450 | 900 | 300 | 600 | 1650 | 2550 |

**Table 4.5.2** Riser Weight-Optimised Section Length Proportions for Design Reference.

| $L_B/wd$ | $upN/L_{BT}$ | $straightH/L_{BT}$ | $straightL/L_{BT}$ | $sagH/L_{BT}$ |
|---|---|---|---|---|
| 0.15 | 0.261 | 0.087 | 0.174 | 0.478 |

where

$wd$ = water depth

$L_A$ = riser arc length

$L_B$ = riser arc length from the end point of section sagH to TDP under static loadings

$L_{AT}$ = riser arc length from top end to TDP under static loadings

$L_{BT}$ = riser arc length before TDP, including sections upN, straightH, straightL and sagH

Illustration is shown in Figure 3.5.45.

SCR configuration F7 is an optimised configuration for water depth 1000 m. How to apply the weight distribution to risers for deeper water depths was still not for sure. However, from previous study in section 4.3 it is found that the end point of sagH section is a controlling point of the maximum von Mises stress at TDA. Riser arc length from top end to TDP under static loadings $L_{AT}$ = 1304 m is obtained by static analysis while riser arc length before TDP $L_{BT}$ = 1150 m is an optimised length with weight coatings. Therefore, the riser arc length from the end point of section sagH to TDP $L_B = L_{AT} - L_{BT} \approx 150$ m. Whether $L_B$ should be a fixed length around 150 m or flexible as a proportional length to water depth ($L_B/wd$ = 0.15 for water depth 1000 m) was needed to be decided. As long as the length $L_B$ is settled, the length $L_{BT}$ for deeper water cases can be deducted by $L_{AT} - L_B$ and the lengths for sections upN,

straightH, straightL and sagH can be decided by proportions as obtained by configuration F7 for water depth 1000 m (see Table 4.5.2).

The riser model for water depth 1500 m was investigated for both methods which means the length $L_B$ was taken as either 150 m or 1500 × 0.15 = 225 m. Simulation results are compared in Table 4.5.3 and Figure 4.5.1 and 4.5.2.

**Table 4.5.3** Weight-Optimised SCRs for Water Depth 1500 m.

| *wd* | $L_A$ | $L_{AT}$ | $L_{BT}$ | $L_B$ | upN (m) | straightH (m) | straightL (m) | sagH (m) | TDAL (m) |
|---|---|---|---|---|---|---|---|---|---|
| 1500 | 3500 | 1953 | 1796 | 150 | 468 | 156 | 312 | 860 | 1704 |
| | | | 1730 | 225 | 450 | 150 | 300 | 830 | 1770 |

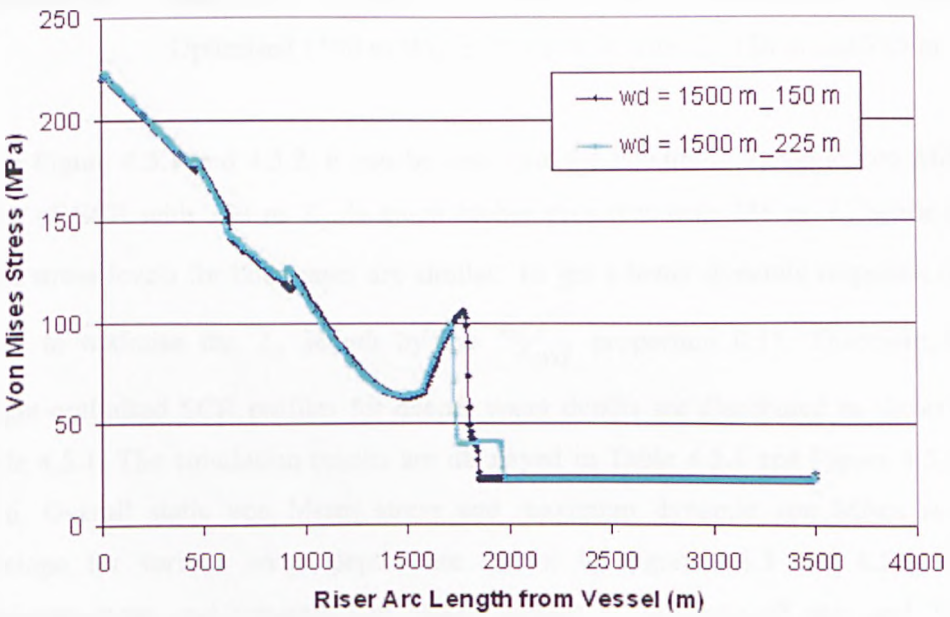


**Figure 4.5.1** Static von Mises Stresses for Weight-Optimised 1500 m Water Depth SCR with $L_B$ 150 m and 225 m.

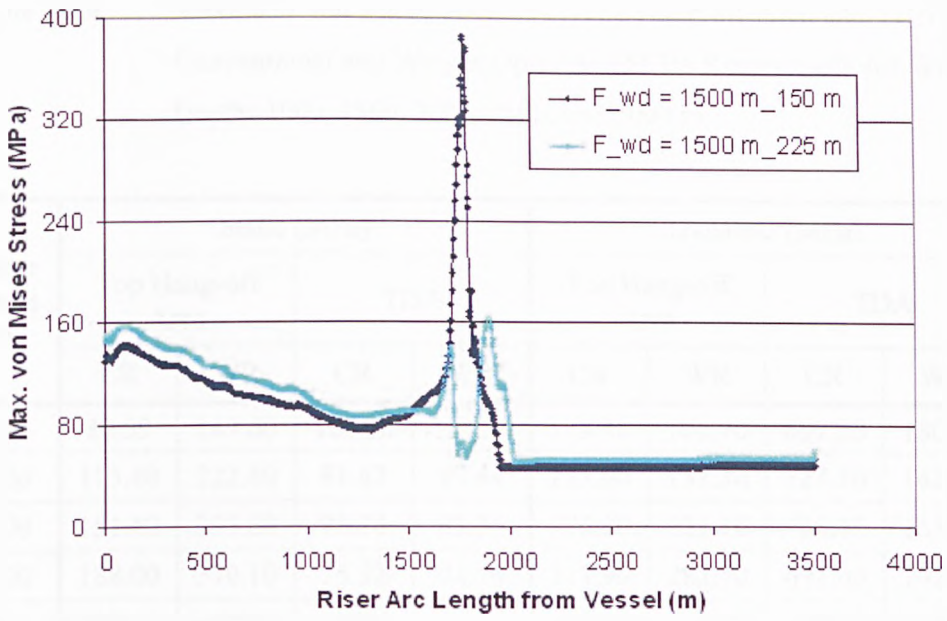


**Figure 4.5.2** Maximum Dynamic von Mises Stress Envelopes for Weight-Optimised 1500 m Water Depth SCR with $L_B$ 150 m and 225 m.

From Figure 4.5.1 and 4.5.2, it can be seen that the maximum dynamic von Mises stress of SCR with 150 m $L_B$ is much higher than that with 225 m $L_B$ while the static stress levels for both cases are similar. To get a better dynamic response, it is better to optimise the $L_B$ length by the $L_B/wd$ proportion 0.15. Therefore, the weight-optimised SCR profiles for deeper water depths are distributed as shown in Table 4.5.1. The simulation results are displayed in Table 4.5.4 and Figure 4.5.3 ~ 4.5.6. Overall static von Mises stress and maximum dynamic von Mises stress envelope for various water depths are shown in Figure 4.5.3 and 4.5.5. The maximum static and dynamic von Mises stresses at top hang-off area and TDA respectively for various water depths are compared in Table 4.5.4 and Figure 4.5.4 and 4.5.6.

**Table 4.5.4** Maximum von Mises Stresses of Top Hang-off Area and TDA for Conventional and Weight-Optimised SCRs Respectively for Water Depths 1000, 1500, 2000, 2500, and 3000 m.

| Water Depth (m) | Static (MPa) | | | | Dynamic (MPa) | | | |
|---|---|---|---|---|---|---|---|---|
| | Top Hang-off Area | | TDA | | Top Hang-off Area | | TDA | |
| | CR | WR | CR | WR | CR | WR | CR | WR |
| 1000 | 80.59 | 149.60 | 100.20 | 133.30 | 113.30 | 101.90 | 657.20 | 180.70 |
| 1500 | 115.40 | 222.60 | 81.47 | 99.44 | 133.00 | 157.30 | 727.10 | 162.80 |
| 2000 | 151.40 | 295.80 | 75.74 | 83.36 | 170.80 | 221.10 | 738.40 | 163.70 |
| 2500 | 188.00 | 370.10 | 75.32 | 74.79 | 217.90 | 282.70 | 691.60 | 242.60 |
| 3000 | 224.30 | 443.80 | 78.50 | 72.29 | 260.90 | 319.80 | 769.20 | 287.80 |

Where CR and WR stand for conventional SCR and weight-optimised SCR respectively.

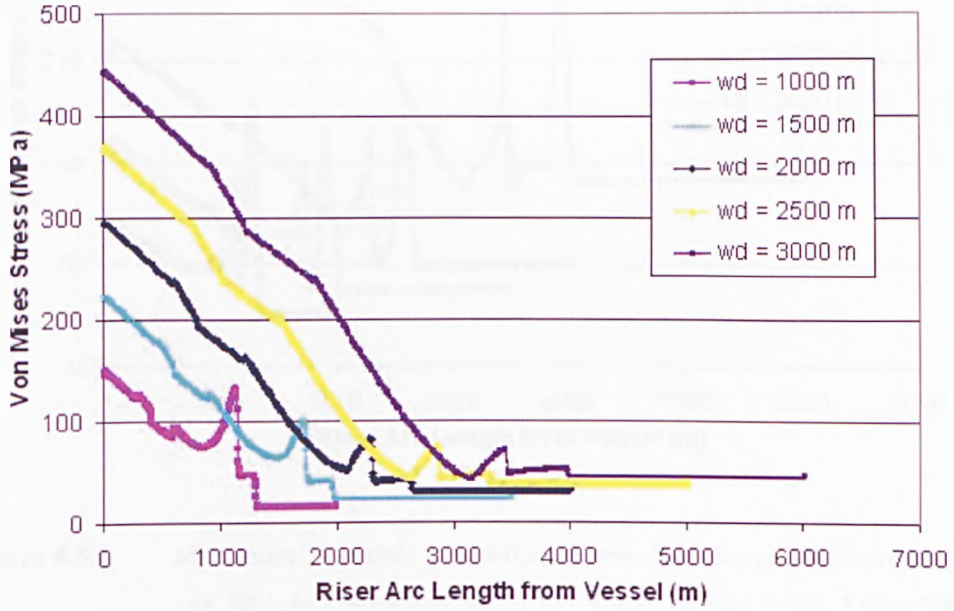


**Figure 4.5.3** Static von Mises Stresses of Conventional and Weight-Optimised SCRs for Water Depths 1000, 1500, 2000, 2500, and 3000 m.

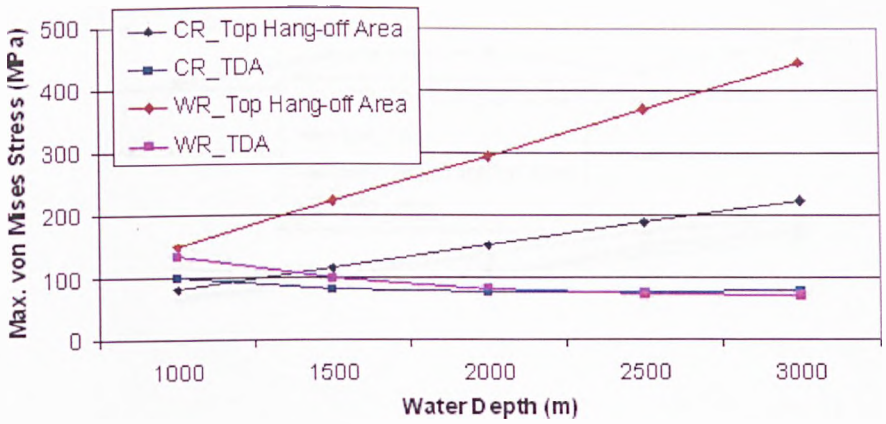


**Figure 4.5.4** Maximum Static von Mises Stresses of Top Hang-off Area and TDA for Conventional and Weight-Optimised SCRs Respectively for Water Depths 1000, 1500, 2000, 2500, and 3000 m.

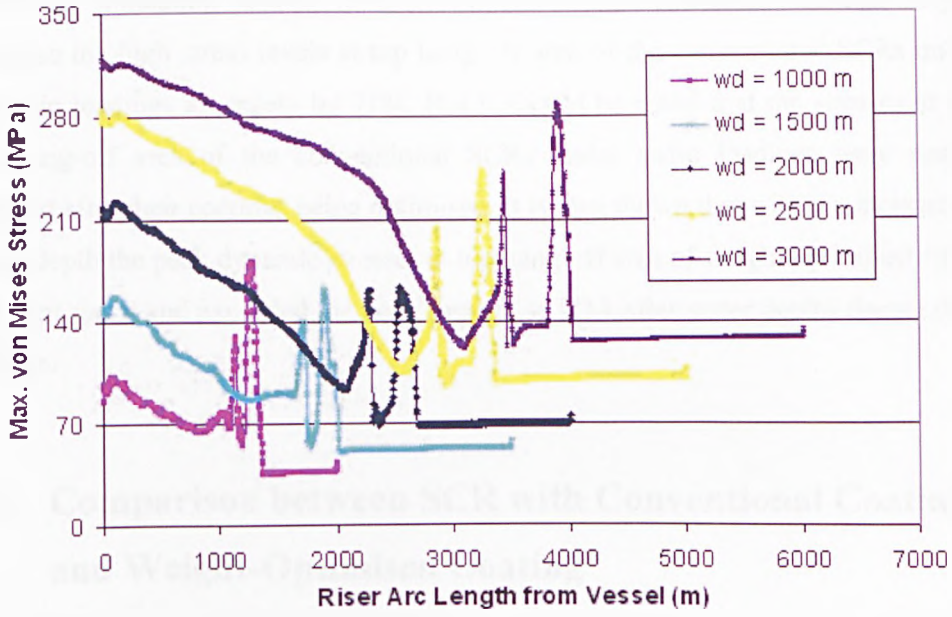


**Figure 4.5.5** Maximum Dynamic von Mises Stress Envelopes of Conventional and Weight-Optimised SCRs for Water Depths 1000, 1500, 2000, 2500, and 3000 m.

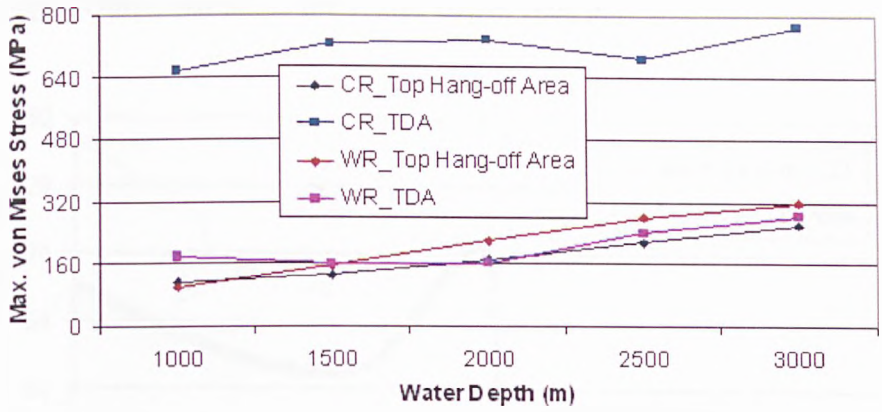


**Figure 4.5.6** Maximum Dynamic von Mises Stresses of Top Hang-off Area and TDA for Conventional and Weight-Optimised SCRs Respectively for Water Depths 1000, 1500, 2000, 2500, and 3000 m.

From the simulation results, it is shown that weight-optimised coatings helped decrease the high stress levels at top hang-off area of the conventional SCRs under dynamic loadings averagely by 71%. But it should be noted that the stresses at the top hang-off area of the conventional SCRs under static loadings were nearly doubled after their coatings being optimised. It is also shown that with the increase of water depth the peak dynamic stresses at top hang-off area of weight-optimised risers had kept rising and exceeded the peak stresses at TDA after water depths deeper than 1500 m.

## 4.6 Comparison between SCR with Conventional Coating and Weight-Optimised Coating

The comparisons between each pair of conventional SCR and weight-optimised SCR for every individual water depth study case are shown in Figure 4.6.1 ~ 4.6.10. It is obviously shown that weight-optimised coatings helped distinctively improve the dynamic response of conventional SCRs which make their services feasible in deep and even deeper waters.

**a) Weight-Optimised SCRs for Water Depth 1000 m**

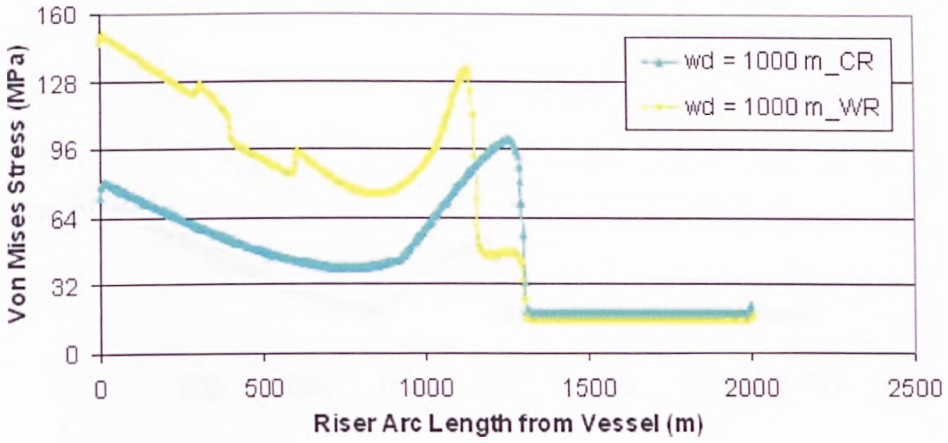


**Figure 4.6.1** Static von Mises Stresses of Conventional and Weight-Optimised SCRs for Water Depth 1000 m.

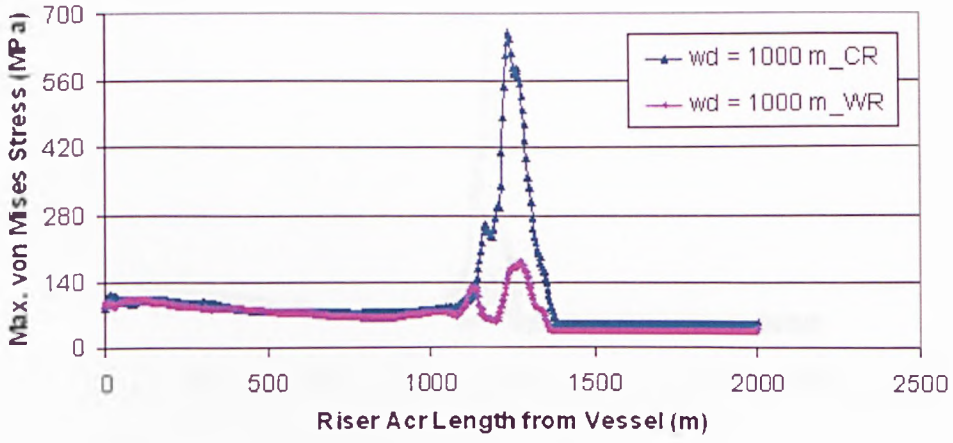


**Figure 4.6.2** Maximum Dynamic von Mises Stress Envelopes of Conventional and Weight-Optimised SCRs for Water Depth 1000 m.

**b) Weight-Optimised SCRs for Water Depth 1500 m**

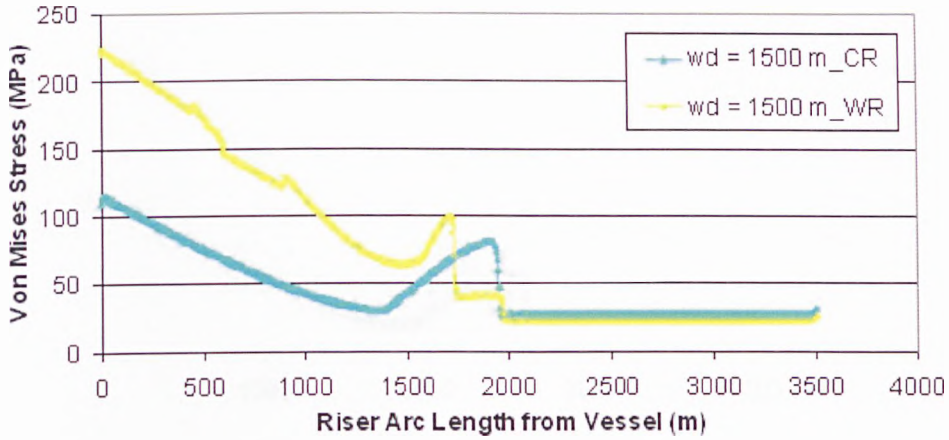


**Figure 4.6.3** Static von Mises Stresses of Conventional and Weight-Optimised SCRs for Water Depth 1500 m.

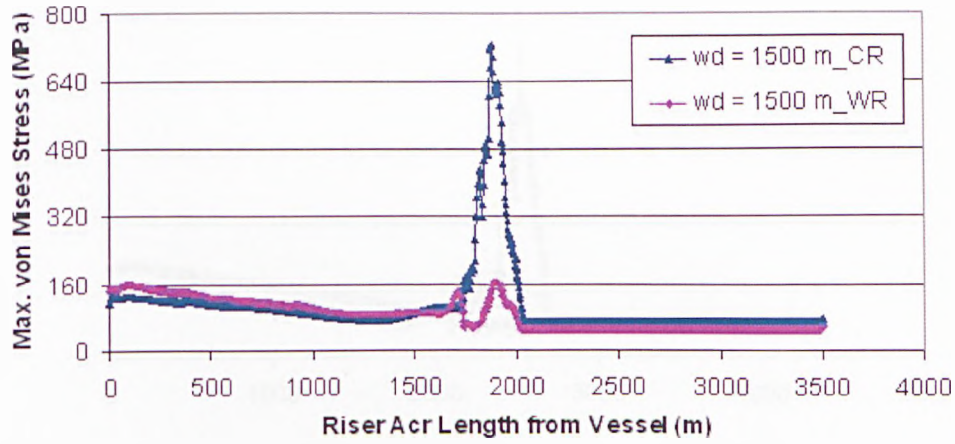


**Figure 4.6.4** Maximum Dynamic von Mises Stress Envelopes of Conventional and Weight-Optimised SCRs for Water Depth 1500 m.

**c) Weight-Optimised SCRs for Water Depth 2000 m**

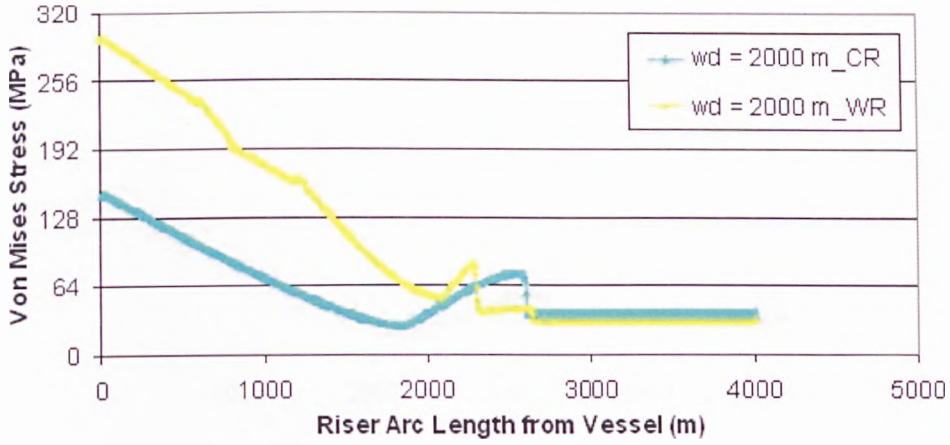


**Figure 4.6.5** Static von Mises Stresses of Conventional and Weight-Optimised SCRs for Water Depth 2000 m.

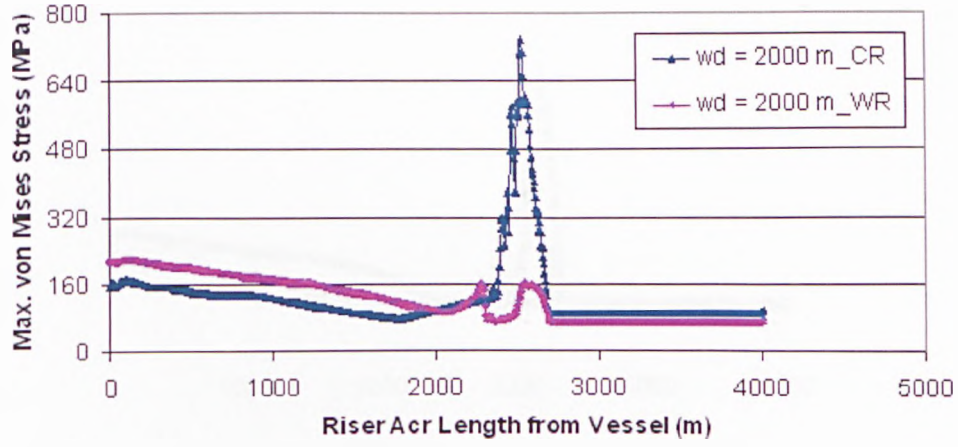


**Figure 4.6.6** Maximum Dynamic von Mises Stress Envelopes of Conventional and Weight-Optimised SCRs for Water Depth 2000 m.

**d) Weight-Optimised SCRs for Water Depth 2500 m**

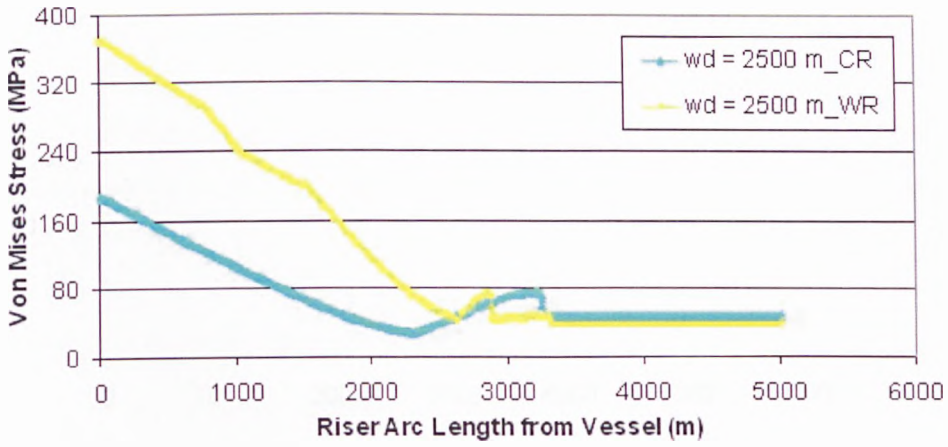


**Figure 4.6.7** Static von Mises Stresses of Conventional and Weight-Optimised SCRs for Water Depth 2500 m.

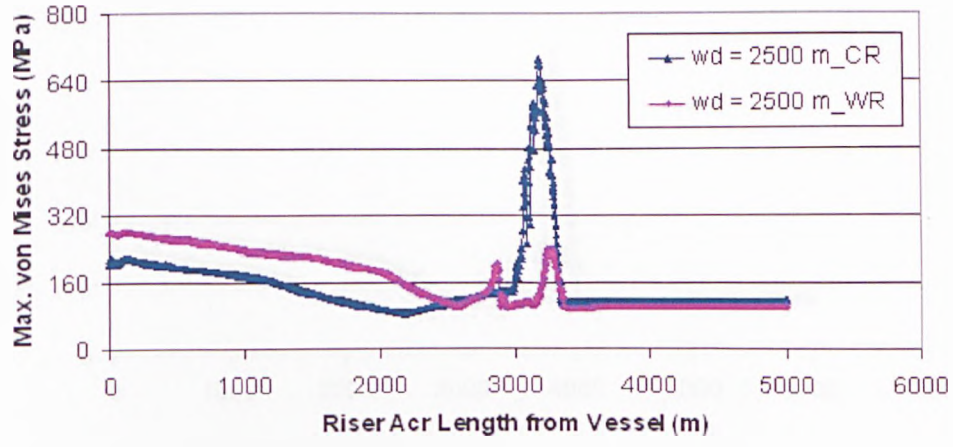


**Figure 4.6.8** Maximum Dynamic von Mises Stress Envelopes of Conventional and Weight-Optimised SCRs for Water Depth 2500 m.

**e) Weight-Optimised SCRs for Water Depth 3000 m**

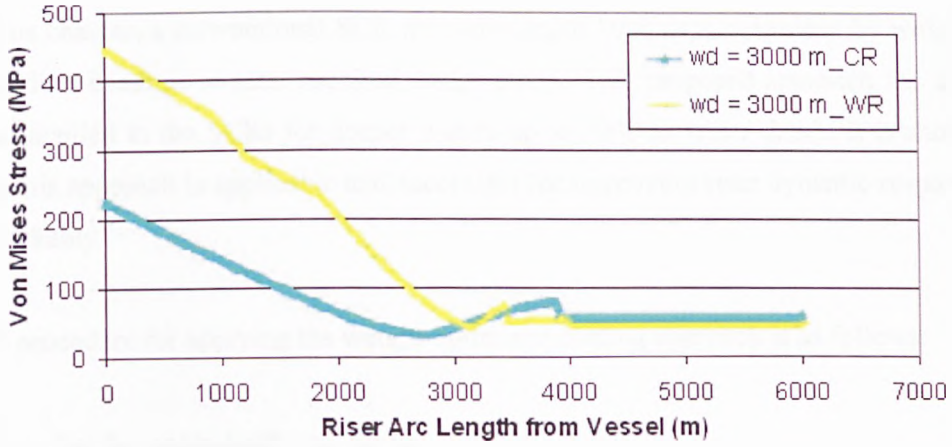


**Figure 4.6.9** Static von Mises Stresses of Conventional and Weight-Optimised SCRs for Water Depth 3000 m.

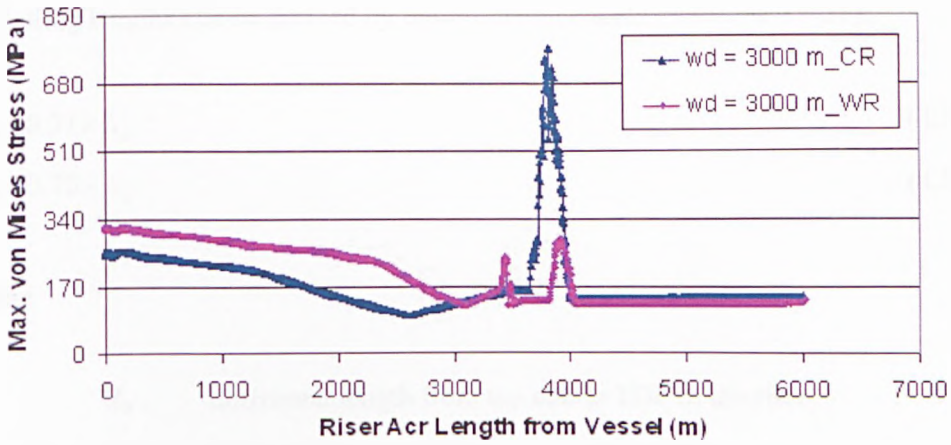


**Figure 4.6.10** Maximum Dynamic von Mises Stress Envelopes of Conventional and Weight-Optimised SCRs for Water Depth 3000 m.

## 4.7 Discussion and Conclusion

In this chapter, a conventional SCR for water depth 1000 m is optimised by weight-optimised coatings to meet required design stress. This proposed approach has also been applied to the SCRs for deeper waters up to 3000 m water depth. It is shown that this approach is applicable and successful for improving riser dynamic response remarkably.

The procedure for applying the weight-optimised coating approach is as follows:

Step 1: Set the water depth $wd$ for the SCR service area.

Step 2: Estimate the riser arc length $L_A$ according to the Table 3.5.19.

Step 3: For a 15 deg deepwater SCR connected to a semi-submersible, the riser modelling lengths can be derived by the following equations (Table 3.5.21):

$$L_T = 0.37 \times L_A \tag{4.7.1}$$

$$L_E = 0.70 \times L_A \tag{4.7.2}$$

where

$L_T$ horizontal length from top end to TDP of the riser

$L_E$ horizontal length from top end to bottom end of the riser

Step 4: Run static analysis of the conventional SCR and obtain riser arc length from top end to TDP under static loadings $L_{AT}$. Check the $L_{AT}$ length with water depth to see whether it satisfies the relationship expressed by equation 4.7.3. If not, adjust the lengths $L_T$ and $L_E$ and rerun the static analysis until it satisfies.

$$L_{AT} = 1.30 \times wd \tag{4.7.3}$$

Step 5: Calculate the riser arc length from the end point of section sagH to TDP under static loadings $L_B$ and the riser arc length before TDP $L_{BT}$ by the following equations:

$$L_B = 0.15 \times wd \tag{4.7.4}$$

$$L_{BT} = L_{AT} - L_B \tag{4.7.5}$$

Step 6: Calculate the arc lengths for sections upN, straightH, straightL, sagH and TDAL by equations 4.7.6 ~ 4.7.10 (also see Table 4.5.2). The thickness and densities of each section are given in Table 4.7.1.

$$L_{upN} = 0.261 \times L_{BT} \tag{4.7.6}$$

$$L_{straightH} = 0.087 \times L_{BT} \tag{4.7.7}$$

$$L_{straightL} = 0.174 \times L_{BT} \tag{4.7.8}$$

$$L_{sagH} = 0.478 \times L_{BT} \tag{4.7.9}$$

$$L_{TDAL} = L_A - L_{BT} \tag{4.7.10}$$

**Table 4.7.1** Weight Coating Thickness and Densities.

| Coating Thickness (m) | Coating Density (kg/m$^3$) | | |
|---|---|---|---|
| | L | N | H |
| 0.1 | 650 | 950 | 3200 |

Step 7: Run dynamic analysis for weight-optimised SCRs and check the response maximum envelopes.

Step 8: Slightly change the relative lengths among sections and rerun dynamic analysis to see if there is any improvement for riser response.

Step 9: Move forward the end point of section sagH around 100 m for final weight-optimised configuration and check ALS conditions.

Chapter 5

# Fatigue Analysis of Deepwater Weight-Optimised SCRs

## 5.1 Introduction

The slender cable-like structure of deepwater SCRs are fatigue sensitive. Hence fatigue is a very important limit state for SCR structural design.

A particular characteristic of fatigue is that the applied loading is not sufficient to cause immediate collapse of the structure. Instead, collapse occurs after a certain number of cyclic variations of the loading, that is, when the cumulative damage reaches a given level. The main parameters in fatigue analysis is, therefore, the component amplitude of variation in stresses and strains, defined by the difference between successive peaks and valleys in the time response.

The evaluation of fatigue behaviour in offshore structures should be performed through dynamic analyses, considering the environmental loading characteristic of the location of the structures. This allows the determination of the long-term time history of local stresses in different point of the structure (the "hot-spots"), in order

to identify all stress cycles and their respective amplitudes (Torres, Sagrilo, Siqueira, and Lima, 1995). Besides, the nonlinear random dynamic analyses in time domain approach for the fatigue analysis of SCRs also allows the representation of the nonlinear characteristics of fluid-soil-structure interaction and also the random characteristics of environmental loadings.

Stress amplitudes are subdivided in intervals; each interval of stress amplitude is associated to the number of observed cycles. A distribution of probability can then be established for each stress cycle, and the evaluation of fatigue life can be calculated either through fracture mechanics, or through a procedure based on the S-N curves and the Palmgren-Miner's rule. The fracture mechanics methodology is more appropriated for the monitoring of crack-growth, while the latter procedure is indicated for the design, since in this case the engineer is concerned with open cracks in their final stages.

In order to determine the structural response and assess the fatigue behaviour, several alternative analysis methods may be adopted, for instance: frequency-domain dynamic analysis that requires linearisation techniques, or time-domain dynamic analysis that can adequately consider all nonlinear characteristics of the model; also, the sea state may be represented by a regular wave allowing deterministic dynamic analysis, or by an irregular (spectral) model, requiring the use of random dynamic analysis methods.

The fatigue damage calculations in this thesis arise from the first order loadings, based on the wave scatter. The second order vessel motions and vortex induced vibrations (VIV) are not included in this thesis.

In general, fatigue performance, especially at the TDA, poses a greater challenge to SCR design than strength response. In instances where low fatigue life in the TDA of the SCR poses seemingly insurmountable difficulties, instead of switching to an entirely different riser concept, it may be possible to add enhancements to the basic SCR configuration in order to achieve acceptable performance. In this chapter,

weight-optimised SCRs obtained from the previous Chapter 4 are assessed for fatigue life.

## 5.2 Fatigue Analysis Approaches

### *5.2.1 The Fracture Mechanics (FM) Approach (Micro Approach)*

The FM approach is based on crack growth data of an initial flaw of known (or assumed) size and geometry. For welded joints, it is assumed that an appropriate initial defect exists, which is just under the threshold of detection, fatigue life can then be predicted using the FM method to determine the number of cycles required to grow the crack to a certain unstable growth. The FM approach is more detailed and it involves examining crack growth and determining the number of load cycles that are needed for small initial defects to grow into cracks large enough to cause fracture. That's why it is also known as a micro approach. The growth rate is proportional to the stress range. It is expressed in terms of a stress intensity factor intensity factor $K$, which accounts for the magnitude of the stress, current crack size, and weld and joint details. The basic equation that governs crack growth is given by

$$\frac{da}{dN} = C\Delta K^{m_p} \tag{5.2.1}$$

where $a$ = crack size, $N$ = number of fatigue cycles, $\Delta K$ = range of stress intensity factor, and $C$ and $m_p$ are empirically derived crack propagation parameters. The range of the stress intensity factor is given by Broek (1986) as

$$\Delta K = SY(a)\sqrt{\pi a} \tag{5.2.2}$$

in which $S$ is stress range and $Y(a)$ is a function of crack geometry. When the crack size $a$ reaches some critical crack size $a_{cr}$, failure is assumed to have occurred. Although most laboratory testing is performed with constant-amplitude stress ranges, equation 5.2.1 is typically applied to variable stress range models that ignore sequence effects (Byers, Marley, Mohammadi, Nielsen, and Sarkani, 1997). Rearranging the variables in equation 5.2.1, the number of cycles can be computed using the following equation:

$$N = \frac{1}{CS^{m_p}} \int_{a_0}^{a} \frac{da}{Y^{m_p}(a)\left(\sqrt{\pi a}\right)^{m_p}} \tag{5.2.3}$$

Equations 5.2.1 and 5.2.3 involve a variety of sources of uncertainty (Harris, 1995). The crack propagation parameter $C$ in both equations is treated as a random variable (Madsen, 1983). However, in more sophisticated models, equation 5.2.1 is treated as a stochastic differential equation and $C$ is allowed to vary during the crack growth as Markov process, while Ditlevsen (1986) treated it as a first-passage problem.

### *5.2.2 The Characteristic S-N Approach*

Since the well-known work of Wöhler in Germany starting in the 1850's, engineers have employed curves of stress versus cycles to fatigue failure, which have been presented in the form of so-called S-N curves or Wöhler's curve (Wöhler, 1871), where $S$ is the engineering stress amplitude and $N$ is the number of cycles to failure, on a semi-log or log-log scale.

The characteristic S-N curve approach is based on S-N curves and on the assumption that fatigue damage accumulation is a linear phenomenon that is independent of previously applied cycles (i.e., that follows Palmgren-Miner's rule). According to Palmgren-Miner's rule (see Appendix D), the total fatigue life under a variety of stress ranges is the weighted sum of the individual lives at constant stress $S$ as given

by the S-N curves, with each being weighted according to fractional exposure to that level of stress range (Hughes, 1988). Upon crack initiation, cracks propagate based on the fracture mechanics concept as shown in Figure 5.2.1.

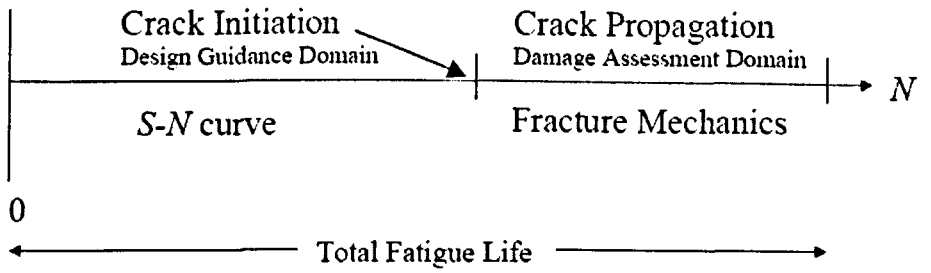


**Figure 5.2.1** Comparison between the Characteristic S-N curve and Fracture Mechanics Approach.

The fatigue behaviour of different types of structural details is generally evaluated in constant-cycle fatigue tests and the results are presented in terms of nominal applied stresses and the number of cycles of loading that produces failure. The resulting S-N curves are usually presented as straight lines on a log-log paper as shown in Figure 5.2.2.

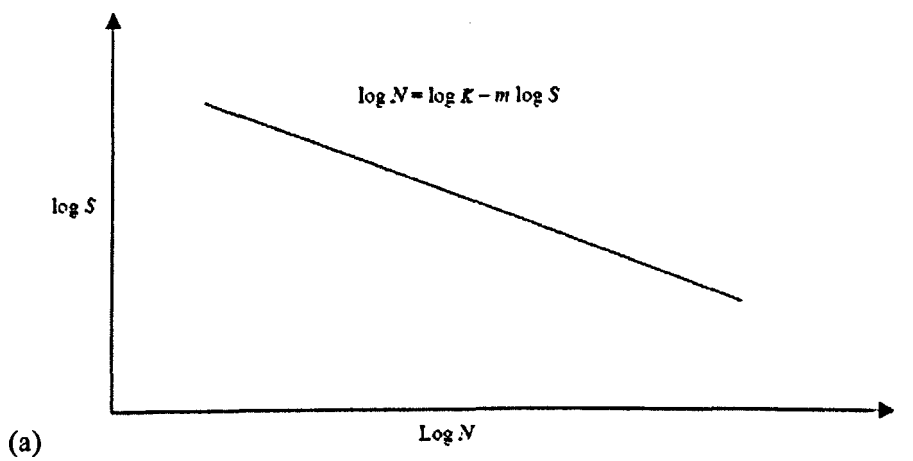

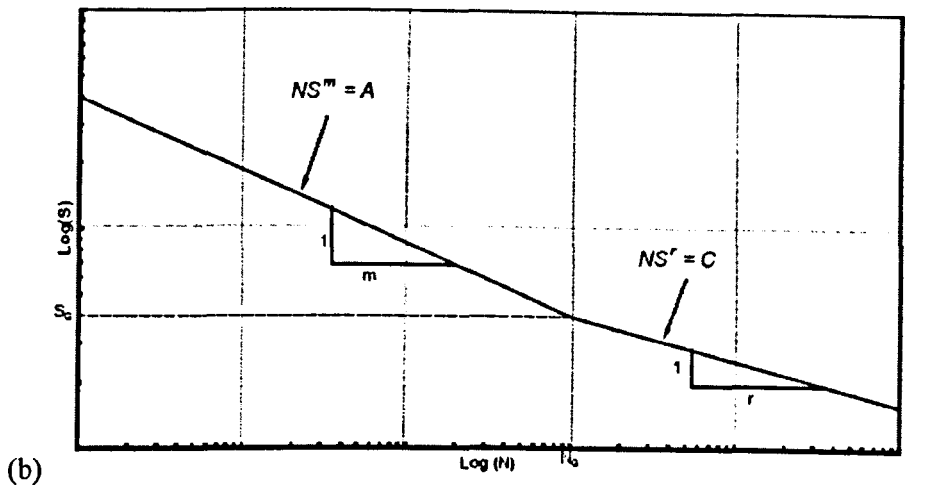


**Figure 5.2.2** Typical S-N Curves: (a) One-Slope S-N Curve; (b) Two-Slope S-N Curve.

The basic equation that represents the S-N curve is given by

$$N = KS^{-m} \tag{5.2.4}$$

where

$N$ = number of cycles to failure initiation (failure)
$S$ = stress range with stress concentration factor (SCF)
$K$ = material constant (empirical constant established by experiments)
$m$ = negative slope of the fatigue curve (empirical constant established by experiments)

Equation 5.2.4 can also be expressed in a linear form as

$$\log N = \log K - m \log S \tag{5.2.5}$$

where log is to the base 10. The fatigue strength can be computed over a range of lives covered by the straight line if the slope of the line and one point on the line are

known. However, only one type of stress cycle and one detail are represented on an individual S-N curve (Munse, Wilbur, Tellalian, Nicoll, & Wilson, 1983). In general, a least-squares analysis of $\log N$ given $S$ fatigue data is used to produce the S-N curve and associated experimental constants $\log K$ and $m$.

The choice of appropriate stress history is an important factor in reliability-based design and analysis for fatigue. The question is not really how to determine the stress history; rather, what constitutes an appropriate stress history. According to Moan and Berge (1997), and based on the terminology adopted by Hobbacher (1996), the following four different approaches are classified for stress determination for fatigue design and analysis:

- The nominal stress approach
- The hot spot stress approach
- The notch stress approach
- The notch strain approach

The concepts of nominal stress, hot spot stress and notch stress in weld joints are defined in Figure 5.2.3. Figure 5.2.4 shows a schematic of the approaches mentioned above. Except for the nominal stress approach, the rest are commonly called local stress approaches. The most common approaches for determining fatigue stresses in marine industry are the nominal stress and the hot spot approaches (Ayyub, Assakkaf, Kihl, and Sieve, 2002).

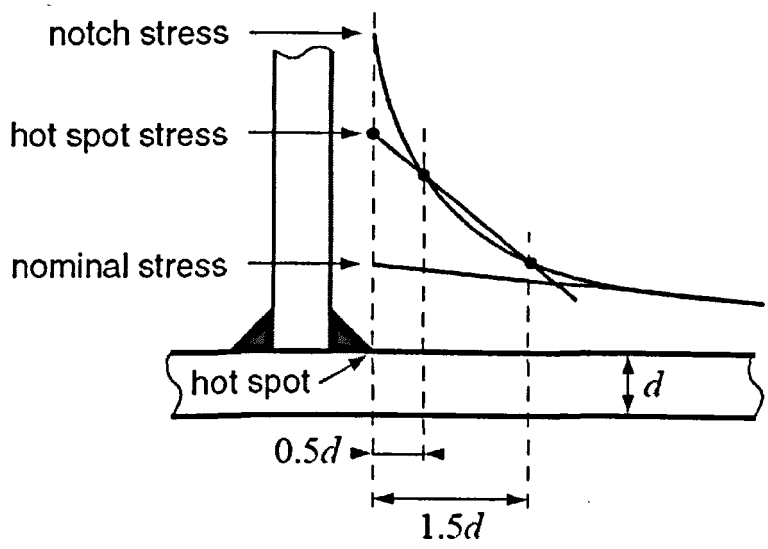


**Figure 5.2.3** Illustration of the Different Stress Levels at Welded Joints from Bureau Veritas Rules (2000).

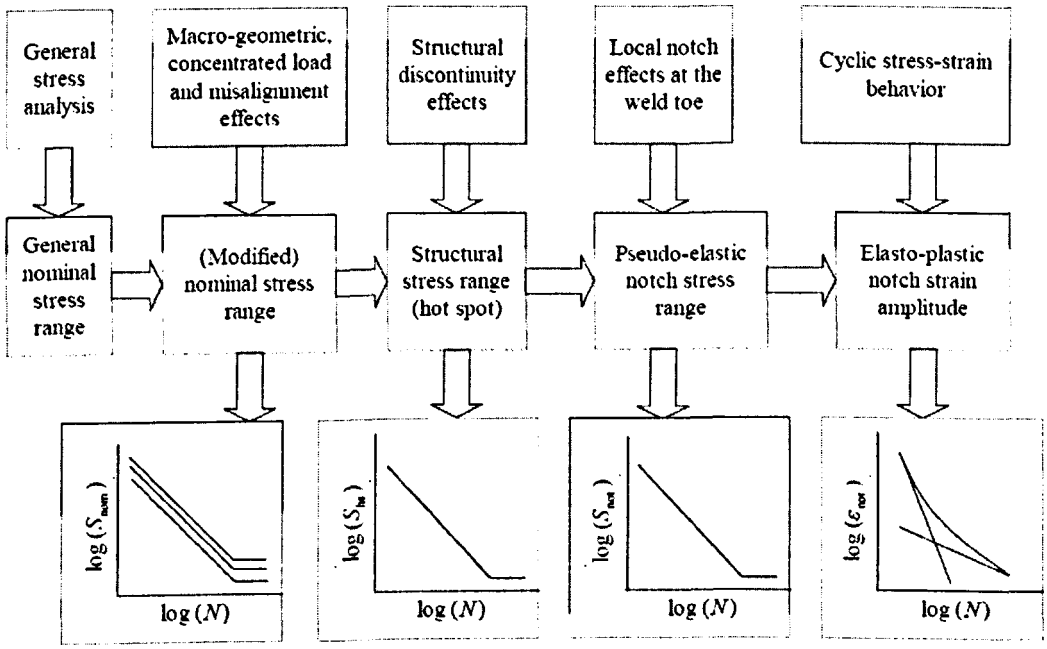


**Figure 5.2.4** S-N Approaches for Fatigue Strength Assessment (Niemi, 1995).

The simplest and most common method for estimating fatigue life is nominal stress approach. Fatigue design codes and ship rules, such as British Standard (BS 5400, 1980) and DNV Offshore Code (DNV-RP-C203, 2008), usually divide various structural details into different classes and provide an S-N curve for each class.

## 5.3 Fatigue under Wave Loadings

The fatigue damage of SCRs is mainly caused by the random sea state waves. Wave loading fatigue contributes significantly to the total fatigue performance of SCRs, through wave induced vessel motions. The SCR wave loading fatigue damage is related to the combined effect of various parameters, such as environmental conditions, fluid density, riser diameter, water depth, host vessel type and its motion behaviour. Wave loading fatigue damage in SCRs is generally greatest in the wave zone and at TDP on the seabed. Catenary geometry may need to be modified to improve response and local improvements in fatigue details may be required in extreme cases.

Wave-induced fatigue analysis of SCRs is best evaluated in the time domain since the nonlinearities of the system can be large, particularly around the critical TDP and the top section close to the top connection. This approach is numerically demanding but is considered necessary to achieve an adequate level of confidence in the results.

The main problems with the traditional deterministic method are related first to the fact that not all waves have the same period and second because assuming all waves are regular does not take into account the stochastic nature of the marine environment. Because of this it has become common practice to perform spectral fatigue analyses instead of deterministic ones, in order that satisfactory statistical representation of behaviour is obtained.

Hence random sea state wave loading is employed and fatigue damage is based on a series of one-half to one-hour dynamic simulations of sea states from a scatter wave

diagram that also includes sea states annual probability of occurrence. The wave sea states in the scatter diagram can be grouped in blocks to reduce the computation time and effort. Rainflow counting (RFC) technique or any acceptable statistical method is applied to calculate fatigue damage associated with each of the individual sea states. Palmgren-Miner's rule is then used to sum the overall fatigue damage along the SCR pipe. The final result given by the analysis is the life of the structure at all the critical points where stress concentrations occur.

Usually the number of waves per wave height and wave direction is given per year, which means that the inverse of the yearly damage is the life of the structure at each point.

$$Fatigue\ Life = \frac{1}{Total\ Damage} \tag{5.3.1}$$

## 5.4 Procedure for SCR Fatigue Analysis (FLS Check)

The nonlinear time-domain analysis program DNV DeepC & Riflex is employed for the determination of the time histories and stress variations in each node of the riser, resulting from the application of cyclic environmental loadings. This determination is performed by the following sequence of analyses:

- **Nonlinear static analysis**

- **Nonlinear time-domain dynamic analysis**: A comprehensive nonlinear time domain fatigue analysis is performed and the response is obtained by completing a nonlinear dynamic response using random irregular waves, applying the Airy wave model.

Several sequences of analyses are performed with the DNV DeepC & Riflex program, for each sea state and each load condition. The results of these sequences of

nonlinear analysis are time histories of forces and stresses, in 16 points around the perimeter of the cross section of selected elements of the model.

These time histories are post-processed by Riserlife, the fatigue analysis module of the DNV DeepC system. The stress ranges and fatigue damage associated with each sea state are calculated using RFC (see Appendix E) method and then weighted with the occurrence probability of each load case to calculate the overall fatigue damage along the SCR pipe by Palmgren-Miner's rule.

The design criteria for fatigue comply with the regulations given in the DNV recommended practice (DNV-RP-C203, 2008; DNV-RP-F204, 2005). The factor of safety to be used for fatigue calculations is normally 10 assuming it will not be feasible to inspect the pipe. The target field life is 20 years so that the criteria for fatigue verification consider a required design life of 200 years.

As the fatigue damage calculation depends on the stresses variations during all life of the structure, the set of loads used in the analysis should be complete enough to represent all possible situations. The use of the complete set of possible environmental load cases leads to high computer time necessary for the analysis in time domain. Therefore, the analysis is performed by dividing the wave scatter diagram into an appropriate number of blocks for the reduction of environmental loads and computation time and effort (Sharks and Fang, 2000). Within each block a nonlinear time domain analysis was performed for a representative sea state. This representative sea state has the highest occurrence rate within that block.

A series of one-half to 1-hour dynamic simulations of sea states considered adequate to assess the fatigue response of the riser. A simulation time of 45 min (2700 s) is suggested by Karunakaran, Meiling, Kristoffersen, and Lund (2005). The base case analysis is conducted for SCRs of riser length 2000 and 3000 m respectively, using the base case riser configuration with the DNV-D-Seawater-cathodic S-N curve and an SCF of 1.0 along the riser length.

The single omni-directional Wave Scatter Diagram (WSD) of Northern North Sea as shown in Figure 5.4.1, with all waves applied in the most critical direction is used to conduct a conservative fatigue analysis.

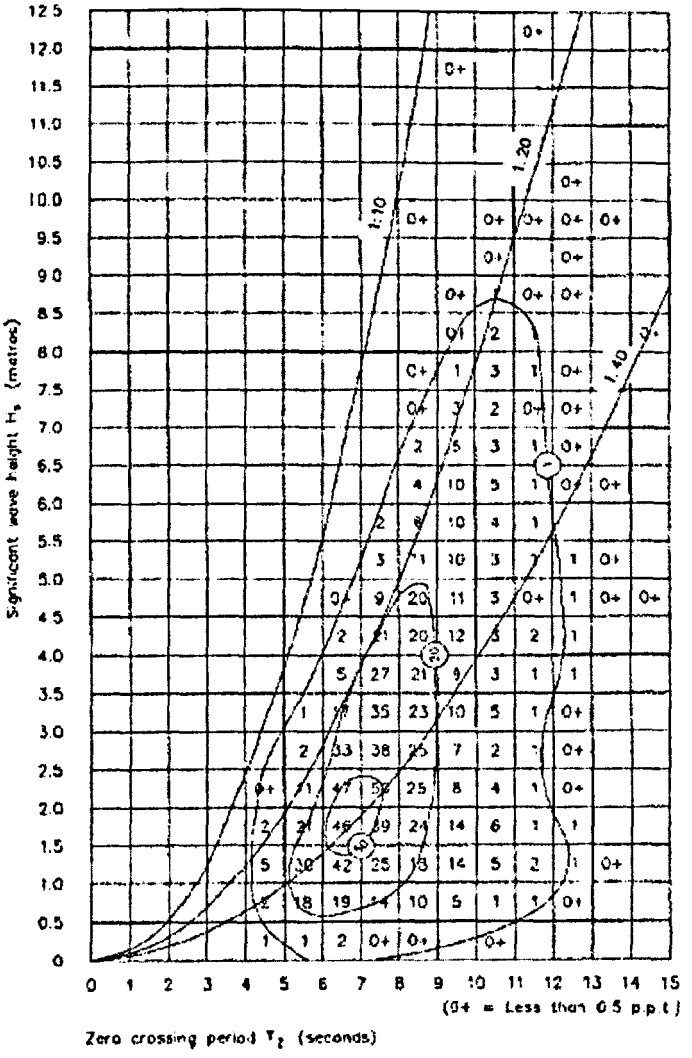


**Figure 5.4.1** Sea State Scatter Diagram (Barltrop and Adams, 1991).

SCR Base Case

Based on the former weight-optimised configuration design of SCRs in Chapter 4, the following parameters are chosen:

- Configuration — P
- Riser length — 2000, and 3000 m
- Mesh length — 4, and 5 m*
- Vessel offset — 0 m, mean position
- Sea-state scatter diagram — Northern North Sea (Figure 5.4.1)
- SCF — 1.0
- S-N curve — DNV-D-Seawater-cathodic

Note that the program Riserlife (which carries out DNV DeepC fatigue analysis) can only read up to 10000 responses from database files. For each line element, a total of 14 responses are stored. Therefore, the maximum number of elements for each riser is 10000 / 14 = 714. If the riser length is to be more than 3000 m, the minimum element length is 3000 m / 714 = 4.2 m. The element length of 5 m was chosen for the fatigue analysis of 3000 m long SCR.

The simplified sea state fatigue blocks are shown in Table 5.4.1 and 5.4.2. A total time series length of 45 min (2700 s) is used for each sea state for the fatigue life evaluation.

**Table 5.4.1** Multiple Wave Spectrums – 6 Sea State Blocks.

| Block | $H_s$ (m) | $T_p$ (s) | Gamma | Type | Probability (%) |
|---|---|---|---|---|---|
| 1 | 3.25 | 7.15 | 3.28 | JONSWAP | 9.4 |
| 2 | 3.25 | 10.4 | 1.00 | | 45.9 |
| 3 | 3.25 | 14.3 | 1.00 | | 7.7 |
| 4 | 6.25 | 10.4 | 2.63 | | 22.9 |
| 5 | 6.25 | 14.3 | 1.00 | | 9.5 |
| 6 | 9.25 | 14.3 | 1.41 | | 4.6 |

**Table 5.4.2** Scatter Discretisation – 6 Sea State Blocks.

| $H_s$ (m) / $T_p$ (s) | 5.85 | 7.15 | 8.45 | 9.75 | 11.05 | 12.35 | 13.65 | 14.95 | 16.25 |
|---|---|---|---|---|---|---|---|---|---|
| 0.25 | 1 | 1 | 2 | 1 | 1 | | | | |
| 0.75 | 2 | 18 | 19 | 14 | 10 | 5 | 1 | 1 | 1 |
| 1.25 | 5 | 30 | 42 | 25 | 18 | 14 | 5 | 2 | 1 |
| 1.75 | 2 | 21 | 46 | 39 | 24 | 14 | 6 | 1 | 1 |
| 2.25 | | 11 | 47 | 50 | 25 | 8 | 4 | 1 | 1 |
| 2.75 | | 2 | 33 | 38 | 25 | 7 | 2 | 1 | 1 |
| 3.25 | | 1 | 17 | 35 | 23 | 10 | 5 | 1 | 1 |
| 3.75 | | | 5 | 27 | 21 | 9 | 3 | 1 | 1 |
| 4.25 | | | 2 | 21 | 20 | 12 | 3 | 2 | 1 |
| 4.75 | | | | 9 | 20 | 11 | 3 | 1 | 1 |
| 5.25 | | | | 3 | 11 | 10 | 3 | 1 | 1 |
| 5.75 | | | | 2 | 6 | 10 | 4 | 1 | |
| 6.25 | | | | | 4 | 10 | 5 | 1 | 1 |
| 6.75 | | | | | 2 | 5 | 3 | 1 | |
| 7.25 | | | | | 1 | 3 | 2 | 1 | 1 |
| 7.75 | | | | | | 1 | 3 | 1 | |
| 8.25 | | | | | | 1 | 2 | 1 | |
| 8.75 | | | | | | | 1 | 1 | |
| 9.25 | | | | | | | 1 | | 1 |

Configuration P of riser lengths 2000 and 3000 m is assessed respectively for FLS (see Figure 5.4.2). The shortest fatigue life of configuration P is 284.8 and 244.5 yr at TDA section for riser lengths 2000 and 3000 m respectively which indicates that the fatigue performance of configuration P with shorter length 2000 m is better than P with longer length 3000 m (see Table 5.4.3).

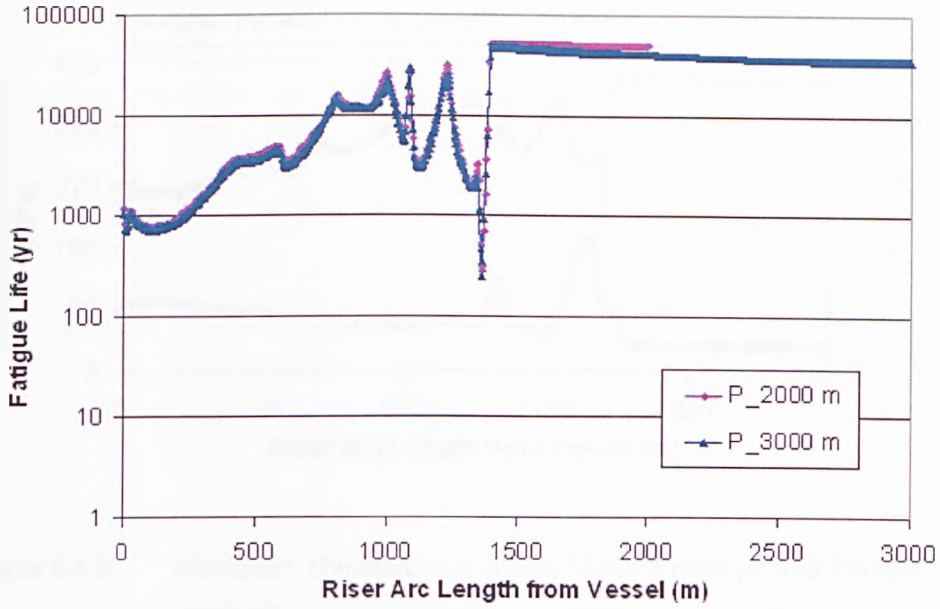


**Figure 5.4.2** Fatigue Life along Riser Arc Length for Configuration P of Riser Lengths 2000 and 3000 m.

**Table 5.4.3** Riser Fatigue Response for Riser Lengths 2000 and 3000 m.

| Riser Length (m) | Shortest Fatigue Life (yr) | |
|---|---|---|
| | At Top | At TDA |
| 2000 | 764.2 | 284.8 |
| 3000 | 713.5 (–6.6%) | 244.5 (–14.2%) |

The maximum dynamic von Mises stress envelope and fatigue life along riser arc length for configuration P of riser length 2000 m is displayed in Figure 5.4.3. It shows that the maximum dynamic von Mises stress and the lowest fatigue life didn't happen at the same point. The riser arc length from vessel for the maximum dynamic von Mises stress point was 1314.06 m while the riser arc length from vessel for the lowest fatigue point was 1365.39 m.

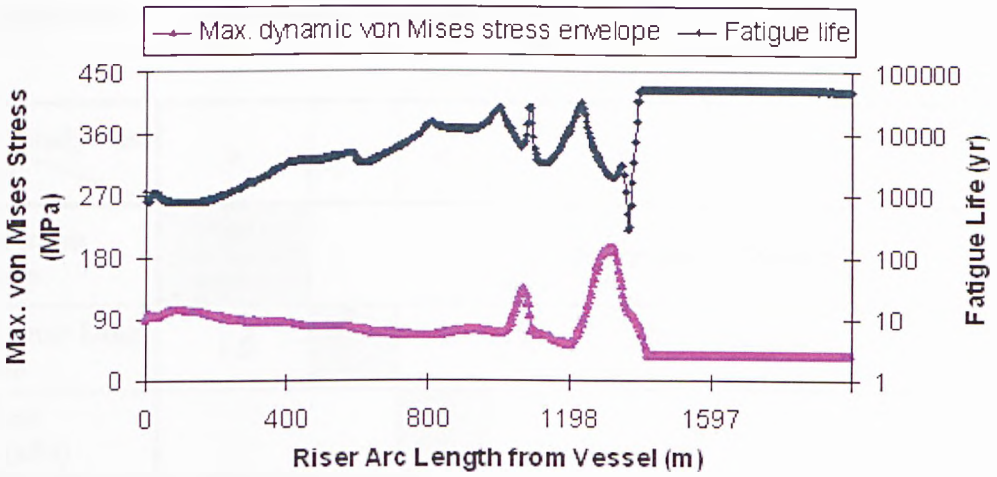


**Figure 5.4.3** Maximum Dynamic von Mises Stress Envelope and Fatigue Life along Riser Arc Length for Configuration P of Riser Length 2000 m.

The impacts on the riser fatigue life of different parameters have been investigated by changing parameters listed below:

- Wave spectral formulation
- Hydrodynamic drag coefficient
- Soil stiffness modelling
- Selection of S-N curve
- Determination of SCF
- Sea state representation
- Selection of safety factor

For each study case, all the parameter values are fixed except the value of the specific parameter which is under investigation, as shown in Table 5.4.4.

**Table 5.4.4** SCR Fatigue Design Parameters for Sensitivity Study.

| Parameter \ Study Case | a | b | c | d | e | f | g |
|---|---|---|---|---|---|---|---|
| Wave Spectrum Formulation | JONSWAP, Bretschneider Spectrum | 3 parameter JONSWAP | | | | | |
| Hydrodynamic Drag Coefficient | 1.0 | 0.7 – 1.2 | 1.0 | | | | |
| Normal Soil Stiffness (kPa) | | | 100 ~ 5000 | | | | |
| Transverse Soil Stiffness (kPa) | 10 | | | | | | |
| S-N Curve | DNV-Seawater-cathodic double-slope D | | | DNV-Seawater-cathodic double-slope C, C1, C2, D, E, DNV single slope D, DOE E, API X' | DNV-Seawater-cathodic double-slope D | | |
| SCF | 1.0 | | | | 0.8 – 1.2 | 1.0 | |
| Sea State Representation | 6 sea state blocks | | | | | 3, 6, 8, 14 sea state blocks | 6 sea state blocks |
| Safety Factor | 10 | | | | | | 3, 6, 10 |

Note that SCF is studied for values 0.8, 0.9, 1.0, 1.1 and 1.2 while there is no realistic meaning in value choices 0.8 and 0.9 for no SCF will be less than 1.0 according to its definition (DNV-RP-F204, 2005). The values of 0.8 and 0.9 for SCF are just for the mathematical study about the effect of SCF variation on the resultant fatigue life.

The riser fatigue performance with different featured parameters is investigated as follows.

### *5.4.1 Wave Spectral Formulation*

The root mean square (RMS) value $\sigma_s$ of the stress variation $S$ for a given sea-state is given by the following equation:

$$\sigma_s = \sqrt{\int_0^\infty S_{\eta\eta}(\omega)\,d\omega} \tag{5.4.1}$$

where $S_{\eta\eta}$ is expressed by equation 3.5.5.

Every $\sigma_s$ has an associated average wave period $T_z$:

$$T_z = \frac{2\pi\sigma_s}{\sqrt{\int_0^\infty \omega^2 S_{\eta\eta}(\omega)\,d\omega}} \tag{5.4.2}$$

Assuming that this given sea-state will occur a fraction $m$ of the entire *Life* of the structure, the corresponding number of cycles will be given by:

$$N = \frac{mLife}{T_z} \tag{5.4.3}$$

The corresponding damage, assuming a Rayleigh distribution is then given by:

$$D = \frac{N}{\sigma_s^2}\int_0^\infty \frac{s}{N(s)}\exp\left[-\left(\frac{s}{2\sqrt{2\sigma}}\right)^2\right]ds \tag{5.4.4}$$

SCR Base Case

- Configuration — P
- Riser length — 2000 m
- Mesh length — 4 m
- Vessel offset — 0 m, mean position
- *Wave spectrum* — *JONSWAP, and Bretschneider Spectrum*
- Sea-state scatter diagram — Northern North Sea (Figure 5.4.1)
- S-N curve — DNV-D-Seawater-cathodic
- SCF — 1.0

The fatigue performance along the riser length for wave spectra JONSWAP and Bretschneider is shown in Figure 5.4.4. The shortest fatigue lives are 764.2 and 815.3 yr at top and 284.8 and 297.2 yr at TDA respectively for wave spectra JONSWAP and Bretschneider (see Table 5.4.5). The overall fatigue lives along the riser are similar by both wave spectra. Spectrum JONSWAP is used for the following study.

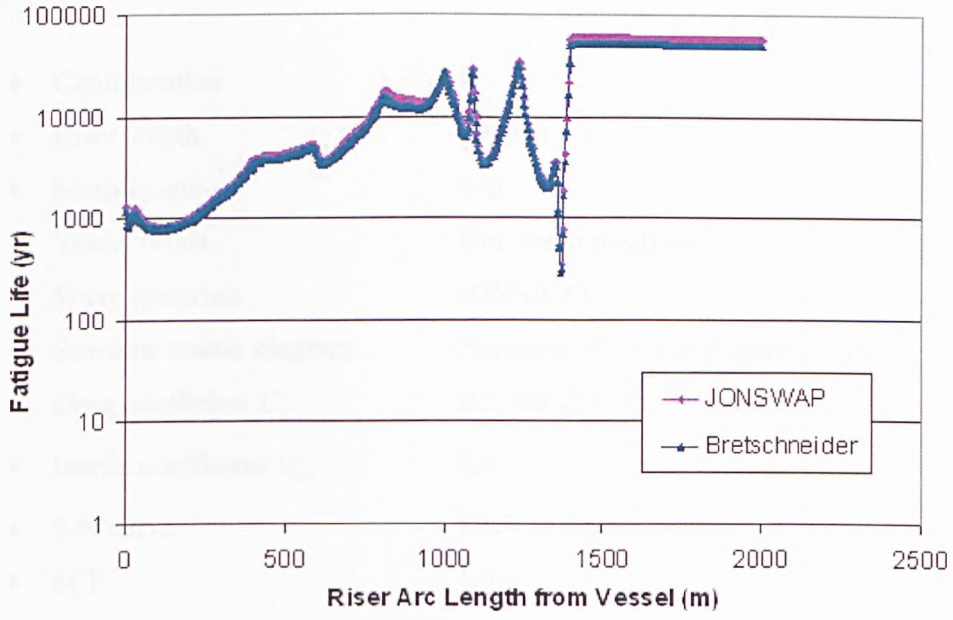


**Figure 5.4.4** Fatigue Life along Riser Arc Length for Wave Spectra JONSWAP and Bretschneider.

**Table 5.4.5** Riser Fatigue Response for Wave Spectra JONSWAP and Bretschneider.

| Hydrodynamic Drag Coefficient $C_d$ | Shortest Fatigue Life (yr) | |
|---|---|---|
| | At Top | At TDA |
| JONSWAP | 764.2 | 284.8 |
| Bretschneider | 815.3 | 297.2 |

### 5.4.2 *Hydrodynamic Drag Coefficient*

The riser fatigue performance with various hydrodynamic drag coefficients $C_d$ is investigated as follows.

SCR Base Case

- Configuration — P
- Riser length — 2000 m
- Mesh length — 4 m
- Vessel offset — 0 m, mean position
- Wave spectrum — JONSWAP
- Sea-state scatter diagram — Northern North Sea (Figure 5.4.1)
- *Drag coefficient* $C_d$ — *0.7, 0.8, 0.9, 1.0, 1.1 and 1.2*
- Inertia coefficient $C_m$ — 2.0
- S-N curve — DNV-D-Seawater-cathodic
- SCF — 1.0

The fatigue performance along the riser length for riser configuration P for various hydrodynamic drag coefficients is shown in Figure 5.4.5. The fatigue critical locations were short and peak at TDA and close to the top end (Table 5.4.6 and Figure 5.4.6). With the increase of hydrodynamic drag coefficient by each 0.1, the lowest fatigue life at Top was decreased averagely by 3.85 % while the lowest fatigue life at TDA was increased decreasingly till decreased when $C_d$ = 1.1 and then increased again which means that hydrodynamic drag coefficient should be carefully chosen also for the sake of accurate fatigue life assessment.

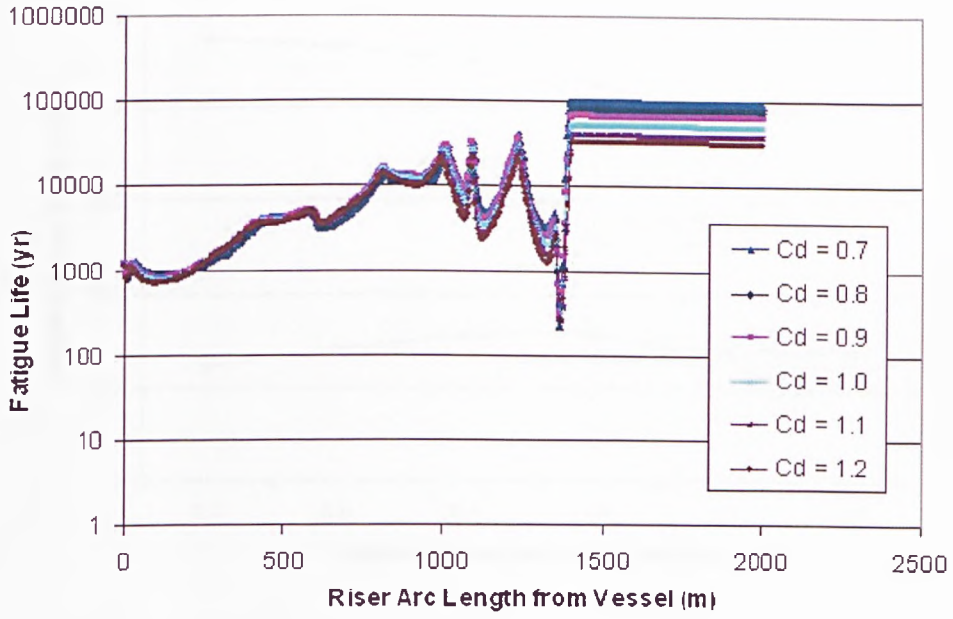


**Figure 5.4.5** Fatigue Life along Riser Arc Length for Various Hydrodynamic Drag Coefficients 0.7 – 1.2.

**Table 5.4.6** Riser Fatigue Response for Various Hydrodynamic Drag Coefficients 0.7 – 1.2.

| Hydrodynamic Drag Coefficient $C_d$ | Shortest Fatigue Life (yr) | |
|---|---|---|
| | At Top | At TDA |
| 0.7 | 849.9 | 218.9 |
| 0.8 | 836.4 (–1.59%) | 252.6 (+15.40%) |
| 0.9 | 812.4 (–2.87%) | 281.0 (+11.24%) |
| 1.0 | 764.2 (–5.93%) | 284.8 (+1.35%) |
| 1.1 | 720.3 (–5.74%) | 247.1 (–13.24%) |
| 1.2 | 698.0 (–3.10%) | 258.0 (+4.41%) |

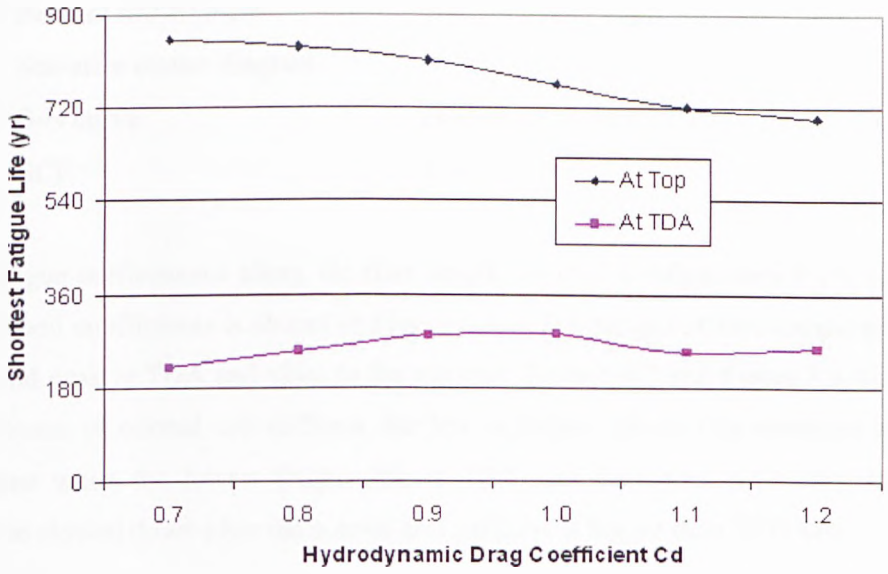


**Figure 5.4.6** Shortest Riser Fatigue Lives at Top and TDA for Various Hydrodynamic Drag Coefficients 0.7 – 1.2.

### *5.4.3 Soil Stiffness Modelling*

The riser fatigue performance with various normal soil stiffness is investigated as follows.

SCR Base Case

- Configuration — P
- Riser length — 2000 m
- Mesh length — 4 m
- Vessel offset — 0 m, mean position
- Wave spectrum — JONSWAP
- Drag coefficient $C_d$ — 1.0
- Inertia coefficient $C_m$ — 2.0
- Transverse soil stiffness — 10 kPa

- *Normal soil stiffness* *100, 300, 600, 2000, and 5000 kPa*
- Sea-state scatter diagram Northern North Sea (Figure 5.4.1)
- S-N curve DNV-D-Seawater-cathodic
- SCF 1.0

The fatigue performance along the riser length for riser configuration P for various normal soil coefficients is shown in Figure 5.4.7. The fatigue critical locations were short and peak at TDA and close to the top end (Table 5.4.7 and Figure 5.4.8). With the increase of normal soil stiffness, the lowest fatigue life at Top remained almost the same while the lowest fatigue life at TDA was decreased noticeably but the decrease slowed down after the normal soil stiffness is bigger than 2000 kPa.

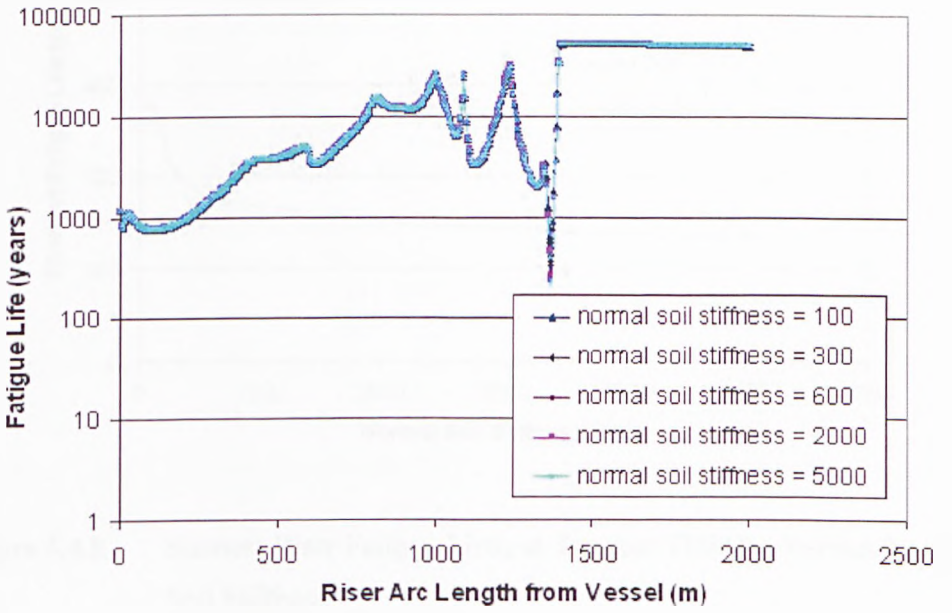


**Figure 5.4.7** Fatigue Life along Riser Arc Length for Various Normal Soil Stiffness.

**Table 5.4.7** Riser Fatigue Response for Various Normal Soil Stiffness.

| Normal Soil Stiffness (kPa) | Shortest Fatigue Life (yr) | |
|---|---|---|
| | At Top | At TDA |
| 100 | 764.3 | 441.2 |
| 300 | 764.4 | 327.6 (–25.75%) |
| 600 | 764.2 | 284.8 (–13.06%) |
| 2000 | 764.3 | 242.3 (–14.92%) |
| 5000 | 764.2 | 217.6 (–10.19%) |

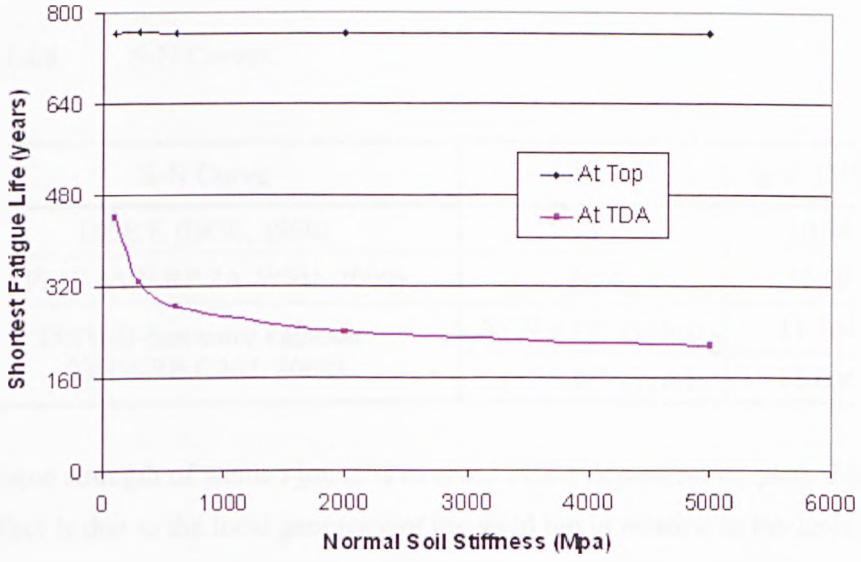


**Figure 5.4.8** Shortest Riser Fatigue Lives at Top and TDA for Various Normal Soil Stiffness.

### *5.4.4 Selection of S-N Curve*

The S-N curves form the basis for description of the SCR's fatigue capacity. These curves relate the number of stress cycles to failure, $N$, to the corresponding stress range $S$ including the effects of stress concentrations. The relevant S-N curves applicable to risers have either a single slope (expressed as equation 5.2.4) or double

slope (bilinear) behaviour. Note that bilinear S-N curves can only be used for risers with corrosion protection. Because the riser material stainless steel super-duplex grade F55 used for SCRs in the current study cases has good corrosion resistance, bilinear S-N curves can be applied here.

It is recommended that an appropriate S-N curve from a recognized national or international standard be the basic component S-N fatigue design curve. Normally, a conservative S-N curve such as the API X', UK DOE E, or DNV curves is assumed. Table 5.4.8 summarises the three most widely used S-N curves for SCR fatigue design.

**Table 5.4.8** S-N Curves.

| S-N Curve | m | $\lg K$ (MPa) |
|---|---|---|
| DOE E (DOE, 1990) | 3 | 10.34 |
| API X' (API RP 2A-WSD, 2000) | 3.74 | 11.09 |
| DNV-D-Seawater-cathodic (DNV-RP-C203, 2008) | 3 ($N \leq 10^6$ cycles) | 11.764 |
| | 5 ($N > 10^6$ cycles) | 15.606 |

The fatigue strength of welded joints is to some extent dependent on plate thickness. This effect is due to the local geometry of the weld toe in relation to thickness of the adjoining plates. It is also dependent on the stress gradient over the thickness. Thus the design S-N curve is given as (DNV-RP-F204, 2005)

$$\log N = \log K - m \log\left[\Delta\sigma\left(\frac{t}{t_{ref}}\right)^{L}\right] \tag{5.4.6}$$

where

$m$ negative inverse double slope of the S-N curve

$\log K$ intercept of $\lg N$ axis

$t_{ref}$ reference thickness equal 25 mm for welded connections other than tubular joints

$t$ thickness through which a crack will most likely grow

$L$ thickness exponent on fatigue strength

SCR Base Case

- Configuration: P
- Riser length: 3000 m
- Mesh length: 5 m
- Vessel offset: 0 m, mean position
- Wave spectrum: JONSWAP
- Sea-state scatter diagram: Northern North Sea (Figure 5.4.1)
- *S-N curve*: *DNV-Seawater-cathodic double-slope C, C1, C2, D, E, DNV single slope D, DOE E, and API X'*
- SCF: 1.0

S-N curves for seawater environment with cathodic protection are given in Table 5.4.9.

The fatigue performance along the riser length for riser configuration P with different S-N curves is shown in Figure 5.4.9. The fatigue critical locations were short and peak at TDA and close to the top end (Table 5.4.10 and Figure 5.4.10). It is noted that with DNV double-slope curves the riser had sufficient design life for fatigue except E curve. However, if the weld quality and pipe matching tolerance can be improved by C1 or C2 curve, the riser can easily get fatigue life with a margin of safety. But when DNV D single-slope, DOE E, and API X' curves were used, the overall fatigue life of the riser dropped dramatically, especially for DOE E and API X' curves. For a same DNV D level curve, the fatigue life at Top and TDA was decreased by 89.70% and 87.81% respectively for single slope compared with double slope. For DOE E and API X' curves, the fatigue lives at TDA dropped to as low as

nearly zero. It is because the feature of SCR fatigue stress is low range high cycle which indicates that double-slope S-N curves may be suitable for deepwater SCRs and can predict much better fatigue life for them.

**Table 5.4.9** S-N Curves for Seawater Environment with Cathodic Protection.

| S-N Curve | m1 | m2 | log $K$ | $L$ | $t_{ref}$ (mm) |
|---|---|---|---|---|---|
| DNV C | 3 | 5 | 12.192 | 0.15 | 25 |
| DNV C1 | 3 | 5 | 12.049 | 0.15 | 25 |
| DNV C2 | 3 | 5 | 11.901 | 0.15 | 25 |
| DNV D | 3 | 5 | 11.764 | 0.2 | 25 |
| DNV E | 3 | 5 | 11.610 | 0.2 | 25 |
| DNV D Single-Slope | 3 | / | 11.764 | 0.2 | 25 |
| DOE E | 3 | / | 10.34 | 0.2 | 25 |
| API X' | 3.74 | / | 11.09 | 0.2 | 25 |

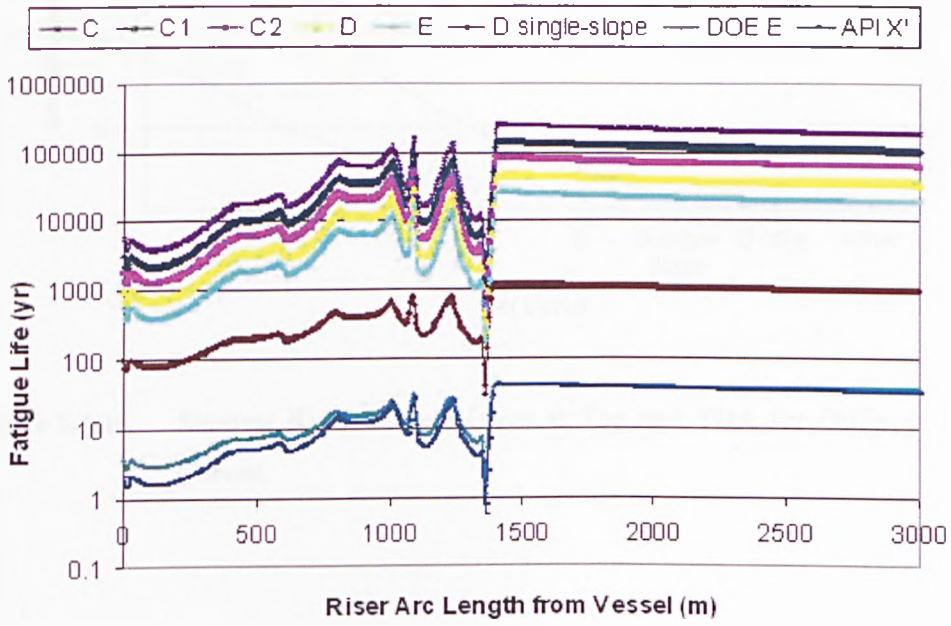


**Figure 5.4.9** Fatigue Life along Riser Arc Length for Different S-N Curves.

**Table 5.4.10** Riser Fatigue Response for Different S-N Curves.

| S-N Curve | Shortest Fatigue Life (yr) | |
|---|---|---|
| | At Top | At TDA |
| DNV C | 3859.2 | 1322.7 |
| DNV C1 | 2229.3 | 764.1 |
| DNV C2 | 1263.3 | 433.0 |
| DNV D | 713.5 | 244.5 |
| DNV E | 395.1 | 135.4 |
| DNV D Single-Slope | 73.5 | 29.8 |
| DOE E | 2.8 | 1.1 |
| API X | 1.5 | 0.6 |

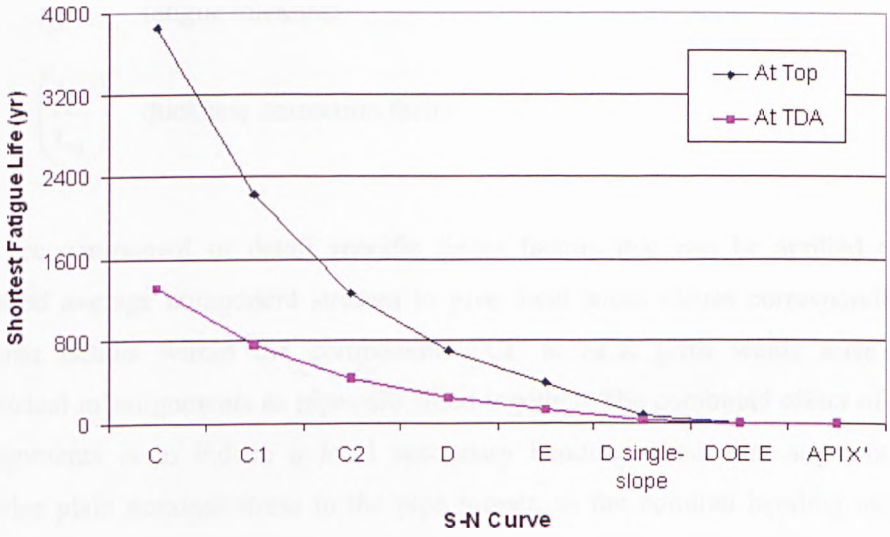


**Figure 5.4.10** Shortest Riser Fatigue Lives at Top and TDA for Different S-N Curves.

### 5.4.5 Determination of Stress Concentration Factor (SCF)

The stress range to be applied in fatigue damage calculations is found by application of an SCF as well as a thickness correction factor to the nominal stress range:

$$S = S_0 \cdot SCF \cdot \left( \frac{t_{fat}}{t_{ref}} \right)^L \tag{5.4.7}$$

where

$S_0$ nominal stress range

$SCF$ stress concentration factor

$t_{fat}$ fatigue thickness

$\left( \frac{t_{fat}}{t_{ref}} \right)^L$ thickness correction factor

SCFs are component or detail specific linear factors that can be applied to the calculated average component stresses to give local stress values corresponding to particular details within the component. SCF at SCR girth welds arise from geometrical misalignments as pipes are fitted together. The combined effect of these misalignments is to induce a local secondary bending stress that augments the otherwise plain nominal stress in the pipe proper, as the nominal bending moment and axial forces are transferred across the weld. Given the good quality of the end preparation in SCRs, angular misalignment is virtually eliminated. Hence, the hi-lo condition arising from thickness mismatch dominates. SCFs are calculated to take this mismatch into account.

In general, there are two approaches to determine the SCF for a given SCR pipe with tolerance. The first approach is based on testing and numerical simulation. An empirical formulation based on data fitting is often used based on Buitrago and Zettlemoyer's findings (1998).

SCR Base Case

- Configuration — P
- Riser length — 3000 m
- Mesh length — 5 m
- Vessel offset — 0 m, mean position
- Wave spectrum — JONSWAP
- Sea-state scatter diagram — Northern North Sea (Figure 5.4.1)
- S-N curve — DNV-D-Seawater-cathodic
- *SCF* — *0.8, 0.9, 1.0, 1.1, and 1.2*

Note that as stated before the SCF values less than 1.0 have no realistic meaning. As shown by Figure 5.4.11 and 5.4.12, Table 5.4.11, the determination of SCF has a significant effect on the fatigue results. The shortest fatigue lives both at Top and TDA decreased with increased SCF value. SCF = 1.0 was suggested to be used with S-N D curve by DNV-RP-C203 (2008). With the increase of SCF by each 0.1, the lowest fatigue life at Top and TDA was both decreased averagely by 40 %.

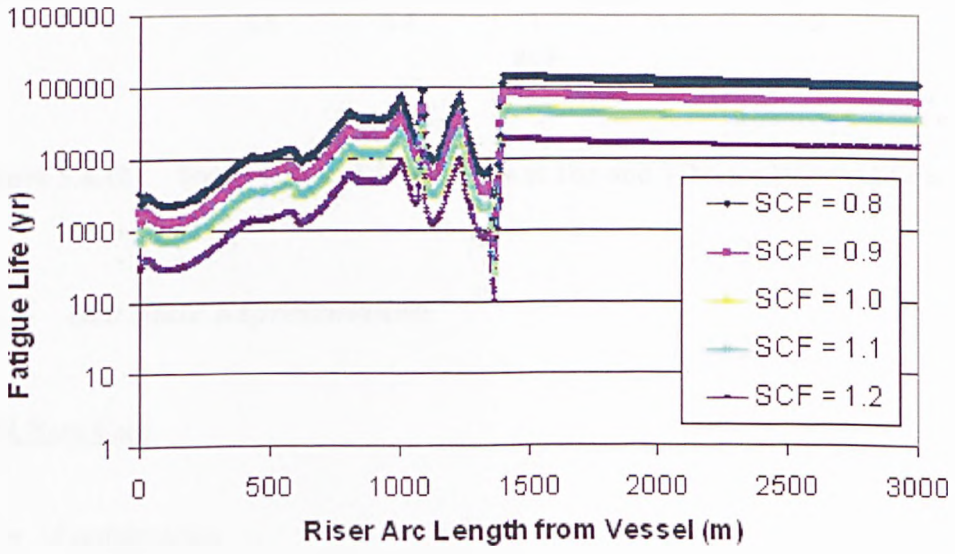


**Figure 5.4.11** Fatigue Life along Riser Arc Length for Various SCFs.

**Table 5.4.11** Riser Fatigue Response for Various SCFs.

| SCF | Shortest Fatigue Life (yr) | |
|---|---|---|
| | At Top | At TDA |
| 0.8 | 2177.3 | 746.3 |
| 0.9 | 1208.3 (-44.50%) | 414.1 (-44.51%) |
| 1.0 | 713.5 (-40.87%) | 244.5 (-40.96%) |
| 1.1 | 443.0 (-37.91%) | 151.8 (-37.91%) |
| 1.2 | 286.7 (-35.28%) | 98.3 (-35.24%) |

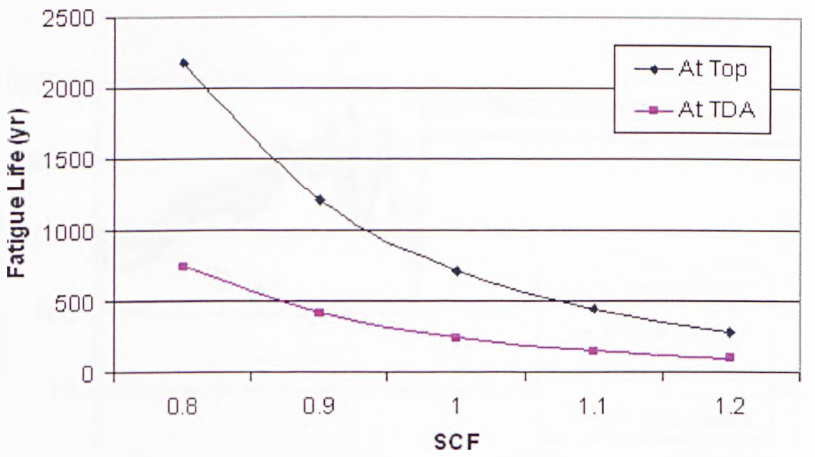


**Figure 5.4.12** Shortest Riser Fatigue Lives at Top and TDA for Various SCFs.

### *5.4.6 Sea State Representation*

SCR Base Case

- Configuration P
- Riser length 3000 m
- Mesh length 5 m
- Vessel offset 0 m, mean position

- Wave spectrum — JONSWAP
- *Sea-state scatter diagram* — *Northern North Sea (Figure 5.4.1)*
  *3, 6, 8, and 14 sea state blocks*
- S-N curve — DNV-D-Seawater-cathodic
- SCF — 1.0

The wave scatter diagram is divided into various blocks for investigation (as shown in Tables 5.4.12 & 5.4.15, 5.4.1 & 5.4.2, 5.4.13 & 5.4.16, 5.4.14 & 5.4.17). The overall fatigue lives calculated under various number of sea state blocks are shown in Figure 5.4.13. Their shortest fatigue lives at Top and TDA are compared in Table 5.3.18 and Figure 5.4.14.

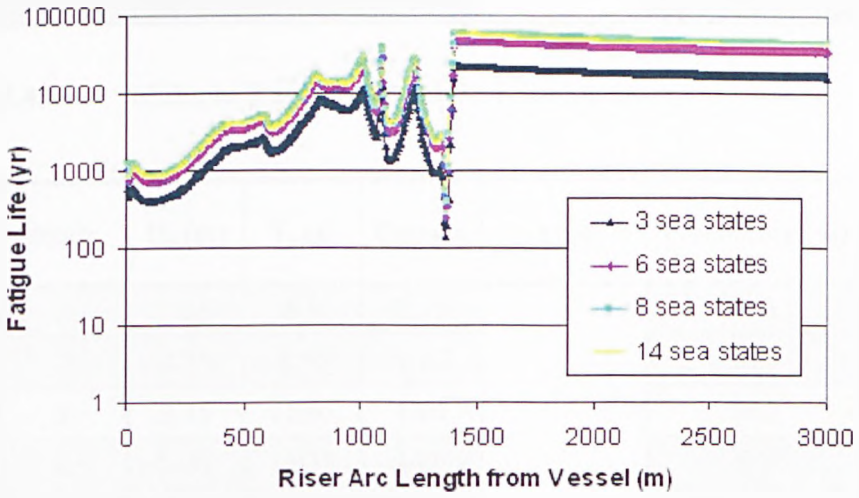


**Figure 5.4.13** Fatigue Life along Riser Arc Length for Various Sea States.

**Table 5.4.12** Multiple Wave Spectrums – 3 Sea States.

| Block | $H_s$ (m) | $T_p$ (s) | Gamma | Type | Probability (%) |
|---|---|---|---|---|---|
| 1 | 4.75 | 8.45 | 3.64 | JONSWAP | 57.1 |
| 2 | 4.75 | 14.3 | 1.00 | | 29.3 |
| 3 | 9.25 | 14.3 | 1.14 | | 13.6 |

**Table 5.4.13** Multiple Wave Spectrums – 8 Sea States.

| Block | $H_s$ (m) | $T_p$ (s) | Gamma | Type | Probability (%) |
|---|---|---|---|---|---|
| 1 | 2.75 | 7.15 | 2.21 | JONSWAP | 9.4 |
| 2 | 2.75 | 10.4 | 1.00 | | 36.3 |
| 3 | 2.75 | 14.3 | 1.00 | | 6.6 |
| 4 | 5.25 | 10.4 | 1.70 | | 29.6 |
| 5 | 5.25 | 14.3 | 1.00 | | 7.6 |
| 6 | 7.75 | 11.05 | 3.27 | | 2.9 |
| 7 | 7.75 | 14.3 | 1.00 | | 6.3 |
| 8 | 9.75 | 14.3 | 1.62 | | 1.3 |

**Table 5.4.14** Multiple Wave Spectrums – 14 Sea States.

| Block | $H_s$ (m) | $T_p$ (s) | Gamma | Type | Probability (%) |
|---|---|---|---|---|---|
| 1 | 2.25 | 6.5 | 2.15 | JONSWAP | 1.0 |
| 2 | 2.75 | 8.45 | 1.00 | | 23.7 |
| 3 | 2.75 | 11.05 | 1.00 | | 20.7 |
| 4 | 2.75 | 13.65 | 1.00 | | 5.7 |
| 5 | 2.75 | 16.25 | 1.00 | | 0.9 |
| 6 | 4.75 | 8.45 | 3.64 | | 6.0 |
| 7 | 5.25 | 11.05 | 1.23 | | 23.9 |
| 8 | 5.25 | 13.65 | 1.00 | | 6.5 |
| 9 | 5.25 | 16.25 | 1.00 | | 1.1 |
| 10 | 7.75 | 11.05 | 3.27 | | 2.9 |
| 11 | 7.75 | 13.65 | 1.12 | | 5.5 |
| 12 | 7.75 | 16.25 | 1.00 | | 0.8 |
| 13 | 9.75 | 13.65 | 2.06 | | 0.9 |
| 14 | 9.75 | 16.25 | 1.00 | | 0.4 |

**Table 5.4.15** Scatter Discretisation – 3 Sea State Blocks.

| $H_s$ (m) / $T_p$ (s) | 5.85 | 7.15 | 8.45 | 9.75 | 11.05 | 12.35 | 13.65 | 14.95 | 16.25 |
|---|---|---|---|---|---|---|---|---|---|
| 0.25 | 1 | 1 | 2 | 1 | 1 | | | | |
| 0.75 | 2 | 18 | 19 | 14 | 10 | 5 | 1 | 1 | 1 |
| 1.25 | 5 | 30 | 42 | 25 | 18 | 14 | 5 | 2 | 1 |
| 1.75 | 2 | 21 | 46 | 39 | 24 | 14 | 6 | 1 | 1 |
| 2.25 | | 11 | 47 | 50 | 25 | 8 | 4 | 1 | 1 |
| 2.75 | | 2 | 33 | 38 | 25 | 7 | 2 | 1 | 1 |
| 3.25 | | 1 | 17 | 35 | 23 | 10 | 5 | 1 | 1 |
| 3.75 | | | 5 | 27 | 21 | 9 | 3 | 1 | 1 |
| 4.25 | | | 2 | 21 | 20 | 12 | 3 | 2 | 1 |
| 4.75 | | | | 9 | 20 | 11 | 3 | 1 | 1 |
| 5.25 | | | | 3 | 11 | 10 | 3 | 1 | 1 |
| 5.75 | | | | 2 | 6 | 10 | 4 | 1 | |
| 6.25 | | | | | 4 | 10 | 5 | 1 | 1 |
| 6.75 | | | | | 2 | 5 | 3 | 1 | |
| 7.25 | | | | | 1 | 3 | 2 | 1 | 1 |
| 7.75 | | | | | | 1 | 3 | 1 | |
| 8.25 | | | | | | 1 | 2 | 1 | |
| 8.75 | | | | | | | 1 | 1 | |
| 9.25 | | | | | | | 1 | | 1 |

**Table 5.4.16** Scatter Discretisation – 8 Sea State Blocks.

| $H_s$ (m) / $T_p$ (s) | 5.85 | 7.15 | 8.45 | 9.75 | 11.05 | 12.35 | 13.65 | 14.95 | 16.25 |
|---|---|---|---|---|---|---|---|---|---|
| 0.25 | 1 | 1 | 2 | 1 | 1 | | | | |
| 0.75 | 2 | 18 | 19 | 14 | 10 | 5 | 1 | 1 | 1 |
| 1.25 | 5 | 30 | 42 | 25 | 18 | 14 | 5 | 2 | 1 |
| 1.75 | 2 | 21 | 46 | 39 | 24 | 14 | 6 | 1 | 1 |
| 2.25 | | 11 | 47 | 50 | 25 | 8 | 4 | 1 | 1 |
| 2.75 | | 2 | 33 | 38 | 25 | 7 | 2 | 1 | 1 |
| 3.25 | | 1 | 17 | 35 | 23 | 10 | 5 | 1 | 1 |
| 3.75 | | | 5 | 27 | 21 | 9 | 3 | 1 | 1 |
| 4.25 | | | 2 | 21 | 20 | 12 | 3 | 2 | 1 |
| 4.75 | | | | 9 | 20 | 11 | 3 | 1 | 1 |
| 5.25 | | | | 3 | 11 | 10 | 3 | 1 | 1 |
| 5.75 | | | | 2 | 6 | 10 | 4 | 1 | |
| 6.25 | | | | | 4 | 10 | 5 | 1 | 1 |
| 6.75 | | | | | 2 | 5 | 3 | 1 | |
| 7.25 | | | | | 1 | 3 | 2 | 1 | 1 |
| 7.75 | | | | | | 1 | 3 | 1 | |
| 8.25 | | | | | | 1 | 2 | 1 | |
| 8.75 | | | | | | | 1 | 1 | |
| 9.25 | | | | | | | 1 | | 1 |

**Table 5.4.17** Scatter Discretisation – 14 Sea State Blocks.

| $T_p$ (s) \ $H_s$ (m) | 5.85 | 7.15 | 8.45 | 9.75 | 11.05 | 12.35 | 13.65 | 14.95 | 16.25 |
|---|---|---|---|---|---|---|---|---|---|
| 0.25 | 1 | 1 | 2 | 1 | 1 | | | | |
| 0.75 | 2 | 18 | 19 | 14 | 10 | 5 | 1 | 1 | 1 |
| 1.25 | 5 | 30 | 42 | 25 | 18 | 14 | 5 | 2 | 1 |
| 1.75 | 2 | 21 | 46 | 39 | 24 | 14 | 6 | 1 | 1 |
| 2.25 | | 11 | 47 | 50 | 25 | 8 | 4 | 1 | 1 |
| 2.75 | | 2 | 33 | 38 | 25 | 7 | 2 | 1 | 1 |
| 3.25 | | 1 | 17 | 35 | 23 | 10 | 5 | 1 | 1 |
| 3.75 | | | 5 | 27 | 21 | 9 | 3 | 1 | 1 |
| 4.25 | | | 2 | 21 | 20 | 12 | 3 | 2 | 1 |
| 4.75 | | | | 9 | 20 | 11 | 3 | 1 | 1 |
| 5.25 | | | | 3 | 11 | 10 | 3 | 1 | 1 |
| 5.75 | | | | 2 | 6 | 10 | 4 | 1 | |
| 6.25 | | | | | 4 | 10 | 5 | 1 | 1 |
| 6.75 | | | | | 2 | 5 | 3 | 1 | |
| 7.25 | | | | | 1 | 3 | 2 | 1 | 1 |
| 7.75 | | | | | | 1 | 3 | 1 | |
| 8.25 | | | | | | 1 | 2 | 1 | |
| 8.75 | | | | | | | 1 | 1 | |
| 9.25 | | | | | | | 1 | | 1 |

**Table 5.4.18** Riser Fatigue Response for Various Sea State Blocks.

| Sea State Blocks | Shortest Fatigue Life (yr) | |
|---|---|---|
| | At Top | At TDA |
| 3 | 397.3 | 136.2 |
| 6 | 713.5 (+79.59%) | 244.5 (+79.52%) |
| 8 | 828.8 (+16.16%) | 278.0 (+13.70%) |
| 14 | 813.4 (–1.86%) | 280.2 (+0.79%) |

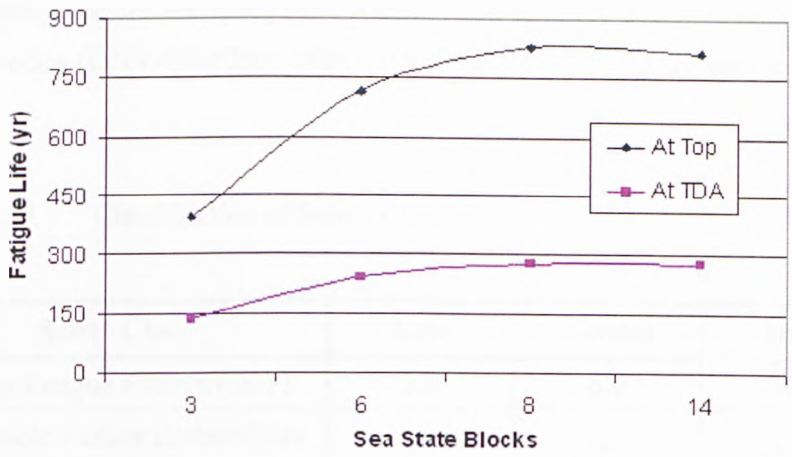


**Figure 5.4.14** Shortest Riser Fatigue Lives at Top and TDA for Various Sea State Blocks.

As shown, fewer blocks of sea state gave lower overall fatigue life prediction which is more conservative. Analyses with more blocks of sea states showed much closer fatigue life estimation but also cost higher computing resources. The multiple dynamic analyse for 14 sea state blocks simulation took 7.40 hr and occupied 20 GB space while the simulation for 3 sea state blocks spent only 2.18 hr and 4.5 GB space. Therefore, a 6 sea state wave spectrum was used which is believed to provide trustworthy fatigue life assessment with margin.

### *5.4.7 Selection of Safety Factor*

At present there is uncertainty regarding the fatigue safety factor for design for deepwater risers. As offshore field development moved into deeper waters where access for structural inspection was practically eliminated and where the consequences of failure increased sharply, the fatigue safety factor required was increased. A factor that has come into common usage is the factor 10, which has as its basis the achievement of specified reliability targets using probabilistic methods (Lotsberg, Fines, and Foss, 1984). The value of 10 is also specified in API RP 2T (1997) and API RP 2RD (1999).

Fatigue safety factors are specified corresponding to three safety classes in DNV offshore codes (DNV-OS-F201, 2001; DNV-RP-F204, 2005) as shown in Table 5.4.19.

**Table 5.4.19** Classification of Safety Classes.

| Safety Class | Low | Normal | High |
|---|---|---|---|
| Design Fatigue Factors (DFF) | 3.0 | 6.0 | 10.0 |
| Acceptable Failure Probabilities (Annual per Riser) | $10^{-3}$ | $10^{-4}$ | $10^{-5}$ |

Therefore, the fatigue criterion may be written:

$$D \cdot DFF \leq 1.0 \tag{5.4.8}$$

where

$D$ Accumulated fatigue damage (Palmgren-Miner's rule)

$DFF$ Design fatigue factor (Table 5.4.14)

Accordingly, the design lives for different safety class are shown in Table 5.4.20. Configuration P of both riser lengths 2000 and 3000 m can satisfied with all three levels of safety class.

**Table 5.4.20** Design Lives according to Different Safety Classes.

| Safety Class | Low | Normal | High |
|---|---|---|---|
| Design Fatigue Factors (DFF) | 3.0 | 6.0 | 10.0 |
| Service Life (yr) | 20 | | |
| Design Life (yr) | 60 | 120 | 200 |

## 5.5 Discussion and Conclusion

The results of the SCR base case analysis show that the majority of the riser has an acceptable fatigue life of more than 1000 years except the two major areas where fatigue damage should be assessed are the lower or touch down section and the top section close to the top connection. Fatigue damage input from all sources should be added along the SCR length.

Sensitivity analysis is performed to determine the sensitivity of riser fatigue life to wave spectral formulation, hydrodynamic drag coefficient, normal soil stiffness, S-N curve, stress concentration factor (SCF), sea state representation, and safety factor.

The sensitivity of fatigue damage due to wave spectra JONSWAP and Bretschneider is minor and JONSWAP was consistently chosen for the all fatigue life analysis as for previous dynamic analysis.

The influence of $C_d$ on the fatigue performance along the riser was not in a consistent trend. With the increase of $C_d$, the lowest fatigue life at Top was decreased while the lowest fatigue life at TDA might be increased or not. Overall, it had a bigger effect on SCR TDA than Top section with variation in $C_d$. Therefore, hydrodynamic drag coefficient $C_d$ should be decided carefully according to the actual local flow regime.

Although the sensitivity of dynamic response due to normal soil stiffness is insignificant, the sensitivity of fatigue life due to normal soil stiffness is unneglectable at TDA especially when normal soil stiffness was less than 1000 kPa. However, the influence of normal soil stiffness on the fatigue life of deepwater SCRs at Top is insignificant. No matter how much the normal soil stiffness value was changed, the variation in the riser lowest fatigue life at Top was within ±0.02%.

The sensitivity of fatigue damage due to S-N curve is significant, not only between linear and bilinear curves, but also among different levels of DNV bilinear curves. The feature of low range high cycle deepwater SCR fatigue stresses make DNV double-slope curves more suitable. Actually in most cases, the standard S-N curve is conservative for a specific project. The actual project based on S-N curve can be used based on full scale fatigue test results. In this study, DNV D curve was chosen for the specific case.

The sensitivity of fatigue damage due to stress concentration factor (SCF) is major. With the increase of SCF by each 0.1, the lowest fatigue life at Top and TDA can be both dropped averagely by as high as 40 % which means reducing SCF by improving weld conditions of fatigue critical welds especially close to the riser top section or at TDA can improve the riser fatigue life significantly.

The sensitivity of fatigue damage due to sea state representation is also important. The predicted fatigue life at critical areas can be even doubled by increasing the number of sea state division. But on the other side, increasing the number of sea state division also means increasing the computation cost which can be a serious problem for a heavy calculation as fatigue life estimation. Therefore, a balance between assessment accuracy and computation cost needs to be established.

Fatigue safety factors are classified into three safety levels in DNV offshore codes. Even for the highest level, the weight-optimised SCR can satisfy with the safety requirement.

The significance effect of all the parameters studied on the riser fatigue life is shown in Table 5.5.1.

Although compared with significant effect parameters, the effect of parameters wave spectrum formulation, hydrodynamic drag coefficient $C_d$ and normal soil stiffness on the riser fatigue life is lesser, their importance for a reliable riser fatigue life prediction is indispensable which requires a careful and proper value choice.

**Table 5.5.1** Significance Effect of Parameters on the Riser Fatigue Life.

| Parameter | Effect on Riser Fatigue Life |
|---|---|
| Wave Spectrum Formulation | Minor Significance |
| Hydrodynamic Drag Coefficient $C_d$ | Minor Significance |
| Normal Soil Stiffness | Minor Significance |
| S-N Curve | Significant |
| SCF | Significant |
| Sea State Representation | Significant |
| Safety Factor | Significant |

*Chapter 6*

# Reliability-Based Fatigue Analysis of Deepwater Weight-Optimised SCRs

## 6.1 Introduction

It should be appreciated that even with high quality NDT inspection experience shows that there is a 1 in 2 chance of missing a weld root flaw as big as 2 mm deep by 12 mm long. Such weld root defects will significantly reduce fatigue life.

Existing approaches for SCR design and analysis are typically based on deterministic methods as performed in Chapter 5. The design process includes requirements of structural strength based on ULS and fatigue criteria. The design procedure of SCRs used in conjunction with a semi-submersible in deepwater harsh environments was carried out by DNV DeepC & Riflex in the former chapters.

However, uncertainties in the loads, strengths and in the modelling of the systems require that methods based on probabilistic techniques in a number of situations have to be used. A structure is usually required to have a satisfactory performance in the expected lifetime, i.e. it is required that it does not collapse or becomes unsafe and

that it fulfils certain functional requirements. Reliability of structural systems can be defined as the probability that the structural under consideration has a proper performance throughout its lifetime. Reliability methods are used to estimate the probability of failure. Therefore, the response histories so obtained in Chapter 5 are employed for the study of probabilistic fatigue reliability by CALREL in the current chapter.

### *6.1.1 Problem Definition*

The probability of failure for a specific structure subjected to loads is a key problem in structural reliability analysis. For a particular structure there exists a limit value of the load it can withstand before failure occurs. The probability of failure herein refers to exceedance of a limit state. CALREL solves general structural system reliability problems of the form

$$p_f = P\left[g(\mathbf{X}) \le 0\right] \tag{6.1.1}$$

where

$p_f$ probability of failure

$g(\cdot)$ limit state function

The limit state function defines the requirement under which the structure is either in the safe region or in the failure region. In a general way this specific $g(\cdot)$-function may consist of n-variables $(X_1, X_2, ..., X_n)$ and the failure criterion is typically expressed as:

$$g(\mathbf{X}) = g(X_1, X_2, ..., X_n) = 0 \tag{6.1.2}$$

Failure occurs when $g(\mathbf{X}) < 0$. On the other hand, positive values of this specific g-function indicate the safe domain. The set of $X$-values giving $g(\mathbf{X})$ a zero value defines the limit surface. The probability of exceeding the limit can be expressed by the joint probability density function, $f_X(\mathbf{x})$, for all time-independent variables in $X$ over the failure domain:

$$p_f = \int_{g(X)\le 0} f_X(\mathbf{x})dx \tag{6.1.3}$$

The reliability index $\beta$ has a one-to-one non-linear relationship with the failure probability (Madsen, Krenk, and Lind, 1986):

$$p_f = \Phi(-\beta) \tag{6.1.4}$$

$$\beta = \Phi^{-1}(1-p_f) \tag{6.1.5}$$

where $\Phi$ is standard normal cumulative distribution function (CDF).

The relationship between reliability index and probability of failure is illustrated in Figure 6.1.1.

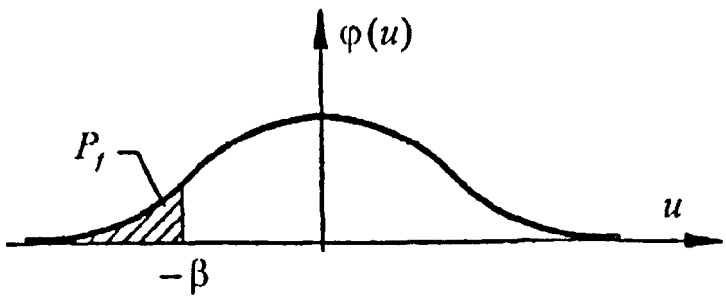


**Figure 6.1.1** Illustration of Reliability Index $\beta$ and Probability of Failure $p_f$.

where $\varphi$ is the standard normal density function.

### 6.1.2 Limit State Function

Both the S-N and FM method can be used to predict time to failure (implicit in SN data and explicitly defined in the FM approach).

The main use of the FM approach is for the assessment of the growth of through-thickness cracks. Fatigue lives predicted by the FM approach are sensitive to some parameters which are difficult to control, but which are implicit in S-N data.

### 6.1.3 Analysis Methods

To establish the probability of failure, two typical types of solution procedures are frequently employed:

- Simulation (numerical integration) algorithm
- Analytical (approximate) algorithm

Monte Carlo simulation (MCS) is a method to determine the probability of failure corresponding to the former type of analysis. The latter type consists typically of first order reliability method (FORM) and second order reliability method (SORM).

In FORM, the limit state surface in the standard normal space is represented by the tangent hyperplane at the design point. In SORM, the limit state surface in the standard normal space is replaced by a quadratic surface, which is tangent at the design point. While MCS is completely general, it is very expensive and time-consuming for small probabilities of failure, which is the major concern in reliability engineering. FORM and SORM are more accurate and efficient for extreme probability of failure; however implementation can be more complex. In the present study, approaches FORM and SORM have been applied to predict the fatigue reliability of SCR.

A brief description of FORM, SORM and MCS algorithms is given in Appendix F.

### *6.1.4 Basic Fatigue Uncertainty Treatment Methods*

There are two distinct approaches for treating uncertainties in fatigue problems:

- Randomised parametric approach
  Uncertainties are modelled by randomising the variables in the deterministic functions.

- Stochastic approach
  This typically uses the Markov chain theory to model the stochastic crack growth.

The stochastic approach provides useful insights for individual studies. However, their general application in engineering analysis has been limited so far.

The randomised parametric approach can be directly related to deterministic methods, e.g. the S-N method or the fracture mechanistic method.

A spectral fatigue analysis involves three major steps:

- Analyses of stresses induced by the random sea (characterised by the scatter diagram) are carried out by using a specific S-N curve.

- Rainflow cycle counting (RFC) in time domain is examined by taking the time history of load as an input. "Stress cycles" and "stress range" are gained accordingly.

- Palmgren-Miner's rule (cumulative damage theory) is used to estimate the fatigue life.

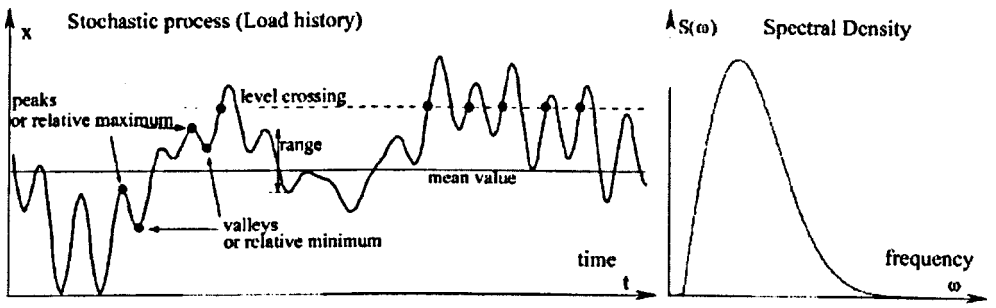


**Figure 6.1.2** Principal Parameters of a Stochastic Process (Tovo, 2002).

### *6.1.5 Analysis Procedure*

The analysis procedure of the reliability-based fatigue analysis of weight-optimised SCRs employed in the current study is as follows:

- Time domain dynamic analyses of the SCR for all sea states by DNV DeepC & RIFLEX;
- Rainflow Counting on the time domain analysis for each sea state by DNV Riserlife;
- Probabilistic fatigue reliability analysis for all sea states by CALREL.

## 6.2 S-N Based Failure Functions

In this approach, the fatigue strength is expressed in terms of S-N relation as given by equation 5.2.4.

The estimation of fatigue damage under stochastic loading is obtained by the Palmgren-Miner's model. In this model response statistics of riser stresses arising

due to the action of random waves are needed. It is assumed that the damage on the structure, per load cycle, $D_i$ is constant at a given stress range $S_i$ and is equal to

$$D_i = \frac{1}{N(S_i)} \tag{6.2.1}$$

where $N(S_i)$ is the number of cycles to failure at stress range $S_i$. The total damage accumulated in time $T_s$ is thus given by

$$D = \sum_{i=1}^{N(T_s)} \frac{1}{N(S_i)} \tag{6.2.2}$$

where $N(T_s)$ is the total number of stress cycles in time $T_s$. In this formulation it is assumed that the accumulated damage $D$ is independent of the sequence in which stress cycles occur.

### 6.2.1 *Linear S-N Model*

Using linear (single-slope) S-N curve, the accumulated damage, $D$, is given as

$$D = \sum_{i=1}^{N(T_s)} \frac{S_i^m}{K} \tag{6.2.3}$$

Since each stress range is a random variable $\sum_{i=1}^{N(T_s)} S_i^m$ is also a random variable. If $N(T_s)$ is sufficiently large, the uncertainty in the sum is very small and the sum can be replaced by its expected value. Therefore

$$E\left[\sum_{i=1}^{N(T_s)} S_i^m\right] = E\left[N(T_s)\right] E\left[S_i^m\right] \tag{6.2.4}$$

The expectation value of $S^m$ is $E[S^m] = \int_0^\infty S^m f(S) dS$, where $f(S)$ is the probability density function of the stress ranges.

For a narrow-band Gaussian process, stress ranges are Rayleigh distributed. The mean value of the stress range follows directly as

$$E[S_i^m] = \int_0^\infty (2x)^m \frac{x}{\sigma_x} \exp\left(-\frac{1}{2}\left(\frac{x}{\sigma_x}\right)^2\right) dx$$
$$= \left(2\sqrt{2}\right)^m \sigma_x^m \Gamma\left(1+\frac{m}{2}\right) \tag{6.2.5}$$

The long term stress range distribution is defined through a short term Rayleigh distribution within each short term period for the different loading conditions, and the accumulated fatigue damage expression can be given as

$$D = \frac{1}{K} E[N(T_s)] E[S^m] \tag{6.2.6}$$

Assuming the offshore environmental condition as a set of stationary short-term sea states, the total fatigue damage can be obtained by summing the accumulated damage over all the sea states. Thus, the total damage $D$ yields:

$$D = \frac{T_s}{K} \Omega \tag{6.2.7}$$

where $T_s$ is the riser life (years in service) and $\Omega$ is a stress parameter as

$$\Omega = \left(2\sqrt{2}\right)^m \Gamma\left(1+\frac{m}{2}\right) \sum_{j=1}^{n} f_j \nu_{0,j} \sigma_j^m \tag{6.2.8}$$

where

| | |
|---|---|
| $f_j$ | fraction of the time spent in $j$ th sea state (to account for long-term sea effect) |
| $\nu_{0_j} = \frac{\pi}{2}\sqrt{\frac{\lambda_2}{\lambda_0}}$ | zero mean crossing frequency of stress process in $j$ th sea state |
| $\sigma_j = \sqrt{\lambda_0}$ | standard deviation of stress process in $j$ th sea state |
| $\lambda_j = \int_0^\infty \omega^n S(\omega) d\omega$ | $j$ th moment of the stress spectrum |

Failure occurs if $D > \Delta$ where $\Delta$ is the value of the Palmgren-Miner's damage index at failure. However, Miner's original paper reported the failure in the range of $0.61 \leq \Delta \leq 1.45$. The large uncertainty in $\Delta$ arises from the empirical nature of equation 6.2.2 and it becomes a random variable denoted as $\Delta_F$. The lognormal distribution with unit median and a coefficient of variation of about 0.3 for $\Delta_F$ is used to account for modelling error associated with Miner's rule, after Wirsching (1984). Replacing the parameter $\Delta$ with the variable $\Delta_F$, the nature of the cumulative damage rule becomes probabilistic.

Letting $D = \Delta_F$, the time for fatigue failure $T$ of a joint is obtained as

$$T = \frac{\Delta_F K}{\Omega} \tag{6.2.9}$$

In order to take into account the uncertainties associated with the above expression, the factors involved in the expression shall be modelled as random variables. The basic operational life is expressed in terms of time to failure

$$T = \frac{\Delta_F K}{B^m \Omega} \tag{6.2.10}$$

where, $\Delta_F$, $K$, $B$ are random variables. $B$ describes the inaccuracies in estimating the fatigue stresses, including modelling error for extreme loads on the riser, environmental conditions in the Northern North Sea, and modelling error in stress analysis by DNV DeepC & Riflex (Wirsching and Chen, 1988). The actual stress range is assumed to be equal to the product of $B$ and the estimated stress range $S$. The uncertainties in fatigue strength, as evidenced by the scatter in S-N data, are accounted by considering $K$ to be a random variable. The random variable $\Delta_F$ quantifies modelling error associated with the Palmgren-Miner's rule.

The fatigue failure occurs when the random variable $T$ is smaller than $T_s$ where $T_s$ is the lifetime of the structure. Thus, the limit state function is

$$g(\mathbf{X}) = \frac{\Delta_F K}{B^m \Omega} - T_s \tag{6.2.11}$$

where

$$\mathbf{X} = (\Delta_F, B, K) \tag{6.2.12}$$

The surface $g(\mathbf{X})$ is the limit state surface, and $\mathbf{X}$ is the vector of basic random variables in the problem.

### *6.2.2 Bilinear S-N Model*

New design approaches based on the S-N curves, e.g. DNV-RP-C203 (2008), BS 7608 (1993), NORSOK (1998), include bilinear (double-slope) curves to account for the effect of variable amplitude loading.

Bilinear S-N curves in log-log scale are frequently applied for representation of the experimental fatigue capacity data (DNV-RP-F204, 2005), i.e.

$$N = \begin{cases} K_1 \cdot S^{-m_1} & S > S_{SW} \\ K_2 \cdot S^{-m_2} & S \le S_{SW} \end{cases} \tag{6.2.13}$$

where $m_1$ and $m_2$ are fatigue exponents (the inverse slope of the bilinear S-N curve) and $K_1$ and $K_2$ are characteristic fatigue strength constants. $S_{SW}$ is the stress at intersection of the two S-N curves given by:

$$S_{SW} = 10^{\left(\frac{\log(K_1)-\log(N_{SW})}{m_1}\right)} \tag{6.2.14}$$

where $N_{SW}$ is the number of cycles for which change in slope appears. $\log(N_{SW})$ is typically 6 ~ 7. For DNV-D-Seawater-cathodic curve, the main parameters are as follows:

$$N_{SW} = 10^6$$

$$S_{SW} = 83.43211043 \text{ MPa}$$

$$m_1 = 3.0$$

$$K_1 = 5.80764E+11$$

$$m_2 = 5.0$$

$$K_2 = 4.03645E+15$$

$$\rho(m_i, K_i) = 0.717 \ (i = 1,2)$$

where $\rho(m_i, K_i)$ is the correlation coefficient of $m_i$ and $K_i$. Accordingly, the correlation matrix of $m_i$ and $K_i$ is $R_i = \begin{bmatrix} 1.0 & 0.717 \\ 0.717 & 1.0 \end{bmatrix} (i = 1,2)$

For further details see DNV-RP-C203 (2008).

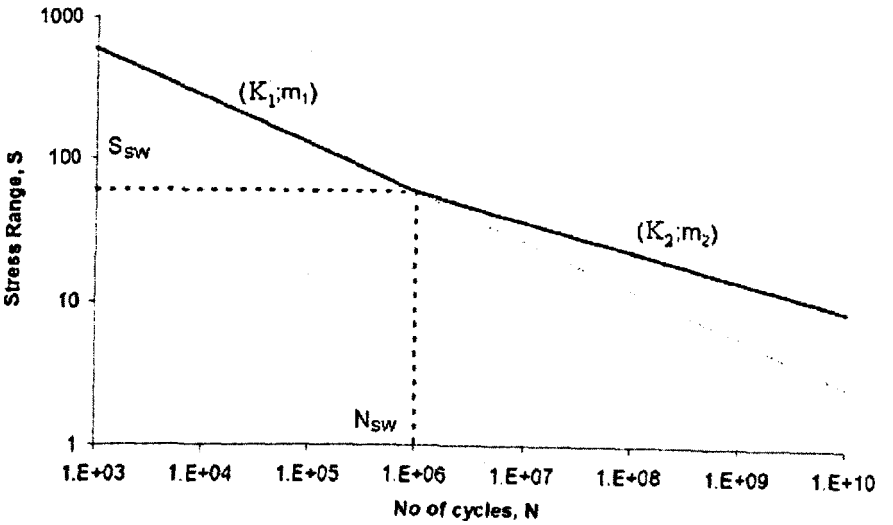


**Figure 6.2.1** Basic Definition for Double-Slope S-N Curves.

For a bilinear S-N curve in log-log scale the corresponding expression of expected fatigue damage becomes:

$$D = E\left[N(T_s)\right]\left(\frac{E\left[S^{m_1}\right]}{K_1} + \frac{E\left[S^{m_2}\right]}{K_2}\right) \tag{6.2.15}$$

The expectation value of Rayleigh distributed stress ranges $S^m$ is written separately for the two parts of the S-N curve

$$E\left[S^{m_1}\right] = \left(2\sqrt{2}\right)^{m_1} \sigma_x^{m_1} \Gamma\left(1 + \frac{m_1}{2}, \frac{S_{SW}^2}{8\sigma_x^2}\right) \tag{6.2.16}$$

$$E\left[S^{m_2}\right] = \left(2\sqrt{2}\right)^{m_2} \sigma_x^{m_2} \gamma\left(1 + \frac{m_2}{2}, \frac{S_{SW}^2}{8\sigma_x^2}\right) \tag{6.2.17}$$

where $\gamma(a,x)$ is the incomplete Gamma function and $\Gamma(a,x)$ is the complementary incomplete Gamma function (Abramowitz and Stegun, 1972).

The complement of the incomplete gamma function is related to the incomplete gamma function by the following identity:

$$\gamma(a,x)+\Gamma(a,x)=\Gamma(a) \tag{6.2.18}$$

Correspondingly, the total fatigue damage $D$ is given as

$$D=T_s\Phi \tag{6.2.19}$$

$$\Phi=\sum_{j=1}^{n} f_j \nu_{0_j}\left[\frac{B^{m_1}\left(2\sqrt{2}\right)^{m_1}\sigma_j^{m_1}\Gamma\left(1+\frac{m_1}{2},\frac{S_{SW}^2}{8\sigma_j^2}\right)}{K_1}+\frac{B^{m_2}\left(2\sqrt{2}\right)^{m_2}\sigma_j^{m_2}\gamma\left(1+\frac{m_2}{2},\frac{S_{SW}^2}{8\sigma_j^2}\right)}{K_2}\right] \tag{6.2.20}$$

$$\Phi=\sum_{j=1}^{n} f_j \nu_{0_j}\left\{\frac{B^{m_1}\left(2\sqrt{2}\right)^{m_1}\sigma_j^{m_1}\Gamma\left(1+\frac{m_1}{2},\frac{S_{SW}^2}{8\left(B\sigma_j\right)^2}\right)}{K_1}+\right.$$
$$\left.+\frac{B^{m_2}\left(2\sqrt{2}\right)^{m_2}\sigma_j^{m_2}\left[\Gamma\left(1+\frac{m_2}{2}\right)-\Gamma\left(1+\frac{m_2}{2},\frac{S_{SW}^2}{8\left(B\sigma_j\right)^2}\right)\right]}{K_2}\right\} \tag{6.2.21}$$

where

$f_j$ – fraction of the time spent in $j$ th sea state (to account for long-term sea effect)

$\nu_{0_j}$ – zero mean crossing frequency of stress process in $j$ th sea state

$B$ – inaccuracies in estimating the fatigue stresses

$\sigma_j$ – standard deviation of stress process in $j$ th sea state

$K_1$, $m_1$ – S-N fatigue parameters for $N \leq 10^6$ cycles

$K_2$, $m_2$ – S-N fatigue parameters for $N > 10^6$ cycles

$\Gamma$, $\gamma$ – complementary incomplete Gamma function and incomplete Gamma function

$S_{SW}$ – stress range for which change of slope curve

The safety margin is expressed as

$$g(X) = T - T_s = \frac{\Delta_F}{\Phi} - T_s \leq 0 \tag{6.2.22}$$

where

$T$ – time for fatigue failure

$\Delta_F$ – value of the Palmgren-Miner damage index at failure

$\Phi$ – defined by equation 6.2.21

$\mathbf{X} = (\Delta_F, B, K_1, m_1, K_2, m_2)$

## 6.3 Fracture Mechanics (FM) Based Failure Functions

Fracture mechanics assessment is becoming a more integral part of the overall SCR design. In almost every SCR project to date, a set of full-scale fatigue tests have been conducted to simulate operational and installation conditions of the SCRs. The acceptance or the rejection of the SCR pipe welds is based on weld acceptance criteria that should be established according to the engineering critical assessment (ECA) procedure. Weld acceptance criteria provide guidelines to either accept or reject flaws that would be detected during the non-destructive examination (NDE) of

the welds. A combination of flaw length and height is considered in the flaw evaluation, as well as the position of the flaw with respect to the weld profile (surface flaws or subsurface flaws).

In this section, fatigue damage was estimated by fracture mechanics approach.

Palmgren-Miner's damage model defines the time for fatigue failure as the time for crack initiation in a material. Fracture mechanics approach deals with the ability of a material to resist crack propagation under a given set of loading and environmental conditions. With the help of fracture mechanics, components may be designed to ensure that cracks do not reach a critical length during the design life of the structure.

For the reliability assessment with respect to the fracture limit state, the crack size which is present at a given time instant is decisive. In particular, the probability that the crack size at the end of the lifetime is larger than or equal to the critical one for the given stress level is required.

Linear elastic fracture mechanics (LEFM) and elastic-plastic fracture mechanics (EPFM) are the two major approaches of fracture mechanics formulation. Since fatigue cracks exist under normally elastic conditions, the principles of LEFM were adopted for studying their behaviour and formulating limit state function in this paper. In this approach, relationships between average increment in crack growth $(\frac{da}{dN})$ during a load cycle and a global parameter are developed. The stress-intensity factor, $K$, which gives the magnitude of the stresses in the crack-tip region as a function of type and magnitude of loading and geometry of the cracked body is usually expressed as

$$K = Y(a)S\sqrt{\pi a} \tag{6.3.1}$$

where $a$ is the crack size, $S$ is the far-field stress due to applied load and $Y(a)$ is the geometry function which takes into account the crack geometry and specimen shape. In general, $Y(a)$ may be defined as:

$$Y(a) = Y_{plate}(a) \cdot M_k(a) \tag{6.3.2}$$

where $Y_{plate}(a)$ is the geometry function corresponding to a semi-elliptical surface crack as proposed by Newman and Raju (1981) from finite element analysis in flat plates subjected to axial and bending remote stresses. $M_k(a)$ is a magnificent factor (or correction factor) which depends on the local weld geometry and accounts for the crack size and loading. There are some formulations of $M_k(a)$ proposed by Bowness and Lee (1999) and recommended in the BS 7910 (2005).

The cases studied herein considering the $Y(a)$ is based on the empirical expression given by Kung and Wirsching (1992) for welded joint:

$$Y(a) = 1.12 \tag{6.3.3}$$

At present, it is a common practice to describe the process of fatigue crack growth by a logarithmic $da/dN$ vs. $\Delta K$ diagram (see e.g. Figure 6.3.1).

In logarithmic scale, the crack propagation law is a straight line, which describes the major part of the crack propagation domain (region II). Below a threshold value $\Delta K_{th}$, the crack propagation is zero due to the existing fatigue limit, which means no crack propagation takes place, while in the upper part the crack propagation rate increases rapidly, which means rapid propagation takes place and crack growth instability occurs (see Figure 6.3.1).

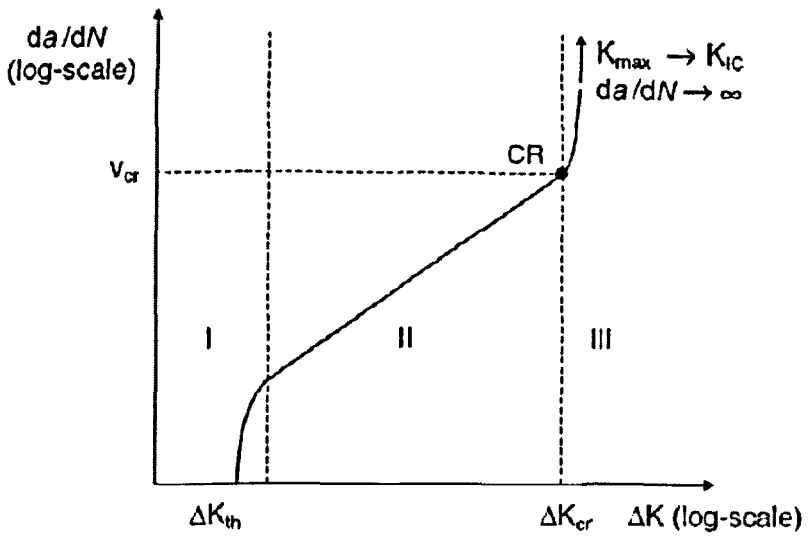


**Figure 6.3.1** Scheme of the Typical Fatigue Crack Propagation Curve.

Many crack growth relationships are available in the literature on fatigue. The application of fracture mechanics to fatigue of steel structures uses the Paris (Paris, Gomez, and Anderson, 1961) and Erdogan (Paris and Erdogan, 1963) law which is one of the most used relations for predicting crack growth rate:

$$\frac{da}{dN} = C(\Delta K)^{m_P} \tag{6.3.4}$$

$$\Delta K = Y(a)\Delta S\sqrt{\pi a} \tag{6.3.5}$$

where $\Delta K$ is the stress-intensity factor range in a stress cycle and $C$ and $m_p$ are material and environment dependent constants. For the stress ranges that are usually of importance for floating structures $C$ and $m_p$ are independent of $\Delta K$. A simplified Paris Law crack growth relationship provided by BS 7910 (2005) is shown in Figure 6.3.2.

Substituting for $\Delta K$ into equation 6.3.3 and integrating over $da$ and $dN$, the following relation between crack size $a$ and a number of cycles $N$ in time $T_s$ is obtained:

$$\frac{1}{C}\int_{a_0}^{a}\frac{dz}{Y^{m_p}\left(\sqrt{\pi z}\right)^{m_p}} = N(T_s)E\left(S^{m_p}\right) \tag{6.3.6}$$

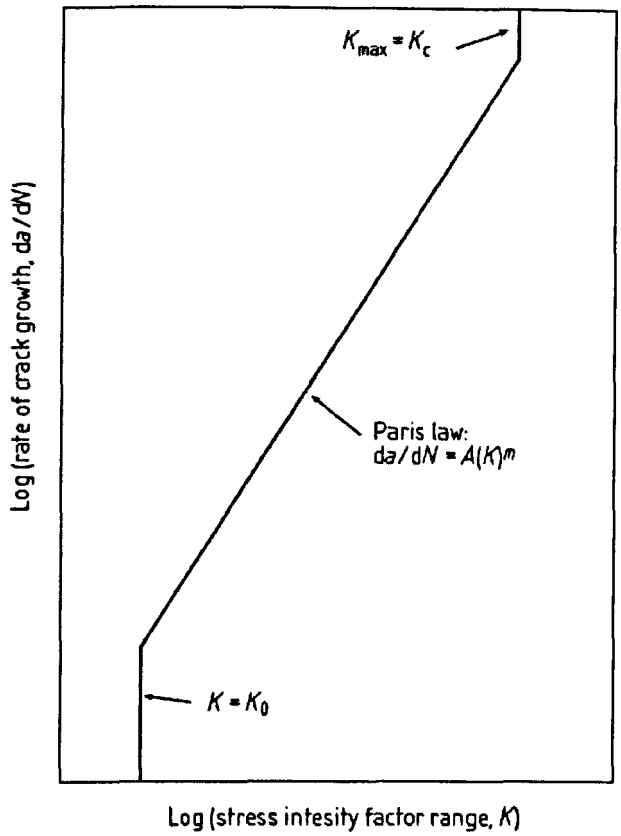


**Figure 6.3.2** Simplified Paris Law Crack Growth Relationship (BS 7910, 2005).

This equation was delivered considering variable-amplitude loading. As described in the previous section, the sum of the values of stress range in each cycle ($\sum_{i=1}^{N(T_s)} S_i$) has been approximated by $N(T_s)E\left(S^{m_p}\right)$. This approximation neglects the effects of load cycle sequence. Assuming the environmental condition being described as a long-term sea states, and the stress range following a Rayleigh distribution in each sea state, we obtain

$$\frac{1}{C}\int_{a_0}^{a}\frac{dz}{Y^{m_P}\left(\sqrt{\pi z}\right)^{m_P}}=T_s\Omega \tag{6.3.7}$$

where $\Omega$ is given by equation 6.2.8. The failure criteria can then be formulated as a function of crack size. Failure occurs when the crack size exceeds a critical value $a_c$ which is based on a serviceability condition. The probabilistic model for the time to failure $T$ of joint $i$ is defined by equation 6.3.7, taking into account the uncertainties involved in the fracture mechanics:

$$T=\frac{1}{CB^{m_P}\Omega}\int_{a_0}^{a_c}\frac{dz}{{\gamma_{FM}}^{m_P}Y^{m_P}\left(\sqrt{\pi z}\right)^{m_P}} \tag{6.3.8}$$

where $C$, $m_P$, $B$, $a_0$, and $\gamma_{FM}$ are random variables.

In the above equation 6.3.8 $B$ and $\gamma_{FM}$ are introduced to the model errors in the estimations of the stress range $S$ and the geometry function $Y$ respectively.

The fatigue failure occurs when the random variable $T$ is smaller than $T_s$, where $T_s$ is the lifetime of the structure. The limit state function is

$$g(\mathbf{X})=\frac{1}{CB^{m_P}\Omega}\int_{a_0}^{a_c}\frac{dz}{{\gamma_{FM}}^{m_P}Y^{m_P}\left(\sqrt{\pi z}\right)^{m_P}}-T_s \tag{6.3.9}$$

$$\mathbf{X}=\left(C,m_P,B,a_0,\gamma_{FM}\right) \tag{6.3.10}$$

The probability of failure $p_f$ is

$$p_f=P\left(T_i\le T_s\right)=P\left[g(X)\le 0\right] \tag{6.3.11}$$

## 6.4 Wide Band Correction

Fatigue stresses are assumed to be narrow band random process. However, if they are wide band random process, the narrow band approximation then gives over-conservative results for wide band processes. Under this circumstance, the stress parameter $\Omega$ has to be modified. Different investigators attempted to approximate damage under wide band spectra loading applying a correction factor to the Rayleigh damage for the narrow band, as listed in Table 6.4.1.

**Table 6.4.1** Damage Correction Factor for Wide Band Spectra.

| Investigator | Correction Factor $\delta_j$ |
|---|---|
| Wirsching and Light (1980); Wirsching (1984) | $\delta_j(\varepsilon_j, m) = a(m) + [1 - a(m)](1 - \varepsilon_j)^{b(m)}$ |
| Hancock and Gall (1985) | $\alpha$ |
| Krenk (1978) | $\alpha^{m-1}$ |
| Madsen, Frandsen, Holley, and Hansen (1983) | $(0.93 + 0.07\alpha^5)^m$ |

where

$$a(m) = 0.926 - 0.033m \tag{6.4.1}$$

$$b(m) = 1.587m - 2.323 \tag{6.4.2}$$

$$\alpha = \frac{\lambda_2}{\sqrt{\lambda_0 \lambda_4}} \tag{6.4.3}$$

$$\varepsilon = \sqrt{1 - \alpha^2} \tag{6.4.4}$$

where $\lambda_i$ is the $i$th spectrum moment.

Because zero mean crossing period $T_z$ and mean local peak period $T_c$ are derived by the following equations:

$$T_z = \sqrt{\frac{\lambda_0}{\lambda_2}} \tag{6.4.5}$$

$$T_c = \sqrt{\frac{\lambda_2}{\lambda_4}} \tag{6.4.6}$$

Therefore, $\varepsilon$ can be obtained by $T_z$ and $T_c$:

$$\alpha = \frac{T_c}{T_z} \tag{6.4.7}$$

$$\varepsilon = \sqrt{1 - \left(\frac{T_c}{T_z}\right)^2} \tag{6.4.8}$$

Currently Wirsching-Light's wide band correction factor is the most widely used formula for offshore structures. Hence Wirsching-Light's wide band correction factor $\delta$ is applied in the present study to modify the expression of stress parameter $\Omega$:

$$\Omega = \left(2\sqrt{2}\right)^m \Gamma\left(1 + \frac{m}{2}\right) \sum_{j=1}^{n} f_j \nu_{0_j} \sigma_j^m \delta_j \tag{6.4.9}$$

where

$\delta_j$ Wirsching-Light's wide band correction factor for $j$th sea state which is estimated by the following empirical expressions given by equations 6.4.1 ~ 6.4.4

In an ideal narrow band process $\varepsilon = 0$, which correctly gives $\delta = 1$. For a typical ocean structure problem if $\varepsilon > 0.5$, then $\delta \cong 0.83$ for $m = 3$ and $\delta \cong 0.76$ for $m = 5$.

The limit state functions for linear S-N, bilinear S-N, and fracture mechanics models accordingly are:

For linear S-N model

$$g(\mathbf{X}) = \frac{\Delta_F K}{B^m \Omega} - T_s = \frac{\Delta_F K}{B^m \left(2\sqrt{2}\right)^m \Gamma\left(1+\frac{m}{2}\right) \sum_{j=1}^{n} f_j \nu_{0_j} \sigma_j^m \delta_j} - T_s \tag{6.4.10}$$

For bilinear S-N model

$$g(X) = \frac{\Delta_F}{B^m \Phi} - T_s$$

$$\Phi = \sum_{j=1}^{n} f_j \nu_{0_j} \left\{ \frac{\delta_j B^{m_1} \left(2\sqrt{2}\right)^{m_1} \sigma_j^{m_1} \Gamma\left(1+\frac{m_1}{2}, \frac{S_{SW}^2}{8\left(B\sigma_j\right)^2}\right)}{K_1} + \right.$$

$$\left. + \frac{\delta_j B^{m_2} \left(2\sqrt{2}\right)^{m_2} \sigma_j^{m_2} \left[\Gamma\left(1+\frac{m_2}{2}\right) - \Gamma\left(1+\frac{m_2}{2}, \frac{S_{SW}^2}{8\left(B\sigma_j\right)^2}\right)\right]}{K_2} \right\} \tag{6.4.11}$$

For fracture mechanics model

$$g(X) = \frac{1}{CB^{m_P}\Omega} \int_{a_0}^{a_c} \frac{dz}{{\gamma_{FM}}^{m_P} Y^{m_P} \left(\sqrt{\pi z}\right)^{m_P}} - T_s$$

$$= \frac{1}{CB^{m_P} \left(2\sqrt{2}\right)^{m_P} \Gamma\left(1+\frac{m_P}{2}\right) \sum_{j=1}^{n} f_j \nu_{0_j} \sigma_j^{m_P} \delta_j} \int_{a_0}^{a_c} \frac{dz}{{\gamma_{FM}}^{m_P} Y^{m_P} \left(\sqrt{\pi z}\right)^{m_P}} - T_s \tag{6.4.12}$$

## 6.5 Uncertainties Associated with Fatigue Analysis

According to the limit state functions Ln (equation 6.2.11), Bn (equation 6.2.22), Lw (equation 6.4.10), and Bw (equation 6.4.11), the basic random variables are used as below:

**Table 6.5.1** Random Variables Used for Reliability Analysis with Limit State Functions Ln, Bn, Lw, and Bw.

| Variable | Used in Limit State Function | Description |
|---|---|---|
| $\Delta_F$ | Ln, Bn, Lw, Bw | Fatigue resistance limit (Palmgren-Miner's index) |
| $B$ | | Stress modelling error |
| $m$ | Ln, Lw | Empirical constant representing the fatigue exponent coefficient |
| $m_1$, $m_2$ | Bn, Bw | Empirical constants representing the fatigue exponent coefficient |
| $K$ | Ln, Lw | Empirical constant representing the fatigue strength coefficient |
| $K_1$, $K_2$ | Bn, Bw | Empirical constants representing the fatigue strength coefficient |

According to the limit state functions Fn (equation 6.3.9) and Fw (equation 6.4.12), the basic random variables are used as below:

**Table 6.5.2** Random Variables Used for Reliability Analysis with Limit State Functions Fn and Fw.

| Variable | Used in Limit State Function | Description |
|---|---|---|
| $C$ | Fn, Fw | Paris coefficient |
| $m_P$ | | Paris exponent |
| $B$ | | Stress modelling error |
| $a_0$ | | Initial crack size |
| $a_c$ | | Critical crack size |
| $\gamma_{FM}$ | | Modelling error in $Y$ |

## 6.6 Probabilistic Distribution

The probabilistic fatigue analysis is performed for the weight-optimised SCR connected to a semi-submersible in the Northern North Sea in a water depth of 1000 m as obtained from the former chapters.

The probabilistic distribution of random variables used for the reliability analysis by limit state functions Ln, Bn, Lw, and Bw are summarised in Table 6.6.1 according to the work by Akpan and Koko (2007), Tapan (2006), and Zhao, Stacey, and Prakash, (2002).

The mean values of random variables $m$, $m_1$, $m_2$, $K$, $K_1$ and $K_2$ are based on DNV-D-Seawater-cathodic curve (DNV-RP-C203, 2008) which was used for the spectral fatigue life analysis.

**Table 6.6.1** Description of Random Variables Used for Reliability Analysis by Limit State Functions Ln, Bn, Lw, and Bw.

| Variable | Used in Limit State Function | Distribution | $\mu$ | COV |
|---|---|---|---|---|
| $\Delta_F$ | Ln, Bn, Lw, Bw | Lognormal | 1.0 | 0.3 |
| $B$ | | Lognormal | 0.9 | 0.25 |
| $m$ | Ln, Lw | Lognormal | 3.0 | 0.16 |
| $m_1$ | Bn, Bw | Lognormal | 3.0 | 0.18 |
| $m_2$ | | Lognormal | 5.0 | 0.18 |
| $K$ | Ln, Lw | Lognormal | 5.81E+11 | 0.5 |
| $K_1$ | Bn, Bw | Lognormal | 5.81E+11 | 0.5 |
| $K_2$ | | Lognormal | 4.04E+15 | 0.5 |

The coefficient of variation (COV) equals the standard deviation divided by the mean.

$$COV = \frac{\sigma}{\mu} \tag{6.6.1}$$

where

$\mu$ mean value

$\sigma$ standard deviation

The probabilistic distribution of random variables used for the reliability analysis by limit state functions Fn1, Fn2, Fw1 and Fw2 are summarised in Table 6.6.2 according to the work by Kung and Wirsching (1992), Zhao, Stacey, and Prakash (2002), and Ayala-Uraga and Moan (2007).

**Table 6.6.2** Description of Random Variables Used for Reliability Analysis by Limit State Functions Fn and Fw.

| Variable | Used in Limit State Function | Distribution | $\mu$ | COV |
|---|---|---|---|---|
| $C\ (\frac{m}{\left(MPa\cdot\sqrt{m}\right)^3})$ | Fn1, Fn2, Fw1, Fw2 | Lognormal | $6.39\times10^{-13}$ | 0.5 |
| $m_P$ | Fn1, Fw1 | Deterministic | 3.0 | |
| | Fn2, Fw2 | Lognormal | 3.0 | 0.3 |
| $B$ | Fn1, Fn2, Fw1, Fw2 | Lognormal | 0.9 | 0.25 |
| $\gamma_{FM}$ | | Lognormal | 1.0 | 0.1 |
| $a_0$ (m) | | Exponential | 0.0001 | 0.0001 |
| $a_c$ (m) | | Exponential | 0.015 | 0.015 |

It is noted that two main methods are available to model the crack growth variability through the use of random variables of Paris parameters $C$ and $m_P$:

(1) $C$ and $m_P$ are correlated variables (Gurney, 1979; Tanaka and Matsuoka, 1977);
(2) $m_P$ is deterministic and $C$ is a variable (Lidiard, 1979; Slatcher, 1987).

Cortie and Garrett (1988) established a least square regression curve, by examining test data obtained by Gurney (1979) and Clark and Hudak (1979) as

$$\ln C = -14.289 - 3.829 m_P \qquad (6.6.2)$$

(units in MPa, m and da/dN in m/cycles)

with the 95% confidence for the slope $m_P$ [-4,-3.66] and the 95% confidence for the intercept as [-14.83,-13.75]. This compares to Tanaka and Matsuoka (1977):

$$\ln C = -15.59 - 3.47 m_P \tag{6.6.3}$$

Cortie and Garrett (1988) further demonstrated that although the correlation of $\ln C$ and $m_P$ is real from experiment, it is of limited use as this is mainly attributed to the use of logarithmic axes commonly used when plotting fatigue crack propagation data. When linear axis of $da/dN$ against $\Delta K$ is used, the scatter is much less. Two points are noted from their study:

(1) lower $m_P$ corresponds to higher growth rate as it comes with higher $C$;

(2) fixing $m_P$ to construct a crack growth curve may oversimplify the problem.

In most reliability calculations, only $C$ is modelled as a variable. The fatigue crack growth is treated as parallel lines with the same $m_P$ values. The commonly used values for $C$ and $m_P$ by various authorities are available from literature by Kung and Wirsching (1992), and Zhao, Stacey, and Prakash (2002).

When $m_P$ is treated as a random variable not deterministic, the relationship between $C$ and $m_P$ is defined correlated by the expression 6.6.2 which is adopted in the present study. Accordingly, the correlation coefficient and correlation matrix of $C$ and $m_P$ are

$$\rho(C, m_P) = 0.773$$

$$R = \begin{bmatrix} 1.0 & 0.773 \\ 0.773 & 1.0 \end{bmatrix}$$

## 6.7 Comparison between Reliability Based Fatigue Analysis of Linear and Bilinear Models

The 2000 m long weight-optimised SCR of configuration P based on the parametric design is chosen for the probabilistic fatigue reliability analysis. Five segments with three different density coatings were used for the riser weight optimisation as shown in Figure 6.7.1.

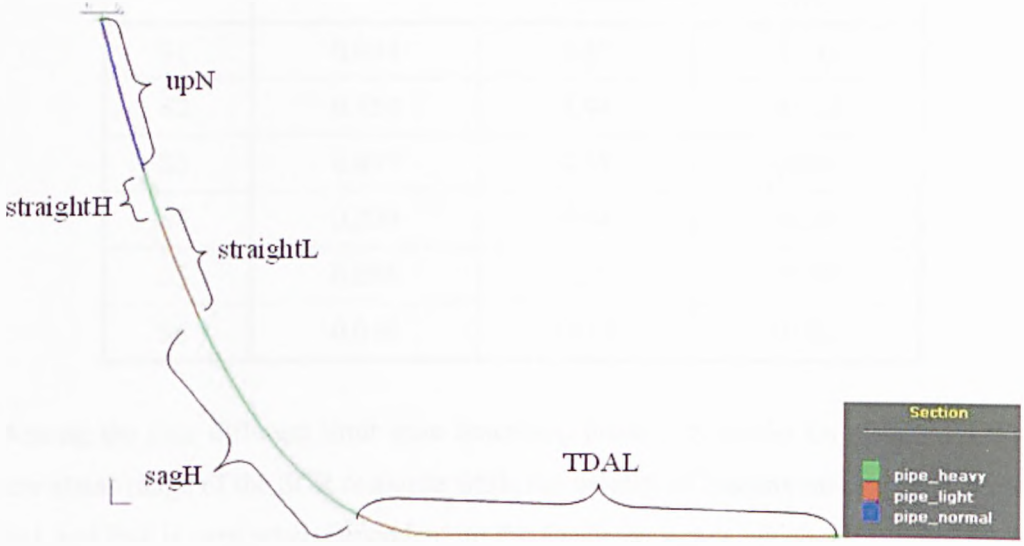


**Figure 6.7.1** 2000 m Long Weight-Optimised SCR of Configuration P.

The estimated fatigue life along the riser arc length was shown in Figure 5.4.2, with a shortest fatigue life of 284.8 yr at TDA. The fatigue stress ranges for all sea states of the point with shortest fatigue life (Point Es in Table 6.8.1) are shown in Table 6.7.1.

Its failure probability $p_f$ and reliability index $\beta$ by various analysis methods for limit state functions with narrow band approximation are shown in Table 6.7.2 and Figure 6.7.2. For all the four limit state functions, the reliability index results of the two SORM curvature-fitting methods are almost the same to each other and also

closer to the results of the two SORM point-fitting methods rather than FORM method.

**Table 6.7.1** Nominal Fatigue Stress Statistics for the Shortest Fatigue Life Point at TDA.

| Sea State Block | Fraction of Time in Each Sea State | Standard Deviation of Stress Process $\sigma_s$ (MPa) | Zero Mean Crossing Frequency $f_z$ (Hz) |
|---|---|---|---|
| S1 | 0.094 | 3.82 | 0.142 |
| S2 | 0.459 | 3.94 | 0.110 |
| S3 | 0.077 | 4.57 | 0.081 |
| S4 | 0.229 | 6.94 | 0.105 |
| S5 | 0.095 | 7.76 | 0.079 |
| S6 | 0.046 | 10.65 | 0.082 |

Among the four different limit state functions, linear S-N model Ln misses out the low stress range of the SCR response while the validity of fracture mechanics models Fn1 and Fn2 is very much dependent on the specimen inputs which are not available and only based on assumptions for the current study. From the results presented in Table 6.7.2, it also shows that linear S-N model Ln and fracture mechanics model Fn2 gives relatively much higher while fracture mechanics model Fn1 gives relatively much lower reliability index for the SCR structure than the bilinear S-N model Bn. The reliability index results by bilinear S-N model Bn meet the requirements of DNV-RP-F204 (2005) within a reasonable range, which also matches well with the fatigue assessment results from Chapter 5 (see the next section 6.8).

**Table 6.7.2** Fatigue Probability and Reliability Index for the Shortest Fatigue Life Point at TDA by Various Reliability Analysis Methods with Narrow Band Assumption.

| Analysis Method | | $p_f$ | | | | $\beta$ | | | |
|---|---|---|---|---|---|---|---|---|---|
| | | Limit State Function | | | | Limit State Function | | | |
| | | Ln ($\times 10^{-10}$) | Bn ($\times 10^{-5}$) | Fn1 ($\times 10^{-3}$) | Fn2 ($\times 10^{-11}$) | Ln | Bn | Fn1 | Fn2 |
| FORM | | 3.133 | 2.760 | 7.183 | 9.272 | 6.1836 | 4.0324 | 2.4480 | 6.3729 |
| SORM | Point-Fitting Method | Improved Breitung Formula | 2.959 | 2.536 | 6.640 | 2.524 | 6.1926 | 4.0523 | 2.4762 | 6.5695 |
| | | Tvedt Formula | 2.958 | 2.534 | 6.634 | 2.489 | 6.1926 | 4.0524 | 2.4765 | 6.5716 |
| | Curvature -Fitting Method | Improved Breitung Formula | 3.017 | 2.690 | 6.657 | 6.459 | 6.1895 | 4.0385 | 2.4753 | 6.4281 |
| | | Tvedt Formula | 3.017 | 2.690 | 6.651 | 6.445 | 6.1895 | 4.0385 | 2.4756 | 6.4285 |

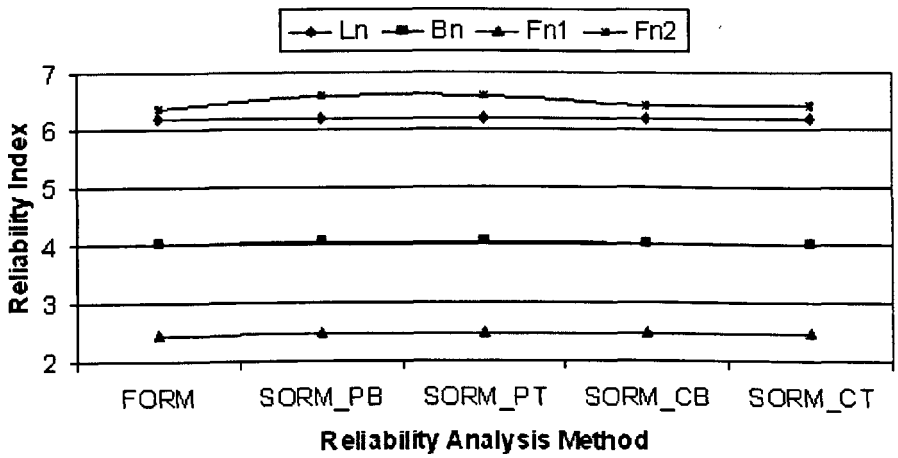


**Figure 6.7.2** Reliability Index for the Shortest Fatigue Life Point at TDA by Various Reliability Analysis Methods with Narrow Band Assumption.

Wide band correction coefficients for each sea state for the shortest fatigue life point at TDA is calculated according to formulas 6.4.1 ~ 6.4.4 and shown in Table 6.7.3.

**Table 6.7.3** Wide Band Correction Coefficients for the Shortest Fatigue Life Point at TDA.

| Sea State Block | Zero Mean Crossing Period $T_z$ (s) | Mean Local Peak Period $T_c$ (s) | $\alpha$ | $\varepsilon$ | $\delta$ | |
|---|---|---|---|---|---|---|
| | | | | | $m=3$ | $m=5$ |
| S1 | 7.031 | 6.569 | 0.934 | 0.357 | 0.89 | 0.78 |
| S2 | 9.122 | 7.895 | 0.865 | 0.501 | 0.86 | 0.77 |
| S3 | 12.39 | 9.783 | 0.790 | 0.614 | 0.84 | 0.76 |
| S4 | 9.507 | 7.941 | 0.835 | 0.550 | 0.85 | 0.76 |
| S5 | 12.62 | 8.940 | 0.708 | 0.706 | 0.84 | 0.76 |
| S6 | 12.22 | 7.459 | 0.610 | 0.792 | 0.83 | 0.76 |

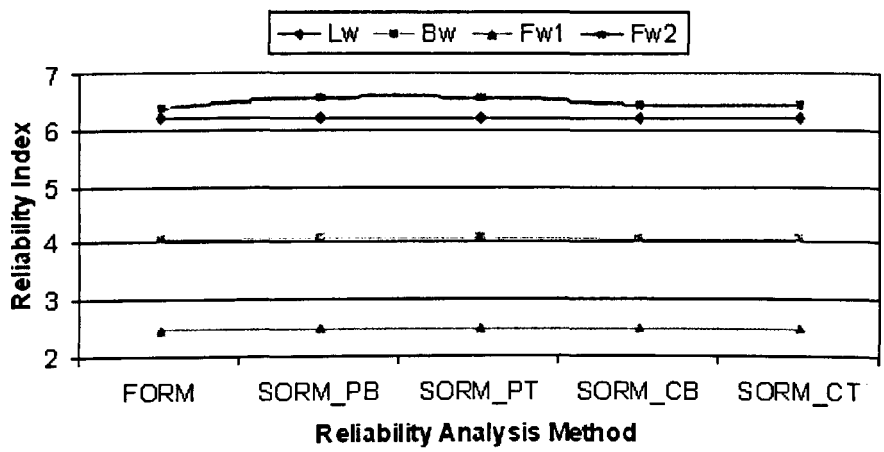


**Figure 6.7.3** Reliability Index for the Shortest Fatigue Life Point at TDA by Various Reliability Analysis Methods with Wide Band Assumption.

**Table 6.7.4** Fatigue Probability and Reliability Index for the Shortest Fatigue Life Point at TDA by Various Reliability Analysis Methods with Wide Band Correction.

| Analysis Method | | $p_f$ | | | | $\beta$ | | | |
|---|---|---|---|---|---|---|---|---|---|
| | | Limit State Function | | | | Limit State Function | | | |
| | | Lw ($\times 10^{-10}$) | Bw ($\times 10^{-5}$) | Fw1 ($\times 10^{-3}$) | Fw2 ($\times 10^{-11}$) | Lw | Bw | Fw1 | Fw2 |
| FORM | | 2.514 | 2.369 | 7.183 | 8.154 | 6.2182 | 4.0682 | 2.4480 | 6.3926 |
| SORM Point-Fitting Method | Improved Breitung Formula | 2.371 | 2.172 | 6.640 | 2.207 | 6.2274 | 4.0884 | 2.4762 | 6.5895 |
| | Tvedt Formula | 2.371 | 2.171 | 6.634 | 2.176 | 6.2274 | 4.0885 | 2.4765 | 6.5916 |
| SORM Curvature -Fitting Method | Improved Breitung Formula | 2.420 | 2.308 | 6.657 | 5.679 | 6.2242 | 4.0742 | 2.4753 | 6.4477 |
| | Tvedt Formula | 2.420 | 2.308 | 6.651 | 5.667 | 6.2242 | 4.0742 | 2.4756 | 6.4480 |

Failure probability $p_f$ and reliability index $\beta$ for the shortest fatigue life point at TDA calculated by various analysis methods for limit state functions with wide band correction are shown in Figure 6.7.3 and Table 6.7.4. For all the four limit state functions, the reliability index results of the two SORM curvature-fitting methods are almost the same to each other and also closer to the results of the two SORM point-fitting methods rather than FORM method, same trends as for the four limit state functions with narrow band approximation studied above. Therefore, the improved Breitung formula of SORM curvature-fitting method is used for the following reliability analysis.

Among the four different limit state functions, linear S-N model Lw and fracture mechanics model Fw2 gives unrealistically high reliability index results for the SCR structure while fracture mechanics model Fw1 gives unrealistically low reliability

index results. Only the bilinear S-N model Bw provides a reasonable and acceptable reliability assessment result, which also matches well with the fatigue assessment result from Chapter 5 (see the next section 6.8).

With wide band correction, the reliability index of the studied point has been increased by all four limit state function as listed in Table 6.7.5, which means the fatigue stresses are not an ideal narrow band random process and wide band correction coefficients are needed for a more accurate fatigue reliability assessment of the SCRs. Therefore, bilinear S-N model with wide band correction Bw is chosen for the reliability-based fatigue analysis of weight-optimised SCRs.

**Table 6.7.5** Increase of Reliability Index for the Shortest Fatigue Life Point at TDA by Various Reliability Analysis Methods with Wide Band Correction.

| Limit State Function | Lw | Bw | Fw1 | Fw2 |
|---|---|---|---|---|
| Average Increase of $\beta$ | $(\beta_{Lw}-\beta_{Ln})/\beta_{Ln}$ (%) | $(\beta_{Bw}-\beta_{Bn})/\beta_{Bn}$ (%) | $(\beta_{Fw1}-\beta_{Fn1})/\beta_{Fn1}$ (%) | $(\beta_{Fw2}-\beta_{Fn2})/\beta_{Fn2}$ (%) |
| | + 0.56 | + 0.89 | + 0.05 | + 0.31 |

Figure 6.7.4 are the pie charts for the distribution of parametric uncertainty importance at points Es and El (as described in Table 6.8.1) for limit state function Bw. Accordingly, the fatigue exponent coefficient $m_2$ and fatigue strength coefficient $K_2$ are the two uncertainty parameters most affecting the reliability of the riser while $m_1$ and $K_1$ have no effect on the fatigue reliability which proves once again that deepwater SCR fatigue stress is low range high cycle and bilinear S-N model is more suitable than linear S-N model for current case study. The third important parameter for SCR fatigue reliability analysis by limit state function Bw is stress modelling error $B$.

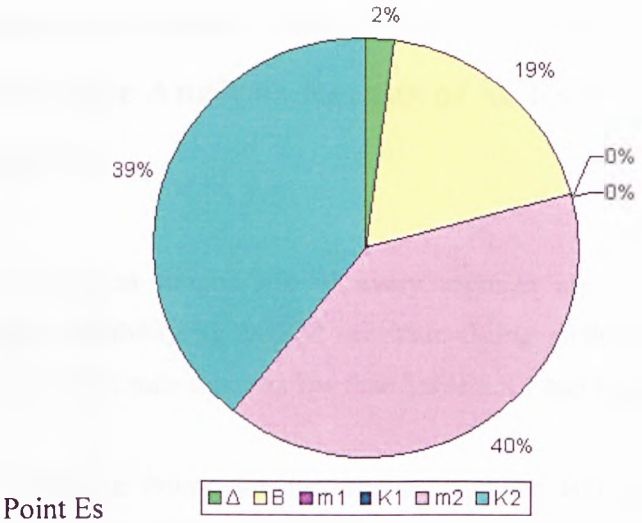


Point Es

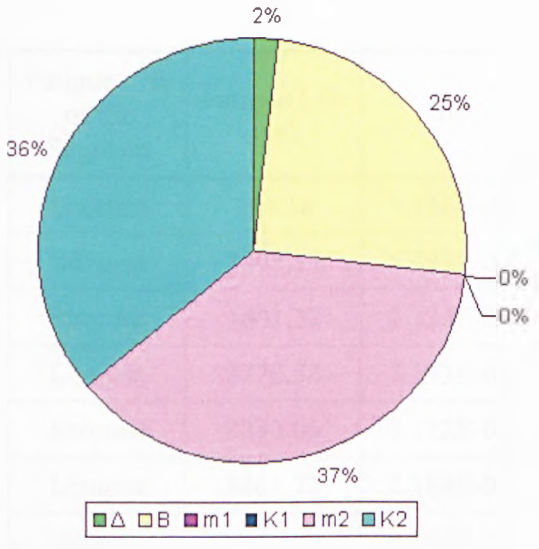


Point El

**Figure 6.7.4** Distribution of Important Factors for the Random Variables of Points Es and El Respectively for Limit State Function Bn.

## 6.8 Comparison between Fatigue Analysis and Reliability-Based Fatigue Analysis Results of SCRs by Bilinear S-N Model Bw

Typical points of shortest fatigue life of every segment are checked for their probabilistic fatigue reliability by SORM curvature-fitting method with improved Breitung formula for limit state function Bw (see Table 6.8.1 and Figure 6.8.1).

**Table 6.8.1** Example Points for Probabilistic Fatigue Reliability Check by Limit State Function Bw.

| Point | Segment | Fatigue Life of the Segment | Fatigue Life (yr) | $p_f$ | $\beta$ |
|---|---|---|---|---|---|
| As | upN | Shortest | 764.18 | 5.136E-06 | 4.4114 |
| Al | | Longest | 3907.17 | 6.483E-07 | 4.8403 |
| Bs | straightH | Shortest | 1601.32 | 2.336E-06 | 4.5790 |
| Bl | | Longest | 3770.54 | 7.133E-07 | 4.8213 |
| Cs | straightL | Shortest | 3333.06 | 9.112E-07 | 4.7722 |
| Cl | | Longest | 8461.72 | 2.388E-07 | 5.0351 |
| Ds | sagH | Shortest | 3316.66 | 7.590E-07 | 4.8088 |
| Dl | | Longest | 159996 | 1.209E-09 | 5.9669 |
| Es | TDAL | Shortest | 284.84 | 2.308E-05 | 4.0742 |
| El | | Longest | 1217560 | 2.766E-13 | 7.2116 |

It can be seen from Table 6.8.1 and Figure 6.8.1 that the fatigue life and reliability index for all 10 points from 5 segments have a very similar trend which shows that the two approaches can be executed together for fatigue assessment of deepwater weight-optimised SCRs and provide a reliable prediction.

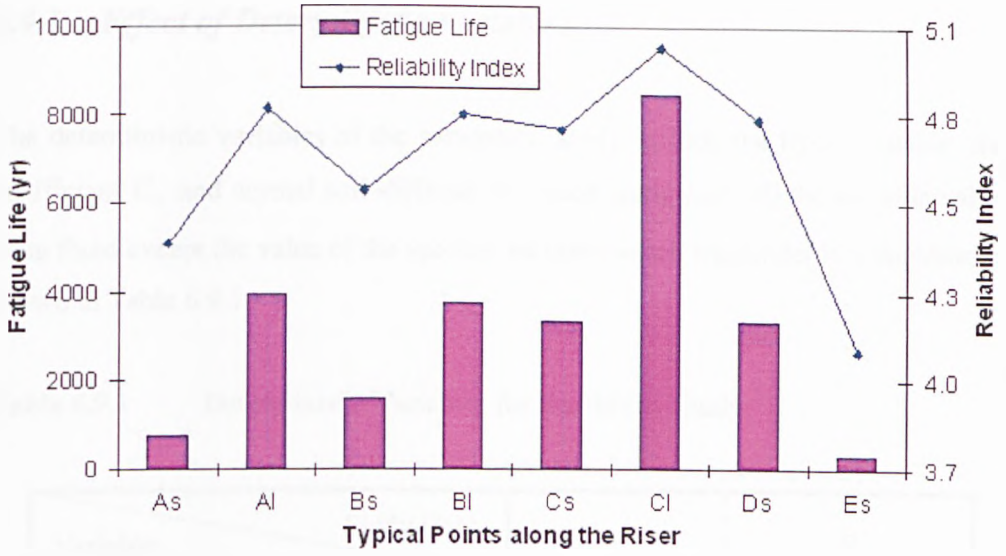


**Figure 6.8.1** Fatigue Life and Reliability Assessment Result by Limit State Function Bw of Typical Points along the Riser.

## 6.9 Sensitivity of Reliability Index by Bilinear S-N Model Bw

To provide insight into the effect of the different deterministic and random variables on the fatigue reliability index, a limited parametric study is carried out. The variables considered are the hydrodynamic drag coefficient $C_d$, normal soil stiffness, fatigue resistance limit $\Delta_F$, stress modelling error $B$, fatigue exponent coefficient $m_2$, and fatigue strength coefficient $K_2$. Because fatigue exponent coefficient $m_1$ and fatigue strength coefficient $K_1$ have no effect on the reliability analysis by limit state function Bw, they are not included in this study.

The values of these studied variables are changed one at a time keeping the remaining variables at their nominal values. The results of this parametric study are presented below.

### 6.9.1 *Effect of Deterministic Variables*

The deterministic variables of the parametric study include the hydrodynamic drag coefficient $C_d$ and normal soil stiffness. For each study case, all the variable values were fixed except the value of the specific variable which was under investigation, as shown in Table 6.9.1.

**Table 6.9.1** Deterministic Variables for Sensitivity Study.

| Variable \ Study Case | a | b |
|---|---|---|
| Hydrodynamic Drag Coefficient $C_d$ | 0.7 – 1.2 | 1.0 |
| Normal Soil Stiffness | 600 | 100 ~ 5000 |

**a) Effect of Hydrodynamic Drag Coefficient $C_d$**

Table 6.9.2 and Figure 6.9.1 give the variation of fatigue reliability index with respect to hydrodynamic drag coefficient $C_d$. It is shown that there is no considerable variation in reliability index with $C_d$ especially for point Es. Therefore, hydrodynamic drag coefficient $C_d$ may be treated as a deterministic variable in the fatigue reliability analysis of weight-optimised SCRs. However, reliability index for point El tends to decrease with increase in $C_d$ after $C_d$ is larger than 0.8 while there is no clear trend for point Es.

**Table 6.9.2** Probabilistic Fatigue Reliability Check for Points Es and El with Variation in Hydrodynamic Drag Coefficient $C_d$ by Limit State Function Bw.

| $C_d$ | $\beta$ | |
|---|---|---|
| | Es | El |
| 0.7 | 4.0164 | 6.5924 |
| 0.8 | 4.0532 (+0.92%) | 7.4566 (+13.11%) |
| 0.9 | 4.0335 (–0.49%) | 7.3615 (–1.28%) |
| 1.0 | 4.0742 (+1.01%) | 7.2116 (–2.04%) |
| 1.1 | 3.9739 (–2.46%) | 7.1438 (–0.94%) |
| 1.2 | 3.9767 (+0.07%) | 7.0231 (–1.69%) |

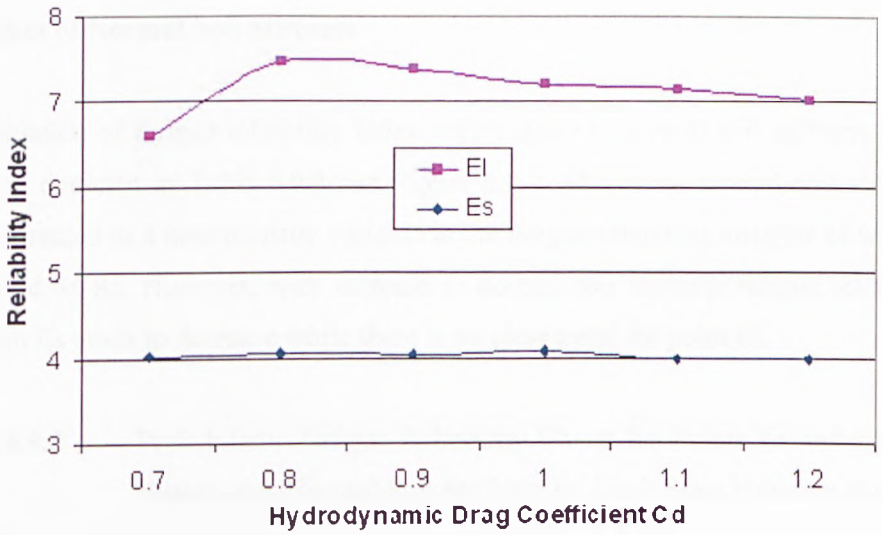


**Figure 6.9.1** Effect of Hydrodynamic Drag Coefficient $C_d$ on Fatigue Reliability for Points Es and El by Limit State Function Bw.

Fatigue life prediction and fatigue reliability assessment result of point Es for various hydrodynamic drag coefficients are shown in Figure 6.9.2. It shows that the trends of the results calculated by two approaches matched well.

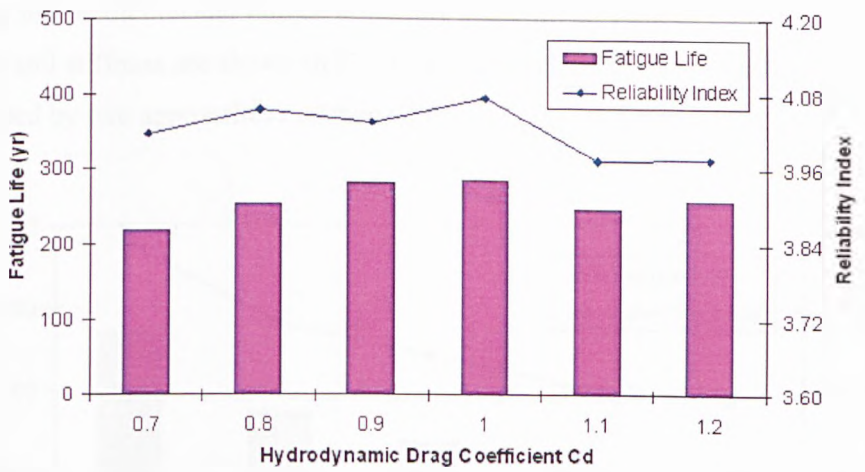


**Figure 6.9.2** Fatigue Life Reliability Assessment Result by Limit State Function Bw of Point Es for Various Hydrodynamic Drag Coefficient $C_d$.

**b) Effect of Normal Soil Stiffness**

The variation of fatigue reliability index with respect to normal soil stiffness is not much as depicted in Table 6.9.3 and Figure 6.9.2. Therefore, normal soil stiffness may be treated as a deterministic variable in the fatigue reliability analysis of weight-optimised SCRs. However, with increase in normal soil stiffness fatigue reliability for point Es tends to decrease while there is no clear trend for point El.

**Table 6.9.3** Probabilistic Fatigue Reliability Check for Points Es and El with Variation in Normal Soil Stiffness by Limit State Function Bw.

| Normal Soil Stiffness (kPa) | $\beta$ | |
|---|---|---|
| | Es | El |
| 100 | 4.1809 | 7.2164 |
| 300 | 4.1032 (–1.86%) | 7.2842 (+0.94%) |
| 600 | 4.0742 (–0.71%) | 7.2116 (–1.00%) |
| 2000 | 4.0427 (–0.77%) | 7.2974 (+1.19%) |
| 5000 | 4.0299 (–0.32%) | 7.2969 (–0.01%) |

Fatigue life prediction and fatigue reliability assessment result of point Es for various normal soil stiffness are shown in Figure 6.9.4. It shows that the trends of the results calculated by two approaches matched well.

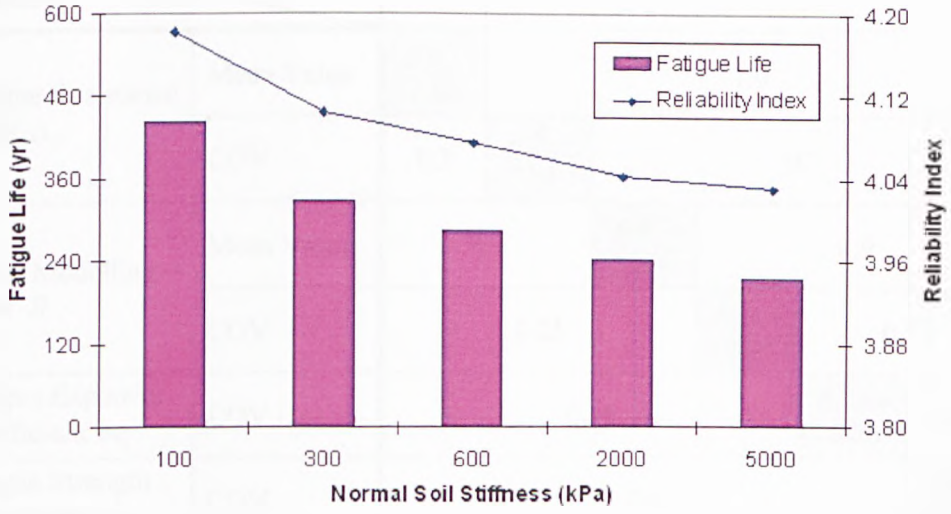


**Figure 6.9.4** Fatigue Life Reliability Assessment Result by Limit State Function Bw of Point Es for Various Normal Soil Stiffness.

### *6.9.2 Effect of Random Variables*

The random variables of the parametric study include fatigue resistance limit $\Delta_F$, stress modelling error $B$, fatigue exponent coefficient $m_2$, and fatigue strength coefficient $K_2$. For each study case, all the variable values were fixed except the value of the specific variable which was under investigation, as shown in Table 6.9.4.

**Table 6.9.4** Random Variables for Sensitivity Study.

| Variable \ Study Case | | a | b | c | d | e | f |
|---|---|---|---|---|---|---|---|
| Fatigue Resistance Limit $\Delta_F$ | Mean Value | 0.9 – 1.10 | 1.0 | | | | |
| | COV | 0.3 | 0.2 – 0.4 | 0.3 | | | |
| Stress Modelling Error $B$ | Mean Value | 0.9 | | 0.8 – 1.0 | 0.9 | | |
| | COV | 0.25 | | | 0.15 – 0.35 | 0.25 | |
| Fatigue Exponent Coefficient $m_2$ | COV | 0.18 | | | | 0.16 – 0.20 | 0.18 |
| Fatigue Strength Coefficient $K_2$ | COV | 0.5 | | | | | 0.48 – 0.52 |

**a) Fatigue Resistance Limit $\Delta_F$**

The variation of reliability index with mean value and COV of fatigue resistance limit $\Delta_F$ is shown in Table 6.9.5 and Figure 6.9.5, and Table 6.9.6 and Figure 6.9.6 respectively. As the mean value of fatigue resistance limit increases by each 0.05, the reliability index increases averagely by 0.16% for point Es and 0.08% for point El (Table 6.9.5 and Figure 6.9.5), which also implies that with a higher target safety index a higher fatigue resistance limit, or in other words, a lower target damage level needs to be established by stricter design criteria or inspection. As the COV of fatigue resistance limit increases by each 0.05, the reliability index decreases averagely by 0.07% for point Es and 0.04% for point El (Table 6.9.6 and Figure 6.9.6). Because the fatigue resistance limit is measured from random fatigue testing, a better measurement can stabilise the testing results which helps improve the riser safety index.

**Table 6.9.5** Probabilistic Fatigue Reliability Check for Points Es and El with Variation in Mean Value of Fatigue Resistance Limit $\Delta_F$ by Limit State Function Bw.

| Mean Value of $\Delta_F$ | $\beta$ | |
|---|---|---|
| | Es | El |
| 0.90 | 4.0605 | 7.1996 |
| 0.95 | 4.0676 (+0.17%) | 7.2057 (+0.08%) |
| 1.00 | 4.0742 (+0.16%) | 7.2116 (+0.08%) |
| 1.05 | 4.0806 (+0.16%) | 7.2171 (+0.08%) |
| 1.10 | 4.0866 (+0.15%) | 7.2224 (+0.07%) |

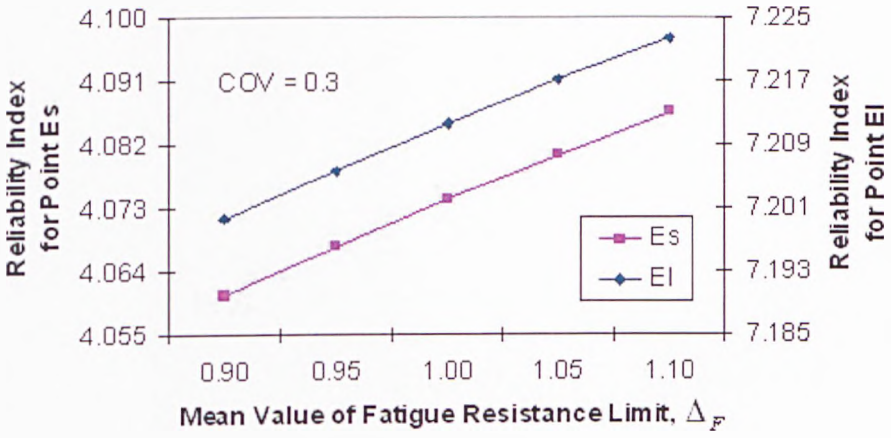


**Figure 6.9.5** Variation of Reliability Index for Points Es and El with Mean Value of Fatigue Resistance Limit $\Delta_F$ by Limit State Function Bw.

**Table 6.9.6** Probabilistic Fatigue Reliability Check for Points Es and El with Variation in COV of Fatigue Resistance Limit $\Delta_F$ by Limit State Function Bw.

| COV of $\Delta_F$ | $\beta$ | |
|---|---|---|
| | Es | El |
| 0.20 | 4.0790 | 7.2165 |
| 0.25 | 4.0768 (–0.05%) | 7.2143 (–0.03%) |
| 0.30 | 4.0742 (–0.06%) | 7.2116 (–0.04%) |
| 0.35 | 4.0713 (–0.07%) | 7.2085 (–0.04%) |
| 0.40 | 4.0679 (–0.08%) | 7.2051 (–0.05%) |

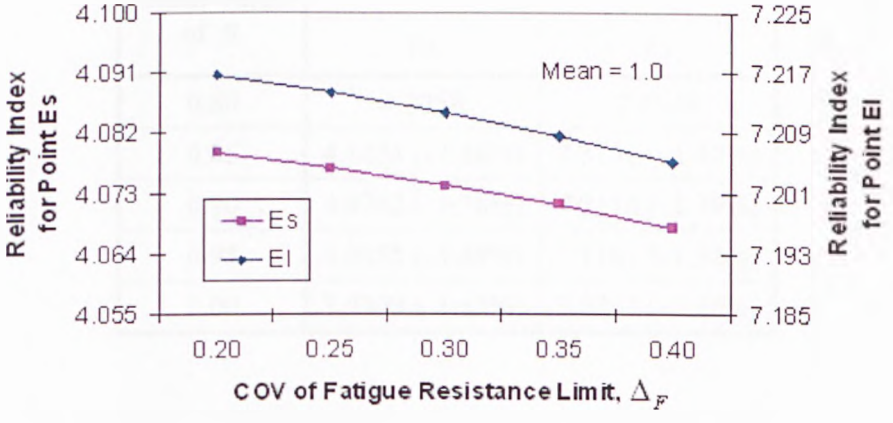


**Figure 6.9.6** Variation of Reliability Index for Points Es and El with COV of Fatigue Resistance Limit $\Delta_F$ by Limit State Function Bw.

**b) Stress Modelling Error** $B$

The variation of reliability index with mean value and COV of stress modelling error $B$ is shown in Table 6.9.7 and Figure 6.9.7, and Table 6.9.8 and Figure 6.9.8 respectively. As the mean value of stress modelling error increases by each 0.05, the reliability index decreases averagely by 1.73% for point Es and 1.36% for point El (Table 6.9.7 and Figure 6.9.7). As the COV of fatigue resistance limit increases by

each 0.05, the reliability index decreases averagely by 1.44% for point Es and 3.23% for point El (Table 6.9.8 and Figure 6.9.8). It means that by improving the accuracy of stress analysis to minimise the stress modelling error, such as applying more appropriate wave spectrum formulation and scatter diagram division to simulate local environmental conditions and more advanced tailor-made riser analysis programs with improved theories and technologies for simulations, the riser safety index can be increased.

**Table 6.9.7** Probabilistic Fatigue Reliability Check for Points Es and El with Variation in Mean Value of Stress Modelling Error $B$ by Limit State Function Bw.

| Mean Value of $B$ | $\beta$ | |
|---|---|---|
| | Es | El |
| 0.80 | 4.2258 | 7.4224 |
| 0.85 | 4.1474 (–1.86%) | 7.3134 (–1.47%) |
| 0.90 | 4.0742 (–1.76%) | 7.2116 (–1.39%) |
| 0.95 | 4.0055 (–1.69%) | 7.1161 (–1.32%) |
| 1.00 | 3.9409 (–1.61%) | 7.0263 (–1.26%) |

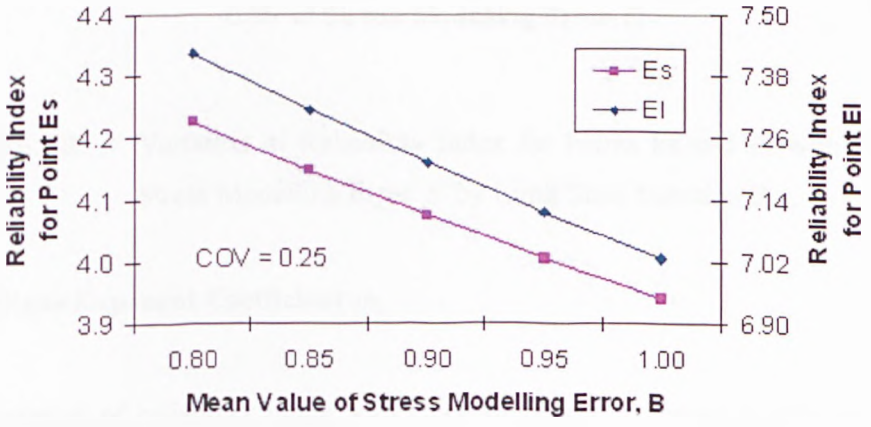


**Figure 6.9.7** Variation of Reliability Index for Points Es and El with Mean Value of Stress Modelling Error $B$ by Limit State Function Bw.

**Table 6.9.8** Probabilistic Fatigue Reliability Check for Points Es and El with Variation in COV of Stress Modelling Error $B$ by Limit State Function Bw.

| COV of $B$ | $\beta$ | |
|---|---|---|
| | Es | El |
| 0.15 | 4.1820 | 7.6944 |
| 0.20 | 4.1321 (–1.19%) | 7.4562 (–3.10%) |
| 0.25 | 4.0742 (–1.40%) | 7.2116 (–3.28%) |
| 0.30 | 4.0114 (–1.54%) | 6.9736 (–3.30%) |
| 0.35 | 3.9461 (–1.63%) | 6.7485 (–3.23%) |

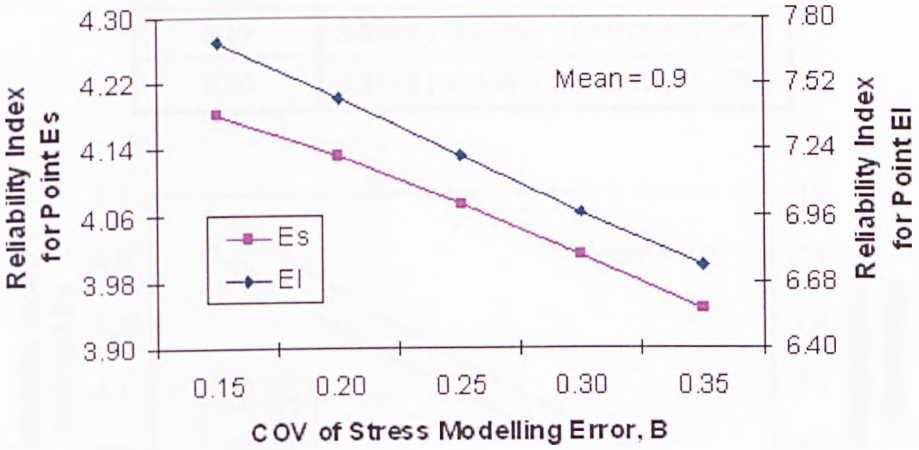


**Figure 6.9.8** Variation of Reliability Index for Points Es and El with COV of Stress Modelling Error $B$ by Limit State Function Bw.

**c) Fatigue Exponent Coefficient $m_2$**

The variation of reliability index with COV of fatigue exponent coefficient $m_2$ is shown in Table 6.9.9 and Figure 6.9.9. As the COV of fatigue exponent coefficient $m_2$ increases by each 0.01, the reliability index decreases averagely by 4.81% for point Es and 4.38% for point El. Because reliability index is sensitive to the fatigue

exponent coefficient $m_2$, proper COV value of $m_2$ should be used to get an accurate measure of reliability index.

**Table 6.9.9** Probabilistic Fatigue Reliability Check for Points Es and El with Variation in COV of Fatigue Exponent Coefficient $m_2$ by Limit State Function Bw.

| COV of $m_2$ | $\beta$ | |
|---|---|---|
| | Es | El |
| 0.16 | 4.5201 | 7.9165 |
| 0.17 | 4.2952 (–5.20%) | 7.5500 (–4.63%) |
| 0.18 | 4.0742 (–4.92%) | 7.2116 (–4.48%) |
| 0.19 | 3.8840 (–4.67%) | 6.9028 (–4.28%) |
| 0.20 | 3.7118 (–4.43%) | 6.6201 (–4.10%) |

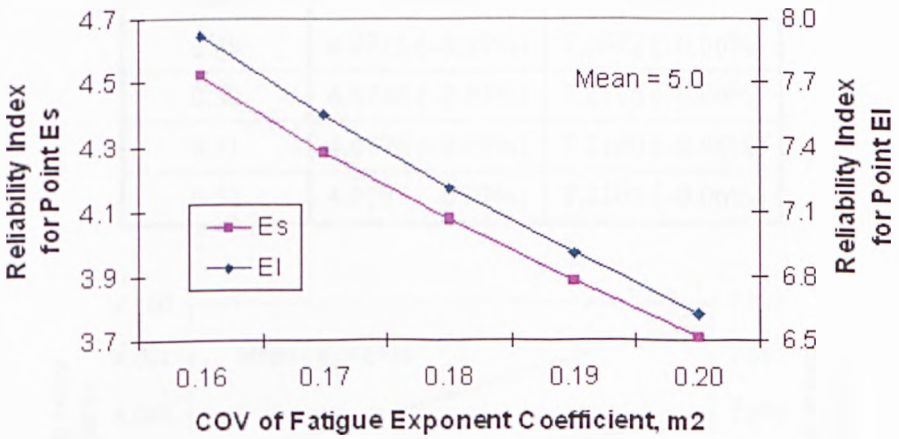


**Figure 6.9.9** Variation of Reliability Index for Points Es and El with COV of Fatigue Exponent Coefficient $m_2$ by Limit State Function Bw.

**d) Fatigue Strength Coefficient $K_2$**

The variation of reliability index with COV of fatigue strength coefficient $K_2$ is shown in Table 6.9.10 and Figure 6.9.10. As the COV of fatigue strength coefficient $K_2$ increases by each 0.01, the reliability index decreases averagely by 0.07% for point Es and 0.06% for point El which does not have as significant effect as fatigue exponent coefficient $m_2$ on reliability index.

**Table 6.9.10** Probabilistic Fatigue Reliability Check for Points Es and El with Variation in COV of Fatigue Strength Coefficient $K_2$ by Limit State Function Bw.

| COV of $K_2$ | $\beta$ | |
|---|---|---|
| | Es | El |
| 0.48 | 4.0687 | 7.2028 |
| 0.49 | 4.0715 (–0.07%) | 7.2072 (–0.06%) |
| 0.50 | 4.0742 (–0.07%) | 7.2116 (–0.06%) |
| 0.51 | 4.0770 (–0.07%) | 7.2160 (–0.06%) |
| 0.52 | 4.0797 (–0.07%) | 7.2203 (–0.06%) |

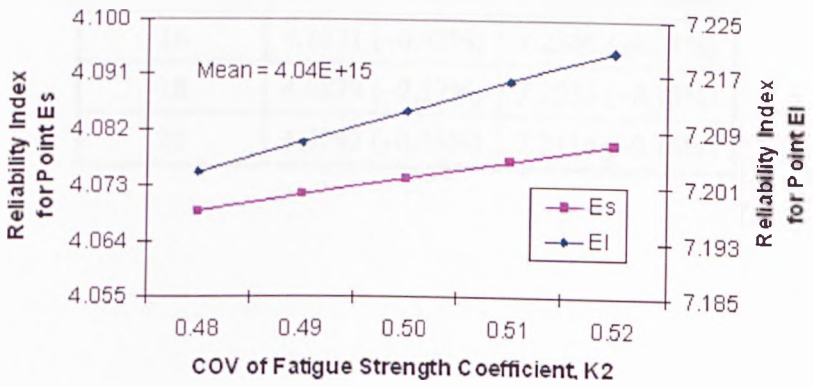


**Figure 6.9.10** Variation of Reliability Index for Points Es and El with COV of Fatigue Strength Coefficient $K_2$ by Limit State Function Bw.

### *6.9.3 SCR Service Life*

The reliability index achieved at various levels of service life is shown in Table 6.9.11 and Figure 6.9.11. The longer the service life, the higher was the probability of failure. Especially within the first 5 years, reliability index dropped down sharply with time wnet by. After 5 years of service time, the decrease of reliability index tended to slow down.

**Table 6.9.11** Probabilistic Fatigue Reliability Check for Points Es and El with Change in SCR Service Life $T_s$ by Limit State Function Bw.

| $T_s$ (yr) | $\beta$ | |
|---|---|---|
| | Es | El |
| 0 | 4.7157 | 7.7749 |
| 2 | 4.3639 (–7.46%) | 7.4651 (–3.98%) |
| 4 | 4.2786 (–1.95%) | 7.3903 (–1.00%) |
| 6 | 4.2280 (–1.18%) | 7.3458 (–0.60%) |
| 8 | 4.1917 (–0.86%) | 7.3142 (–0.43%) |
| 10 | 4.1634 (–0.68%) | 7.2894 (–0.34%) |
| 12 | 4.1401 (–0.56%) | 7.2691 (–0.28%) |
| 14 | 4.1203 (–0.48%) | 7.2518 (–0.24%) |
| 16 | 4.1031 (–0.42%) | 7.2368 (–0.21%) |
| 18 | 4.0879 (–0.37%) | 7.2235 (–0.18%) |
| 20 | 4.0742 (–0.34%) | 7.2116 (–0.16%) |

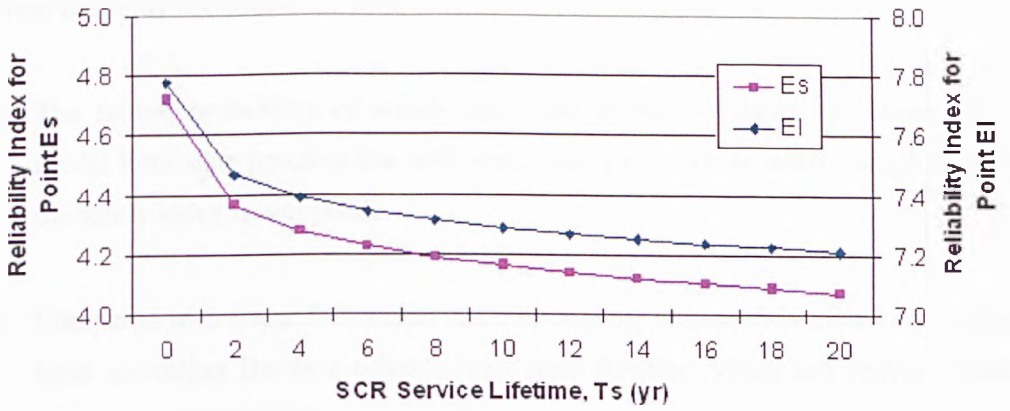


**Figure 6.9.11** Variation of Reliability Index for Points Es and El with SCR Service Life $T_s$ by Limit State Function Bw.

## 6.10 Discussion and Conclusion

In this chapter, a procedure for the probabilistic fatigue reliability analysis at critical points in the weight-optimised SCRs by combining using DNV DeepC, RIFLEX, Riserlife and CALREL has been outlined and illustrated through sample calculations. Four limit state functions with narrow band approximation or wide band correction were formulated respectively and compared for fatigue reliability analysis. The fatigue loading function may be extended further to include other uncertainties. There is no limit on the number of uncertainties. The random variables are varied for different limit state functions. Based on the results during spectral fatigue analysis, the probabilistic fatigue life of the typical points with both the shortest and longest fatigue life of each segment along a weight-optimised SCR connected to a semi-submersible was evaluated. The reliability index indicates the level of safety and quantifies the risk and whether the probability of failure is small enough to be acceptable. This is seen as a way forward for the rational design of deepwater weight-optimised SCRs. A limited parametric study has also been conducted providing insight into the effect of various parameters on the fatigue reliability index.

From the study conducted the following specific conclusions can be drawn:

- The failure probability of weight-optimised SCRs calculated by bilinear S-N model limit state function Bw with wide band correction is small enough so that the safety index is acceptable.

- Compared with linear S-N model and FM models, bilinear S-N model with wide band correction Bw is a suitable limit state function which can provide more stable and reliable fatigue reliability assessment for the deepwater weight-optimised SCRs.

- Uncertainty analysis shows that not only mean value but also COV of random variables plays a very significant role in determining the reliability or safety of SCRs. If the uncertainties of random variables can be reduced through appropriate care and control, the reliability of risers can be increased.

- Fatigue exponent coefficient $m_2$ and fatigue strength coefficient $K_2$ are the two most important uncertainty parameters affecting the reliability of weight-optimised SCRs by limit state function Bw while fatigue exponent coefficient $m_1$ and fatigue strength coefficient $K_1$ have no effect on the reliability index at all. Increasing the COV of fatigue exponent coefficient $m_2$ or fatigue strength coefficient $K_2$ by each 0.01 will reduce the reliability index of deepwater weight-optimised SCRs at TDA by 4.8% and 0.07 respectively.

- With a higher target safety index a higher fatigue resistance limit $\Delta_F$, or in other words, a lower target damage level needs to be established by stricter design criteria or inspection. In addition, a better measurement of fatigue testing will help reduce the variation in fatigue resistance limit $\Delta_F$ and improve the reliability or safety index of deepwater weight-optimised SCRs.

- Improving the accuracy of stress analysis, such as by applying more appropriate wave spectrum formulation and scatter diagram division to simulate local environmental conditions and more advanced tailor-made riser analysis programs with improved theories and technologies for simulations, can minimise the stress modelling error and its variation so as to increase the riser safety index.

- With the increase of riser service life, the probability of failure was correspondingly increased. Especially within the first 5 years, reliability index dropped down sharply with time went by. After 5 years of service time, the decrease of reliability index tended to slow down.

- The significance effect of all the variables studied on the reliability index is shown in Table 6.10.1.

**Table 6.10.1** Significance Effect of Variables on the Reliability Index.

| Variable | | Effect on Reliability Index |
|---|---|---|
| Deterministic | Hydrodynamic Drag Coefficient $C_d$ | Minor Significant |
| | Normal Soil Stiffness | Minor Significant |
| Random | Fatigue Resistance Limit $\Delta_F$ | Minor Significant |
| | Stress Modelling Error $B$ | Minor Significant |
| | Fatigue Exponent Coefficient $m_1$ | Insignificant |
| | Fatigue Exponent Coefficient $m_2$ | Significant |
| | Fatigue Strength Coefficient $K_1$ | Insignificant |
| | Fatigue Strength Coefficient $K_2$ | Minor Significant |

- According to Table 6.10.1, fatigue exponent coefficient $m_2$ is the most important parameter for the fatigue reliability assessment of deepwater weight-optimised SCRs which necessitates the use of proper value of $m_2$ in the analysis.

*Chapter 7*

# Design Procedure for Deepwater Weight-Optimised SCRs

## 7.1 Outline of Design Procedure

From preceding Chapters, the design procedure for deepwater weight-optimised SCRs can be summarised in the following diagram.

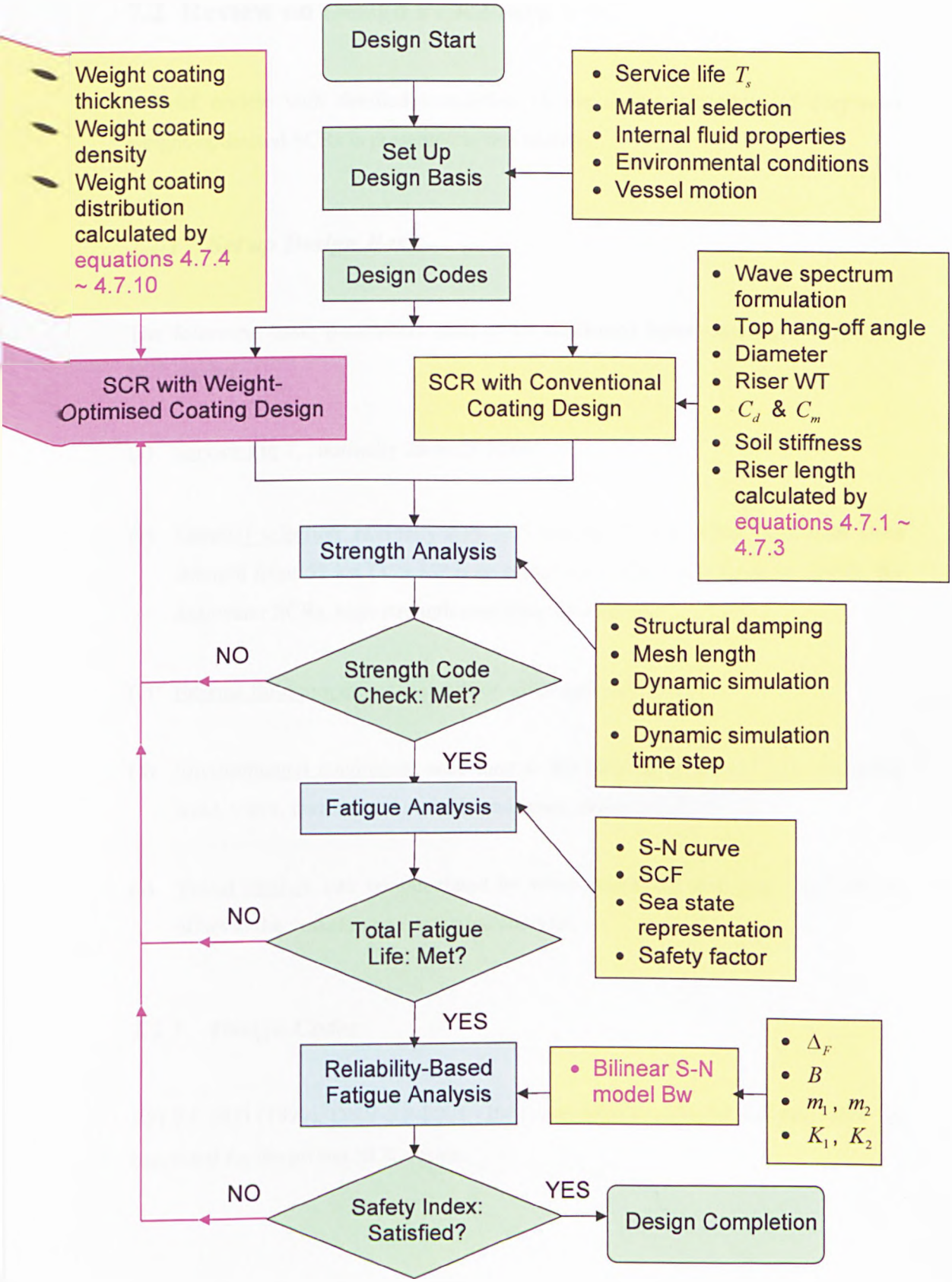
Design Start
Set Up Design Basis
Service life $T_s$
Material selection
Internal fluid properties
Environmental conditions
Vessel motion
Design Codes
Weight coating thickness
Weight coating density
Weight coating distribution calculated by equations 4.7.4 ~ 4.7.10
SCR with Weight-Optimised Coating Design
SCR with Conventional Coating Design
Wave spectrum formulation
Top hang-off angle
Diameter
Riser WT
$C_d$ & $C_m$
Soil stiffness
Riser length calculated by equations 4.7.1 ~ 4.7.3
Strength Analysis
Structural damping
Mesh length
Dynamic simulation duration
Dynamic simulation time step
Strength Code Check: Met?
NO
YES
Fatigue Analysis
S-N curve
SCF
Sea state representation
Safety factor
Total Fatigue Life: Met?
NO
YES
Reliability-Based Fatigue Analysis
Bilinear S-N model Bw
$\Delta_F$
$B$
$m_1$, $m_2$
$K_1$, $K_2$
Safety Index: Satisfied?
NO
YES
Design Completion

## 7.2 Review on Design Procedure

A brief review with detailed instruction on the design procedure of deepwater weight-optimised SCRs is presented in this section.

### *7.2.1 Set up Design Basis*

The following basic parameters need to be confirmed before starting a deepwater SCR design.

(a) Service life $T_s$: normally 20 to 25 years.

(b) Material selection: normally API X52 through X70 pipeline steel, with yield strength from 52 ksi (359 MPa) to 70 ksi (483 MPa) (API Spec 5L, 2000); for deepwater SCRs, high strength steel may be needed.

(c) Internal fluid properties: depends on oil or gas production.

(d) Environmental conditions: according to the local geographical data, including wind, wave, current, and seabed conditions, and water depth $wd$.

(e) Vessel motion: can be calculated by wave and RAO data combined with an offset to the vessel in an uncoupled analysis.

### *7.2.2 Design Codes*

API RP 2RD (1999), DNV-RP-F201 (2001) and related codes by API and DNV are suggested for deepwater SCR design.

### *7.2.3 SCR with Conventional Coating Design*

The key parameters for the SCR with conventional coating design are as follows:

(a) Wave spectrum formulation: JONSWAP is suggested for simulation of North Northern Sea conditions.

(b) Top hang-off angle: typical top hang-off angles for vessel types Spar, semi-submersible, TLP and FPSO are 8 – 14, 10 – 18, 10 – 14, and 12 – 16 degrees respectively (also see Table 3.5.7); for a deepwater SCR connected to a semi-submersible, its dynamic response at critical area TDZ can be improved by decreasing its top hang-off angle.

(c) Diameter: for a deepwater SCR connected to a semi-submersible, its dynamic response at critical area TDZ can be improved by increasing its internal diameter.

(d) Riser wall thickness: for a deepwater SCR connected to a semi-submersible, its dynamic response at critical area TDZ can be improved by increasing its wall thickness.

(e) Hydrodynamic drag coefficient $C_d$: decided by Reynolds number; 0.7 for supercritical flow condition, 0.6 – 1.2 for critical flow condition, and 1.0 for subcritical condition (also see Table 3.5.13); for a deepwater SCR connected to a semi-submersible, the dynamic response at critical area TDA gets worse with the increase of $C_d$ value. Hydrodynamic drag coefficient $C_d$ also has an effect on riser fatigue performance and reliability. Therefore, its value needs to be properly chosen.

(f) Hydrodynamic inertia coefficient $C_m$: normally 2.0 for deepwater SCRs.

(g) Soil stiffness: a linear stiffness simulation is suggested; for normal soil stiffness from 100 kPa to 5000 kPa, its influence on deepwater SCR dynamic response is minor; however, note that higher value of normal soil stiffness needs shorter riser mesh length to get stable dynamic analysis result. Normal soil stiffness also has an effect on riser fatigue performance and reliability. Therefore, its value needs to be properly chosen.

(h) Riser length: a proper riser length with no redundant length for a 15 deg top hang-off angle deepwater SCR connected to a semi-submersible can be calculated by the following equations:

$$L_T = 0.37 \times L_A$$

$$L_E = 0.70 \times L_A$$

where

$L_A$ riser arc length which can be referred to Table 7.2.1

$L_T$ horizontal length from top end to TDP of the riser

$L_E$ horizontal length from top end to bottom end of the riser

$L_A$, $L_E$, and $L_T$ are depicted in Figure 7.2.1.

**Table 7.2.1** Various Riser Arc Lengths for Water Depths 500, 800, 1000, 1500, 2000, 2500, and 3000 m.

| *wd* (m) | 500 | 800 | 1000 | 1500 | 2000 | 2500 | 3000 |
|---|---|---|---|---|---|---|---|
| $L_A$ (m) | 1100 | 1500 | 2000 | 3500 | 4000 | 5000 | 6000 |

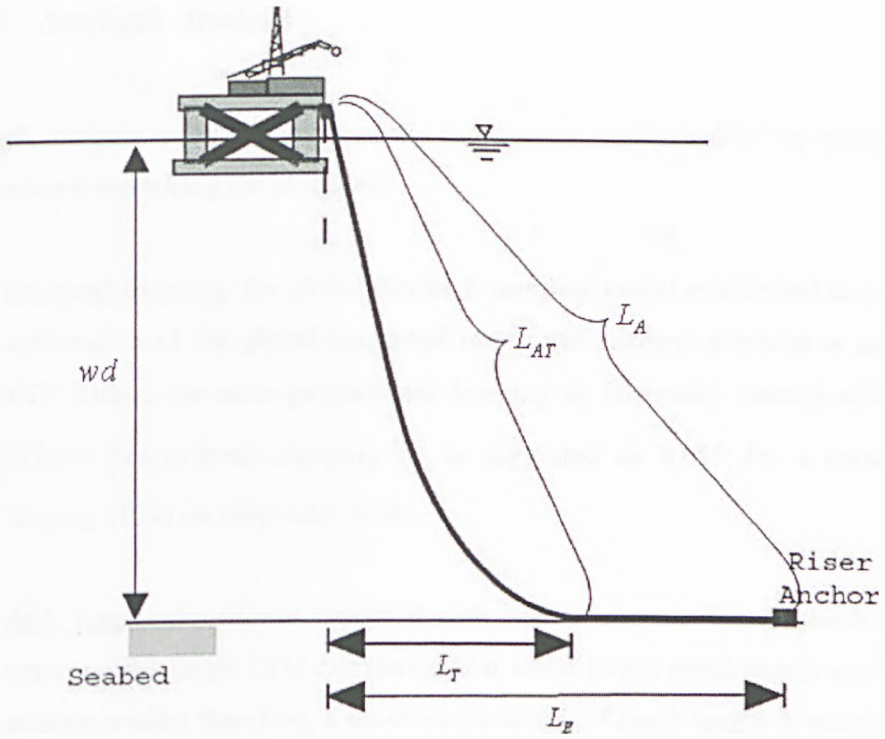


**Figure 7.2.1** Outline of a Typical Deepwater SCR.

After running static analysis of the conventional SCR, riser arc length from top end to TDP under static loadings $L_{AT}$ is obtained. Check the $L_{AT}$ length with water depth to see whether it satisfies the relationship expressed by the following equation. If not, adjust the lengths $L_T$ and $L_E$ and rerun the static analysis until it satisfies.

$$L_{AT} = 1.30 \times wd$$

where

$wd$ water depth

### 7.2.4 Strength Analysis

Strength analysis includes static analysis and dynamic analysis. The key parameters for structural modelling are as follows:

(a) Structural damping: the global Rayleigh damping model established as a linear combination of the global tangential mass- and stiffness matrices is used by DNV Riflex; the mass proportional damping $a_1$ is usually omitted while the stiffness proportional damping $a_2$ is suggested as 0.015 for a reasonable damping effect on deepwater SCRs.

(b) Mesh length: the riser is modelled with beam elements. Shorter mesh length may consume larger CPU calculating cost while longer mesh length may cause unstable results; therefore, a sensitivity analysis of mesh length is necessary; a constant mesh length of 4 m was used for the majority of strength analysis in the present study.

(c) Dynamic simulation duration: normally a 3 h simulation is needed for a proper convergence for a deepwater SCR dynamic analysis; however, considering its high CPU consumption and hard disk occupation, a 1 h simulation is suggested for a large amount of parametric studies which can also provide reliable comparison results with similar riser response trends as 3 h simulation.

(d) Dynamic simulation time step: too small time step may cost too large CPU consumption while too big time step may cause unstable results; a time step of 0.1 s is suggested for deepwater SCR dynamic analysis.

Check the strength analysis results for deepwater SCR with conventional coating design with codes API RP 2RD (1999) and DNV-RP-F201 (2001). If the results satisfy the riser strength requirements of design codes, fatigue analysis can be performed for the designed SCRs; if not, deepwater SCRs need to be redesigned with weight-optimised coating.

### 7.2.5 SCR with Weight-Optimised Coating Design

The suggested weight coating thickness for deepwater SCR with weight-optimised coating design is 0.1 m and suggested coating densities are 650, 950, and 3200 kg/m$^3$ for light, normal, and heavy coating respectively (also see Table 4.7.1).

The weight coating distribution plan including sections upN, straightH, straightL, sagH and TDAL for deepwater SCR with weight-optimised coating design is depicted in Figure 7.2.2, where N, H, and L stand for normal coating, heavy coating, and light coating respectively.

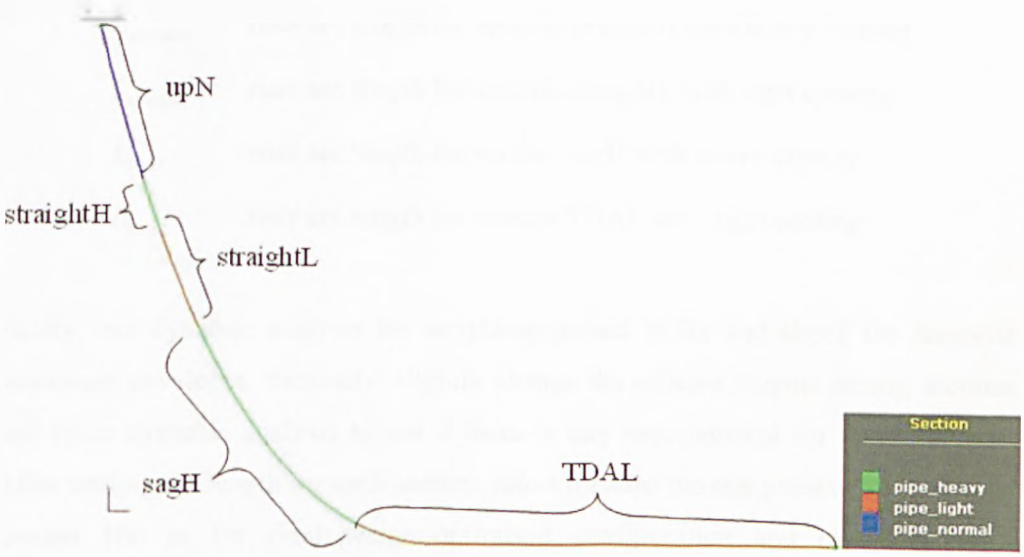


**Figure 7.2.2** Weight Coating Distribution Plan for Deepwater SCR with Weight-Optimised Coating Design.

The length for each section is determined by the following equations:

$$L_B = 0.15 \times wd$$

$$L_{BT} = L_{AT} - L_B$$

$$L_{upN} = 0.261 \times L_{BT}$$

$$L_{straightH} = 0.087 \times L_{BT}$$

$$L_{straightL} = 0.174 \times L_{BT}$$

$$L_{sagH} = 0.478 \times L_{BT}$$

$$L_{TDAL} = L_A - L_{BT}$$

where

| | |
|---|---|
| $L_B$ | riser arc length from the end point of section sagH to TDP under static loadings |
| $L_{upN}$ | riser arc length for section upN with normal coating |
| $L_{straightH}$ | riser arc length for section straightH with heavy coating |
| $L_{straightL}$ | riser arc length for section straightL with light coating |
| $L_{sagH}$ | riser arc length for section sagH with heavy coating |
| $L_{TDAL}$ | riser arc length for section TDAL with light coating |

Firstly, run dynamic analysis for weight-optimised SCRs and check the response maximum envelopes. Secondly, slightly change the relative lengths among sections and rerun dynamic analysis to see if there is any improvement for riser response. After settling the length for each section, move forward the end point of section sagH around 100 m for final weight-optimised configuration and check its ALS performance.

### *7.2.6 Fatigue Analysis*

The key parameters for SCR fatigue analysis are as follows:

(a) S-N curve: DNV-D-Seawater-cathodic bilinear curve (DNV-RP-C203, 2008) is suggested for deepwater SCR fatigue analysis.

(b) Stress concentration factor (SCF): normally 1.0 is suggested to be used with S-N D curve. SCF has a significant effect on riser fatigue life which necessitates proper use of value according to practical weld quality.

(c) Sea state representation: wave scatter diagram can be divided into various blocks for wave simulation; fewer blocks of sea state gives lower overall fatigue life prediction which is more conservative while analyses with more blocks of sea states provides much closer fatigue life estimation but also costs higher computing resources; a 6 to 8 sea state wave spectrum is suggested for a trustworthy fatigue life assessment with margin.

(d) Safety factor: normally 10 for deepwater SCR design, which is considered as "High" safety class by DNV offshore codes (DNV-OS-F201, 2001; DNV-RP-F204, 2005).

Check the fatigue analysis results for deepwater SCR with weight-optimised coating design with code DNV-RP-F204 (2005). If the results satisfy the riser fatigue requirement of design code, reliability-based fatigue analysis can be performed for comparison design; otherwise, design parameters for deepwater SCRs with weight-optimised coating need to be adjusted and reassessed.

### *7.2.7 Reliability-Based Fatigue Analysis*

A bilinear S-N model with wide band correction is suggested for the reliability-based fatigue analysis of deepwater SCRs:

$$g(X)=\frac{\Delta_F}{B^m\Phi}-T_s$$

$$\Phi = \sum_{j=1}^{n} f_j \nu_{0_j} \left\{ \frac{\delta_j B^{m_1} \left(2\sqrt{2}\right)^{m_1} \sigma_j^{m_1} \Gamma\left(1+\frac{m_1}{2}, \frac{S_{SW}^2}{8\left(B\sigma_j\right)^2}\right)}{K_1} + \right.$$

$$\left. + \frac{\delta_j B^{m_2} \left(2\sqrt{2}\right)^{m_2} \sigma_j^{m_2} \left[\Gamma\left(1+\frac{m_2}{2}\right) - \Gamma\left(1+\frac{m_2}{2}, \frac{S_{SW}^2}{8\left(B\sigma_j\right)^2}\right)\right]}{K_2} \right\}$$

where

| | |
|---|---|
| $\Delta_F$ | fatigue resistance limit |
| $B$ | stress modelling error |
| $T_s$ | riser service life |
| $f_j$ | fraction of the time spent in $j$ th sea state |
| $\nu_{0_j}$ | zero mean crossing frequency of stress process in $j$ th sea state |
| $\sigma_j$ | standard deviation of stress process in $j$ th sea state |
| $K_1$, $m_1$ | S-N fatigue parameters for $N \le 10^6$ cycles |
| $K_2$, $m_2$ | S-N fatigue parameters for $N > 10^6$ cycles |
| $\Gamma$, $\gamma$ | complementary incomplete Gamma function and incomplete Gamma function |
| $S_{SW}$ | stress range for which change of slope curve |
| $\delta_j$ | Wirsching-Light's wide band correction factor for $j$th sea state |

The random variables that affect the riser fatigue reliability by bilinear S-N model with wide band correction are as follows:

(a) Fatigue resistance limit $\Delta_F$: lognormal distribution with $\mu$ = 1.0 and COV = 0.3 is suggested; compared with $m_2$, $K_2$ has a minor effect on deepwater SCRs' fatigue reliability.

(b) Stress modelling error $B$: lognormal distribution with $\mu$ = 0.9 and COV = 0.25 is suggested; compared with $m_2$, $K_2$ has a minor effect on deepwater SCRs' fatigue reliability.

(c) Fatigue exponent coefficient $m_1$: lognormal distribution with $\mu$ = 3.0 and COV = 0.18 is suggested, according to DNV-D-Seawater-cathodic curve (DNV-RP-C203, 2008); however, for deepwater SCRs with low fatigue stress and high cycle, $m_1$ won't have any effect on the riser fatigue reliability.

(d) Fatigue exponent coefficient $m_2$: lognormal distribution with $\mu$ = 5.0 and COV = 0.18 is suggested, according to DNV-D-Seawater-cathodic curve (DNV-RP-C203, 2008); with respect to deepwater SCRs' low fatigue stress and high cycle, $m_2$ has a significant effect on the riser fatigue reliability.

(e) Fatigue strength coefficient $K_1$: lognormal distribution with $\mu$ = 5.81E+11 and COV = 0.5 is suggested, according to DNV-D-Seawater-cathodic curve (DNV-RP-C203, 2008); however, for deepwater SCRs with low fatigue stress and high cycle, $K_1$ won't have any effect on the riser fatigue reliability.

(f) Fatigue strength coefficient $K_2$: lognormal distribution with $\mu$ = 4.04E+15 and COV = 0.5 is suggested, according to DNV-D-Seawater-cathodic curve (DNV-RP-C203, 2008); compared with $m_2$, $K_2$ has a minor effect on deepwater SCRs' fatigue reliability.

Check the reliability-based fatigue analysis results for typical points along the deepwater SCR with weight-optimised coating design. If the fatigue reliability index

trend for SCR typical points match well with their fatigue life and the lowest reliability is higher than 4.0, the riser considered to be safe within the required service life. Otherwise, design parameters for deepwater SCRs with weight-optimised coating need to be adjusted and reassessed.

Chapter 8

# Discussion and Conclusions

## 8.1 Discussion

On the basis of the work outlined in this thesis a number of issues deserve brief discussion, and they are considered as follows.

### *8.1.1 Reflection of the Approach Adopted*

#### a) Taking a Broader View

The study began with a critical review of the information on problems related to severe dynamic response and low fatigue life at TDA of deepwater SCRs connected to semi-submersibles in harsh environment and possible methods of dealing with it, among which there hasn't yet a certain mitigation approach universally accepted formulised for practice. This revealed that the existing methods have made significant contributions to the acquiring of knowledge on the physical phenomena of severe dynamic response and low fatigue life at TDA of deepwater SCRs and attempt

of minimising it. But majority of those methods are biased more towards the technical field rather than providing a clarified and effective approach for practical application.

Based on the available information related to subject of mitigation of riser dynamic response and fatigue damage, an impression was created that the problem could be solved by methods based upon the simplified mathematical representations of physical processes involved.

In order to understand the nature of deepwater SCRs' problem and to generate appropriate solutions necessary for the assessment of its fatigue life, reliability approach based on bilinear S-N model with wide band correction was introduced. It expends the traditional focus on linear S-N model for SCR design and concentrates on the function which is more suitable for the behaviour of deepwater SCRs.

**b) The Need to Focus on Key Factors**

The number of parameters affecting dynamic analysis alone for deepwater SCRs was 13, not even mention the parameters that affect its fatigue life and reliability. A comprehensive analysis including as many elements as possible can provide a wide view on the problem and produce a large number of findings and recommendations. But it is necessary to narrow the focus to specific issues capable of solving the problem effectively. The Pareto principle (also know as the 80-20 rule) states that, for many events, roughly 80% of the effects come from 20% of the causes. The activity aided in mitigating the dynamic response and fatigue damage and probability of deepwater SCRs is not an exception. The study provides a good understanding of where effort should be directed in order to tackle the problem efficiently.

### 8.1.2 Contributions of the Thesis

The main contributions of this thesis are:

**a) Adopting a Fresh Approach to Optimising Deepwater SCRs and Formulising Its Application**

The novel approach, called weight-optimised coating, was applied in this thesis for mitigating dynamic response and fatigue damage at TDA for deepwater SCRs. This new approach was further developed into formulisation for an easier practical implementation.

**b) Establishing the Key Parameters**

The comprehensiveness of the approach adopted, with its systematic way of thinking, makes the severe dynamic response and fatigue damage at SCR TDA traceable from many perspectives. The dynamic response as well as fatigue damage at SCR TDA is better understood and optimisation design of deepwater SCRs can be focused on the decision of a fewer parameters for an efficient and effective solution.

**c) Checking the Fundamental Basis of Methods**

Methods and techniques of disciplines related to riser static analysis, dynamic analysis, fatigue analysis and reliability-based fatigue analysis were brought together in an organised way, which gradually proved that the new bilinear S-N model is more suitable for the feature and design of deepwater SCRs compared with the conventional linear S-N model. The integrity of the new approach is based on the principle that all aspects of the problem should be treated together in a rational manner and continuously developing with advantages in knowledge.

**d) Effective Transfer of Research Advances to Practical Application**

A generalised guidance with simple formulations for applying the weight-optimised coating approach for deepwater SCRs with various water depths, which can assist riser engineer to improve deepwater SCR response in harsh environment, was developed as one of facilitators for transferring the research findings into practice. A suitable bilinear S-N model with wide band correction function was also provided for fatigue reliability assessment. It is applicable to deepwater SCRs and can be utilised for a comprehensive and effective preliminary design.

## 8.2 Conclusions

The present study has addressed the use of weight-optimised SCRs for semi-submersibles in deepwater and harsh environment. Focus has been on the mitigation of the severe dynamic response, fatigue performance and reliability at critical area TDZ of the riser.

A deepwater SCR with conventional coating was designed and analysed with a finite element beam model through a comprehensive parametric study. However, no matter how the design parameters had been adjusted, the dynamic response at TDA of the deepwater SCR with conventional coating was much higher than the strength limit required by the adopted design codes.

Therefore, a deepwater SCR with weight-optimised coating was designed and analysed based on the obtained SCR with conventional coating. The distribution plan, thickness, and densities of the 3 types of weight coating (normal coating, light coating, and heavy coating) had been tested and compared. Finally, a deepwater SCR with weight-optimised coating distribution plan, thickness, and densities was established. Extreme dynamic analysis showed that the deepwater SCR with weight-optimised coating could satisfy the strength requirements according to the design codes.

Since the weight-optimised SCR had past strength design requirement, fatigue assessment should be executed to see whether it can meet the service life requirement. Sensitivity study on the fatigue design parameters had been performed and proper values had been chosen for a reliable prediction analysis.

Paralleled with fatigue life assessment, a reliability-based fatigue analysis was also applied. Limit state functions with various models were assessed and compared. A proper limit state function was found for a comparative prediction with fatigue life assessment. Sensitivity analyses were performed for mean value and coefficient of variation (COV) of random variables.

The following conclusions can be made on the basis of the present study:

*Deepwater SCR strength design and analysis with conventional coating*

- Before any structural modelling, sensitivity analyses need to be conducted to ensure that modelling features such as mesh length, mass and stiffness damping, time step size, and dynamic simulation duration are suitable to obtain reliable results with affordable computation cost.

- Normally a 3 h simulation is required to give a proper convergence for riser dynamic analysis. But 1 h dynamic simulation is suggested for sensitivity analysis for preliminary design with a reduction of CPU calculation time by 78.2% and dynamic result file size by 66.7% for a 3000 m long deepwater SCR.

- A mesh sensitivity study is demanded, not only in space domain (mesh length) but also in time domain (time step).

- The global Rayleigh damping model was used during SCR dynamic simulation with mass proportional damping $a_1 = 0$ and stiffness proportional damping coefficient $a_2 = 0.015$ for a reasonable damping of 0.5%.

- JONSWAP spectrum is suggested for wave spectral simulation for Northern North Sea offshore region.

- The dynamic response at the highly stressed SCR TDZ area on seabed can be improved by decreasing the top hang-off angle by each 1 deg or increasing the ID and WT by each 1 in (0.0254 m) and 0.01 m respectively to reduce the maximum dynamic stress level by approximately 3%.

- With the increase of hydrodynamic drag coefficient $C_d$ by each 0.1, the average change in stress level at SCR TDZ could be as high as 8.27%.

- Sensitivity analysis is needed to obtain an optimised riser length with a balance between dynamic response and computation and riser cost. The determination process for riser arc length was formulised based on the study in Chapter 3 and also summarised in Chapter 7 with an attempt to reduce the testing effort for SCR preliminary design.

- Soil stiffness has little influence on the SCR dynamic response, but element length may need to be reduced to get stable results when soil stiffness becomes larger.

- Compared with mild environments such as GoM and WoA, the harsh environment in Northern North Sea had a significant impact on deepwater SCR dynamic response and caused an applicable riser in mild environments into severe dynamic response condition which needed mitigation methods for improvement to achieve acceptable response.

- Deeper water depth has a bigger effect on the top hang-off area of the riser rather than the TDA. With the increase of water depth by each 500 m, the maximum dynamic von Mises stress at Top increased averagely by 20.6%, where attention should be raised during design.

- After all possible adjustment of design parameters, the deepwater SCR with conventional coating for 1000 m water depth and Northern North Sea offshore region still could not meet riser strength design requirement.

*Deepwater SCR strength design and analysis with weight-optimised coating*

- The previous conventional SCR for 1000 m water depth was optimised by weight-optimised coating and satisfied riser strength design requirement. This proposed approach has also been applied to the SCRs for deeper waters up to 3000 m water depth. It is shown that this approach is applicable and successful for improving riser dynamic response remarkably.

- The weight coating optimisation design includes the parameter adjustment of weight coating distribution plan, thickness, and densities.

- The procedure for applying the weight-optimised coating approach has been summarised and formulised in Chapter 4 and 7 for a user-friendly application.

*Fatigue Analysis of Deepwater Weight-Optimised SCRs*

- The majority of the weight-optimised riser had an acceptable fatigue life of more than 1000 years except the two major areas where fatigue damage should be assessed are the SCR TDZ area and top section.

- JONSWAP is consistently suggested for fatigue life analysis as for dynamic analysis of SCRs in Northern North Sea offshore region.

- Variation in hydrodynamic drag coefficient $C_d$ had a bigger effect on SCR TDA than Top section.

- Variation in normal soil stiffness had almost no effect on riser Top section but significant influence on TDA section especially when normal soil stiffness was less than 1000 kPa.

- A suitable bilinear S-N curve is suggested for deepwater SCR fatigue analysis.

- With the increase of SCF by each 0.1, the lowest fatigue life at Top and TDA can be both dropped averagely by as high as 40 %.

- Increasing the sea state division from 3 blocks to 14 blocks raised riser fatigue life prediction by 105% with a reduction in computation time by 71%. Therefore, a balance between assessment accuracy and computation cost should be established.

- The current weight-optimised SCR can satisfy the highest level of safety requirement in DNV offshore codes.

- The significance effect of all the parameters studied on the riser fatigue life has been summarised in Chapter 5 (see Table 5.5.1).

*Reliability-Based Fatigue Analysis of Deepwater Weight-Optimised SCRs*

- A procedure for the probabilistic fatigue reliability analysis at critical points along the weight-optimised SCRs has been outlined and illustrated through sample calculations.

- Four limit state functions, linear S-N model Ln, bilinear S-N model Bn, FM based model with constant $m$ Fn1, and FM based model with correlated $C$ and $m$ Fn2, with narrow band approximation or wide band correction (Lw, Bw, Fw1, and Fw2), were formulated respectively and compared for fatigue reliability analysis.

- A bilinear S-N model based limit state function Bw with wide band correction is suggested for reliability-based fatigue analysis of deepwater weight-optimised SCRs, which can provide more stable and reliable fatigue reliability assessment and also match well with fatigue life prediction.

- Uncertainty analysis shows that not only mean value but also COV of random variables plays a very significant role in determining the reliability or safety of SCRs. If the uncertainties of random variables can be reduced through appropriate care and control, the reliability of risers can be increased.

- Fatigue exponent coefficient $m_2$ and fatigue strength coefficient $K_2$ are the two most important uncertainty parameters affecting the reliability of weight-optimised SCRs by limit state function Bw while fatigue exponent coefficient $m_1$ and fatigue strength coefficient $K_1$ have no effect on the reliability index at all.

- With the increase of riser service life, the probability of failure was correspondingly increased. SCR reliability index dropped down sharply within the first 5 years but afterwards the decrease rate slowed down.

- The significance effect of all the variables studied on the reliability index was summarised in Chapter 6 (see Table 6.10.1).

A full design procedure with indicated important influential parameters, starting from using conventional coating to optimised weight coating for deepwater SCRs connected to vessels with severe motion such as semi-submersibles in harsh environment to meet design requirements including strength, fatigue life, and reliability was summarised and detailedly instructed in Chapter 7 based on the current thesis study for reference, which can be applicable for deepwater SCRs with various water depths.

## 8.3 Recommendations for Future Research

### a) Collect Data Relating to Deepwater SCR Fracture Mechanics (FM) Features

Use of qualitative and quantitative methods of reliability assessment allows focusing on the most important parameters affecting deepwater SCR fracture mechanics. The former is based upon judgement skill gained through practice and experience, while the latter is built by judgement based on available statistical information (data) used. The study on the fatigue reliability analysis based on FM model can be considered as a starting point in the establishment of the general framework. There were the problems with the data that are not well defined or that are incomplete. More information about such as the initial crack size and critical crack size is needed in order to make more realistic assumptions about consequences and probabilities of the identified fatigue crack growth in deepwater SCRs. There is a need for ongoing data collection efforts to improve the understanding of the uncertainties associated with the fatigue reliability analysis of deepwater SCRs based on FM model. Once an adequate and sufficient data could be gathered and numerical values can be assigned to the various parameters, quantification of fatigue reliability can be performed with more precision showing the probability of fatigue crack growth and their consequences more accurately.

### b) Improve Fracture Mechanics (FM) Model for Fatigue Reliability Analysis

The introduction and development of fracture mechanics and reliability-based methods for crack growth assessment will signify substantial benefit and understanding of the different parameters and corresponding uncertainties involved in the fatigue damage process. FM represents a potential tool to describe the gradual development of crack and hence accounts for the effect of inspection and possible repair at the different stages of crack growth. Recently, the use of an FM-based bilinear crack growth law for fatigue analysis has been introduced by BS 7910 (2005), which reduces the excessive conservatism believed to be implicit in the linear Paris law approach. A limit state function based on an FM bilinear crack growth law

might be a way to improve the FM model for a better fatigue reliability assessment of deepwater SCRs.

**c) Research into Other Vessel Situations**

It would be very helpful to examine how the weight-optimised coating formulisation and bilinear S-N model can be used for deepwater SCRs connected to other kinds of vessels, especially an FPSO which may cause similar or even worse dynamic response and fatigue damage at SCR TDA. This approach might be expected to have an increased level of application for deep and even deeper water SCRs.

# References

**Abramowitz**, M., & Stegun, I.A. (1972). *Handbook of Mathematical Functions with Formulas, Graphs and Mathematical Tables*. Dover, New York, 1972. Retrieved September 15, 2008, from http://www.convertit.com/Go/Convertit/Reference/AMS55.ASP?Res=150&Page=260&Submit=Go.

**Aggarwal**, R.K. et al. (2005). Qualification of Solutions for Improving Fatigue Life at SCR Touch Down Zone. Paper presented at Deep Offshore Technology (DOT) Conference, Vitoria, Espirito Santo, Brazil.

**Aggarwal**, R.K. et al. (2007). Development and Qualification of Alternate Solutions for Improved Fatigue Performance of Deepwater Steel Catenary Risers. *Proceedings of the 26th International Conference on Offshore Mechanics and Arctic Engineering OMAE2007*, San Diego, USA.

**Airy**, G.B. (1841). Tides and Waves. *Encyclopaedia Metropolitana*, Mixed Sciences, 3, 1817-1845.

**Akpan**, U.O., Koko, T.S., Rushton, P.A., Tavassoli, A., & Else, M. (2007). Probabilistic Fatigue Reliability of Large Diameter Steel Catenary Risers (SCR) for Ultra-Deepwater Operations. *Proceedings of the 26th International Conference on Offshore Mechanics and Arctic Engineering OMAE2007*, San Diego, USA.

**Amicis**, L.D., Mahoney, G., Grealish, F., & Connaire, A. (2008). Advanced Design Methodologies for SCRs. *Proceedings of the Eighteenth (2008) International Offshore and Polar Engineering Conference*, Vancouver, Canada.

**Amzallag**, C., Gerey, J.P., Robert, J.L., & Bahuaud, J. (1994). Standardization of the Rainflow Counting Method for Fatigue Analysis. *International Journal of Fatigue*, 16, 287-293.

**Andrade**, E.Q.D., Siqueira, E.F.N., Mourelle, M.M., & Caldwell, C. (2007). Titanium Stressjoint Design for the Top Connection of A SCR in HPHD. *Proceedings of the 26th International Conference on Offshore Mechanics and Arctic Engineering OMAE2007*, San Diego, USA.

**ANFLEX** (1999). *Computational System for the Nonlinear Analysis of Risers and Anchoring Systems – Users Manual* (in Portuguese). Petrobras/CENPES/DIPREX/ SEDEM, Rio de Janeiro.

**API** RP 1111 (1999). *Design, Construction, Operation, and Maintenance of Offshore Hydrocarbon Pipelines* (Limit State Design) (1st ed.). American Petroleum Institute.

**API** RP 2A-WSD (2000). *Planning, Designing and Constructing Fixed Offshore Platforms – Working Stress Design* (21st ed.). American Petroleum Institute.

**API** RP 2RD (1999). *Design of Risers for Floating Production Systems (FPSs) and Tension Leg Platforms (TLPs)* (1st ed.). American Petroleum Institute.

**API** RP 2T (1997). *Recommended Practice for Planning, Designing, and Constructing Tension Leg Platforms*. American Petroleum Institute.

**API** Spec 5L (2000). *Specification for Line Pipe* (42nd ed.). American Petroleum Institute.

**Aranha**, J.A.P., Martins, C.A., & Pesce, C.P. (1997). Analytical Approximation for the Dynamic Bending Moment at the Touch-Down Point of a Catenary Riser. *International Journal of Offshore and Polar Engineering*, 7(4), 293-300.

**Arnesen**, G. et al. (2006). Integrated Semi and Steel Catenary Risers (SCR) in Deep Water and Harsh Environment Conditions. Paper presented at the Offshore Technology Conference, Houston, USA.

**ASME** B31.8 (2000). *Gas Transmission Distribution and Piping Systems*. American Society of Mechanical Engineers.

**ASTM** (1985). *Standard Practices for Cycle Counting in Fatigue Analysis*. Designation E 1049-85, Philadelphia, PA.

**Aubeny**, C.P., Biscontin, G., & Zhang, J. (2006). Seafloor Interaction with Steel Catenary Risers. Minerals Management Service (MMS) Project Number 510 and OTRC Industry Consortium, final project report.

**Averbuch**, D., Cunff, C.L., Costa, D., & Biolley, F. (2003). Analytical Methods for Predicting Displacements and Stresses in SCRs Subjected to Static Loading. *Proceedings of the Thirteenth (2003) International Offshore and Polar Engineering Conference*, Honolulu, Hawaii, USA.

**Ayala**-Uraga, E., & Moan, T. (2007). Fatigue Reliability-Based Assessment of Welded Joints Applying Consistent Fracture Mechanics Formulations. *International Journal of Fatigue*, 29, 444-456.

**Ayyub**, B.M., Assakkaf, I.A., Kihl, D.P., & Sieve, M.W. (2002). Reliability-Based Design Guidelines for Fatigue of Ship Structures. *Naval Engineers Journal*, ASNE, 114(2), 113-138.

**Bai**, Y., & Bai, Q. (2005). *Subsea Pipelines and Risers* (1st ed.). Amsterdam: Elsevier.

**Bai**, Y., Tang, A., O'Sullivan, E., Uppu, K.C., & Ramakrishnan, S. (2004). Steel Catenary Riser Fatigue due to Vortex Induced Spar Motions. Paper presented at the Offshore Technology Conference, Houston, USA.

**Barltrop**, N.D.P., & Adams, A. (1991). *Dynamics of Fixed Marine Structures*. MTD / Butterworth – Heinemann.

**Bathe**, K.J. (1982). Finite Element Procedures in Engineering Analysis. Prentice Hall, Englewood Cliffs, New Jersey.

**Bech**, A., & Skallerud, B. (1992). Structural Damping in Flexible Pipes: Comparisons between Dynamic Tests and Numerical Simulations. *Proceedings of the 2nd International Offshore and Polar Engineering Conference*, San Fransisco, USA.

**Bell**, J.M., Chin, Y.D., & Hanrahan, S. (2005). State of the Art of Ultra Deepwater Production Technologies. Paper prepared for the Offshore Technology Conference, Houston, USA.

**Bhat**, S., Dutta, A., Wu, J., & Sarkar, I. (2004). Pragmatic Solutions to Touch-Down Zone Fatigue Challenges in Steel Catenary Risers. Paper presented at the Offshore Technology Conference, Houston, USA.

**Bishop**, N.W.M., & Sherratt, F. (2000). *Finite Element Based Fatigue Calculations*, NAFEMS Ltd, Glasgow, UK.

**Bjørset**, A., Remseth, S., Leira, B.J., & Larsen, C.M. (2003). Titanium Pipes Subjected to Bending Moment and External Pressure. *Computers and Structures*, 81, 2691-2704.

**Bjørset**, A., Leira, B.J., & Remseth, S. (2004). Probabilistic Analysis of Bending Moment Capacity of Titanium Pipes. *Structural Safety*, 26, 241-269.

**Borgen**, J.E. (2002). Large Diameter Steel Riser for Semi Submersible Floater in Harsh Environment. Paper presented at Deep Offshore Technology (DOT), New Orleans, USA.

**Borgen**, J.E., Fosterud, E.K., & Larsen, T.J. (2003). L-Riser: Steel Dynamic Riser for Severe Vessel Motions. Paper presented at the Offshore Technology Conference, Houston, USA.

**Bowness**, D., & Lee, M.M.K. (1999). Weld Toe Magnification Factors for Semi-Ellipitical Cracks in T-Butt Joints. *Offshore Technology Report* – OTO 1999 014, Health Safety Executive.

**Braga**, V., Bomfimsliva, C., Critsinelis, A., Monteiro, C., & Azevedo, F. (2000). Deepwater Steel Pipelines and SCRs Installation. *Proceedings of 3rd Deepwater Pipeline and Riser Technology Conference*, Houston, USA.

**Breitung**, K. (1984). Asymptotic Approximations for Multinormal Integrals. *Journal of Engineering Mechanics*, ASCE, 110(3), 357-366.

**Bridge**, C., & Laver, K. (2004). Steel Catenary Riser Touchdown Point Vertical Interaction Models. Paper presented at the Offshore Technology Conference, Houston, USA.

**Brinkmann**, C.R., & Whooley, K.T. (2002). Design Study of a Deepwater Compliant Vertical Access Riser for the Gulf of Mexico. *Proceedings of OMAE'02 21st International Conference on Offshore Mechanics and Arctic Engineering*, Oslo, Norway.

**Broek**, D. (1986). *Elementary Engineering Fracture Mechanics* (4th ed.). Martinus Nijhoff Publishers, Dordrecht, The Netherlands.

**Brooks**, J., Masson, C., & Reeves, D. (2007). Atlantis Oil Export SCR, Treatment fo Girth Welds for Enhanced Fatigue Performance. *Proceedings of the 26th International Conference on Offshore Mechanics and Arctic Engineering OMAE2007*, San Diego, USA.

**Brugmans**, J. (2005). *Parametric Instability of Deep-Water Risers*. Master's Thesis, Delft University of Technology.

**BS** 5400 (1980). Steel, Concrete, and Composite Bridges; Part 10. Code of Practice for Fatigue. British Standards Institute.

**BS** 7608 (1993). *Code of Practice for Fatigue Design and Assessment of Steel Structures*. British Standards Institute.

**BS** 7910 (2005). Guide to Methods for Assessing the Acceptability of Flaws in Metallic Structures. British Standards Institute.

**Bucher**, C., Hintze, D., & Boos, D. (2000). Advanced Analysis of Structural Reliability Using Commercial FE-Codes. European Congress on Computational Methods in Applied Sciences and Engineering, ECCOMAS 2000, Barcelona, Spain.

**Buitrago**, J., Weir, M.S., & Kan, W.C. (2003). Fatigue Design and Performance Verification of Deepwater Risers. *Proceedings of OMAE 2003 22nd International Conference on Offshore Mechanics and Arctic Engineering*, Cancun, Mexico.

**Buitrago**, J., & Zettlemoyer, N. (2004). Fatigue Design of Critical Girth Welds for Deepwater Applications. *Proceedings of OMAE '98, 17th International Conference on Offshore Mechanics and Arctic Engineering*, Lisbon, Portugal.

**Bureau** Veritas Rules (2000). *BV Rules for the Classification of Steel Ships*. Bureau Veritas, Marine Department, Paris.

**Byers**, W.G., Marley, M.J., Mohammadi, J., Nielsen, R.J., & Sarkani, S. (1997). Fatigue Reliability Reassessment Procedures: State-of-the-Art Paper. *Journal of Structural Engineering*, 123(3), 271-276.

**Campbell**, M. (1999). The Complexities of Fatigue Analysis for Deepwater Risers. Paper presented at Deepwater Pipeline Conference, New Orleans, USA.

**Campbell**, M., Jones, S., & Korloo, J. (2003). The Role of ECA in the Development of Dynamic Riser Systems. *Proceedings of OMAE 2003 22nd International Conference on Offshore Mechanics and Arctic Engineering*, Cancun, Mexico.

**Campos**, L.D.A., & Martins, C.A. (2001). Nonlinear Dynamic Response of a Steel Catenary Riser at the Touch-Down Point. *Proceedings of the Eleventh (2001) International Offshore and Polar Engineering Conference*, Stavanger, Norway.

**Chai**, Y.T., Varyani, K.S., & Barltrop, N.D.P. (2001). Three-Dimensional Lump-Mass Formulation of A Catenary Riser with Bending, Torsion and Irregular Seabed Interaction Effect. *Ocean Engineering*, 29, 1503-1525.

**Chai**, Y.T., & Varyani, K.S. (2005). An Absolute Coordinate Formulation for Three-Dimensional Flexible Pipe Analysis. *Ocean Engineering*, 33, 23–58.

**Chandwani**, R., Timbrell, C.M., & Wiehahn, M. (2005). An FE Simulation Tool for Fracture Mechanics. Paper presented at International Seminar on "Fatigue, Reliability & Performance Considerations in Design", Bangalore, India.

**Chatjigeorgiou**, I.K. (2008). A Finite Differences Formulation for the Linear and Nonlinear Dynamics of 2D Catenary Risers. *Ocean Engineering*, 35, 616-636.

**Chaudhury**, G., & Kennefick, J. (1999). Design, Testing and Installation of Steel Catenary Risers. *Proceedings of Offshore Technology Conference 1999*, Houston, USA.

**Chen**, H.C., Chen, C.R., & Mercier, R.S. (2006). CFD Simulation of Riser VIV. Prepared for the MMS under the MMS/OTRC Cooperative Research Agreement 1435-01-99-CA-31003, Task Order 74521 and 1435-01-04-CA-35515, Task Order 35983; MMS Project No. 481, Offshore Technology Research Center Library No. 10/2006A176.

**Cheng**, Y., Song, R., Mekha, B., Torstrick, A., & Liu, H. (2007). Compression Assessment of Deepwater Steel Catenary Risers at Touch Down Zone. *Proceedings of the 26th International Conference on Offshore Mechanics and Arctic Engineering OMAE2007*, San Diego, USA.

**Clark**, W.G., & Hudak, S.J., Jr. (1979). The Analysis of Fatigue Crack Growth Rate Data. *Application of Fracture Mechanics to Design*, 22, 67-81.

**Clukey**, E., Jacob, P., & Sharma, P. (2008). Investigation of Riser Seafloor Interaction Using Explicit Finite Element Methods. Paper presented at the Offshore Technology Conference, Houston, USA.

**Collins**, J.A. (1993). *Failure of Materials in Mechanical Design, Analysis, Prediction, Prevention* (2nd ed.). A Wiley-Interscience Publication.

**Compbell**, M. (1999). The Complexities of Fatigue Analysis for Deepwater Risers. Paper presented at Deepwater Pipeline Technology Conference, New Orleans, USA.

**Cunliffe**, N., Baxter, C., McCarthy, T., & Trim, A. (2004). Evolutionary Design of Marine Riser Systems. *Proceedings of OMAE04 23rd International Conference on Offshore Mechanics and Arctic Engineering*, Vancouver, Canada.

**Connaire**, A., Kavanagh, K., Ahilan, R.V., & Goodwin, P. (1999). Integrated Mooring & Riser Design: Analysis Methodology. Paper presented at the Offshore Technology Conference, Houston, USA.

**Cortie**, M.B., & Garrett, G.G. (1988). On the Correlation between C and m in the Paris equation for fatigue crack propagation. Engineering Fracture Mechanics, 30(1), 49-58.

**Dantas**, C.M.S. et al. (2004). A Frequency Domain Approach for Random Fatigue Analysis of Steel Catenary Risers at Brazil's Deep Waters. *Proceedings of OMAE04 23rd International Conference on Offshore Mechanics and Arctic Engineering*, Vancouver, Canada.

**Dantas**, C.M.S. et al. (2005). A Frequency Domain Approach for the Random Fatigue Analysis of SCR Considering Bimodal/Bidirectional Characteristic of Campos Basin Sea States. *Proceedings of OMAE2005 24th International Conference on Offshore Mechanics and Arctic Engineering*, Halkidiki, Greece.

**Deepwater** Engineering & Technology Research Centre (2008). Offshore Riser Design and Analysis, 01 – Overview. Harbin Engineering University, China. Retrieved September 22, 2008, from http://sy.zlgc.edu.cn/upload/20070918094847015.pdf.

**Ditlevsen**, O. (1986). Random Fatigue Crack Growth – A First-Passage Problem. *Engineering Fracture Mechanics*, 23, 467-477.

**Ditlevsen**, O., & Madsen, H.O. (1996). *Structural Reliability Methods*. Wiley, New York, USA.

**DNV**-OS-F201 (2001). *Dynamic Risers*. Det Norske Veritas.

**DNV**-RP-F204 (2005). *Riser Fatigue*. Det Norske Veritas.

**DNV**-RP-B401 (2005). *Cathodic Protection Design*. Det Norske Veritas.

**DNV**-RP-C203 (2008). *Fatigue Design of Offshore Steel Structures*. Det Norske Veritas.

**DNV**-RP-F103 (2003). Cathodic Protection of Submarine Pipelines by Galvanic Anodes. Det Norske Veritas.

**DNV**-RP-F201 (2001). *Dynamic Risers*. Det Norske Veritas.

**DNV**-RP-F204 (2005). *Riser Fatigue*. Det Norske Veritas.

**DNV** Software (2005). *RIFLEX Theory Manual*. Det Norske Veritas.

**DNV** Software (2008). *DeepC Deep Water Floater Motion Analysis*, SESAM User Manual. Det Norske Veritas.

**DOE** (1990). *Offshore Installations: Guidance on Design, Construction and Certification* (4th ed.). UK Department of Energy, HMSO, London.

**DOT** 49 CFR PT 192 (2007). *Transportation of Natural or Other Gas by Pipeline: Minimum Federal Safety Standards*. U.S. Department of Transportation.

**Dowling**, N.E. (1972). Fatigue-Failure Predictions for Complicated Stress-Strain Histories. *American Society for Testing and Materials, Journal of Materials*, 7(1), 71-87.

**Dowling**, N.E. (1979). Fatigue at Notches and the Local Strain and Fracture Mechanics Approaches. *Fracture Mechanics*, ASTM STP 677, American Society of Testing and Materials.

**Ellyin**, F. (1997). *Fatigue Damage, Crack Growth and Life Prediction*. Chapman & Hall, London; New York.

**Faltinsen**, O.M. (1990). *Sea Loads on Ships and Offshore Structures.* Cambridge University Press, Cambridge, UK.

**Fatemi**, A., & Yang, L. (1997). Cumulative Fatigue Damage and Life Prediction Theories: A Survey of the State of the Art for Homogeneous Materials. *International Journal of Fatigue*, 20(1), 9-34.

**Fiessler**, B., Neumann, H.J., & Rackwitz, R. (1979). Quadratic Limit States in Structural Reliability Theory. *Journal of Engineering Mechanics*, ASCE, 105, 661-676.

**Fisher**, J.W. (1984). *Fatigue and Fracture in Steel Bridges – Case Studies.* Wiley, New York.

**FloaTEC**. Deepwater Floating Facilities – An Overview. FloaTEC LLC, Houston, USA. Retrieved September 22, 2008, from http://www.floatec.com/images/mm_content/Deepwater_Floater_Intro.pdf.

**Foyt**, E., Griffin, C., Campbell, M., Wang, H.H., & Kan, W.C. (2007). Weight Optimized SCR – Enabling Technology for Turret Moored FPSO Developments. *Proceedings of the 26th International Conference on Offshore Mechanics and Arctic Engineering OMAE2007*, San Diego, USA.

**Franciss**, R., & Riberiro, E. (2004). Analyses of a Large Diameter Steel Lazy Wave Riser for Ultra Deepwater in Campos Basin. *Proceedings of OMAE04 23rd International Conference on Offshore Mechanics and Arctic Engineering*, Vancouver, Canada.

**Fuchs**, H.O., & Stephens, R.I. (1980). *Metal Fatigue in Engineering.* Wiley, New York.

**Fylling**, I., Larsen, C.M., Sødahl, N., Passano, E., Bech, A., Engseth, A.G., Lie, E., & Ormberg, H. (1998). Riflex User's Manual. Marintek Report, Trondheim, Norway.

**Galvin**, C., & Hill, R. (2007). Independence Trail – Steel Catenary Riser Design and Material. Paper presented at the Offshore Technology Conference, Houston, USA.

**Garrett**, D.L. (2005). Coupled Analysis of Floating Production Systems. *Ocean Engineering*, 32, 802-816.

**Garrett**, D.L., Chappell, J.F., & Gordon, R.B. (2002). Global Performance of Floating Production Systems. Paper presented at the Offshore Technology Conference, Houston, USA.

**Gassner**, E., & Schültz, W. (1962). Evaluating Vital Vehicle Components by Program Fatigue Tests. *Proceedings of 9th International Auto. Tech. Congress*, International Mechanical Engineering, 195-205.

**Giertsen**, E., Verley, R., & Schrøder, K. (2004). CARISMA A Catenary Riser/Soil Interaction Model for Global Riser Analysis. *Proceedings of OMAE04 23rd International Conference on Offshore Mechanics and Arctic Engineering*, Vancouver, Canada.

**Gollwitzer**, S., Kirchgässner, B., Fischer, R., & Rackwitz, R. (2006). PERMAS-RA/SREUREL System of Programs for Probabilistic Reliability Analysis. *Structural Safety*, 28(1-2), 108-129.

**Gonzalez**, E.C., Mourelle, M.M., Mauricio, J., Lima, T.G., & Moreira, C.C. (2005). Steel Catenary Riser Design and Analysis for Petrobras Roncador Field Development. Paper presented at the Offshore Technology Conference, Houston, USA.

**Gore**, C.T., & Mekha, B.B. (2002). Common Sense Requirements (CSRs) for Steel Catenary Risers (SCRs). Paper presented at the Offshore Technology Conference, Houston, USA.

**Grealish**, F., Kavanagh, K., Connaire, A., & Batty, P. (2007). Advanced Nonlinear Analysis Methodologies for SCRs. Paper presented at the Offshore Technology Conference, Houston, USA.

**Gurney**, T.R. (1979). *Fatigue of Welded Structures* (2nd ed.). Cambridge University Press, Cambridge.

**Hancock**, J.W., & Gall, D.S. (1985). *Fatigue under Narrow and Broad Stationary Loading*. Final report of the cohesive program of research and development into the fatigue of offshore structures. MTD Ltd.

**Hansen**, V.L., Wang, L., Sodahl, N., & Ward (2004). Guidelines on Coupled Analyses of Deepwater Floating Systems. Paper presented at the Offshore Technology Conference, Houston, USA.

**Harris**, D.O. (1995). Probabilistic Fracture Mechanics. *Probabilistic Fracture Mechanics Handbook*, Sundarajan, C., Editor, Chapman and Hall, New York.

**Hasofer**, A.M., & Lind, N.C. (1974). Exact and Invariant Second-Moment Code Format. *Journal of Engineering Mechanics Division*, ASCE, 100(1), 111-121.

**Hasselmann**, K. et al. (1973). Measurements of wind-wave growth and swell decay during the Joint North Sea Wave Project (JONSWAP). *Deutsche Hydrographische Zeitschrift*, Supplement, A8(12), 1-95.

**Hatton**, S.A. (1999). Update on the Design of Steel Catenary Riser Systems. Deep and Ultra Deep Water Offshore Technology Conference, Newcastle, UK.

**Hesar,** M. (2004). Pipeline-Seabed Interaction in Soft Clay. *Proceedings of OMAE04 23rd International Conference on Offshore Mechanics and Arctic Engineering*, Vancouver, Canada.

**Heurtier,** J.M. et al. (2001). Coupled Dynamic Response of Moored FPSO with Risers. *Proceedings of the Eleventh (2001) International Offshore and Polar Engineering Conference*, Stavanger, Norway.

**Hobbacher,** A. (1996). *Recommendations on Fatigue of Welded Components*, International Institute of Welding (IIW) Document, XIII-1539/XV-845-96.

**Hogg,** B., Harte, A., & Grealish, F. (2003). A Combined Riser Mooring System for Deepwater Applications. *Proceedings of OMAE 2003 22nd International Conference on Offshore Mechanics and Arctic Engineering*, Cancun, Mexico.

**Horn,** A.M., Hauge, M., Røstadsand, P., Bjørnbakk, B., Dahlberg, P., & Fossesholm, T. (2002). Cost Effective Fabrication of Large Diameter High Strength Titanium Catenary Riser. *Proceedings of OMAE'02 21st International Conference on Offshore Mechanics and Arctic Engineering*, Oslo, Norway.

**Hughes,** O.F. (1988). Ship Structural Design, A Rationally-Based, Computer-Aided Optimization Approach. The Society of Naval Architects & Marine Engineers, Jersey City, New Jersey, USA.

**IIJIMA,** T. (2005). Simplified Modeling and Detailed Crack Propagation Analysis for Cracked Pipes. *Proceedings of PVP2005 ASME Pressure Vessels and Piping Division Conference*, Denver, USA.

**Izquierdo,** A. et al. (2008). Qualification of Weldable X65 Grade Riser Sections with Upset Ends to Improve Fatigue Performance of Deepwater Steel Catenary Risers. *Proceedings of the Eighteenth (2008) International Offshore and Polar Engineering Conference*, Vancouver, Canada.

**ISO** 15589-2 (2004). Cathodic Protection of Pipeline Transportation Systems – Part 2: Offshore Pipelines. International Organization for Standardization.

**Jain,** A.K. (1994). Review of Flexible Risers and Articulated Storage Systems. *Ocean Engineering*, 21, 733-750.

**Jeary,** A. (1998). *Designer's Guide to the Dynamic Response of Structures*. Brunner-Routledge.

**Jesudasen,** A.S., McShane, B.M., McDonald, W.J., Vandenbossche, M., & Souza, L.F. (2004). Design Considerations Particular to SCRs Supported by Spar Buoy Platform Structures. Paper presented at the Offshore Technology Conference, Houston, USA.

**JIP** Report (2008). New Touch Down Zone (TDZ) Solutions for Steel Catenary Risers (SCRs) – Development and Qualification of Alternative Design Solutions. US Department of Interior, Minerals Management Service & US Department of Transportation, Pipeline and Hazardous Materials Safety Administration.

**Karunakaran**, D. (2006). Weight-Distributed Steel Catenary Risers A Harsh Environment Plus. *Offshore*, 66(8). Retrieved September 19, 2008, from http://www.offshore-mag.com/display_article/262128/120/ARTCL/none/none/1/Weight-distributed-steel-catenary-risers-a-harsh-environment-plus/.

**Karunakaran**, D., Dutta, A., Clausen, T., & Lund, K.M. (2002). Steel Catenary Riser Configurations for Large Motion Semi Submersibles with Lightweight Coating. Paper presented at Deep Offshore Technology (DOT), New Orleans, USA.

**Karunakaran**, D., & Meling, T.S. (2006). Robust Design against Fatigue in Deepwater Harsh Environments. Paper presented at Deep Offshore Technology (DOT), Houston, USA.

**Karunakaran**, D., Meiling, T.S., Kristoffersen, S., & Lund, K.M. (2005). Weight-Optimized SCRs for Deepwater Harsh Environments. Paper presented at the Offshore Technology Conference, Houston, USA.

**Kavanagh**, W.K., Harte, G., Farnsworth, K.R., Griffin, P.G., Hsu, T.M., Jefferies, A., & Desalos, A.P. (2004). Matterhorn Steel Catenary Risers: Critical Issues and Lessons Learned for Reel-Layed SCRs to a TLP. Paper presented at the Offshore Technology Conference, Houston, USA.

**Kavanagh**, W.K., Lou, J., & Hays, P. (2003). Design of Steel Risers in Ultra Deep Water – The Influence of Recent Code Requirements on Wall Thickness Design for 10,000ft Water Depth. Paper presented at the Offshore Technology Conference, Houston, USA.

**Keppel** FELS Limit (2007). DSS™ 51 Semisubmersible Drilling Rig. Retrieved October 22, 2008, from http://www.keppelfels.com.sg/capabilities/pdf/dss51.pdf.
Khan, R.A., & Ahmad, S. (2007a). Safety of a Deep Water Marine Riser under Random Loads. *Maritime Engineering*, 160, 175-183.

**Khan**, R.A., & Ahmad, S. (2007b). Dynamic Response and Fatigue Analysis of Marine Riser under Random Loads. *Proceedings of the 26th International Conference on Offshore Mechanics and Arctic Engineering OMAE2007*, San Diego, USA.

**Kim**, M.H. (2004). Dynamic Analysis Tool for Moored Tanker-Based FPSO's including Large Yaw Motions. Final project report prepared for the Minerals Management Service under the MMS/OTRC Cooperative Research Agreement 1435-01-99-CA-31003, Task Order 16181, Project 366.

**Kiureghian**, A.D., Lin, H.Z., & Hwang, S.J. (1987). Second-Order Reliability Approximations. *Journal of Engineering Mechanics Division*, ASCE, 113(8), 1208-1225.

**Kiureghian**, A.D., Haukaas, T., & Fujimura, K. (2006). Structural Reliability Software at the University of California, Berkeley. *Structural Safety*, 28, 44-67.
Lalanne, C. (1999). *Fatigue Damage*. Mechanical Vibration & Shock, VI. Taylor and Francis Books, Inc.

**Kopp**, F., Perkins, G., Prentice, G., & Stevens, D. (2003). Production and Inspection Issues for Steel Catenary Riser Welds. Paper presented at the Offshore Technology Conference, Houston, USA.

**Korth**, D.R., Chou, B.S.J., & McCullough, G.D. (2002). Design and Implementation of the First Buoyed Steel Catenary Risers. Paper presented at the Offshore Technology Conference, Houston, USA.

**Krenk**, S. (1978). *A Double Envelope for Stochastic Processes*. Report No. 134. Danish Center for Applied Mathematics and Mechanics.

**Ku**, A. et al. (2004). Structural Reliability Applications in Developing Risk-Based Inspection Plans for a Floating Production Installation. *Proceedings of OMAE04 23rd International Conference on Offshore Mechanics and Arctic Engineering*, Vancouver, Canada.

**Kung**, C.J., & Wirsching, P.H. (1992). Fatigue and Fracture Reliability and Maintainability of TLP Tendons. *Proceedings of OMAE1992 11th International Conference on Offshore Mechanics and Arctic Engineering*, Calgary, Canada.

**Lalanne**, C. (1999). *Fatigue Damage*. Mechanical Vibration & Shock, VI. Taylor and Francis Books, Inc.

**Landes**, J., Lee, K., Bose, W.W., & Ito, H. (2001). Evaluation of Fatigue Lives of Steel Catenary Risers. *Proceedings of OMAE'01 20th International Conference on Offshore Mechanics and Arctic Engineering*, Rio de Janeiro, Brazil.

**Langner**, C.G. (2003). Fatigue Life Improvement of Steel Catenary Risers due to Self-Trenching at the Touchdown Point. Paper presented at the Offshore Technology Conference, Houston, USA.

**Langner**, C.G., & Bharat C.S. (1997). Code Conflicts for Harsh Pressure Flowlines and Steel Catenary Risers. Paper presented at the Offshore Technology Conference, Houston, USA.

**Larsen**, C.M., and Passano, E. (2006). Time and Frequency Domain Analysis of Catenary Risers Subjected to Vortex Induced Vibrations. Efficient Analysis of A Catenary Riser. *Proceedings of OMAE2006 25th International Conference on Offshore Mechanics and Arctic Engineering*, Hamburg, Germany.

**Lee**, J.Y., & Clauss, G.F. (2007). Automated Development of Floating Offshore Structures in Deepwater with Verified Global Performances by Coupled Analysis. *Proceedings of the Seventeenth (2007) International Offshore and Polar Engineering Conference*, Lisbon, Portugal.

**Lee**, Y.L., Pan, J., Hathaway, R.B., & Barkey, M.E. (2005). *Fatigue Testing and Analysis*. Elsevier Butterworth-Heinemann.

**Leira**, B.J., Passano, E., Karunakaran, D., Farnes, K.A., and Giertsen, E. (2004). Analysis Guidelines and Application of a Riser-Soil Interaction Model including Trench Effects. *Proceedings of OMAE04 23rd International Conference on Offshore Mechanics and Arctic Engineering*, Vancouver, Canada.

**Lemaire**, M., & Pendola, M. (2006). PHIMECA-SOFT. *Structural Safety*, 28(1-2), 130-149.

**Li**, Y., Lo, K.H., & Zhang, H. (2007). An Alternative Top Termination for A Steel Catenary Riser. *Proceedings of the 26th International Conference on Offshore Mechanics and Arctic Engineering OMAE2007*, San Diego, USA.

**Lidiard**, A.B. (1979). Probabilistic Fracture Mechanics. *Proceedings of Fracture Mechanics – Current State, Future Prospect*, Pergammon Press.

**Lim**, F. (2006). Paper presented at Installation of Risers in Deep Waters. 4th PetroMin Deepwater & Subsea Technology Conference & Exhibition. Kuala Lumpur, Malaysia.

**Lin**, H.Z., & Khalessi, M.R. (2006). General Outlook of UNIPASS™ V5.0: A General-Purpose Probabilistic Software System. *Structural Safety*, 28(1-2), 196-216.

**Liu**, P.L., & Kiureghian, D.A. (1990). Optimization Algorithms for Structural Reliability. *Structural Safety*, 9(3), 161-177.

**Liu**, P.L., Lin, H.Z., & Kiureghian, A.D. (1989). *CalREL User Manual*. Report No. UCB/SEMM-89/18, Structural Engineering, Mechanics and Materials, Department of Civil Engineering, University of California, Berkeley, USA.

**Lotsberg**, I., Fines, S., & Foss, G. (1984). Reliability of Calculated Fatigue Lives of Offshore Structures. *Fatigue 84, Proceedings of the 2nd International Conference on Fatigue and Fatigue Thresholds*, Birmingham, UK.

**Low**, Y.M., & Langley, R.S. (2006a). Time and Frequency Domain Coupled Analysis of Deepwater Floating Production Systems. *Ocean Engineering*, 28, 371-385.

**Low**, Y.M., & Langley, R.S. (2006b). Dynamic Analysis of a Flexible Hanging Riser in the Time and Frequency Domain. *Proceedings of OMAE2006 25th International Conference on Offshore Mechanics and Arctic Engineering*, Hamburg, Germany.

**Luenberger**, D.G. (1986). *Introduction to Linear and Nonlinear Programming.* Reading (MA): Addison-Wesley.

**Luk**, C.H., and Wang, T.J. (2007). ECA Methodology for Fatigue Design of Risers and Flowlines. *Proceedings of the 26th International Conference on Offshore Mechanics and Arctic Engineering OMAE2007*, San Diego, USA.

**Macdonald**, K.A., & Maddox, S.J. (2003). New Guidance for Fatigue Design of Pipeline Girth Welds. *Engineering Failure Analysis*, 10, 177-197.

**Madhavan**, P.T.M., & Veena, G. (2006). Fatigue Reliability Analysis of Fixed Offshore Structures: A First Passage Problem Approach. Journal of Zhejiang University SCIENCE A, 7(11), 1839-1845.

**Madsen**, H.O. (1983). Probabilistic and Deterministic Models for Predicting Damage Accumulation due to Time Varying Loading. DIALOG 5-82, Danish Engineering Academy, Lyngby, Denmark.

**Madsen**, H.O., Krenk, S., & Lind, N.C. (1986). *Methods of Structural Safety.* Prentice Hall Inc., Englewood Cliffs, New Jersey, USA.

**Madsen**, P.H., Frandsen, S., Holley, W.E., & Hansen, J.C. (1983). *Dynamic Analysis of Wind Turbine Rotors for Lifetime Prediction.* RISO contract report 102-43-51.

**Mansour**, G. (2004). The Impact of the Second Order Vessel Motion on the Fatigue Life of Steel Catenary Risers. *Proceedings of OMAE04 23rd International Conference on Offshore Mechanics and Arctic Engineering*, Vancouver, Canada.

**Mansour**, G. (2007). *Deepwater Riser Design, Fatigue Life and Standards Study Report.* Minerals Management Service (MMS) TA&R Project Number 572, Document No. 86330-20-R-RP-005.

**Mazzoni**, S., McKenna, F., Scott, M.H., & Fenves, G.L. (2006). *Open System for Earthquake Engineering Simulation User Command – Language Manual.* Retrieved August 19, 2008, from Pacific Earthquake Engineering Research Centre, University of California, Berkeley web site http://opensees.berkeley.edu/OpenSees/manuals/usermanual/index.html.

**McNamara**, J.F., O' Brien, P.J., & Gilroy, S.G. (1988). Non-Linear Analysis of Flexible Risers Using Hybrid Finite Elements. *Journal of Offshore Mechanics and Arctic Engineering*, 110 (3), 197–204.

**Mekha**, B.B. (2001). New Frontiers in the Design of Steel Catenary Risers for Floating Production Systems. *Journal of Offshore Mechanics and Arctic Engineering*, 123, 153-158.

**Mekha**, B.B. (2002). On the Wave and VIV Fatigue of Steel Catenary Risers Connected to Floating Structures. *Proceedings of OMAE'02 21st International Conference on Offshore Mechanics and Arctic Engineering*, Oslo, Norway.

**Mekha**, B.B., & Heijermans, B. (2003). The Prince TLP Steel Catenary Risers: Design and Fatigue Challenges. *Proceedings of OMAE 2003 22nd International Conference on Offshore Mechanics and Arctic Engineering*, Cancun, Mexico.

**Mekha**, B.B., Johnson, C.P., & Roesset, J.M. (1996). Implications of Tendon Modelling on Nonlinear Response of TLP. *Journal of Structural Engineering*, 122 (2), 142-149.

**Mekha**, B.B., Mirza, S., & Lang, P. (2000). An Assessment of Fatigue Damage for A Deepwater Steel Catenary Riser. *Proceedings of ETCE/OMAE2000 Joint Conference Energy for the New Millenium*, New Orleans, USA.

**Miner**, M.A. (1945). Cumulative Damage in Fatigue. *Journal of Applied Mechanics*, 12, 159-164.

**Mitsunaga**, K., & Endo, T. (1968). Fatigue of Metals Subjected to Varying Stress. Presented to the Japan Society of Mechanical Engineers, Fukuoka, Japan.

**Moan**, T., & Berge, S. (1997). Fatigue and Fracture, Committee III.2, *Proceedings of the 13th International Ship and Offshore Structures Congress*, Norwegian University of Science and Technology, Trondheim, Norway, 292-294.

**Moan**, T., Uraga, E.A., & Wang, X. (2004). Reliability-Based Service Life Assessment of FPSO Structures. ABS Technical Papers.

**Moe**, G., & Arntsen, Ø. (2001). An Analytic Model for Static Analysis of Catenary Risers. *Proceedings of the Eleventh (2001) International Offshore and Polar Engineering Conference*, Stavanger, Norway.

**Morais**, M.C.D., & Jacob, B.P. (2002). Application of a Modified Truss Element to the Analysis of Flexible Riser. *Proceedings of OMAE'02 21st International Conference on Offshore Mechanics and Arctic Engineering*, Oslo, Norway.

**Mungall**, C. et al. (2004). Semisubmersible Based Dry Tree Platform with Compliant Vertical Access Risers. Paper presented at the Offshore Technology Conference, Houston, USA.

**Munse**, W.H., Wilbur, T.W., Tellalian, M.L., Nicoll, K., & Wilson, K. (1983). *Fatigue Characterization of Fabricated Ship Details for Design*. SSC Report 318, Ship Structure Committee, Washington, D.C., USA.

**NACE** MR0175/ISO 15156-2 (2003). *Petroleum and Natural Gas Industries – Materials for Use in H2S-containing Environments in Oil and Gas Production.* NACE International.

**NACE** SP0169-2007 (2007). Control of External Corrosion on Underground or Submerged Metallic Piping Systems. NACE International.

**Nakhaee**, A., and Zhang, J. (2007). Dynamic Interaction between SCR and the Seabed. *Proceedings of the 26th International Conference on Offshore Mechanics and Arctic Engineering OMAE2007*, San Diego, USA.

**Nazir**, M., Khan, F., & Amyotte, P. (2008). Fatigue Reliability Analysis of Deep Water Rigid Marine Risers Associated with Morison-Type Wave Loading. *Stoch Environ Res Risk Assess*, 22, 379-390.

**Netto**, T.A., Lourenço, M.I., & Botto, A. (2007). Fatigue Life Assessment of Reeled Risers. Paper presented at the Offshore Technology Conference, Houston, USA.

**Netto**, T.A., Lourenço, M.I., & Botto, A. (2008). Fatigue Performance of Pre-strained Pipes with Girth Weld Defects: Full-Scale Experiments and Analyses. *International Journal of Fatigue*, 30(5), 767-778.

**Newman**, J.C., & Raju, J.S. (1981). An Empirical Stress-Intensity Factor Equation for the Surface Crack. *Engineering Fracture Mechanics*, 15(1-2), 185-192.

**Niemi**, E. (1995). Stress Determination for Fatigue Analysis of Welded Components. Abington Publishing, Cambridge.

**Nolop**, N.C., Wang, H.H., Kan, W.C., Sutherland, J.B., Elholm, E.S., Hoyt, D.S., Montbarbon, S., & Quintin, H. (2007). Erha and Erha North Development: Steel Catenary Risers and Offloading System. Paper presented at the Offshore Technology Conference, Houston, USA.

**Norsok** Standard N-001 (2004). *Structural Design* (4th rev.). Norway.

**Norsok** Standard N-003 (2007). *Actions and Action Effect* (2nd ed.). Norway.
Ong, P.P.A., & Pellegrino, S. (2003). Modelling of Seabed Interaction in Frequency Domain Analysis of Mooring Cables. *Proceedings of OMAE 2003 22nd International Conference on Offshore Mechanics and Arctic Engineering*, Cancun, Mexico.

**O'Brien**, M.D., & Morison, J.R. (1952). *The Forces Exerted by Waves on Objects*. Transactions of the American Geophysical Union, 33(1).

**Palmgren**, A.Z. (1924). Die Lebendauer von Kugellagern. *Zeichscrift des Verein Deutscher Ingenieure*, 68, 339–341.

**Paris**, P., Gomez, M., & Anderson, W. (1961). A Rational Analytic Theory of Fatigue. *The trend in Engineering*, 13, 9-14.

**Paris**, P., & Erdogan, F. (1963). A Critical Analysis of Crack Propagation Laws. *Journal of Basic Engineering*, Transactions of the American Society of Mechanical Engineers, 528-534.

**Pasqualino**, I.P., Valeriano, I.A., & Alves, T.M.J. (2002). Crack Growth Prediction in Girth Welds of Steel Catenary Risers. *Proceedings of the Twelfth (2002) International Offshore and Polar Engineering Conference*, Kitakyushu, Japan.

**Passano**, E., & Laesen, C.M. (2006). Efficient Analysis of a Catenary Riser. *Proceedings of OMAE2006 25th International Conference on Offshore Mechanics and Arctic Engineering*, Hamburg, Germany.

**Passano**, E., & Laesen, C.M. (2007). Estimating Distributions for Extreme Response of A Catenary Riser. *Proceedings of the 26th International Conference on Offshore Mechanics and Arctic Engineering OMAE2007*, San Diego, USA.

**Patel**, S.K., Kumar, D., Master, B., & Karunakaran, D. (2001). Design of Steel Catenary Riser for Deepwater Fields in Indian Offshore – A Case Study. *Proceedings of OMAE 2001 20th International Conference on Offshore Mechanics and Arctic Engineering*, Rio de Janeiro, Brazil.

**Patel**, H.M., Seyed, F.B. (1995). Review of Flexible Risers Modelling and Analysis Techniques. *Engineering Structures*, 17, 293-304.

**Pellissetti**, M.F., & Schuëller, G.I. (2006). On General Purpose Software in Structural Reliability – An Overview. *Structural Safety*, 28(1-2), 3-16.

**Pesce**, C.P. et al. (2003a). Riser Technology and Industry – University Cooperation. Part I – Riser Mechanics. *Proceedings of OMAE 2003 22nd International Conference on Offshore Mechanics and Arctic Engineering*, Cancun, Mexico.

**Pesce**, C.P. et al. (2003b). Riser Technology and Industry – University Cooperation. Part II – Risers Loading: VIV, Heading and Dynamic Positioning. *Proceedings of OMAE 2003 22nd International Conference on Offshore Mechanics and Arctic Engineering*, Cancun, Mexico.

**Pesce**, C.P., & Martins, C.A. (2004). Riser-Soil Interaction: Local Dynamics at TDP and A Discussion on the Eigenvalue Problem. *Proceedings of OMAE04 23rd International Conference on Offshore Mechanics and Arctic Engineering*, Vancouver, Canada.

**Petruska**, D.J., Zimmermann, C.A., Krafft, K.M., Thurmond, B.F., & Duggal, A. (2002). Riser System Selection and Design for a Deepwater FSO in the Gulf of Mexico. Paper presented at the Offshore Technology Conference, Houston, USA.

**Phifer**, E.H., Kopp, F., Swanson, R.C., Allen, D.W., & Langner, C.G. (1994). Design and Installation of Auger Steel Catenary Risers. *Proceedings of Offshore Technology Conference 1994*, Houston, USA.

**Pierson**, W.J., & Moskowitz, L. (1964). A proposed spectral form for full-developed wind sea based on the similarity law of S. A. Kitaigorodoskii. *Journal of Geophysical Research*, 69, 5191–5203.

**Pollack**, J., Davies, K.B., & Riggs, D.C. (2003). A Feasibility Study for Steel Catenary Risers Connected to a Spread-Moored FPU Monohull in A Field Offshore Brazil. *Proceedings of OMAE03 22nd International Conference on Offshore Mechanics and Arctic Engineering*, Cancun, Mexico.

**Power**, E.M. (1978). *Cycle Counting Methods and the Development of Block Load Fatigue Programs*. SAE 780102.

**Quintin**, H., Legras, J.L., Huang, K., & Wu, M. (2007). Steel Catenary Riser Challenges and Solutions for Deepwater Applications. Paper presented at the Offshore Technology Conference, Houston, USA.

**Rackwitz**, R., & Fiessler, B. (1978). Structural Reliability under Combined Random Load Sequences. *Computers and Structures*, 9, 489-494.

**Reh**, S., Beley, J.D., Mukherjee, S., & Khor, E.H. (2006). Probabilistic Finite Element Analysis Using ANSYS. *Structural Safety*, 28(1-2), 17-43.

**Riha**, D.S., Thacker, B.H., Millwater, H.R., Wu, Y.T., & Enright, M.P. (2000). Probabilistic Engineering Analysis Using the NESSUS Software. Southwest Research Institute, San Antonio, USA. Retrieved August 19, 2008, from http://www.nessus.swri.org/publications/2000%20AIAA%20SDM41%20Paper.pdf.

**Rubinstein**, R.Y. (1981). *Simulation of the Monte Carlo Method*. John Wiley & Sons Inc., New York, USA.

**Rustad**, A.M., Larsen, C.M., & Sørensen, A.J. (2007). FEM Modelling and Automatic Control for Collision Prevention of Top Tensioned Risers. *Marine Structures*, 20, ISSN 0951-8339.

**Rychlik**, I. (1987). A New Definition of the Rainflow Cycle Counting Method. International Journal of Fatigue, 9(2), 119-121.

**Rychlik**, I. (1993). Characterisation of Random Fatigue Loads. *Stochastic Approach to Fatigue, CISM Course and Lectures n. 334*, Springer, Wienn.

**Sánchez**, H.A.S., & Salas, C.C. (2005). Riser Stability under External Pressure and Axial Compression Observing Geometrical Imperfections. *Proceedings of OMAE2005 24th International Conference on Offshore Mechanics and Arctic Engineering*, Halkidiki, Greece.

**Schittkowski**, K. (1985). NLPQL: A FORTRAN Subroutine Solving Constrained Nonlinear Programming Problems. *Annals of Operations Research*, 5, 485-500.

**Schowalter**, D., Menon, R., & Allen, D. (2007). Accurately Model Deepwater Risers. *E&P Magazine*, 80(4), 77-80.

**Schuëller**, G.I., & Pradlwarter, H.J. (2005). Computational Stochastic Structural Analysis (COSSAN) – A Software Tool. *Proceedings of the 9th International Conference on Structural Safety and Reliability (ICOSSAR'05)*, Rome, Italy.

**Sele**, A., Dretvik, S., Nygård, M., & Støme, S. (2001). Installing Steel Catenary Risers for Production Vessels in Modest Water Depths. *Proceedings of OMAE 2001 20th International Conference on Offshore Mechanics and Arctic Engineering*, Rio de Janeiro, Brazil.

**Sen**, T.K. (2006). Probability of Fatigue Failure in Steel Catenary Risers in Deep Water. *Journal of Engineering Mechanics*, 132, 1001-1006.

**Sen**, T.K., & Hesar, M. (2007). Riser Soil Interaction in Soft Clay near the Touchdown Zone. Paper presented at the Offshore Technology Conference, Houston, USA.

**Senra**, S.F., Jacob, B.P., Torres, A.L.F.L., & Mourelle, M.M. (2002). Sensitivity Studies on the Fatigue Behavior of Steel Catenary Riser. *Proceedings of the Twelfth (2002) International Offshore and Polar Engineering Conference*, Kitakyushu, Japan.

**Sertã**, O.B., Mourelle, M.M., Grealish, F.W., Harbert, S.J., & Souza, L.F.A. (1996). Steel Catenary Riser for the Marlim Field FPS P-XVIII. Paper presented at the Offshore Technology Conference, Houston, USA.

**Shabakhty**, N., Gelder, P.V., & Boonstra, H. (2002). Reliability Analysis of Jack-Up Platforms Based on Fatigue Degradation. *Proceedings of OMAE'02 21st International Conference on Offshore Mechanics and Arctic Engineering*, Oslo, Norway.

**Sharks**, J., & Fang, J. (2000). Field, Platform Specifics for the Design of Steel Catenary Risers – Fatigue Prediction for Deepwater Applications. *Proceedings of Offshore Technology Conference 2000*, Houston, USA.

**Sheehan**, J.M., Grealish, F.W., Smith, R.J., & Harte, A.M. (2005). Characterisation of the Wave Environment in the Fatigue Analysis of Flexible Risers. *Proceedings of OMAE2005 24th International Conference on Offshore Mechanics and Arctic Engineering*, Halkidiki, Greece.

**Siddiqui**, N.A., & Ahmad, S. (2001). Fatigue and Fracture Reliability of TLP Tethers under Random Loading. *Marine Structures*, 14, 331-352.

**Silveira**, L.M.Y.D., & Martins, C.D.A. (2004). A Numerical Method to Solve the Static Problem of a Catenary Riser. *Proceedings of OMAE04 23rd International Conference on Offshore Mechanics and Arctic Engineering*, Vancouver, Canada.

**Simos**, A.N., Fujarra, A.L.C., & Alves, K.H. (2003). Dynamic Compression of Rigid and Flexible Risers. Part II: Comparison of Theoretical and Experimental Results.

*Proceedings of OMAE03 22nd International Conference on Offshore Mechanics and Arctic Engineering*, Cancun, Mexico.

**Siqueira**, M.Q.D., Sousa, J.R.M.D., & Mourelle, M.M. (2003). Analysis of the Dynamic Behaviour of Flexible Risers Considering *Hysteretic Damping. Proceedings of OMAE03 22nd International Conference on Offshore Mechanics and Arctic Engineering*, Cancun, Mexico.

**Slatcher**, S. (1987). The Probability of Failure due to Fatigue Crack Growth from a Weld Toe. *Proceedings of the International Conference on Fatigue and Welded Constructions*, The Welding Institute, Brighton, UK.

**Song**, R., Mekha, B., & Sebastian, A. (2006). Independent Design Verification of SCRs for Ultra Deepwater IHF Development. *Proceedings of OMAE2006 25th International Conference on Offshore Mechanics and Arctic Engineering*, Hamburg, Germany.

**Song**, R., & Stanton, P. (2007a). Advances in Deepwater Steel Catenary Riser Technology State-of-the-Art: Part I – Design. *Proceedings of 26th International Conference on Offshore Mechanics and Arctic Engineering OMAE2007*, San Diego, USA.

**Song**, R., and Stanton, P. (2007). Advance in Deepwater Steel Catenary Riser Technology State-of-Art: Part I – Design. *Proceedings of the 26th International Conference on Offshore Mechanics and Arctic Engineering OMAE2007*, San Diego, USA.

**Song**, R., & Stanton, P. (2007b). Deepwater Tie-Back SCR: Unique Design Challenges and Solutions. *Proceedings of Offshore Technology Conference 2007*, Houston, USA.

**Stahl**, B., & Banon, H. (2002). Fatigue Safety Factors for Deepwater Risers. *Proceedings of OMAE'02 21st International Conference on Offshore Mechanics and Arctic Engineering*, Oslo, Norway.

**Tahar**, A., & Kim, M.H. (2003). Hull/Mooring/Riser Coupled Dynamic Analysis and Sensitivity Study of a Tanker-Based FPSO. *Applied Ocean Research*, 25, 367-382.

**Tanaka**, K., & Matsuoka, S. (1977). A Tentative Explanation for Two Parameters, C and m, in Paris Equation of Fatigue Crack Growth. *International Journal of Fatigue*, 13, 563-583.

**Tanaka**, R.L., & Martins, C.D.A. (2006). A Genetic Algorithm Approach to Steel Riser Optimization. *Proceedings of OMAE2006 25th International Conference on Offshore Mechanics and Arctic Engineering*, Hamburg, Germany.

**Tapan**, K.S. (2006). Probability of Fatigue Failure in Steel Catenary Risers in Deep Water. *Journal of Engineering Mechanics*, ASCE, 132(9), 1001-1006.

**Thethi**, R. (2001). Soil Interaciton Effects on Simple Catenary Riser Response. Paper presented at Deepwater Pipelines & Riser Technology Conference, Houston, USA.

**Thompson**, H.M., Grealish, F.W., Young, R.D., & Wang, H.K. (2002). Typhoon Steel Catenary Risers: As-Built Design and Verification. Paper presented at the Offshore Technology Conference, Houston, USA.

**Torres**, A.L.F.L., Mourelle, M.M., & Silva, R.M.C.D. (2001). Fatigue Damage Verification of Steel Catenary Risers. *Proceedings of OMAE'01 20th International Conference on Offshore Mechanics and Arctic Engineering,* Rio de Janeiro, Brazil.

**Torres**, A.L.F.L., Sagrilo, L.V.S., Siqueira, M.Q., & Lima, E.C.P (1995). A Procedure for Random Fatigue Analysis of Offshore Structures. *Proceedings of the 9th International Symposium on Offshore Engineering, Brazil Offshore 95*, Rio de Janeiro.

**Torres**, A.L.F.L. et al. (2002). Lazy-Wave Steel Rigid Risers for Turret-Moored FPSO. *Proceedings of OMAE'02 21st International Conference on Offshore Mechanics and Arctic Engineering*, Oslo, Norway.

**Torres**, A.L.F.L. et al. (2003). Lazy-Wave Steel Rigid Risers for FPS with Spread Mooring Anchoring System. *Proceedings of OMAE03 22nd International Conference on Offshore Mechanics and Arctic Engineering*, Cancun, Mexico.

**Torselletti**, E., Vitali, L., & Bruschi, R. (2005). Design Criteria vs. Line Pipe Requirements for Offshore Pipelines. Retrieved September 24, 2008, from http://www.msm.cam.ac.uk/phase-trans/2005/LINK/192.pdf.

**Torsethaugen**, K. (1993). A Two Peak Wave Spectral Model. *Proceedings of the 12th International Conference on Offshore Mechanics and Arctic Engineering OMAE'93*, Glasgow, UK.

**Torsethaugen**, K. (1994). Model for a Doubly Peaked Spectrum. Lifetime and Fatigue Strength Estimation Implications. Paper presented at International Workshop on Floating Structures in Coastal Zone, Hiroshima.

**Torsethaugen**, K. (1996). Model for a Doubly Peaked Wave Spectrum. SINTEF report STF22 A96204.

**Torsethaugen**, K. (2004). Simplified Double Peak Spectral Model for Ocean Waves. Retrieved November 6, 2008, from http://www.sintef.no/upload/Fiskeri_og_havbruk/Havbruksteknologi/2004-JSC-193.pdf.

**Tovo**, R. (2002). Cycle Distribution and Fatigue Damage under Broad-Band Random Loading. *International Journal of Fatigue*, 24, 1137-1147.

**Tvedt**, L. (1983). Two Second-Order Approximations to the Failure Probability. *Veritas Report RDIV/20-004-83*, Det Norske Veritas, Oslo, Norway.

**Tvedt**, L. (1990). Distribution of Quadratic Forms in Normal Space: Application to Structural Reliability. *Engineering Mechanics*, ASCE, 116(6), 1183-1197.

**Tvedt**, L. (2006). Proban – Probabilistic Analysis. *Structural Safety*, 28(1-2), 150-163.

**Vandenbossche**, M. et al. (2007). Fatigue Design of Atlantis Export SCRs. *Proceedings of 26th International Conference on Offshore Mechanics and Arctic Engineering OMAE2007*, San Diego, USA.

**Vandiver**, J.K., & Li, L. (1999). *Shear 7 for Vortex Induced Vibration Response Prediction of Beams or Cables with Slowly Varying Tension in Sheared or Uniform Flow* (Version 3). User's Guide, Atlantia Corporation.

**Vieira**, L.T., Jacob, B.P., Fernandes, A.C., & Franciss, R. (2002). Studies on VIV Fatigue Behavior in SCRs of Hybrid Riser Systems. *Proceedings of OMAE'02 21st International Conference on Offshore Mechanics and Arctic Engineering*, Oslo, Norway.

**Wang**, L., Hansen, V., & Katla, E. (2005). Independent Verification of Deepwater SCR Designs. Paper presented at the Offshore Technology Conference, Houston, USA.

**Ward**, E.G., Haring, R.E., & Devlin, P.V. (1999). Deepwater Mooring and Riser Analysis for Depths to 10,000 Feet. *Proceedings of Offshore Technology Conference 1999*, Houston, USA.

**Watson**, P., & Dabell, B.J. (1975). Cycle Counting and Fatigue Damage. Symposium on Statistical Aspects of Fatigue Testing, Warwick University.

**Wessel**, H.J. (1986). *Fracture Mechanics Analysis of Crack Growth in Plate Girders* (Dissertation). Trondheim: Division of Marine Structures, The University of Trondheim, The Norwegian Institute of Technology.

**Wichers**, J.E.W., & Devlin, P.V. (2001). Effect of Coupling of Mooring Lines and Risers on the Design Values for a Turret Moored FPSO in Deep Water of the Gulf of Mexico. *Proceedings of the Eleventh (2001) International Offshore and Polar Engineering Conference*, Stavanger, Norway.

**Willis**, N. (2000). Steel Catenary Risers in Deepwater Environments. Paper presented at Offshore Pipeline Technology (OPT) Conference, Oslo.

**Willis**, N. (2001). Steel Catenary Risers – Allegheny Offshore VIV Monitoring Campaign and Large Scale Simulation of Seabed Interaction. Retrieved September 25, 2008, from http://www.2hoffshore.com/technical_library/papers/2001/pap053.pdf.

**Willis**, N. (2002). Steel Catenary Risers – Results and Conclusions from Large Scale Simulations of Seabed Interaction. Retrieved September 25, 2008, from http://www.2hoffshore.com/technical_library/papers/2002/Paper64.pdf.

**Willis**, N.R.T., & West, P.T.J. (2001). Interaction between Deepwater Catenary Risers and a Soft Seabed: Large Scale Sea Trials. Paper presented at the Offshore Technology Conference, Houston, USA.

**Wirsching**, P.H. (1984). Fatigue Reliability for Offshore Structures. *Journal of the Structural Division* (ASCE). 110(10), 2340-2356.

**Wirsching**, P.H., & Chen, Y.N. (1988). Considerations of Probability-Based Fatigue Design for Marine Structures. *Marine Structures*, 1, 23-45.

**Wirsching**, P.H., & Light C.L. (1980). Fatigue under Wide Band Random Stresses. *Journal of the Structural Division* (ASCE). 106(7), 1593-1607.

**Wirsching**, P.H., Paez, T.L., & Ortiz, K. (1995). *Random Vibrations: Theory and Practice*. A Wiley-Interscience Publication, John Wiley & Sons, Inc.

**Wöhler**, A. (1871). Tests to Determine the Forces Acting on Railway Carriage Axles and the Capacity of Resistance of the Axles. *Engineering*, 11.

**Wu**, Y.T., Shin, Y., Sues, R.H., & Cesare, M.A. (2006). Probabilistic Function Evaluation System (ProFES) for Reliability-Based Design. *Structural Safety*, 28(1-2), 164-195.

**Xu**, J., Jesudasen, A.S., Fang, J., & Else, M. (2006). Wave Loading Fatigue Performance of Steel Catenary Risers (SCRs) in Ultra-Deepwater Applications. Paper presented at the Offshore Technology Conference, Houston, USA.

**Yao**, X., & Sun, L. (2006). Fatigue Mitigation Design of Deepwater Steel Catenary Risers. *Proceedings of OMAE2006 25th International Conference on Offshore Mechanics and Arctic Engineering*, Hamburg, Germany.

**Ye**, W., Shanks, J., & Fang, J. (2003). Effects of Fully Coupled and Quasi-Static Semi-Submersible Vessel Motions on Steel Catenary Riser's Wave Loading Fatigue. Paper presented at the Offshore Technology Conference, Houston, USA.

**Zhao**, W., Stacey, A., & Prakash, P. (2002). Probabilistic Models of Uncertainties in Fatigue and Fracture Reliability Analysis. *Proceedings of OMAE'02 21st International Conference on Offshore Mechanics and Arctic Engineering*, Oslo, Norway.

**Zimmermann**, C.A., Petruska, D., & Duggal, A.S. (2002). Effective Riser Solutions for a Deepwater FPSO. *Proceedings of 26th International Conference on Offshore Mechanics and Arctic Engineering OMAE2007,* San Diego, USA.

*Appendix A*

# Riser Design Codes

## A.1 API RP 2RD

The design of a deepwater riser system is a challenge since no shallow water concept or experience can be transferred for deepwater application. To address this need, the American Petroleum Institute (API) formed a task group in 1992. In June 1998, the first deepwater riser design code – "Design of Risers for Floating Production Systems (FPSs) and Tension Leg Platforms (TLPs)" was issued officially as API RP 2RD. It has been widely used for deepwater riser system design since then.

API RP 2RD addresses structural analysis procedure, design guidelines, component selection criteria, and typical design for new riser systems used on FPSs.

This standard applies traditional WSD format where structural safety is taken into account by using a single safety factor.

## A.2 New Revision of API RP 2RD

Since the release of API RP 2RD in 1998, tremendous efforts have been spent on deepwater riser engineering, and the focus on deepwater exploration and production also has increased significantly worldwide.

The existing Working Stress Design (WSD) based API RP 2RD applies a single safety factor. In general, the more uncertainty about an event, the larger the safety factor should be. This is general true for WSD based design. Compared to Limit State Design (LSD), WSD in most cases is more conservative. Another limitation of WSD based design compared to Load and Resistance Factor Design (LRFD) approach is that a single safety factor often leads to a varying safety level strongly dependent on the load conditions.

Limit state design philosophy has been successfully applied to offshore pipelines and other marine structures for many years. The obvious advantages of adopting such design philosophy include less conservative, consistent safety level, and const savings.

Considering the different types of floating production concepts and the dynamic feature of the deepwater riser systems, the new revision of API RP 2RD has been renamed "Dynamic Risers for Floating Production Installations". The revised API RP 2RD is also being turned into an ISO standard.

The proposed new version uses a limit state based design and presents more materials than the existing one including loads, design criteria for riser pipe, connectors and riser components, materials, fabrication and installation, and riser integrity management. In addition to the main body, annexes provide including a typical design basis, worked examples, and analysis guidelines that should be more useful for the design of the riser system.

The revised API RP 2RD will serve as

- An industry standard, recommended practice and a reference;
- An ISO standard.

## A.3 DNV OS F201

In 2001, DNV released a new DNV Offshore Standard (OS) F201 for dynamic risers, which is the second riser design code based on a Joint Industry Program (JIP). Similar to DNV OS F101 pipeline design code, DNV OS F201 applies LSD in a LRFD format, which is based on reliability and risk concept to calibrate partial safety factors.

The basic design principles and functional requirements of DNV OS F201 are not in conflict with API RP 2RD.

The most pronounced difference compared to existing API RP 2RD is the adoption of reliability-based limit state design with explicit design checks against different failure models.

*Appendix B*

# Wave Spectrum Formulation

## B.1 JONSWAP

The equation that governs JONSWAP spectra is given below:

$$S_{\eta\eta}(\omega) = \alpha g^2 \omega^{-5} \exp\left(-\beta_w \left(\frac{\omega_p}{\omega}\right)^4\right) \cdot \gamma^{a_J} \tag{B.1.1}$$

where

$\omega$ – angular wave frequency $\rightarrow \omega = \dfrac{2\pi}{T_\omega}$

$T_\omega$ – wave period

$T_p$ – peak or significant wave period (period with maximum energy density)

$T_z$ – zero up-crossing wave period $\rightarrow \dfrac{T_p}{T_z} = 1.407\left(1 - 0.287 \ln \gamma\right)^{1/4}$

$\omega_p$ – angular spectral peak frequency → $\omega_p = \frac{2\pi}{T_p}$

$H_s$ – significant wave height which is approximately equal to the average of the highest one third of the waves)

$g$ – acceleration of gravity

$\alpha$ – generalised Philip's constant → $\alpha = 1.2905 \frac{H_s^2}{T_z^4}$

$\beta_w$ – spectral width parameter → $\beta_w = 1.25$ for North Sea conditions

$a_J$ – JONSWAP formulation parameter → $a_J = \exp\left(-\frac{1}{2}\left(\frac{\omega - \omega_p}{\sigma_w \cdot \omega_p}\right)^2\right)$

$\sigma_w$ – spectral width parameter

$\sigma_{wa}$ – left width parameter $\sigma_{wa} = 0.07$ for $\omega \leq \omega_p$

$\sigma_{wb}$ – right width parameter $\sigma_{wb} = 0.09$ for $\omega \geq \omega_p$

$\gamma$ – peakedness parameter

$$= 1.0 \qquad T_p \geq 5\sqrt{H_s}$$

$$= \exp\left(5.75 - 1.15 \frac{T_p}{\sqrt{H_s}}\right) \qquad 3.6\sqrt{H_s} \leq T_p < 5\sqrt{H_s}$$

$$= 5.0 \qquad T_p < 3.6\sqrt{H_s}$$

In the case of a 3 parameter JONSWAP spectrum the parameters need to be specified by users are $\gamma$, $H_s$ and $T_p$. JONSWAP 5 parameter wave spectra are also defined by the equation B.1.1. The only difference is that the values for $\sigma_{wa}$ and $\sigma_{wb}$ need to be defined by users.

## B.2 Pierson-Moskovitz Spectrum

Pierson-Moskovitz spectra are defined by the following equation:

$$S_{\eta\eta}(\omega) = A_{PM}\omega^{-5}\exp\left(-\frac{B_{PM}}{\omega^4}\right);\ 0<\omega<\infty \qquad \text{(B.2.1)}$$

where

$$A_{PM} = 0.081g^2$$

$$B_{PM} = \frac{3.11}{H_s^2}$$

The input to the model is significant wave height $H_s$.

## B.3 Bretschneider Spectrum

Bretschneider spectrum is also known as 2 parameter Pierson-Moskovitz spectrum and is defined by the same equation as equation B.2.1 except:

$$A_B = 124.2\frac{H_s^2}{T_z^4}$$

$$B_B = \frac{496}{T_z^4}$$

The input to the model is significant wave height $H_s$ and spectral peak period $T_p$.

## B.4 Torsethaugen Spectrum

Low frequency waves can propagate faster than the generating wind field and reach areas not influenced by this wind field or at least before the area is influenced directly by it. This swell component will add to the locally generated wind sea and create double (or multiple) peak spectra. The spectra for the various sea systems will usually correspond to different peak frequencies and different directions of propagation. Sea wave spectra can be rather complicated and be a result of several swell systems in addition to local generated waves. Some spectral models have been developed to give a realistic approach for double peak cases. Torsethaugen spectrum is one of such cases.

Torsethaugen spectrum is a double peak JONSWAP spectrum with 2 parameters which was developed based on measured spectra for Norwegian waters (Torsethaugen, 1993, 1994, 1996, and 2004). The input to the model is significant wave height, $H_s$, for total sea and spectral peak period, $T_p$, for the primary (highest) peak.

Torsethaugen wave spectra may only be used when all vessels employ coupled vessel/line motion.

*Appendix C*

# Applicable Materials of Protective Coatings

## C.1 Heavy Weight Coating

During the DEMO2000 project Ti-Rise the Vikoweight coating from Trelleborg Viking was qualified for offshore use through an extensive testing program (Horn et al., 2002). Vikoweight is a rubber based weight coating where the density is equal to 3000 kg/m$^3$.

Qualification tests for the heavy weight coating were presented by Karunakaran, Meling, Kristoffersen, and Lund (2005).

## C.2 Light Weight Coating

There are different methods to achieve low density coating and usually a multi-layer technology is applied to fulfil the various functional requirements in a most optimal way. The project readiness of the various materials for deepwater application including the proven five-layer syntactic PP coating, which is qualified by SocoRIL

and used in several recent projects such as Roncador project at 2000 m water depth and the Bonga project at 1200 m water depth. Pipe dimensions installed range from 8'' – 12'' with coating thickness ranging from 34 mm – 102 mm. The coating density for Bonga was 680 kg/m$^3$.

The five layers of this coating system shown in Figure C.2.1 are as follows:

- 1$^{st}$ Layer: Fusion Bond Epoxy
- 2$^{nd}$ Layer: PP adhesive
- 3$^{rd}$ Layer: Solid PP
- 4$^{th}$ Layer: Syntactic PP
- 5$^{th}$ Layer: Solid PP

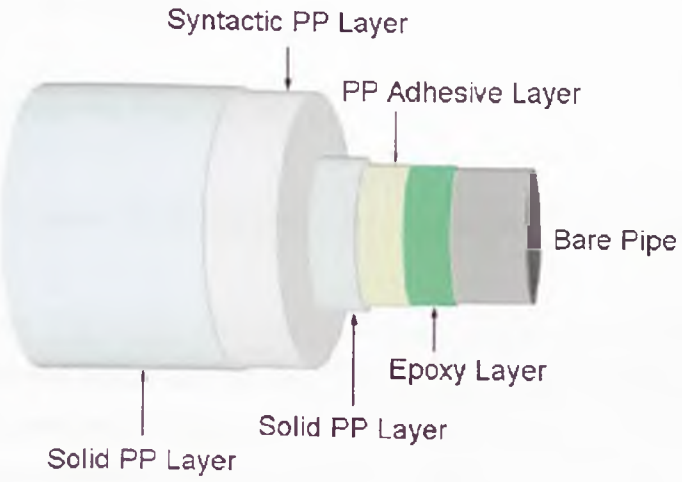


(a)

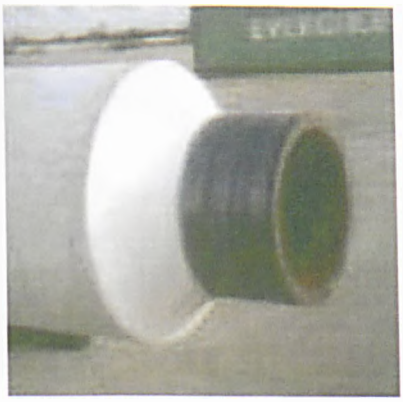

(b)

**Figure C.2.1** Syntactic PP Coating Structure: (a) Illustrative Model (Aggarwal et al., 2005); (b) Real Model (Karunakaran, Meling, Kristoffersen, and Lund, 2005)

The functions of the five layers are illustrated below:

- $1^{st} \sim 3^{rd}$ Layers: The first three layers in this design are for anti-corrosion.

- $4^{th}$ Layer: The fourth layer is for buoyancy and thermal insulation, and its conventional design is varied by introduction of higher percentage of hollow glass microspheres (Figure C.2.2) to obtain lower density, in addition to achieving required thermal insulation properties and hydrostatic pressure resistance.

- $5^{th}$ Layer: The function of the fifth layer is to provide protective coating (top coat), and its thickness at TDZ can be varied for applications in regions with potential for higher wear and abrasion.

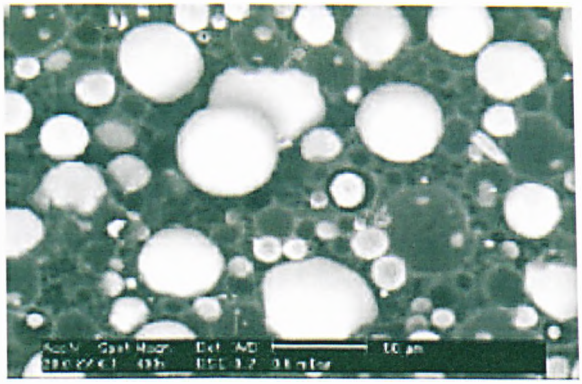

**Figure C.2.2** Hollow Glass Microsphere.

The syntactic PP coating is presently qualified for use in water depths greater than 2500 m targeting a service life of 20 to 25 years. More detailed information can be found in the work of Karunakaran, Meling, Kristoffersen, and Lund (2005) and JIP Report (2008).

*Appendix D*

# Palmgren-Miner's Rule

Many different cumulative damage theories have been proposed for the purposes of assessing fatigue damage caused by operation at any given stress level and the addition of damage increments to properly predict failure under conditions of spectrum loading. A linear damage rule, originally suggested by Palmgren (1924) and later developed by Miner (1945), which is still widely used, is referred to as the Palmgren-Miner's rule or the Miner's rule (Wirsching, Paez, and Ortiz, 1995), assuming that

- The variable load that takes place irregularly can be replaced using a sequence of blocks of uniform cycles (see Figure D.1 (a) and (b)).

- The number of stress cycles imposed on a component, expressed as a percentage of the total number of stress cycles of the same amplitude necessary to cause failure, gives the fraction of damage.

- The order in which the stress blocks of different amplitudes are imposed does not affect the fatigue life.

- Failure occurs when the linear sum of the damage from each load level reaches a critical value.

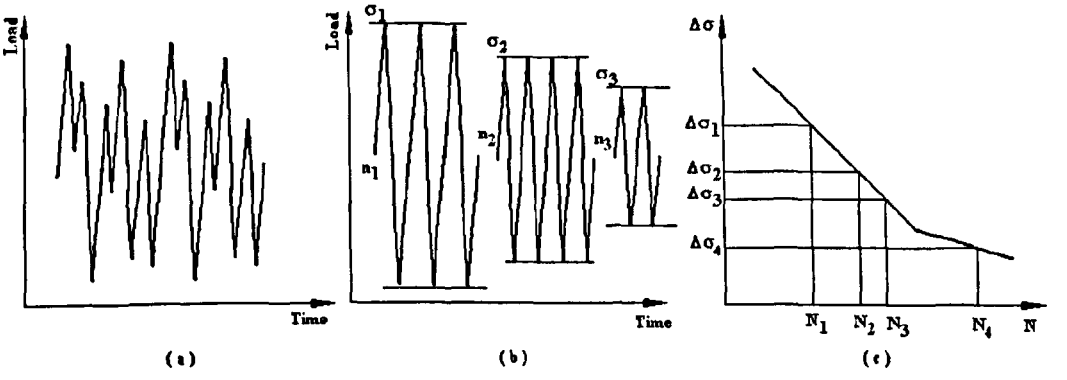


**Figure D.1** Scheme of Palmgren-Miner's Rule.

Fatigue damage (or damage ratio) can be written as

$$D = \sum_{i=1}^{k} \frac{n_i}{N_i} \leq \eta \tag{D.1}$$

where

| | |
|---|---|
| $n_i$ | number of constant amplitude range $S_i$ stress cycles in block $i$ |
| $N_i$ | number of cycles to failure at constant stress range $S_i$ |
| $k$ | number of stress blocks |
| $\eta$ | allowable fatigue damage ratio |

The fatigue damage ratio $D$ theoretically equals 1.0 at failure, however in practice, because of various uncertainties regarding loads, fabrication, operation, and other modelling errors, the value of $D$ is usually made less than one. The scheme of Palmgren-Miner's rule is shown in Figure D.1 (c).

*Appendix E*

# Rainflow Counting (RFC) Method

Cycles can be counted using time histories of the loading parameter of interest, such as force, torque, stress, strain, acceleration, or deflection. Cycle counting techniques can be used to reduce a complicated variable amplitude loading history into a number of discrete simple constant amplitude loading events, which are associated with fatigue damage. Various methods of cycle counting have been proposed to convert the irregular load histories to blocks of constant amplitude cycles. These counting methods can be subdivided into two groups:

- One-parameter cycle counting methods
  - Level crossing counting (LCC) (Gassner and Schültz, 1962)
  - Peak counting (PC) (Rychlik, 1993)
  - Range counting (RC) (Power, 1978)

- Two-parameter cycle counting methods
  - Rainflow counting (RFC)

The RFC method is currently the most preferred one.

Matsuishi and Endo (1968) originally developed the RFC method based on the analogy of raindrops falling on a pagoda roof and running down the edges of the roof. This method has proved to be the most accurate method for estimating fatigue damage under random processes by e.g. Dowling (1972) and Watson and Dabell (1975). The RFC method is briefly described in the following.

A stress time series of peaks and valleys is considered with the time axis vertically downward as shown in Figure E.1 and in this way the lines connecting peaks and valleys form a series of pagoda roofs. The RFC method applies the following general rules to produce stress cycles.

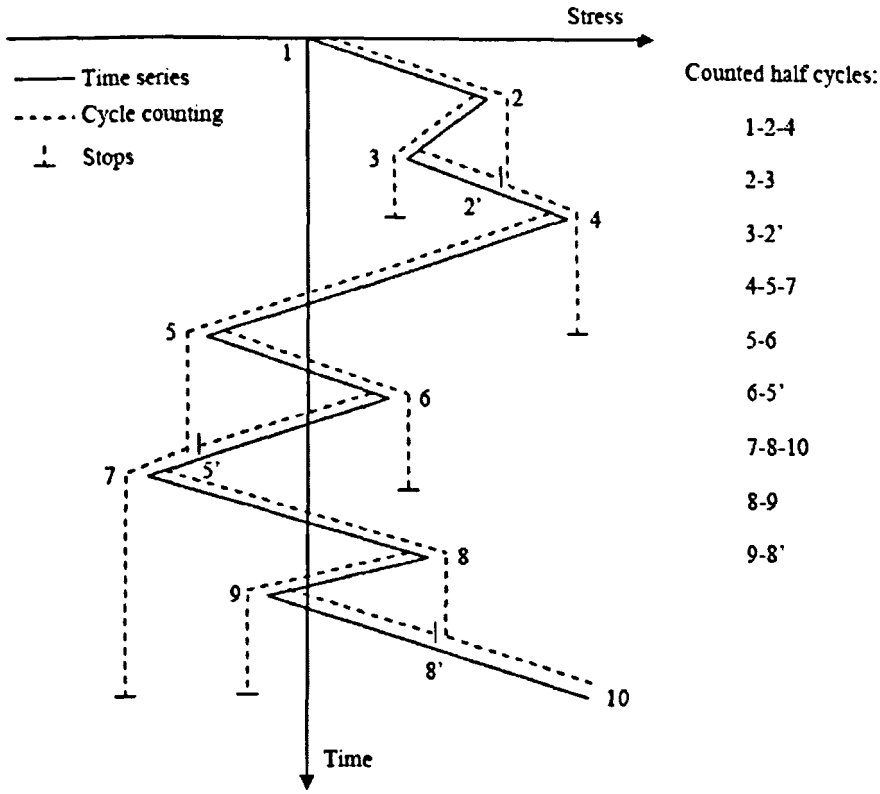


**Figure E.1** Illustration of the Rainflow Counting Method.

1. Each rainflow begins at the beginning of the time series and successively at the inside of every peak and valley.

2. Rainflow initiating at a peak (or a valley) drops down until it reaches opposite a peak more positive (or a valley more negative) than the peak (or the valley) it stated from.

3. Rainflow also stops when it meets the rainflow from a roof above.

4. Rainflow must terminate at the end of the time series.

5. The horizontal length of each rainflow is counted as a half cycle with that stress range.

As shown in Figure E.1, the first rainflow starts from the beginning at 1 as a valley, the second one from the peak 2, the third one from the valley 3, and so on. The end at 10 is considered as a peak herein. There are totally 9 half cycles can be extracted from this time series. When all of the 9 half cycles have been identified, the horizontal length of each cycle is used as an effective stress range to calculate the fatigue damage based on e.g. the linear damage accumulation law.

This is the original proposal of the RFC method (Matsuishi and Endo, 1968). Other versions of the method can be found such as the 3-point method (ASTM, 1985), the 4-point method (Amzallag, Gerey, Robert, and Bahuaud, 1994) and the non-recursive definition proposed by Rychlik (1987). All these methods lead to the same results of fatigue damage.

## E.1 RFC in Time Domain

When the response time history is irregular with time as shown in Figure E.1.1, RFC is used to decompose the irregular time history into equivalent stress of block loading. The number of cycles in each block is usually recorded in a stress range histogram. This can be used in Palmgren-Miner calculation to obtain the fatigue life.

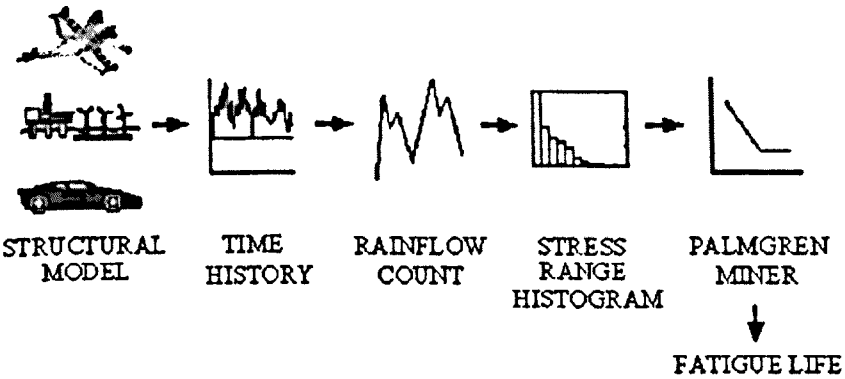


**Figure E.1.1** General Procedure for Time Domain Fatigue Life Calculation (Bishop and Sherratt, 2000).

## E.2 RFC in Frequency Domain

In frequency domain, firstly, time signal data is transferred into power spectral density values. Power spectral density versus frequency data is used to find the first four moments of the power spectral density functions and these four moments are used in finding the probability density function. Then, fatigue life is obtained as the steps of the process are also given in Figure E.2.1.

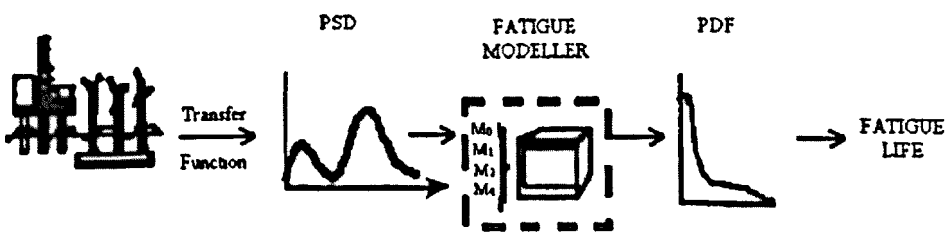


**Figure E.2.1** General Procedure for Frequency Domain Fatigue Life Calculation (Bishop and Sherratt, 2000).

*Appendix F*

# Reliability Analysis Method

CALREL incorporates several methods and algorithms for reliability analysis of structural components and systems, including the FORM, the SORM, MCS, importance sampling (IM), directional simulation (DS), and orthogonal plane sampling (OPS).

## F.1 First Order Reliability Method (FORM)

FORM is an approach for obtaining the failure probability by approximating the limit state function at the most probable failure point (Ditlevsen and Madsen, 1996). The most probable failure point, which is also called the design point, is defined in a standardised normal space that is also known as u-space. Generally speaking, the design point is located on the failure surface which is defined by the limit state function. In a u-space, a normally distributed probability density function (PDF) is rotationally symmetric and exponentially decaying. Therefore, the point on the limit state surface which has the shortest distance from the origin is the one with the highest probability of failure. This is the definition of the most probable failure point (MPP) and it can be found mathematically by iteration procedures.

For a limit state function $g(\mathbf{X})$, the design point is obtained by solving the constrained optimization problem. CALREL offers four alternative algorithms for solving this problem:

- The HL-RF method (Hasofer and Lind, 1974; Rackwitz and Fiessler, 1978);
- The modified HL-RF method (Liu and Kiureghian, 1990);
- The gradient projection method (Luenberger, 1986);
- The sequential quadratic programming method (Schittkowski, 1985).

Once the design point $u^*$ is specified in a u-space, the probability of failure is analytically estimated as in the equation 6.2.4 where the safety index $\beta$ represents the shortest distance to define the MPP. The mathematical expression of $\beta$ is shown in the following equation

$$\beta = \|u^*\| = \sqrt{u_1^{*2} + u_2^{*2} + \ldots u_n^{*2}} \tag{F.1.1}$$

The direct method to evaluate failure probability as in equation 6.2.4 is usually applied to the linear limit state function. In cases of nonlinear limit state function, Taylor expansion is generally applied at the design point. The first order based failure probability evaluation algorithm is usually called First Order Reliability Method, also referred to as FORM. Its expression is written as (Wu, 1994):

$$g(u) = a_0 + \sum_{i=1}^{n} a_i \left(u_i - u_i^*\right) \tag{F.1.2}$$

Due to its simplicity, FORM is widely used to obtain the failure probability. Unfortunately, the accuracy of FORM is highly dependent on the nonlinearity of the limit state function. A linear approximation of the failure surface at the design point will be accurate if the failure function is linear or weakly nonlinear. For heavily nonlinear failure function, the FORM methods may not be always adequate to find a reasonably correct failure probability. In such cases, a better approximation of the

failure surface at the design point is required. For this purpose, a second order (parabolic) failure surface is fitted to the nonlinear failure function at the design point (Tvedt, 1983; Fiessler, Neumann, and Rackwitz, 1979; Kiureghian, Lin, and Hwang, 1987), which is known as the Second Order Reliability Method (SORM).

## F.2 Second Order Reliability Method (SORM)

As shown from the terminology, Second Order Reliability Method (SORM) is to linearise the nonlinear limit state function with a second order Taylor expansion (Breitung, 1984). The failure surface of the system is obtained as a quadratic surface with the following form:

$$g(u) = a_0 + \sum_{i=1}^{n} a_i \left(u_i - u_i^*\right) + \sum_{i=1}^{n} b_i \left(u_i - u_i^*\right)^2 + \sum_{i=1}^{n} \sum_{j=1}^{i-1} c_{ij} \left(u_i - u_i^*\right)\left(u_j - u_j^*\right) \qquad \text{(F.2.1)}$$

CALREL incorporates two distinct methods for second order reliability analysis:

Point-Fitting Method

The limit state surface is approximated by a paraboloid surface with its principal curvatures fitted to the principal curvatures of the limit state surface at the design point. This approach is advantageous for reliability problems with large number of random variables, since calculations can be stopped when the magnitude of the last curvature found is sufficiently small. Once the principal curvatures are determined, the asymptotic formula by Breitung (1984) or the exact formula by Tvedt (1990) is used to compute the probability content of the fitted paraboloid as the SORM approximation of the failure probability for each component.

The curvature-fitting SORM approximating is applicable when the limit state function is twice differentiable and the second derivatives can be easily and accurately computed. When the limit state function involves numerical computations

that are subject to truncation or other errors (e.g., finite element computations), the resulting noise makes the computation of curvatures problematic. For such problems, CalREL has a point-fitting SORM approximation.

Curvature-Fitting Method

In this method the limit state function is approximated by a piecewise paraboloid surface, which is tangent to the limit state surface at the design point and coincides with the limit state surface at two points on each axis selected on both sides of the origin. The SORM approximation of the failure probability is again computed by the Breitung or Tvedt formulas. This approach is advantageous when the computation of curvatures is problematic, or when the problem has a large number of random variables.

In brief, it is a four step process for the solution of the failure probability by utilising FORM / SORM:

1. Formulation of the limit state equation $g(X)$.

2. The "transformation" requires that each random variable be associated with an uncorrelated, unit variance, normally distributed random variable. For independent variables this is achieved by equating the cumulative distribution functions of the input variable and its associated standard normal variate. The failure state function $g(X)$ is evaluated in normal u-space and gradient search methods are employed to find design point.

3. An "approximation" of the failure probability is obtained by fitting a tangent line (FORM) or a parabola (SORM) to the failure state function at the design point (see Figure F.2.1).

4. The direction cosines, $\alpha_i$, of the vector $\beta$, that define the design point are measures of the relative importance of each of the random variables. The symmetry of standard normal space simplifies the "computation" of the failure probabilities and the importance factors as the final step of the solution algorithm.

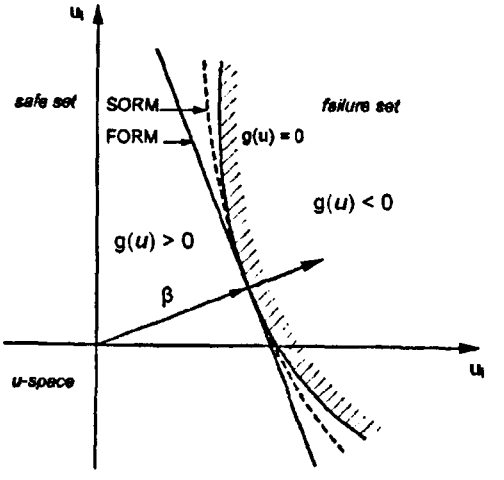


**Figure F.2.1** FORM and SORM Approximations to $g(u) < 0$.

## F.3 Monte Carlo Simulation (MCS)

Monte Carlo simulation (Rubinstein, 1981) uses statistics to mathematically model a real-life process and then estimate the likelihood of possible outcomes. MCS is an empirical method utilizing a large sample size to obtain the integral value through rejection scheme (see Figure F.3.1). With samples generated from the given random variable generators, it is an algorithm based on a recursive experiment to count the numbers of the samples falling into interested region. The failure probability obtained from MCS is calculated as:

$$p_f = \frac{N_f}{N_T} \tag{F.3.1}$$

where $N_T$ is the total sampling number and $N_f$ is the number of samples falling into failure region. This estimator of the failure probability, i.e. equation F.3.1, can also be written as

$$p_f = \frac{1}{N_T}\sum_{i=1}^{N} I_i \tag{F.3.2}$$

where $I_i$ is indication function where $I_i = 1$ when failure occurs ($g < 0$) and $I_i = 0$ for survival ($g > 0$).

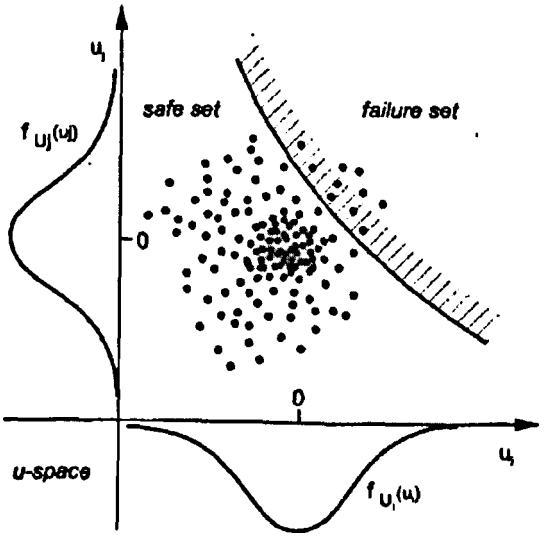


**Figure F.3.1** Visualisation of Results from Monte Carlo Simulations.

Probability of failure evaluated using Monte Carlo method is usually referred to as the exact value. $p_f$ is generally extremely small for most of the structural and mechanical structures. The number of needed simulations rapidly grows with decreasing probability. Thus, it requires a fairly huge number of samples to perform the simulation to achieve the satisfied accuracy. Subsequently, this increases the computation cost. In structural engineering, for a typical $\beta$ of 3-4, this may lead to

100,000 – 10,000,000 samples. Therefore, this method is not effective for small-probability problems.

The basic procedure of performing Monte Carlo Simulation is as follows:

1. Define the limit state function;

2. Randomly generate values for the random variables (using their probability distribution information);

3. Assign generated values to the limit state;

4. Repeat steps 1-4 until a sufficient number of simulations have been conducted;

5. Calculate probability of failure by equation F.3.2.

Figure F.3.2 gives the accuracy / speed ratio for some solution methods as mentioned above.

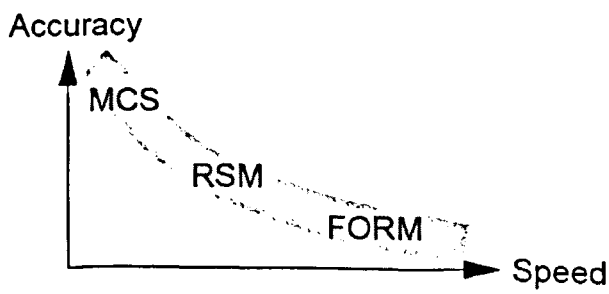


**Figure F.3.2** Performance of Methods for Stochastic Analysis (Bucher, Hintze, and Boos, 2000).

*Appendix G*

# Papers

The papers written based on the thesis and published in journal or presented for international conferences are as follows:

[1] Xia, J., Das, P.K., & Karunakaran, D. (2008). A Parametric Design Study for a Semi/SCR System in Northern North Sea. *Ocean Engineering*, 35, 1686-1699.

[2] Xia, J., Das, P.K., & Karunakaran, D. (2008). A Parametric Study for the Design of Steel Catenary Riser System in Deepwater Harsh Environments. *Proceedings of the 27th International Conference on Offshore Mechanics and Arctic Engineering OMAE 2008*, Estoril, Portugal.

[3] Xia, J., & Das, P.K. (2008). Probabilistic Fatigue Reliability Analysis of Deepwater Steel Catenary Risers. *Proceedings of the 27th International Conference on Offshore Mechanics and Arctic Engineering OMAE 2008*, Estoril, Portugal.

[4] Xia, J., Das, P.K., & Karunakaran, D. (2008). Wave Loading Fatigue Evaluation of Deepwater Steel Catenary Riser. Paper reviewed and accepted by the Eighteenth (2008) International Offshore and Polar Engineering Conference, Vancouver, Canada.